

STUDIES OF THE
ELECTRICAL PROPERTIES AND ELECTROFORMING
OF THIN INSULATING FILMS

by

ROBERT DAVID GOULD, B.A., M.Sc.

This thesis was submitted in fulfilment
of the requirements for the degree of
Doctor of Philosophy
at Brunel University

SEPTEMBER 1973

To my wife, whose help has been invaluable.

'Nature and Nature's laws lay hid in night:

God said, "Let Newton be!" and all was light.'

Alexander Pope

1688 - 1744

ABSTRACT

Evaporated thin film sandwich structures of Au-SiO_x-Au have been studied. These normally show electroforming effects and subsequently electron emission, electroluminescence, negative resistance and thermal-voltage memory effects. Previous work in the field is critically reviewed.

It was shown that the time dependence of the device current and emission current can be explained by making certain modifications to the filamentary conduction theory of Dearnaley. Detailed direct current-voltage measurements have revealed the existence of two different types of breakdown behaviour. At voltages less than 20 V single-hole breakdowns were observed, while in the voltage range 20-30 V large scale irreversible breakdown behaviour took place. The dependence of the voltage at which this occurs (V_{β}) on insulator thickness and temperature, together with measurements of the device temperature at breakdown and visual evidence of damage after breakdown, has led to the conclusion that this type of breakdown is a thermal effect. Such measurements also pointed to the existence of a high field region within the insulator, and potential distribution measurements confirmed this hypothesis. The high field region was also in evidence at low temperatures where the device current (I_c) showed a $\log I_c \propto V_b^{\frac{1}{2}}$ dependence on applied voltage (V_b).

Measurements of electron attenuation lengths in SiO_x gave values of 400-1000 Å irrespective of temperature. The temperature independence was consistent with the emitted electron energy distributions at 77 and 300 K.

It was shown that electrons underwent Bragg diffraction through the top Au electrode. The angular distribution of emitted electrons became more isotropic with increasing voltage.

(ii)

Measurements on other systems showed that Al-SiO_x/B₂O₃-Al devices could withstand very high voltages and give improved emission efficiency, while Au-CaBr₂-Au and Au-Si₃N₄-Au devices showed very high initial currents and current-voltage characteristics which were irreversible.

CONTENTS

	Page
Abstract	(i)
Acknowledgements	(iii)
Contents	(iv)
1 A Review of Electrical Conduction in Amorphous Thin Films	1
1.1 Introduction	1
1.2 DC Conduction Mechanisms in Insulating Films	2
1.3 Negative Resistance and Switching Phenomena	7
1.3.1 Current Controlled Negative Resistance	8
1.3.2 Voltage Controlled Negative Resistance	10
1.4 A History of the Forming Effect	12
1.5 Models of the Forming Process and Conduction Phenomena in Formed Materials	52
1.5.1 Hickmott	52
1.5.2 Simmons, Verderber and Eales	54
1.5.3 Greene, Bush and Rawlings	60
1.5.4 Barriac, Pinard and Davoine	64
1.5.5 Dearnaley, Morgan and Stoneham	68
1.5.6 Ralph and Woodcock	73
1.5.7 Discussion	77
1.6 Aim of the Experimental Work	79
2 Apparatus and Experimental Techniques	81
2.1 Preparation of Devices	81
2.1.1 The Evaporation System	81
2.1.2 Deposition Procedures	82

2.1.3	Thickness Measurements	85
2.2	Electrical Measurements	86
2.2.1	The Vacuum Test System	86
2.2.2	Forming	87
2.2.3	Circuits	88
2.2.4	Current-Voltage-Time Characteristics	89
2.2.5	Temperature Measurements	89
2.2.6	Attenuation Lengths	90
2.2.7	Spatial Distribution of Emitted Electrons	91
2.2.7.1	Diffraction of Emitted Electrons	91
2.2.7.2	Angular Distribution of Emitted Electrons	93
3	Results and Discussion	95
3.1	DC Device Stability and Operation	95
3.1.1	Variation of I_c and I_e with V_b	95
3.1.2	Time Dependence of I_c and I_e	104
3.1.3	Device Temperature During Operation	114
3.1.4	Microscopic Investigation of Device Damage	115
3.2	The High Field Region	120
3.2.1	Dependence of V_β on Insulator Thickness	120
3.2.2	Dependence of V_β on Temperature	123
3.2.3	Potential Distribution Measurements	126
3.2.4	Low Temperature Characteristics	133
3.3	Attenuation Lengths in SiO_x	140
3.4	Spatial Distribution of Emitted Electrons	147
3.4.1	Electron Diffraction Through the Top Electrode	147
3.4.2	Angular Distribution of Emitted Electrons	150
3.5	The Forming Effect in Other Materials	152
3.5.1	$\text{SiO}_x/\text{B}_2\text{O}_3$	153

3.5.2	CaBr ₂	156
3.5.3	Si ₃ N ₄	160
4	Conclusions and Summary	162
4.1	DC Device Stability and Operation	162
4.2	The High Field Region	164
4.3	Attenuation Lengths in SiO _x	165
4.4	Spatial Distribution of Emitted Electrons	166
4.5	The Forming Effect in Other Materials	166
	References	168
	Figures	175

CHAPTER 1

A REVIEW OF ELECTRICAL CONDUCTION IN AMORPHOUS THIN FILMS

1.1 Introduction

Materials in their thin film form have been used for many years for lens and mirror coating and other optical purposes. Only more recently, however, with the ready availability of commercial evaporating units have their electrical properties received significant attention. At first this was restricted to the performance of passive circuit elements such as resistors and to insulating film layers used to isolate various components. Subsequently the use of evaporated metal-insulator-metal (M-I-M) structures for capacitors was investigated and in some cases these have proved superior to conventional devices. With the introduction of integrated circuit technology evaporated films are widely used for contact, capacitor and insulator areas of such circuits.

In this thesis we are mainly concerned with the conduction properties of M-I-M structures, although metal-semiconductor-metal devices are also discussed. Non-metallic evaporated materials are normally deposited as an amorphous layer containing a large number of donor and acceptor centres and traps. These are due to the defect nature of the film and to impurities incorporated into the film during deposition. The amorphous nature of the films would lead us to assume that band theory, which is strictly only applicable to crystalline materials, would not apply. However, amorphous materials retain their short range order and local binding forces are essentially the same as in crystalline forms¹. Thus it is not necessary to abandon band theory, but only to modify it in the light of the new circumstances. Two very

important deviations from the band structure of crystalline materials are manifest.

(i) Donors and acceptors do not form discrete energy levels. Due to the ill-defined potential energy of the levels, trapping effects and the non-periodicity of the "lattice" a smearing out of the levels into an impurity band occurs². A very similar effect also takes place in heavily doped semiconductors³.

(ii) Band edges do not undergo a sudden transition from allowed to forbidden energy levels. Mott⁴ has shown that a one dimensional energy band model for a completely amorphous material, results in a series of localised states. In real amorphous materials a transition from the band to a localised tail of states takes place. This transition, at which a significant change in mobility occurs, is termed the mobility edge. The gap between the mobility edges of conduction and valence bands is then termed the mobility gap, a concept which is more appropriate to amorphous materials than the energy gap employed for crystalline semiconductors.

A fuller discussion of the band model for amorphous materials is contained in section 1.5.6, where the model of Ralph and Woodcock⁵ for forming in oxide films is reviewed.

1.2 DC Conduction Mechanisms in Insulating Films

In this section the conduction mechanisms most frequently observed in thin film work will be reviewed. Further reviews of these processes are given by Lamb⁶ and Simmons⁷. The equations show the variation to be expected in current density J , with respect to applied field F , and temperature T . k is Boltzmann's constant and J_I , J_{FN} , J_R , J_S , J_{PF} , J_{TH} and J_{SCL} are particular constants for each of the conduction mechanisms.

Similarly β_I , β_{FN} , β_S and β_{PF} are constants. ϕ is used as a general symbol for barrier height or activation energy. The particular meaning will be indicated in each case.

Conduction normally takes place by the transference of carriers across the insulating layer. Sometimes, however, ionic conduction is important. This is the transference of ionic charges between adjacent defect sites under the influence of the applied field. Conduction takes place by a series of ionic jumps between neighbouring sites over a potential barrier ϕ . The electric field lowers the potential barrier by an amount $\beta_I F$ in the forward direction, and increases it by the same amount in the backward direction. For a DC electric field where $\beta_I F$ is not negligible compared to kT the probability of ionic jumps in the backward direction can be ignored and the current density is given by

$$J = J_I \exp\left(-\frac{\phi}{kT}\right) \exp\left(\frac{\beta_I F}{kT}\right) \quad (1.1)$$

When conduction is by electronic means, the conductivity is normally dominated by either potential barriers at the electrode-insulator interface or by the high resistivity of the insulator. These two categories are referred to respectively as electrode limited and bulk limited conduction. Simmons⁷ has shown that whether the conduction is electrode or bulk limited depends primarily on the type of contact at the metal-insulator interface. If the metal work-function (ψ_m) is greater than the insulator work-function (ψ_i) thermal equilibrium conditions require that electrons flow from the insulator into the metal, giving a blocking contact. A depletion region is formed in the insulator at the interface and the free electron density is then lower than in the bulk. The rate

of electron flow through the system is limited by the rate of flow over (or through) the barrier and the conduction process is electrode limited. Conversely if $\psi_i > \psi_m$ electrons flow from the electrode into the conduction band of the insulator and an accumulation region results. This type of contact is termed an ohmic contact. The space-charge region thus formed in the insulator at the interface acts as a charge reservoir and can continuously supply electrons for conduction processes. The electron flow rate is then determined by the resistivity of the insulator and the process is bulk limited. Six further types of conduction will be described, the former three of which are electrode limited and the latter three bulk limited.

Under certain conditions thin insulating films can conduct current by means of quantum mechanical tunnelling through the potential barrier at the contacts, without the need to surmount the barrier. The insulator must be thin (typically less than 100 Å) so that the electron wave function is not significantly attenuated at the opposite electrode. The tunnelling equation gives a complicated dependence of current on the barrier heights at the two electrodes, which differs for the forward and reverse bias directions. At higher voltages (when $V_b \gg \phi/e$, where V_b is the applied voltage and e is the electronic charge) the equation reduces to the well known Fowler-Nordheim tunnelling equation

$$J = J_{FN} F^2 \exp\left(-\frac{\beta_{FN} \phi^{3/2}}{F}\right) \quad (1.2)$$

where ϕ is the height of the interfacial barrier. Note there is no temperature dependence in this equation.

Normally the thickness of the insulator is such that tunnelling cannot take place. Under these conditions electrons must be

thermally excited over the barrier (of height ϕ) into the insulator conduction band. The thermionic emission equation of Richardson then applies, thus

$$J = J_R T^2 \exp\left(-\frac{\phi}{kT}\right) \quad (1.3)$$

where J_R is the Richardson constant.

Usually a lowering of the barrier height ϕ occurs, due to the high fields present. This is known as the Schottky effect and the above equation is modified to the Richardson-Schottky form

$$J = J_S T^2 \exp\left(-\frac{\phi}{kT}\right) \exp\left(\frac{\beta_S F^{\frac{1}{2}}}{kT}\right) \quad (1.4)$$

By far the most important high field bulk effect in insulators is the Poole-Frenkel effect, which is directly analogous to the Schottky effect at a potential barrier. In this case internal centres (donors) are affected by the high field. The donors, at an energy ϕ below the conduction band, are subjected to a lowering of the coulombic potential barrier which increases the probability of emission into the conduction band. The usual Poole-Frenkel equation associated with thin film insulators is⁷⁻⁹

$$J = J_{PF} F \exp\left(-\frac{\phi}{kT}\right) \exp\left(\frac{\beta_{PF} F^{\frac{1}{2}}}{kT}\right) \quad (1.5)$$

where

$$\beta_{PF} = 2\beta_S \quad (1.6)$$

The higher value of β in the Poole-Frenkel case is related to the different geometry of the potential barriers at the immobile positive charge centres. Certain modifications to equation (1.5) sometimes

apply. Indeed, the original Frenkel equation (derived for bulk semiconductors) has a factor $2kT$ replacing kT in the denominators of the exponentials. Mead⁸ has suggested that the experimental behaviour described by equation (1.5) is a result of the existence of a large number of shallow traps which exhibit Poole-Frenkel emission at high fields. However Simmons¹⁰ has questioned this explanation and shown that if a more realistic value of dielectric constant is used, Mead's results are compatible with Schottky emission. Nevertheless equation (1.5) is still generally used to describe the Poole-Frenkel effect in thin film insulators. Simmons¹⁰ has pointed out that a further variation to equation (1.5), applicable for wide energy gap insulators with shallow neutral traps and donor centres which are situated below the Fermi level, can also occur. In this case the kT factor is also replaced by $2kT$ and thus the coefficient of F^2/kT is $\frac{1}{2}\beta_{PF}$, which is equivalent to β_S . Thus great difficulty is often incurred in distinguishing between the two processes.

Conduction often takes place by means of the transference of electrons between neighbouring localised impurity sites. This is known as impurity conduction and there is no need for electrons to be excited into the insulator conduction band. Electrons can be transferred between adjacent sites either by tunnelling through or by hopping over the potential barrier between the sites. This potential barrier or activation energy is denoted by ϕ . Both the tunnelling and the hopping type of impurity conduction give a thermally activated equation of the form

$$J = J_{TH} F \exp\left(-\frac{\phi}{kT}\right) \quad (1.7)$$

where J_{TH} is a function of the majority carrier concentration, and the activation energy differs for the two processes.

Finally we must consider an effect which can sometimes occur when ohmic contacts exist at the electrodes. As we have seen a negative charge is injected into the conduction band of the insulator, resulting in a semi-permanent space-charge accumulation region. The width of this region, which is a sensitive function of trapping parameters, determines whether space-charge limited conduction occurs. If the widths of the two accumulation regions are such that an overlap between them occurs, there is a space-charge throughout the insulator which determines the conduction process. Near the injecting cathode the field is approximately zero and the current is carried by diffusion processes only. The current density under these conditions is given by

$$J = J_{SCL} F^2 \quad (1.8)$$

The expression becomes more complicated when a single discrete trap level is introduced, the right-hand side of equation (1.8) must then be multiplied by a temperature dependent function of the trap density. When an exponential trap distribution is considered the current density shows a power law dependence on F , with the exponent greater than 2.

1.3 Negative Resistance and Switching Phenomena

Amorphous thin films normally show conduction properties which can be explained by a combination of one or more of the conduction mechanisms described in 1.2. All the mechanisms described previously for films of thickness greater than that at which

tunnelling predominates, show an increase in current with field. However many materials also show negative resistance effects, sometimes only after a voltage forming process. There are two types of negative resistance which are distinguished by the shape of their current-voltage characteristic. These are S-type current controlled negative resistance (CCNR) and N-type voltage controlled negative resistance (VCNR). Although we will be concerned only with VCNR it is appropriate at this point to also briefly describe CCNR behaviour. Devices showing both types of characteristic frequently exhibit related switching and memory phenomena, and it appears that the two types of negative resistance are not entirely unrelated. Dearnaley et al⁹ have pointed out that both CCNR and VCNR can occur in the same oxide and suggest that differences in stoichiometry may determine which type develops.

1.3.1 Current Controlled Negative Resistance

CCNR has been extensively observed in semiconducting chalcogenide glass thin films, although it has also been observed in bulk devices. A review is given by Henisch¹¹ and the effect is also discussed, as part of a wider review, by Simmons⁷ and Dearnaley et al⁹. Two types of switch have been reported¹². These are the threshold or Ovshinsky switch and the memory switch. In the threshold switch at low voltages a high impedance characteristic is exhibited. However when the voltage is increased above a certain threshold V_t , the device switches to a very low impedance "on" state. It remains in this state provided a holding voltage $V_h < V_t$ and a holding current I_h are exceeded. When the current is reduced below I_h the device switches back to the high impedance "off" state. V_t follows an approximately linear variation with electrode separation

while V_h is almost independent of separation. The memory switch also shows a high impedance "off" state and a low impedance "on" state, but the switching behaviour is different. Switching from the "off" to the "on" state is accomplished by applying a high voltage pulse, whereas switching back to the "off" state can only occur after a high current power pulse is applied. The "off" state cannot be re-obtained merely by reducing the current through the device, and the "on" state is thus a stable memory state. The disparity in switching times between the two types of switch (about 10^{-10} s for the threshold and 10^{-6} s for the memory switch) has led to different explanations of the switching process. The fast switching time of the threshold switch is an indication that electronic (probably space-charge limited) processes are responsible. It has also been shown that a thermal runaway effect could be responsible for the switching process and current opinion is divided between these alternatives. Thermal runaway does not appear to be applicable to the thicker chalcogenide films. The rather slower switching time of the memory switch is compatible with atomic re-arrangement in the glass and this is normally ascribed to the growth of a crystallised filament between the electrodes. Erasure of the "on" state occurs when the filament is destroyed or when it undergoes a phase change due to the high current pulse.

Memory switching has also been observed in transition metal glasses¹³. These consist of inorganic oxides containing an appreciable amount of transition metal ions (Fe, Cu, V, Co, W, Mn) which can enter the glass in two or more valence states. As with the chalcogenide glass memory switch, switching from high to low impedance states is by means of a voltage pulse, while switching from low to high impedance states is by means of a current pulse.

CCNR is also exhibited in some simple oxide films. Chopra¹⁴ observed this after a forming process in oxides of Nb, Ta and Ti. Forming took place when the reverse current density was increased above 100 mA cm^{-2} . Current-voltage behaviour below the current peak suggested a space-charge limited mechanism. Beyond the negative resistance region the impedance of the device is effectively zero. A thickness independent holding voltage is required to keep the device in this state. Hiatt and Hickmott¹⁵ have also reported switching between CCNR states and a high conductivity state which appears after breakdown in Nb_2O_5 .

1.3.2 Voltage Controlled Negative Resistance

VCNR is observed in a wide variety of oxides, halides and sulphides. It has also been observed in organic monomolecular layers of cadmium arachidate¹⁶. This type of conduction only occurs after a voltage forming process. Prior to forming the current through the device (or circulating current, I_c) shows $\log I_c \propto V_b^{\frac{1}{2}}$ dependence where V_b is the voltage bias. From equations (1.4) and (1.5) this is characteristic of Schottky or Poole-Frenkel emission. When the voltage is increased to a value in excess of the forming voltage V_F , a large increase in conductivity (sometimes 8 orders of magnitude¹⁷) takes place. Reducing the current to zero results in the permanent establishment of a VCNR characteristic. The following general features connected with the forming process have been established by many workers. They should not be taken as hard and fast conditions which must be satisfied to ensure forming, as exceptions to most of them have been reported.

(i) A low partial pressure of oxygen in the device environment is usually required.

(ii) The nature of the negatively biased cathode electrode is unimportant. Anode materials of high conductivity "noble metals" such as Au or Ag give good formed characteristics, while reactive metals like Al only form with difficulty. Mg anode electrodes never show forming behaviour.

(iii) Forming is an essentially permanent change. Un-forming normally only takes place if the device is run in a high partial pressure of oxygen, or if non-symmetrical devices with only one suitable electrode are run at a sufficient reverse bias.

(iv) V_F does not depend on the insulator thickness, but varies with different insulators.

(v) V_F is only slightly dependent on temperature. Forming does not occur at low temperatures.

(vi) Forming does not normally occur if the insulator thickness is greater than 3000 Å.

The general device properties after forming are described below and illustrated in figure 1. Exceptions to these properties are also sometimes exhibited.

(vii) Devices display VCNR characteristics. The maximum current is denoted by I_m and the voltage at which this occurs by V_m . The voltage for the current minimum is denoted by V_u .

(viii) V_m is normally independent of thickness and temperature.

(ix) Negative resistance behaviour is destroyed at low temperatures, but can be re-established if the temperature is increased.

(x) The negative resistance part of the characteristic is exceptionally noisy.

(xi) Electrons are hot enough to be emitted from the device and can be collected with a suitable anode. The emission current is denoted by I_e and increases rapidly in the negative resistance region.

(xii) Switching behaviour is exhibited. If the device is quickly turned off (in less than 0.1 ms) in the negative resistance region at B, C or D, the new characteristic will follow the paths OB' , OC' or OD' . At the threshold voltage $V_T < V_m$ the device switches back to the low impedance characteristic. In principle there are an infinite number of memory states.

(xiii) AC characteristics do not show VCNR but follow the curves OA, OB, OC or OD.

Quantitative values of device parameters are not given above. These will be found in the historical section 1.4. Likewise models of the forming process and subsequent device behaviour are discussed in section 1.5.

1.4 A History of the Forming Effect

The forming effect and negative resistance phenomena were first reported for structures of Al-Al₂O₃-Ag by Kreynina et al¹⁸. Samples were produced by anodisation and many showed negative resistance effects for both polarities with the maximum current occurring at approximately 3 V. Electron emission was detected, the voltage at which this first occurred varying with the thickness of the film. Extending this work¹⁹ it was found that up to three maxima could be observed in the $I_c - V_b$ characteristic. The position of these maxima was not dependent on the thickness of the insulating layer. After a period of operation under dynamic conditions the characteristic stabilised to a single maximum at 3-4 V. This was reproducible even

after the specimen had been stored in air for long periods. However, after storage in air a dependence on electrode polarity was evident in the characteristic, lower currents being passed when the Al base layer was positively biased. The negative resistance disappeared on cooling to liquid nitrogen temperature although new maxima re-appeared when the samples were returned to room temperature. Further work²⁰ was performed using base layers of Mg, Cu, Ta and 0.5% Nb, steel, duralumin and an alloy of Mg/Al. Negative resistance effects were also detected and the location of the maximum depended on the base material. In some specimens when the base layer was of positive polarity very low currents were passed. This occurred only with base layers of Al, duralumin, Mg/Al and Ta. Thus the basic effects of negative resistance, electron emission and dependence on the positively biased electrode were observed, but a theoretical basis was not proposed.

Mead²¹ suggested that an improvement in frequency response in the tunnel diode could be brought about by replacing the n-type semiconductor by a metal. This would increase the number of carriers available which effectively limits the frequency response. The structure investigated as an emitter had a bottom metal electrode which injected electrons through an insulating layer and into a top electrode through which emission occurred. The thickness of the insulating layer was such that electrons could tunnel directly through to the top electrode, while the top electrode was kept thin in order to reduce electron attenuation. The principal limitations to the efficiency of such an emitter are this electron attenuation, and also breakdown effects caused by high fields generated over the thin tunnelling layer.

In principle the tunnel structure could be used as the emitter in a three terminal M-I-M-I-M high frequency amplifying device, but structures of this type (Al-Al₂O₃-Al-SiO-Al) failed at currents of 1 mA. Further work²² on two terminal devices gave maximum emission transfer ratios ($\alpha = I_e/I_c$) as high as 0.01 but α varied widely between individual samples.

Because the emitting properties of the top electrode were of such importance, especially when incorporated into a triode configuration, Mead measured the energy mean free path of hot electrons in Au²³. This was accomplished by using a tunnel structure of Be-BeO-Au to inject electrons into and through the counter electrode. The mean free path was deduced from measurements of the transfer ratio with respect to the top electrode thickness, measured values being 109 and 103 Å for electrons injected at voltages of 7 and 10 V respectively. These values are obviously not those for electrons injected into the counter electrode with energies of 7 and 10 eV, but rather those for an electron distribution with energies ranging up to the tunnelling voltage. Thus, mean free paths measured in the counter electrode, reflect previous scattering behaviour in the insulator. The significance of this will become more apparent when discussing attenuation lengths measured in formed devices where the insulating layer is thicker and scattering more prevalent. Attenuation length measurements in formed samples are all based on the above method, originally used by Mead for tunnel cathodes.

② Kanter and Feibelman²⁴ performed an exhaustive study on electron emission from Al-Al₂O₃ (67-150 Å)-Au(200-300 Å) structures. For most samples the characteristic could be explained in terms of Fowler-Nordheim tunnelling although some samples exhibited different

behaviour. After operation for some time at voltages sufficient for electron emission and then reducing the voltage to less than 4 V a considerable increase in I_c was observed. On increasing the voltage the current dropped again and the subsequent characteristic showed a reproducible negative resistance region. Although at the time this was described as a "breakdown" region it now seems certain that this was the normal negative resistance region observed in formed devices, and that the sudden current increase occurred at the onset of forming. There is a marked similarity between this behaviour and that previously reported by Hickmott²⁵.

The experimental arrangement included a positively biased anode system and retarding potential measurements could be made. Emitted electron energy distributions were derived by graphically differentiating retarding potential curves. Typically the distribution showed a peak at a voltage much lower than that across the device and very few maximum energy electrons were observed. Furthermore the average energy of the emitted energy distribution increased linearly with the applied voltage. Values of α were deduced for different thicknesses of Al_2O_3 and Au and were generally found to lie in the range 10^{-6} - 10^4 . By depositing Ba, a low work-function metal, on top of the Au electrode the value of α could be significantly increased.

Kanter²⁶ also measured the attenuation length of hot electrons in Au using the method described by Mead for tunnel cathodes. Using an Al_2O_3 layer of thickness 100 \AA , the value of the attenuation length for a pure Au top electrode was 57 \AA when a bias of 6 or 7 V was applied. The attenuation length was increased to 75 \AA when devices including the additional Ba layer were investigated.

③ Pollack et al^{27,28} observed a field dependent forming process in evaporated Pb-Al₂O₃-Pb diodes, which occurred even in air at atmospheric pressure. Forming took place at about 12 V for a 340 Å film and un-forming of samples occurred when the bias was removed. Forming was uni-directional and only low currents were passed if the applied voltage was in a different direction to that used to induce forming. VCNR was also evident and the current peak was generally at about 3 V irrespective of insulator thickness. The ease of forming was greatly reduced at low temperatures and for samples formed at room temperature the current fell rapidly between 300 and 235 K. Below this temperature the current remained relatively constant. A qualitative model was presented to explain these results. This included the establishment of a positive ionic space-charge which drifts towards the cathode producing a local field as high as 10^8 V cm⁻¹ in the cathode region. The high field region is also consistent with lowered metal-insulator work-functions, which allow Schottky emission of electrons into the insulating layer.

④ Hickmott²⁵ observed forming and negative resistance phenomena in anodically grown diodes of Al-SiO-Au, Al-Al₂O₃-Au, Ta-Ta₂O₅-Au, Zr-ZrO₂-Au and Ti-TiO₂-Au. As the voltage across the freshly made Al-Al₂O₃-Au films was increased, a critical voltage was reached at which a sharp increase in current occurred. For a 350 Å film this occurred at 4.1 V. On lowering the voltage the current through the device increased and reached a peak value at 2.3 V. (This voltage for maximum current was independent of film thickness between 150 and 1000 Å, but varied if materials other than Au were used for the counter electrode.) The negative resistance region was observed for either polarity. Forming only occurred when the devices were

tested under vacuum conditions. Attempts to induce forming at atmospheric pressure proved unsuccessful.

The temperature dependence of I_c was determined and it was found that the current passed was considerably reduced as the temperature was lowered. The shape of the current-voltage characteristic remained unchanged down to temperatures of 195 K, but the negative resistance region disappeared completely at low temperatures. Negative resistivity was readily re-established by increasing the temperature to a value exceeding 195 K. A thermal-voltage memory effect was also observed. When the current-voltage characteristic was first traced out at 188 K (where there is normally no negative resistance region) a characteristic very similar to that observed at room temperature was obtained. However, on reducing the voltage the current did not exhibit the room temperature behaviour and very low currents were observed. Negative resistance was not again observed at this temperature unless the device was once more recycled to above 195 K.

AC conduction was also investigated. At 60 Hz no negative resistance was apparent, but the locus of the maximum AC voltage traced out the DC negative resistance region. Since switching from peak current to valley current in the DC characteristic could be accomplished in approximately 0.5 μ s it was not clear why a 60 Hz voltage (1 cycle lasts about 16 ms) would not trace out the DC curve. Hickmott concluded that the different conduction processes present must have vastly different time constants.

Experiments on triode structures yielded extremely interesting results. A negative resistance region and high conductivity could be established between base and top electrode, without high conductivity developing between middle and base or top electrodes.

For example, 0.5 V between base and top electrode produced a current of 43 mA, but the same voltage between the middle and either of the other electrodes produced a current of only 0.1 mA. However, if conductivity was then established to the middle electrode by applying the forming voltage between it and one of the other electrodes, high current levels could be detected between any pair of electrodes. This unusual effect could be explained if one assumed that the overriding factor in determining conductivity is the condition of the metal-oxide interface region. High currents could only be drawn between electrodes if the forming voltage had previously been applied across the electrodes. A barrier to conductivity must therefore be present at electrodes where this has not been accomplished.

A clear linear correlation between V_m and the square root of the dielectric constant was obtained for all the oxides investigated. This indicated that forming and other related effects were characteristic of thin film insulating oxides and were not specific to Al_2O_3 .

Observations of electron emission were qualitatively similar to those of Kreynina¹⁸. There was a very sharp increase in the magnitude of the electron emission at the same voltage as the negative resistance region appeared, and there seemed to be a close correlation between these two effects. Emission commenced at voltages as low as 2.5 V, and since this would not give enough energy to surmount the Au-vacuum barrier it was concluded that electrons were probably emitted directly from the insulator conduction band and then through pinholes in the Au film. On the basis of later evidence²⁹ another explanation was suggested. There was a marked increase in I_e at about 5 V, which is just above the

work-function of Au. This was detected in Al_2O_3 , SiO , Ta_2O_5 and ZrO_2 , all with Au counter electrodes. The increase in I_e was apparently due to electrons reaching the Au film with an energy sufficient to overcome the metal work-function. Attempts to float off the counter electrode and observe pinholes gave positive results with Al_2O_3 ; however devices using SiO had continuous counter electrodes with no pinholes. Since electron emission can occur when the Au is continuous and the applied potential is less than the metal work-function, some other mechanism must be responsible. The possibility of patches of low work-function was eliminated by photoelectric measurements, and thermionic emission seemed unlikely in view of the observed sensitivity to applied voltage rather than power input. Therefore, either some mechanism was operating whereby electrons with energy of only 2 eV could escape into vacuum, or (more likely) electrons in the oxide received additional energy such that their total energy exceeded the work-function of Au.]

During further studies of the current-voltage characteristic in formed devices Hickmott³⁰ observed that the conductivity of a device could be reduced to a lower value by applying a voltage greater than V_m and then rapidly reducing it to zero. The low conductivity persisted provided that voltages in excess of about 1.8 V were not applied. If this voltage was exceeded full conductivity was restored at some value between 1.8 V and V_m . A further investigation of this switching phenomenon was later performed by Simmons and Verderber³¹.)

There appeared to be some correlation between the purity of samples and their forming voltage. Impure bisulphate anodised Al films showed a value of V_F (3.7-4.1 V) nearly independent of thickness. For SiO and purer Al_2O_3 diodes, the forming voltage

increased with oxide thickness. This dependence of forming on the purity of the insulator, together with the temperature dependence results discussed earlier, led Hickmott to suggest that the device properties were probably dependent on impurity conduction through the insulator.

(Samples were also fabricated with different counter electrode materials which included Ag, Au, Cu, Co, Pb, Sn, Bi, In, Al and Mg. The base electrode and insulator were Al and Al_2O_3 in each case. Ag electrodes frequently induced shorting between the electrodes, and forming was not generally possible unless the Ag electrode was negatively biased during forming. With thicker films Ag appeared to be the optimum anode material. It was impossible to develop conductivity using Mg electrodes, and the conductivity for peak currents using the other metals diminished in the order of the sequence given above. Some device properties were dependent on the device polarity during forming, but forming itself would generally occur for either polarity.)

Further measurements on triode structures were made by Hickmott³² in order to ascertain the potential distribution inside the insulating layer. Al-SiO-Al-SiO-Au samples were fabricated by evaporation. The bottom electrode was referred to as the cathode, the middle electrode as the grid, and the top electrode as the plate, by analogy with vacuum triode tubes. The voltages across the two insulating layers could then be referred to as V_{pg} and V_{gc} , while the total voltage across both layers is V_{pc} . Forming was accomplished by applying a voltage between the plate and cathode with the Au electrode positive. Before forming the potential divided over the two layers in rough proportion to their thicknesses. During the forming process the potential shifted until nearly the whole

voltage drop was between grid and cathode, and V_{gc} was almost equal to V_{pc} . The (very low) voltage drop V_{pg} , between the plate and grid followed the same characteristic as I_c and thus conduction in the low field region follows an ohmic pattern. Device conduction is dominated by the high resistance region between the grid and cathode. On reversal of polarity the high resistance region still remained between the cathode and grid, although the plate was now at a negative bias, and the negative resistivity and high conductivity behaviour persisted. Thus negative resistance effects cannot be the result of having a high field at the negative electrode which can assist emission of electrons into the insulator. Further cycling of the characteristic did sometimes cause a shift of the high resistance region to between the plate and grid, but device properties did not vary with the new potential distribution. The salient factor appeared to be only that there was somewhere in the insulator a high field region, which was estimated to be of thickness approximately 120 \AA . A model for the forming process and subsequent operation of the samples, which was based on the existence of such a high field region and which assumed an impurity conduction process, was proposed to account for the various device properties (see 1.5.1).

Electroluminescence was observed from small distinct spots at voltages greater than 1.8 V. This did not follow the electron emission curve, falling rapidly when V_b exceeded 2.9 V. Emitted light was detected at energy greater than the maximum expected from the applied voltage. A process, whereby impartation of energy to carriers inside the oxide occurs, is supported by this and by the anomalous electron emission results.

Measurements³³ of the attenuation lengths of hot electrons in the Au top electrode were also attempted using the following definition

of attenuation length, λ

$$\frac{I_e}{I_c} = K \exp\left(-\frac{d}{\lambda}\right) \quad (1.9)$$

where d is the thickness of the Au layer and K is the pre-exponential factor, itself dependent on V_b , oxide thickness and metal work-function. For values of V_b up to 9 V the measured attenuation lengths were about 200 Å, with slightly higher values below 3 V and above 8 V. These high values were thought to be due to differences in the electron energy distribution of electrons entering the Au, or to differences in scattering at the metal-insulator interface. The variation of K with V_b was also deduced and the major variations in emission current were reflected in K . An inflexion in K was apparent at 8.2 V, probably due to transitions between the insulator conduction and valence bands.

Retarding potential measurements were taken at different values of V_b and certain features were evident. For V_b greater than the Au work-function there was an inflexion in the curve, and the proportion of low energy electrons was increased. The proportion of current due to high energy electrons was about 10^{-8} of the total current and remained constant with respect to V_b . The proportion of low energy electrons increased rapidly with V_b . The steep rise in emission at voltages greater than the work-function was due to electrons coming through the top electrode, while emission at low voltages must have been due to pinhole emission or electron energy enhancement in the insulator. In view of the fact that thickened top electrodes reduce the maximum energy of the emitted electrons (which would not be the case for pinhole emission) it was concluded that at least some of the emitted electrons came through the top

electrode.

Electron attenuation lengths in Al_2O_3 films were also estimated. A value of approximately 200 \AA was obtained, and as with the attenuation lengths for Au measured by Hickmott, this greatly exceeded values previously measured by other authors.

Preliminary measurements of current-voltage characteristics by Cachard et al³⁴ gave results closely resembling those previously reported by Hickmott. A similar explanation, involving the formation of centres which are neutralised by the field at higher voltages, was presented.

Filaretov et al³⁵ conducted experiments with Al- Al_2O_3 -M structures and found that the conducting properties were drastically affected by the nature of the top electrode. It was proposed that a junction layer was formed in the insulator by the diffusion of metal atoms from the electrode. Due to the low thickness of the Al_2O_3 layer ($100\text{-}500 \text{ \AA}$) it was suggested that the metal atoms could diffuse right across the insulator to form deep impurity levels in the forbidden band of the insulator, which could behave as recombination or trapping centres. By ionisation of these centres a space-charge could be formed which would decrease the density of free carriers and precipitate the negative resistance region. The observed decrease in current with oxygen pressure may also be dependent on a decrease in conductivity because of oxygen adsorption on the surface of the Al_2O_3 layer.

Barriac et al³⁶ observed the normal device properties for Al- Al_2O_3 ($100\text{-}1000 \text{ \AA}$)-Al films prepared by anodisation and atmospheric oxidation of Al. It was observed that forming occurred more readily when the top electrode was positively biased even though the devices were of a symmetrical construction. Subsequent device

properties, after forming, were not polarity dependent. Rare and inert gases did not modify the conduction properties, but the presence of oxygen caused the complete disappearance of the negative resistance region. Increasing the temperature to 100°C did not increase the conductivity and the usual low temperature behaviour was observed at liquid nitrogen temperature. Microscopic examination of the top electrode revealed localised cavities up to 10 μm in diameter and it was suggested that conduction was not uniform but took place via the defect regions.]

Simmons et al³⁷ observed the spatial distribution of emitted electrons by replacing the metal anode with a flat phosphor screen. Imposed on an illuminated background were many circular arcs, all of approximately the same radius. Reducing the accelerating potential and increasing the voltage across the devices both increased the size of the image formed. This was consistent with the following equation.

$$r = \frac{24.54 \text{ s}}{d_{hkl} V_a^{\frac{1}{2}}} \left(1 - \frac{36}{d_{hkl}^2 (V_b + \eta)} \right)^{\frac{1}{2}} \quad (1.10)$$

where r is the radius in cm, s is the cathode-screen separation, d_{hkl} is the lattice spacing in Å, V_a is the accelerating potential and η is the Fermi energy of the Au electrode. The circular arcs were explained in terms of coherent scattering processes in the Au electrode. For the most intensely diffracting (111) Au planes it can be shown from equation (1.10) that 10 eV electrons would be diffracted nearly into the plane of the electrode, and would be unlikely to escape. If diffraction occurs in the region of a pinhole, however, the diffracted electrons would still retain sufficient energy to be emitted through the wall of the pinhole and escape into vacuum. Further work³⁸ in which small area devices were used to cut down the number of arcs

appeared to substantiate this view. Thick Au electrodes were used containing a small square hole. The reason for this configuration was to stop emission through the top electrode and to confine it to the edges of the hole. Radii of emission patterns appeared to be consistent with (111) diffraction. Simmons argued that the fact that emission was only possible by coherent scattering near pinholes, other electrons being reflected back into the top electrode, was probably the reason for the low emission efficiency generally exhibited by cold cathodes.

(12) [Verderber and Simmons³⁹ described the use of the devices as cold cathode electron emitters. The variation of I_c and I_e could be split up into four distinct voltage ranges thus

V_b	I_c	I_e
0-2.5 V	$I_c \propto \sinh K V_b$	No emission
2.5-3.0 V	Maximum current	Exponential increase
3.0-7.0 V	Negative resistance	Slow exponential increase
7.0 V upwards	Slight current increase	Sharp increase

Electron emission at voltages less than the work-function of Au were attributed to the acquisition of energy from the lattice, in agreement with the previous work of Hickmott³³.

(13) [Simmons and Verderber³¹ reported the memory phenomenon in Al-SiO-Au diodes. This was essentially the same as that earlier described by Hickmott³⁰ for Al_2O_3 devices. If voltage was returned to zero in less than 1 ms from some point in the negative resistance region and a voltage less than the threshold voltage V_T re-applied a new higher impedance characteristic was traced out. This characteristic remained unless the voltage exceeded V_T , when the low impedance state was restored. In principle the device could be used as a multi-state

analogue memory with each state corresponding to a different point in the negative resistance region (see figure 1). Similar AC characteristics to those described by Hickmott were observed, the locus of the end points of the characteristics corresponding to the DC curve.]

② [Simmons et al^{2,17} studied the factors involved in the forming of Al-SiO-Au devices. Results were very similar to those of Hickmott. Oxygen pressure had to be less than 10^{-2} torr or forming was inhibited, but the reasons for this effect were not discussed. Samples formed at a high temperature formed faster and passed more current than those formed at lower temperatures. There was also a slight decrease in forming voltage with temperature over a range of 300 K. Samples could not be formed when the Al electrode was positive, and samples which had been formed with the Au electrode positive could be un-formed by applying an increased voltage in the reverse direction. The temperature dependent forming process and reversibility of forming were taken to be a strong indication of ionic migration. On the basis of these observations a new model of the forming process was developed in which a band of localised states were introduced into the forbidden band of the insulator¹⁷. This was later extended to include most of the subsequent conduction phenomena² (see 1.5.2).]

Lomax and Simmons⁴⁰ later described an alpha-numeric display panel consisting of a 5 x 5 array of cold cathodes. Although the preparation of these panels was relatively easy and inexpensive, poor lifetimes caused by dielectric breakdown and continued forming limited their exploitation.

Using a 20 V DC voltage on which a pulsed bias was superimposed Lancaster⁴¹ was able to observe emission patterns for voltages up to 30 V. Electron energy was then sufficient to allow them to be

transmitted through the surface of the top electrode. Emission was not restricted to pinhole edges as was observed by Simmons for lower electron energies. Emission patterns were obtained showing circular arcs with radii consistent with diffraction from the (111) planes of Au, and at voltages greater than 26 V a secondary arc was sometimes observed which was attributed to (200) diffraction.

① Dearnaley⁴² proposed the novel theory that conduction took place through a matrix of conducting filaments which were propagated during the forming process. This idea was to be the basis of a new model which was described to account for some of the previously unexplained device properties⁴³ (see 1.5.5).

② Barriac et al⁴⁴ explained the I_c-V_b characteristics in terms of a combination of ionic and tunnelling mechanisms. At higher voltages tunnelling occurs over a narrow region established as a result of the accumulation of positive ionic space-charge (see 1.5.4).

Pinto and Shaha⁴⁵ observed VCNR in sputtered films of Nb-Nb₂O₅-Al or Au films. The effect was observed in air as well as under vacuum and was not dependent on device polarity. Differences from the normal I_c-V_b curves were apparent, the main point being the sharp rise in current after the negative resistance region at voltages of approximately 3 V. This effect was attributed to non-destructive avalanche breakdown. Negative resistance behaviour was explained in terms of a model whereby a trapping process causes a space-charge to accumulate, finally giving rise to a dipole layer at the metal-insulator interface. As the trapped charge increases the barrier height increases resulting in a sharp decrease in current.

In a series of theoretical publications Hrach⁴⁶ investigated many of the properties of M-I-M structures, although his results were not applied directly to formed materials. In particular the effects of

elastic scattering, optical phonons and traps were considered and their effects on the emission current were discussed. A theoretical expression was obtained for a assuming Fowler-Nordheim tunnelling and the existence of a distribution of traps in the insulator. An expression for the angular distribution of emitted electrons was derived, and it was shown that an isotropic angular distribution required short mean free paths for elastic interactions and long mean free paths for collisions with traps.

⑤ [Greene et al⁴⁷ investigated the dependence of device properties on the nature of the anode material. They found that the effectiveness (maximum current density under specified conditions) of anode materials was in the following order Pd, Ir, Pt, Au, Ag, Cu, C, Si, Ni, Co, Fe, Zn, Sn, Pb, Cr, In, Mn, Be, Al, Mg. The most effective anode materials were those of low chemical reactivity, while reactive anode metals gave poor results.

During forming devices were monitored with a mass spectrometer and results indicated the evolution of fluorine from fluoride devices. Similar experiments on oxide devices were not attempted because of the high background level of atmospheric oxygen.

A correlation was found between observed forming voltages and values of the Gibbs free energy of formation of various halides. The Gibbs free energy corresponds to the minimum voltage for normal solid state electrolysis and the correlation observed was close enough to suggest strongly that forming was by this process.

The growth of current during switching from the high to the low impedance state was investigated. Switching was not instantaneous and current growth took place over several milliseconds. The current did not rise smoothly with time but increased in a series of irregular current steps. This was indicative of a number of separately switching

areas, each of which switched at a different time.

A new model was presented in which a form of high field solid state electrolysis occurs in certain localised regions of the insulator. A series of chemical reactions takes place leading to the establishment of chains of defect centres across the insulator. Conduction takes place through these chains by a tunnelling process. Various device properties, particularly the poor performance of devices in an oxygen atmosphere and the evolution of fluorine from fluoride devices, could be satisfactorily explained by this model (see 1.5.3).

Dearnaley⁴⁸ described a filamentary model to account for the properties of oxide coated cathodes. It was suggested that the filaments consist of chains of metal atoms separated by oxygen vacancies which are produced when the cathodes are thermally activated. The vacancies can take up oxygen atoms from an oxygen atmosphere, and thus poisoning of the cathodes is adequately explained. Emission is originally field emission, but the filament current raises the local temperature and initiates thermionic emission from the ends of the filaments to a suitable anode. Flicker noise which is characteristic of oxide coated cathodes is caused by the thermal rupture and subsequent field-assisted re-forming of the filamentary paths.

Barriac et al⁴⁹ studied various aspects of I_c-V_b and I_e-V_b characteristics in Al-Al₂O₃-Al or Au films. They investigated the dependence of I_m and V_m with the frequency of an AC signal applied to the device. While V_m remained roughly independent of frequency the value of I_m dropped sharply between 0.1 and 10 Hz. Increasing the partial pressure of oxygen from 10^{-5} to 0.2 torr produced a significant change in the device properties. The first trace gave the normal negative resistance characteristic, but the reverse trace gave a high impedance characteristic which did not exhibit negative resistance.

Subsequent traces for both increasing and decreasing voltage followed the high impedance curve. Emission current measurements showed a peak value at a voltage slightly above that of V_m and then a region of low emission at approximately 5 V. A very sharp increase in I_e with V_b was detected at about 6 V. Barriac et al extended their ionic/tunnelling theory noted earlier⁴⁴ and gave experimental values for the constants used to characterise the electron emission (see 1.5.4).

Hartmann et al⁵⁰ made careful quantitative measurements of the spatial distribution of the emission current from Al-Al₂O₃-Au samples. Using a Lallermann electronic camera, plates were produced of which the optical density was proportional to the local emission current. Densitometer tracings then gave the actual emission current. They observed emission from localised areas and noted that the intensity and number of emitting spots increased with time. Short circuits through the alumina at which localised heating caused increased emission, were tentatively suggested to be the predominant source of electron emission.

(17) [Bernard et al⁵¹ observed VCNR in Al-Al₂O₃-Au structures of thickness 25-500 Å. A study of the capacitance of these samples at 1000 Hz showed a linear correlation between anodising voltage and capacitance. They concluded that VCNR was dominated by conduction in a narrow high field region, in agreement with the observations of Hickmott³². Since VCNR was apparent in devices of thickness as low as 25 Å they concluded that the high field region must be of thickness less than 25 Å. Increasing diode voltage increases the width of the high field domain which decreases the efficiency of the tunnel effect and lowers the current carried.]

Galkin and Ignat'ev⁵² observed VCNR in Al-Al₂O₃-Al devices at low temperatures. They suggested the effect was due to a space-charge limited current controlled by traps near the Al-Al₂O₃ interfaces. The

origin of these surface traps was probably due to interaction of the Al with adsorbed molecules of gases on the Al surface and water vapour in the diffusion pump oil.

(18) [Forming at atmospheric pressure and subsequent VCNR was reported in Zr-ZrO₂-Au diodes by Park and Basavaiah⁵³. Optical and electron microscope studies revealed the formation of spots of diameter 5-7 μm during forming and switching operations. Observation of the devices when covered with a liquid crystal, indicated that the current was concentrated in the region of a specific spot. Oxygen deficient areas round the rims of the spots were detected by electron microprobe analysis.]

(19) [The forming process was observed in diodes of Yb-YbO-M by Jawelekar⁵⁴ who noted two differences from the normal negative resistance behaviour. Firstly the current in the negative resistance region was stable in contrast to the normal noisy behaviour. Secondly, a sharp current increase occurred at higher voltages in agreement with the results of Pinto and Shaha⁴⁵ and Barriac et al⁴⁹. Electron emission was detected at voltages in excess of 10 V. He explained the VCNR in terms of a heavily doped p-n junction formed in the YbO layer by excess metal and oxygen atoms. Negative resistance is then a result of a similar process to that in the tunnel diode, where the heavy doping causes the Fermi level to drop into the valence band of the p-type layer.]

Thevenard et al⁵⁵ measured the angular distribution of emitted electrons from Al-Al₂O₃-Al films which exhibited VCNR. They used a hemispherical collecting anode, divided into circular zones which were insulated from each other. Two distinct types of angular distribution were observed. At very low voltages a nearly isotropic distribution was found which was thought to be due to radiative recombination processes in the oxide producing a sea of photoelectrons in the electrodes.

At higher voltages a highly non-isotropic distribution, corresponding to heavy scattering in the insulator was determined. With increasing voltage the distribution became more isotropic, in accordance with the predictions of Hrach^{46(d)} for insulators with traps and where electron-phonon scattering is important.

Hrach⁵⁶ showed that penetration of the electric field intensity into the electrodes could modify the angular distribution of emitted electrons and vary the value of I_c by an appreciable amount.

Attenuation length measurements of hot electrons in Au were performed by Niquet et al⁵⁷. Samples were fabricated with the top electrode thickness ranging from 100-450 Å. Emission current was measured by an electronic camera and results were calculated by the method of Hickmott³³. They found values of the attenuation length in Au to vary from 60-88 Å for voltages of 2.8-3.4 V. The thickness of insulating Al_2O_3 was only 55-75 Å and tunnelling must have been the predominant conduction mechanism.

Gould and Collins⁵⁸ studied the spatial distribution of hot electrons emitted from Au-SiO-Au films. Emission patterns for voltages up to approximately 20 V were very similar to those observed by Simmons et al³⁷, and were composed of a number of brightly illuminated arcs of the same radii, none of which subtended an angle greater than 180° . The arc radii were consistent with the diffraction of hot electrons by the (111) planes of the polycrystalline Au counter electrode prior to emission from pinhole edges. At higher voltages (using a pulsed biased system suggested by Lancaster⁴¹) they clearly observed almost completely circular arcs which they assumed to arise from emission through the top electrode. The first arc appeared at a bias of 20 V and a second lower intensity arc appeared at 26 V. Using the condition for emission from the Au derived by Gould⁵⁹ and assuming that the two rings corresponded to emission from

the (111) and (200) planes of the Au, they calculated that emission should be initiated at 26.8 and 33.0 V respectively for the two rings. The discrepancy between this and the observed values were explained by the distortion of the electric field at the Au surface by irregularities in the Au film, and emission through localised surface regions inclined to the plane of the film. Furthermore, if the filamentary model of Dearnaley⁴³ is assumed to apply, electrons are not necessarily injected into the Au layer in a direction normal to the surface, and this was suggested as a further reason for the observance of diffracted rings at lower voltages than expected.

In order to study changes in the insulating film as a result of the high field existing between the metal electrodes Pivot et al⁶⁰ used electron diffraction to detect crystallinity in the insulator. They used structures of Al-SiO-Al which exhibited forming at approximately 15 V, in contrast to similar devices used by Simmons^{2,17} which failed to form. At low voltages below 5 V the diffraction pattern showed a completely amorphous structure. Between 5 and 15 V electron microdiffraction revealed an isometric cell ($a = 5.40 \text{ \AA}$) which they suggested were due to the presence of Si and SiO₂ in the SiO film. After the appearance of forming at 15 V diffraction patterns indicated the presence of a distorted quartz compound and also a spinal structure formed from Al and Si. At voltages above 20 V the existence of β -cristobalite and certain aluminium silicates was detected. The existence of Al compounds strongly suggest the diffusion of the Al electrode material into the insulator. Chains of SiO₄ tetrahedrons, which were detected parallel to the electric field, pointed to the existence of conducting filaments of a type similar to those proposed by Dearnaley et al^{42,43}.

(20) (Dearnaley et al⁴³ tried to detect the existence of Au ions in formed SiO_x . Energy analysis of the back-scattering of a collimated beam of 1.2 MeV protons generated by a 5 MV Van de Graaf generator is capable of isolating the masses of different nuclei present. The sensitivity of the method was sufficient to detect the 10^{19} Au atoms per cc needed to support the forming theory of Verderber et al¹⁷, but results showed no evidence of any Au ions in the SiO_x . An apparent contradiction is therefore present between these results and those of Pivot et al discussed above, who detected Al in formed film of SiO using Al electrodes.

The non-appearance of Au ions in SiO_x led Dearnaley et al to propose a new phenomenological model based on the growth of filamentary paths which had previously been mooted by Dearnaley⁴² (see 1.5.5).

Bernard et al⁶¹ studied the characteristics of devices in the presence of various gases and found that for voltages less than 2 V, I_c was reduced. By far the greatest diminution of current was observed using O_2 with N_2 , Ar, He and H_2 respectively producing progressively less reduction in current. A memory effect depending on the ambient gas was also exhibited. If current was reduced by introducing a gas into the test system and the system was then re-evacuated the lower current characteristic persisted. The original characteristic could only be restored by applying a voltage in excess of 4 V to the device under vacuum conditions. They explained these variations in terms of the variation of a positive space-charge distribution, as a result of interactions of the gas molecules with the Al electrode. The extremely large effect shown when O_2 was used corresponds to almost complete neutralisation of the positive charge by the O_2 molecules.

(21) (Tronc⁶² observed the behaviour of devices using an insulating layer of SiO_2 doped with B. The top electrode used was Ag while the bottom

contact electrode was Ta. He found that for low voltages the device behaved as an insulator but that at lower voltages with the Ag electrode positive the device showed ohmic conductivity. Insulating behaviour could be re-established by reversing the polarity of the applied voltage.)

Sutherland et al⁶³ suggested that the ohmic characteristic observed by Tronc was merely a consequence of the low bias applied. Furthermore the lack of negative resistance and differences from the normal formed characteristic could be explained by the use of Ag instead of Au counter electrodes. Al-SiO_x-Ag devices prepared by Sutherland et al sometimes showed an ohmic characteristic at low voltage and the negative resistance phenomena were unstable compared to those obtained using Au electrodes. Al-ZnS-Ag devices also showed VCNR, some of which were already formed and did not need to undergo the normal voltage forming process. A noisy higher voltage characteristic was ascribed to the existence of filaments of larger diameter (due to a faster Ag diffusion rate) which would not rupture as easily as those in Au devices. The noisy behaviour was attributed to normal rupture and re-joining of small diameter filaments.

② [A pressure dependent switching effect was reported by Emmer⁶⁴ in Al-Al₂O₃-Au structures. The devices were formed at a pressure of 10⁻² torr. When an AC voltage of value V_m was applied the usual AC characteristic was exhibited. If the pressure was slowly increased to atmospheric pressure the device switched into a very high impedance state at approximately 1 torr, the conductivity then being of the same order as that in an un-formed device. For AC voltages less than V_m the devices switched into an intermediate high impedance state which was stable until the bias was increased to V_m. Further switching of the device then took place into the very high impedance state.

Re-forming of the sample at reduced pressure restored the normal device characteristic. A similar effect was also detected in the DC characteristic. It was proposed that the decrease in current was caused by the adsorption of oxygen atoms on states located on the walls of conducting filaments.]

In an extensive review of conduction in amorphous oxides by Dearnaley et al⁹, it was pointed out that the forming effect could be a source of leakage current in devices such as MOS capacitors and transistors where a high dielectric strength is required. Worthing⁶⁵ had revealed a polarity dependent breakdown effect in capacitors of Au-SiO₂-Si. With the Au electrode positive, breakdown tests showed a breakdown voltage dependent on the previous device history. Dearnaley et al suggested that a small degree of forming may occur in the SiO₂ films, probably in localised regions where the oxide departed from the SiO₂ compound. Thus the consequences of forming in devices where this effect may be troublesome must be considered.)

Hrach and May⁶⁶ measured the angular distribution of emitted electrons from Al-Al₂O₃-Au devices as a function of voltage in the temperature range 80-300 K. A hemispherical anode divided into five parts was employed. The angular distribution exhibited two features, an isotropic background and a central maximum in the forward direction. With increasing voltage the central maximum decreased and the isotropic part of the distribution became increasingly pronounced, in agreement with the results of Thevenard et al⁵⁵. At low temperatures the central maximum was the predominant feature, the isotropic background only appearing at higher temperatures. The non-appearance of the isotropic background at low temperatures was ascribed to the increase in mean free path for electron-phonon interactions, low temperatures thus drastically reducing the level of elastic scattering.

Frank^{67,68} considered the conduction process in Al-Al₂O₃-Au or Al devices to take place through an impurity band caused by the presence of Al ions in the Al₂O₃. These ions were assumed to occur during the Al oxydisation process and then to diffuse into the oxide from the electrodes. VCNR was argued to be the result of two processes, one increasing the current (increased number of carriers at higher voltages due to the increased probability of injection through the cathode potential barrier) and one decreasing the current (low mobility due to a reduction in the number of unoccupied states because of the increased number of carriers). The resultant of these two processes was an increasing current with voltage, which fell in the negative resistance region due to the lower carrier mobility in this voltage range.

Structural work was performed on SiO films by Cachard et al⁶⁹. Infrared spectrophotometry was employed as well as energy analysis of emitted protons from a target bombarded with deuterons. Earlier work by Cachard et al⁷⁰ had shown that VCNR only occurred in films prepared by resistive heating. Films produced by electron bombardment did not exhibit negative resistivity. Analysis of films prepared by the two methods showed a difference in the structural features. Films prepared by electron bombardment were a stable pseudophase of SiO, while resistively prepared SiO was a mixture of an SiO₂ phase and SiO and Si₂O₃ pseudophases. The VCNR was ascribed to the appearance of the Si₂O₃ pseudophase. Further absorption and dielectric loss measurements⁷¹ led them to propose that conducting filaments of Si₂O₃ short-circuited the insulator and gave rise to VCNR.

Bernard et al⁷² showed that the behaviour of Al-Al₂O₃-Au devices could be radically changed by exposing them to high temperatures under ultra-high vacuum conditions for a period of approximately 4 hours. Diodes which had been taken to a temperature not exceeding 150°C showed

increased conductivity for the first characteristic, with subsequent traces reverting to the lower conductivity. Devices for which the temperature had exceeded 150°C also exhibited VCNR with increased conductivity for the first trace, but the conductivity of subsequent traces was lower than for devices which had not undergone heat treatment. When the temperature had exceeded 200°C all traces, except the first, were of lower conductivity and failed to show VCNR. VCNR was gradually restored, however, over a waiting period of 10-20 hours. They related these results to an increase in the dead-time between cycles. The dead-time is normally of the order of 1 ms^{31} , and an increase to several hours is an effect of some magnitude. They suggested that a step in the restoration of higher conductivity was the passage of electrons from traps to "liberation states" in a time corresponding to the dead-time. Exposing the devices to high temperatures could cause an increase in the activation energy for this process, with a corresponding increase in the dead-time.

(2) (Sutherland⁷³ extended the work to semiconducting films of Au-ZnS-Au. The normal DC I_c-V_b characteristics were observed with occasional secondary maxima at voltages in excess of V_m . In contrast with previous work it was found possible to increase the value of V_m by holding the voltage in the region of the original current minimum (V_u) for a period of several minutes. The value of V_m increased to values somewhat in excess of twice its original value. Similar shifts of V_m were also detected in the AC characteristic and in one case an original value of 4 V increased to 25 V. The variability of V_m coupled with the high values sometimes observed led Sutherland to reject theories based on a band structure model. Instead, a modification to the filamentary theory of Dearnaley was presented, in which a change in the distribution of filaments was considered. This implied the permanent destruction of

highly conducting filaments and the establishment of extra centres in the remaining filaments which reduced the value of the average spacing between centres. This model was sufficient to explain all the observed phenomena of ZnS devices reported at that time.)

(Collins and Gould⁷⁴ were able to form Au-SiO-Au devices of thickness up to 6400 Å in contrast to the results of Simmons et al¹⁷ where forming was restricted to oxide layers of less than 3000 Å. The electroforming properties of the virgin devices were found to be in agreement with the previous observations of Simmons et al. The I_c - V_b plots showed the usual peak at 3 V followed by a negative resistance region and a second peak at 16 V which was not evident in previous work. This peak was voltage and not field dependent, remaining at 16 V for a wide range of insulator thicknesses. It was suggested that the gradual fall of I_c after the second peak was the result of a more permanent mechanism than that responsible for the first peak. It was proposed that normal dielectric breakdown, which causes destruction of regions of diameter up to 100 μm ⁷⁵ and thus reduces the effective device area, was the mechanism responsible. Emission current measurements also revealed a secondary maximum at 16 V which was clearly dependent on the same process.)

Electron attenuation length measurements gave a value of the Au attenuation length (λ_{Au}) of approximately 1000 Å for V_b in the range 3-9 V, which then rose roughly linearly with V_b to 3000 Å at 20 V. The divergence of these measurements from the predictions of Quinn⁷⁶ and Motozuki and Sparks⁷⁷ was attributed to prior scattering in the oxide layer. Other attenuation length measurements available at that time showed a similar divergence from theory^{33,57,78}. Variations of K with V_b (see equation 1.9) deduced from transmission ratio measurements showed a point of inflexion at 6-8 V, indicating that a similar effect

apparent in emission current curves is a property of the oxide and not of the top Au layer. Retarding potential measurements showed evidence of electrons emitted with no energy loss, and also the emission of electrons with energy less than the Au work-function. It was estimated that the electrons could obtain energy of between 2.9 and 4.1 eV from the lattice, which would be sufficient to allow excitation over the work-function barrier.

(Collins et al⁷⁹ studied the forming properties of certain fluorides at atmospheric pressure. They found that CaF_2 , LiF and LaF_2 would all form when using Cu or Ag counter electrodes, but that only CaF_2 would form with an Au counter electrode. Devices formed under vacuum often un-formed when the pressure was raised, but sometimes these could be re-formed at atmospheric pressure by the application of a higher bias. Thus both the electrode materials and atmospheric environment were clearly of importance in the forming process of fluoride devices.)

Measurements by Doucas and Walsh⁸⁰ showed that forming was also exhibited in four layer structures of M-CdS-I-M. The bottom metal electrode was Al while the counter electrode was either Al or Au; no difference in device properties was apparent between devices using different counter electrode metals. Typically the CdS was of thickness 10,000 Å while the insulator (SiO_x or MgF_2) was approximately 2000 Å. Room temperature measurements showed an increase in I_c with V_b up to 10 V, followed by current saturation and the negative resistance region. At liquid nitrogen temperatures a power law dependence was observed with $I_c \propto V_b^n$. The value of n changed discontinuously at a value of voltage slightly in excess of that at which negative resistance occurred in the room temperature curve. Typically the change was from $2 < n < 3$ to $3 < n < 5$. The variation of I_e showed a $\log I_e / V_b^2$ versus $1/V_b$ dependence, indicative of a field emission mechanism. Photographs of

the spatial distribution of emitted electrons showed a marked non-uniformity; no correlation was drawn, however, between the arcs observed and scattering processes in the metal electrode. There was no significant difference in the frequency response of the AC conductivity between M-CdS-I-M and M-I-CdS-M devices, although the conductivity of simple M-CdS-M devices was substantially higher (about 2 orders of magnitude) as expected. A polyfilamentary conduction model was assumed and it was suggested that the filament density was much higher in the CdS than in the insulating layer. Thus higher conductivity in M-CdS-M structures was explained, as was the importance of the insulating layer. High current in the CdS layer caused thermal breakdown to occur before localised filamentary rupture. The insulating layer serves the purpose of providing a region where this can take place.

Commenting on the results of Doucas and Walsh, Collins⁸¹ suggested that preferential deposition of Cd atoms may well have given rise to a Cd rich layer of CdS which would have exhibited metallic conduction properties. Apparent forming in the four layer devices would therefore merely be the result of forming in the insulator. The similarity of the results of Doucas and Walsh with those for simple SiO_x devices was pointed out, as was the peculiar behaviour observed by Collins for CdS devices. This included the time dependence of the voltage for voltage maximum which had also been observed previously by Sutherland⁷³ in ZnS devices. Doucas and Walsh⁸² did not accept that metallic conduction properties were shown by the CdS. They stressed that samples which are deposited at temperatures greater than 100°C show a decrease in the number of excess Cd atoms, leading to an increase in the resistivity of the film. Furthermore, in M-I-CdS(10,000 Å)-M devices the probability of hot electron emission through the CdS layer (as required by Collins)

would be very low, and would not be in agreement with experimental results.

(25) (Collins et al⁷⁸ investigated the effects of replacing the Au electrode by Ag to produce Al-SiO_x-Ag cathodes. Certain differences were observed, clearly dependent on the nature of the counter electrode. V_F was much more variable than in the case of devices using Au, varying in the range 3-12 V. In contrast with previous results on Al-SiO_x-Au devices, forming was also possible with the Al electrode positively biased. I_c-V_b curves showed VCNR characteristics which were symmetrical about the origin. The devices appeared to behave in an essentially symmetrical way with respect to the metal contacts and it appeared that forming by the migration of Ag ions under forward bias was unlikely. Spontaneous switching between impedance states at voltages between 10 and 20 V was also characteristic of this configuration. Electron emission was more spatially uniform than in Au devices, the circular arcs indicative of coherent scattering being absent. However, emission did appear to arise at certain localised areas of the device and transmission ratios were typically lower than in corresponding Au devices.)

Attenuation lengths measured in Ag gave a value of λ_{Ag} varying from 150 Å at 9 V to 450 Å at 20 V. The results varied in a similar way to those previously measured by the same technique in Au^{33,57,74}, but did not show the theoretical E^{-2} energy dependence predicted by Quinn⁷⁶. It was considered that the discrepancy was probably due to structural features of the sandwich, in particular preferential electron emission through locally thin areas and localised emission from breakdown craters and the surrounding material. Because of these inhomogenities it was thought unlikely that a correlation could be obtained between the attenuation lengths measured by this technique

and those measured by other means.

Dittmer⁸³ investigated the behaviour of Al-Al₂O₃-Au devices consisting of a complicated layer structure of thermal and anodic oxide layers. The structure consisted of a series of holes of diameter 50-200 μm etched through a sandwich structure of Al(1000 Å)-KTR photo-resist or sputtered SiO₂(10,000 Å)-Al(1000 Å). The exposed base Al layer was thermally oxidised to give a dense Al₂O₃ layer of 20-150 Å thickness. Anodic oxidisation then produced a porous Al₂O₃ layer, which was referred to as Al₂O₃[']. The upper Au electrode was evaporated over the entire surface and in the region of the holes was deposited as a discontinuous layer. The entire structure then consisted of an array of Al-thermal Al₂O₃-porous anodic Al₂O₃[']-discontinuous Au, connected in parallel and imbedded in a matrix of highly resistive material. Devices grown using different anodising current densities showed different characteristics. Anodising current densities of 1 mA cm⁻² produced a fairly high density anodic layer, and an exponential dependence of I_c on V_b was shown for V_b > 9 V. Further traces of the I_c-V_b characteristic showed increasingly higher current densities. The value of I_c was greatly reduced by altering the polarity and making the Al electrode positive. The lifetime of such cathodes was only a few minutes, probably as a result of Au ion diffusion. Conversely devices prepared using 20 mA cm⁻² anodising current showed a forming effect and VCNR, there being no apparent difference in the formed characteristic for devices of opposite polarity. At low voltages the conductivity was increased by raising the temperature, changing approximately 3 orders of magnitude between 77 and 500 K; at higher voltages the temperature dependence was not very strong. VCNR was still apparent at 77 K although it is not clear whether this behaviour disappeared with repeated traces of the low temperature I_c-V_b characteristic. Devices exposed to the atmosphere gave reduced current levels and did not

exhibit VCNR. Negative resistance regions were evident when the thermally oxidised layer was of thickness 25 Å. Increasing this thickness to 50 Å made the negative resistance region extremely pronounced, although using thicker thermally oxidised layers of 75 and 150 Å destroyed the VCNR behaviour. Varying the thickness of the anodic layer between 150 and 600 Å did not substantially change the characteristics. Retarding potential measurements elicited the existence of three different energy ranges of emitted electrons. These could be related to the excitation of electrons by photons of 2.3 and 4.2 eV as well as to electrons not involved in photon interactions.

Dittmer suggested that Al ions, introduced as a result of the anodising procedure, would produce a narrow positive space-charge region near the cathode. The diffusion of Au ions from the counter electrode along grain boundaries would result in the growth of precipitates of Au in the form of field emitting needles. At voltages less than 3.5 V electrons are emitted through a thermal Al_2O_3 layer into an Al impurity band in the anodic Al_2O_3 layer. At higher voltages the impurity band becomes saturated and the Au precipitations (at an energy equivalent to the Al_2O_3 Fermi level) are raised up into the impurity band. The main voltage drop then occurs at the positive Au electrode and the current through the anodic layer is carried by tunnelling between the Au precipitations. Field emission from these points in the high field region greatly enhances the electron emission. This type of elaborate band structure could explain most of the features of this specific type of device which used a series of thermal and anodic layers. Its application to a wider range of structures, in particular single evaporated insulating layers, is questionable and was not proposed by the author.

In order to ascertain the role of impurities on the forming effect Hickmott⁸⁴ produced Al-Al₂O₃-M diodes taking special care to obtain a "clean" anodised layer. This was accomplished by anodising in an ammonium borate-ethylene glycol solution. Results of forming voltage measurements on these devices was compared with those previously obtained³⁰ for "dirty" Al₂O₃ layers produced by anodising in NH₄HSO₄-KHSO₄ eutectic. Al, Mg, Pb and Sn counter electrodes would not induce forming in the "clean" Al₂O₃ of either polarity, destructive dielectric breakdown normally taking place. For Ag and Au VCNR could be induced with the counter electrode positive (occurring at 8 V for Ag and 14 V for Au), but was not possible with the Al layer positive. V_F was not constant and appeared to be field dependent. In contrast, the previous measurements³⁰ on "dirty" oxides had shown that the forming voltage was practically independent of thickness and of counter electrode material. Forming had also been observed with the Al electrode positive although the value of V_F had been somewhat variable. Reducing the impurity content in the Al₂O₃ thus made it impossible to form devices with the Al base electrode positive, and decreased the number of counter electrode materials which were easily formable with the counter electrode positive. Forming voltages were increased and were dependent on the counter electrode material; forming appeared to be field dependent in the "clean" oxides.

Electroluminescence measurements on Al-Al₂O₃-Au diodes revealed peaks at energies of 1.6-1.8, 2.3 and 3.5 eV. Retarding potential measurements indicated a value of excess energy obtained in the insulator to vary between 3.1 and 4.2 eV. It was suggested that this effect took place at the Al-Al₂O₃ interface, although the precise nature of the process remained unknown.

The low voltage dependence ($V_b < 0.6$ V) was virtually unchanged over a temperature range from 2 K to room temperature. Thermal activation of carriers from the metal into the insulator in formed devices was thus considered unlikely.

(Gundlach and Kadlec¹⁶ observed forming and VCNR in organic monomolecular layers. The particular substance investigated was cadmium arachidate, and it was possible to deposit this as a series of layers of thickness 26 Å. Monomolecular layers of arachidic acid were spread on the surface of water containing Cd ions. When the substrate was dipped into the solution for the first time, one monolayer of cadmium arachidate was deposited; this monolayer remained when the substrate was removed from the solution. Subsequently a monolayer was deposited each time the substrate was immersed with a further monolayer deposited when the substrate was removed. Forming was only possible when the counter electrode of Al or Au was positively biased, and the forming voltage V_F was 5-6 V. VCNR was only observed in the temperature range 110-225 K. At higher temperatures there was an increase in conductivity but VCNR behaviour disappeared completely. On repeated voltage cycling the current maximum shifted towards lower voltages and after a number of cycles VCNR disappeared. The peak-to-valley ratio in the $I_c - V_b$ characteristic increased with the number of monolayers in the cadmium arachidate layer, from 1.45 for 7 monolayers to 4.2 for 11 monolayers. Sandwiches with less than 5 monolayers did not show VCNR.

It was proposed that injection of metal ions could be easier in these devices where the monomolecular layers consisted of long chains perpendicular to the plane of the film, because the binding force between such chains is weak. This might, therefore, be the reason why monomolecular layer sandwiches could be formed at low temperatures.

The disappearance of VCNR after a few voltage cycles of the device was ascribed to dead-time effects which had previously been observed in amorphous insulating films; this effect would be more pronounced at low temperatures. In view of the fact that forming and VCNR behaviour have been detected in so many different types of insulator it was thought that specific energy band models were unlikely to apply.)

(A new filamentary model was proposed by Ralph and Woodcock⁵. This involved associating a band structure to each filament, which switched on and off as a result of bias conditions. The effects of band tailing of the conduction and valance bands and of an impurity band, formed an intrinsic part of this theory (see 1.5.6). Work by Woodcock and Ralph⁸⁵ on electroluminescence from M-I-M (Au-SiO_x-Au) and M-I-S (Au-SiO_x-GaAs) structures showed light emission for both polarities and both configurations. The total intensity of light emission in both types of device fell rapidly when voltages greater than V_m were applied. M-I-S devices showed a spectral distribution directly comparable to photoluminescence spectra of GaAs, indicating that the electroluminescence originated in the GaAs. M-I-M spectra showed higher light intensities at lower energies (1.2 eV) with much reduced levels at higher energy (3.0 eV). This type of spectrum was associated with recombination in the forbidden gap of formed SiO_x filamentary regions of the type described above.)

(Hogarth and Taheri⁸⁶ measured I_c - V_b characteristics of Al-SiO_x/B₂O₃-Al co-evaporated films of thickness 3000-6000 Å. This was an extension to the previous work of Timson and Hogarth⁸⁷ on thicker co-evaporated films (approximately 1 μm) who had found a power law dependence of current on voltage thus

$$I_c \propto V_b^n \quad (1.11)$$

where n was of the order of 4-6. As expected the current density of the thinner films was higher than that in the thicker films. More important, however, were the effects observed in some $\text{SiO}_x(70\%)/\text{B}_2\text{O}_3(30\%)$ films. A decrease in current above the current peak was apparent, and the current continued to fall or oscillate until breakdown occurred. It was suggested that in these films a filamentary forming process occurred; this was not apparent in the thicker films described by Timson and Hogarth where the internal field was not high enough to induce filament growth.)

(Sutherland et al⁸⁸ investigated forming phenomena in Al-ZnS or CdS-Ag or Au devices. Al-ZnS-Au and Al-ZnS-Ag formed at 2.5 and 2 V respectively. Al-ZnS-Au devices showed the normal VCNR behaviour and also the time dependent variation of V_m previously observed in Au-ZnS-Au structures⁷³. Al-ZnS-Ag devices showed characteristics markedly different from normal VCNR behaviour if the evaporation pressure was greater than 10^{-6} torr. The characteristics were very similar to those observed by Hiatt and Hickmott¹⁵ for Nb-Nb₂O₅-In diodes which showed CCNR. There was a slight negative resistance, the peak-to-valley ratio being little greater than 1. Large increases in current after the valley region were also observed. The value of the threshold voltage V_T in this case was greater than V_m , in contrast to the case with SiO_x devices. Switching into a high impedance state was possible by applying a reverse bias of value equal to V_F . Conversely Al-ZnS-Ag structures evaporated at less than 10^{-6} torr initially showed the above characteristics, but this gave way to bipolar VCNR characteristics, closely akin to those observed in oxides.

Al-CdS-Au or Ag devices showed a two stage forming process, where initially the current followed a low resistance ohmic characteristic. Finally this gave way to a bipolar VCNR characteristic. In common with

ZnS devices, V_m was time dependent.

Electron emission was detected from Al-ZnS or CdS-Au devices but was not observed with Al-ZnS-Ag. Some structure was observed in the emission patterns, but was not as well defined as patterns observed in Au-SiO_x-Au devices by Gould and Collins⁵⁸.)

In common with the previous results of Hickmott⁸⁴ these results showed that impurity content (determined by evaporation pressure) and also electrode material were very important in determining device properties.

Sutherland⁸⁹ proposed a scheme of classifying materials which would undergo forming. Greene⁴⁷ had suggested that forming of local regions may be due to a form of solid state electrolysis. Because this is a phenomenon which occurs in ionic crystals, it was argued that the amount of ionic character for a given material would give a good indication of its likelihood of forming. An equation for the amount of ionic character of a single bond between atoms A and B, with electronegativities X_A and X_B was given by Pauling⁹⁰ thus

$$\text{Amount of ionic character} = 1 - e^{-\frac{1}{4}(X_A - X_B)} \quad (1.12)$$

Sutherland showed that with the exception of sulphides all formable materials had an ionic content of greater than 50%. It was thought that in formed sulphides, which appeared to be an exception to this rule, forming was initiated by a somewhat different process. This was probably diffusion of the electrode into the insulator as a result of the heat dissipated at the start of the two stage forming process.

Gundlach and Kadlec⁹¹ extended their work on cadmium arachidate to include triode structures using Al electrodes. The voltage drop between the cathode and centre electrode (grid) was referred to as V_{gc}

and that between the grid and counter electrode (plate) as V_{pg} . At 77 K negative resistance was observed and the voltage divided over the two regions in an ohmic fashion; this type of behaviour had been observed by Hickmott³² for SiO layers during the initial stages of forming. At higher temperatures the voltage began to divide in an essentially non-symmetric way, with a high voltage drop in one region and ohmic behaviour in the other. The probability of the high field region appearing in the plate-grid or in the grid-cathode region was approximately equal. This was in contrast to Hickmott's results, where the voltage drop was usually in the cathode-grid region. After a sufficient number of cycles the high field region became firmly established and subsequently no change could be induced in the potential distribution by changing polarities. A tentative explanation of some of these effects was given. It was suggested that current carrying filaments initially did not contact the grid structure, passing through pinholes from cathode to plate; the potential distribution was not then affected by the grid. At higher temperatures and voltages conductivity to the grid was developed in (say) the plate-grid region. Thus the conduction in this region was ohmic along the filaments, and the device behaviour was determined in the high field region between the cathode and grid.

Cachard et al⁹² reviewed their previous work on the structure of SiO_x in formed devices, especially the differences shown between films produced by resistive heating and by electron beam evaporation. In addition they extended their structural work to Al_2O_3 using deuteron radiation and infrared absorption techniques. They concluded that excess oxygen in Al_2O_3 films led to VCNR effects in this material.

Eckertova and Bocek⁹³ made careful measurements of the transmission coefficient α in Al- Al_2O_3 -Au sandwiches. A normal exponential

variation of α with thickness of Au was obtained yielding values of λ_{Au} varying from 75 Å at 3 V to 187 Å at 6.5 V. However the variation of α_0 (transmission coefficient calculated for zero Au thickness) did not show the normal exponential behaviour demanded by theory for trap interactions^{46(c)}. It was argued that this indicated a non-linear variation of the field in the insulator, most probably due to a high field region near the cathode. Strong variations of α_0 with oxide thickness for constant values of the average field, supported this view.

• (In an effort to improve the conduction and emission properties of borosilicate devices of the type investigated by Taheri et al⁹⁴ and described in section 3.5.1, Hogarth and Bidadi⁹⁵ replaced the Al electrodes with higher conductivity Ag. The device structure was Ag-SiO_x (70%)/B₂O₃ (30%)-Ag with the Ag and SiO_x/B₂O₃ layers of thickness 400-500 Å and 1600 Å respectively. As expected both I_c and I_e were considerably higher than in devices using Al electrodes. The emission current density was then of the order of 10^{-4} A cm⁻² compared with 10^{-5} A cm⁻² using Al electrodes.)

Hrach⁹⁶ measured the variation of the energy distribution of emitted electrons with the angle θ at which they were emitted. θ was measured from the normal to the plane of the film. The energy distribution showed the normal peak at an energy less than V_b and the maximum of the distribution shifted from low energies in the forward direction ($\theta = 0^\circ$), to a higher value almost in the plane of the film ($\theta = 80^\circ$). The width of the distribution also increased with θ . At 80 K similar behaviour was observed but the width of the distribution decreased with higher θ . Hrach concluded that the higher energy electrons which were emitted at $\theta > 40^\circ$ were the result of scattering by optical phonons. The low energy electrons which comprised the central maximum

were the result of electronic excitation from traps. Further evidence of two separate emitted energy distributions was provided by the behaviour of the energy distribution maximum with V_b . This increased with V_b from 1.6 V at $V_b = 8$ V to 5.8 V at $V_b = 13$ V for $\theta = 60^\circ$, but over the same range of V_b it only increased from 0.8 to 1.2 V for $\theta = 0^\circ$.

• Recently Morgan et al⁹⁷ have compared electroforming and dielectric breakdown in Al-Al₂O₃ (500 Å)-Au films. Using a pulsed bias in the range at which breakdown was expected (26 V) they observed the voltage over the device to rise, then discontinuously fall and finally to rise again over a time period of 80 μs. They ascribed this to self-healing breakdown of the type described by Klein⁹⁸. The discontinuous fall in voltage corresponds to destruction of an area of the device; this then isolates itself from the remaining device area and the voltage increases once more. Subsequently devices did not show DC conduction. In contrast to this normal type of breakdown another effect was observed in the voltage range 2-10 V. Here a similar discontinuous fall in voltage occurred, but was not followed by recharging of the device; instead a constant voltage level remained indicating that a conducting path through the insulator had been established. Subsequent DC voltage tests showed a new conducting state. They suggested that forming is the result of a localised avalanche initiated by field emission of charge carriers at a defect, where an extremely high field exists.

1.5 Models of the Forming Process and Conduction Phenomena in Formed Materials

1.5.1 Hickmott

This model of functioning of M-I-M devices assumes that there are present in the un-formed insulator an appreciable number of neutral impurity centres of energy E_I , situated approximately at the centre of

the band gap. A high field region exists in the insulator which dominates the conduction process; this is normally near the cathode but can exist in any region of the insulator³². A diagrammatic representation of the centres in the high field region is shown in figure 2a for an Al-SiO-Au device. E_C and E_V are the conduction and valence band edges and E_F is the Fermi level. ψ_{Au} is the Au work-function. The quantity and types of centres are dependent on the conditions of preparation, but it is suggested that foreign atoms and structural faults in the insulator are probable. On applying a DC voltage across the device Schottky emission takes place from both the cathode and the impurity centres. When the voltage is increased to a sufficient value there are enough ionised centres to form an impurity band in the insulator which can greatly assist subsequent conduction processes through the insulator. Thus conductivity of the structure is determined by these positive impurity centres. Ionisation of the centres is followed by modifications occurring to the metal-insulator interface such that electrons can easily be injected into the insulator without thermal activation. The charge carriers are low mobility injected electrons which hop from one centre to another as indicated by (1) in figure 2b. Conduction in the low field regions of the insulator is also by this process.

The above process, while indicating how conduction can take place at voltages below V_m , cannot explain the phenomena of negative resistance, electron emission and electroluminescence. In order to accommodate these effects Hickmott postulates an immobile hole level at energy E_H , between the impurity band and the valence band. As the voltage is increased the hole levels are filled by electrons tunnelling from the valence band or excited by impact ionisation, (2). A mobile hole is left behind in the valence band which is accelerated towards the cathode under the

influence of the high field, (3). The hole is neutralised by an electron from the impurity levels (4), which in turn imparts its recombination energy to another electron trapped in an impurity state. This electron is then excited into the conduction band of the insulator (5), where it is accelerated in the high field towards the anode, (6). At sufficient voltages electrons can also tunnel directly from the impurity band to the conduction band, where they too will be accelerated towards the anode. Electrons with sufficient energy to overcome the Au work-function may be emitted from the device while others can be captured by the impurity band (7), with the consequent emission of light. Radiative transitions between the valence band, hole levels and impurity levels can also contribute to the observed electro-luminescence.

The decrease in current after the voltage maximum at 2.8 V is caused by neutralisation of impurity sites by electrons tunnelling from the hole levels under the influence of the high electric field, (8). Since neutralisation is an exponential function of voltage, when the voltage is increased beyond V_m the number of impurity centres that are ionised and capable of conduction decreases rapidly, and the current level decreases. Thus the current is limited by a fall in the number of ionised impurity levels in the high-field region.

1.5.2 Simmons, Verderber and Eales

When an insulator is brought into contact with a metal electrode there is in general a flow of charge from one layer to the other in order that thermal equilibrium requirements be satisfied. Effectively this means that the vacuum and Fermi levels of the two layers must be continuous. The direction of charge flow depends only on the relative work-functions of the metal and the insulator, ψ_m and ψ_i . Usually

insulator work-functions are not defined; here we can take $\psi_i = \chi_i + \phi_b$ where χ_i is the insulator electron affinity and ϕ_b is the height of the bottom of the insulator conduction band above the Fermi level in the un-formed device, known as the bulk activation energy. In the example considered by Verderber et al¹⁷ (Al-SiO-Au) these parameters were approximately $\psi_m = 4$ eV, $\chi_i = 1$ eV and $\phi_b = 0.4$ eV. Thus $\psi_m > \chi_i + \phi_b$ and electrons flow from the insulator to the metal. A depletion region of positive charge is created in the insulator and an equal negative charge on the metal electrode. As a result of these two charge accumulations a local field exists within the surface of the insulator. This causes the bottom of the insulator conduction band in the centre of the insulator to bend downwards until it lies at an energy ϕ_b above the Fermi level. Thus the band structure for a zero bias Al-SiO-Au device, with approximate numerical values of parameters as given above, will resemble that shown in figure 3a. Barrier heights at both interfaces have been taken as equal and from figure 3a can be seen to be

$$\phi_o = \psi_m - \chi_i \quad (1.13)$$

which is approximately 3 eV in this case.

Ionisable centres are assumed to exist in the SiO probably due to the presence of free silicon. It is therefore possible to form a depletion region in the SiO. The field at the metal-insulator interface is

$$F = \left(\frac{n_d e^2}{2\epsilon\epsilon_0} \right) (\phi_o - \phi_b - V_d)^{\frac{1}{2}} \quad (1.14)$$

where V_d is the voltage drop across the depletion region, n_d is the

donor density, ϵ the dielectric constant, ϵ_0 the permittivity of free space and e the electronic charge.

For an applied voltage $V_b < V_F$ across the device the energy diagram of the un-formed sample is shown in figure 3b. At the negatively biased electrode the field at the interface and width of the depletion region are increased; at the positive electrode the reverse is the case. Ions are not yet able to migrate from the anode into the insulator because a reduced positive field still exists at the anode and inhibits migration.

When V_b is increased to values exceeding V_F the field at the anode interface falls to zero as indicated in figure 3c. There is now no retarding field to inhibit injection and positive ions are free to enter and migrate through the insulator. From equation (1.14) the field at the interface falls to zero when

$$V_d = \phi_o - \phi_b \quad (1.15)$$

Assuming that a similar voltage is dropped across the depletion region at the negative electrode the forming voltage is given by

$$V_F = 2V_d = 2 (\phi_o - \phi_b) \quad (1.16)$$

ϕ_o and ϕ_b are constants independent of oxide thickness and evaporating conditions, thus revealing why V_F is not affected by variations in evaporating procedure. Furthermore, the value of V_F calculated from equation (1.16) and using $\phi_o = 3$ eV and $\phi_b = 0.4$ eV is 5.2 V which is in excellent agreement with experimental observations.

The Au ions injected into the insulator act as donor centres, but not in one discrete energy level². The reasons are twofold. Firstly,

in an amorphous material there is no consistency of nearest neighbour distances and no recognisable lattice exists. Consequently the Au ions are not restricted to predetermined lattice positions, with the result that their potential energies are not well defined. Secondly, filling of traps present in the insulator up to the Fermi level gives a net negative charge. A coulombic interaction between the negative traps and positive donors perturbs the potential energy of the donor centres. The result of these two effects is to create a band of localised states within the energy gap of the insulator (figure 4a). ψ_m is the metal work-function, ϕ_0 the metal-insulator barrier height and ψ_I and ϕ_i the energies of the bottom of the conduction band and the top of the localised levels in the formed sample. All energies are measured from the Fermi level.

When a voltage less than ϕ_i is applied, an electron at the Fermi level can pass straight through the band of allowed states to the other electrode by a tunnel hopping process (figure 4b). If a voltage greater than ϕ_i is applied electrons at the Fermi level can only tunnel as far as the top of the allowed band and cannot contribute to the conduction process (figure 4c). They are, however, stored in local levels near the top of the allowed band. Electrons with an energy greater than $V_b - \phi_i$ below the Fermi level can still contribute to conduction, but since the contribution to current of injected electrons falls off rapidly with energy below the Fermi level the current through the device decreases. Thus the maximum current always occurs when $V_b = \phi_i$ and is independent of the thickness of the insulator in accordance with experiment. When voltages are sufficiently large, electrons injected at the Fermi level of the metal can find a path into the conduction band of the insulator. Thermal excitation (AC in figure 4c) and tunnelling through the gap between the top of the allowed states and the conduction

band (AB) become possible. It is suggested that these processes are responsible for the rising tail in the $I_c - V_b$ characteristic at voltages greater than 8 V.

The memory phenomenon is also explained on the stored charge hypothesis. As previously mentioned when a bias $V_b > \phi_i$ is applied to a device electrons with energies between E_F and $E_F - (V_b - \phi_i)$ cannot contribute to the conduction process and are stored near the top of the band of allowed states. In general when the voltage is removed slowly, the stored charge can leak out via the anode and the device remains in its original state. If the voltage is removed very quickly the electrons will remain in the states in which they are stored. After a time the electrons will diffuse through the insulator by tunnelling towards the centre of the insulator in the direction of lowered potential barriers. At the centre of the insulator, potential barriers rise on both sides so the charge remains in this position. Energetically, the stored charge is still near the top of the allowed band. Electrons do not drop down below the Fermi level or to another lower energy level because the probability of this happening is less than that for simple oscillation of the electrons between two states of equal energy. The stored charge within the insulator reduces the field at the metal-insulator interfaces. On substituting the reduced field into the theoretical $I_c - V_b$ equation (equation 5 of reference 2) it is evident that for $V_b < \phi_i$ the circulating current is reduced. Moreover the higher the voltage at which the current is rapidly reduced to zero, the higher the charge stored and hence the lower the field at the interface. Thus the subsequent impedance state of the device can be predetermined by the voltage at which the memory is induced. The memory is not therefore restricted to an "on" and "off" state, but in principle gives an infinite number of analogue memory states.

Experimentally the device switches back into the low impedance state when the threshold voltage V_T is reached. This appears to be a natural consequence of the stored charge located just below the top of the band of allowed states. For $V_b < \phi_i$ the stored charge is energetically higher than the Fermi level of both the cathode and anode. Therefore the occupation probabilities of energy levels in the cathode and anode, of equal energy to those occupied by the stored electrons, are approximately equal to zero. It follows that both the cathode and anode electron densities for these levels are also zero. Thus there is no electron concentration gradient between cathode and anode to drive the stored charge through the potential barrier region at the anode, and the stored charge remains. As V_b is increased towards ϕ_i the cathode Fermi-level moves up towards the stored charge levels. Thus the occupation probability for electrons in the cathode, at a potential energy equal to that of the stored charge, approaches that of the Fermi level. Consequently the electron density in the cathode at the equivalent energy to that of the stored charge is high, while that at the anode remains approximately zero. We therefore have an electron concentration gradient existing, the stored charge is swept away to the anode and the device switches back into its low impedance state. Note that switching occurs when the band diagram is such that the stored charge lines up with the cathode Fermi level; negative resistance starts when the top of the impurity band in the bulk lines up with the cathode Fermi level. Since the stored charge is located just below the top of the allowed band, switching occurs at $V_b = V_T$ which is slightly lower than the voltage at which the onset of negative resistance occurs ($V_b = \phi_i$). Therefore switching must always occur just before the start of the negative resistance region, as is observed.

Electron emission arises when hot electrons are injected from the lower electrode into and through the top electrode. For $V_b < \phi_i$ electrons tunnel-hop through the insulator and arrive in the anode with a maximum energy ϕ_i above the Fermi level (figure 4b). Since ϕ_i is less than the electrode work-function ψ_m , no electrons can surmount the barrier and be emitted. When $V_b > \phi_i$ electrons injected at the Fermi level can only reach the point A in figure 4c. There is, however, a probability that the electron can be excited into the conduction band by obtaining energy from the lattice (AC). E_i , the energy difference between the top of the impurity band and the bottom of the conduction band, is the minimum energy necessary to excite an electron into the conduction band. Hence an electron excited into the conduction band can arrive at the anode with energy $eV_b + E_i$ above the anode Fermi level. It can then be emitted into vacuum provided

$$eV_b + E_i > \psi_m \quad (1.17)$$

Anomalous electron emission, when $eV_b < \psi_m$ is therefore allowed by this model as long as the above condition is fulfilled.

1.5.3 Greene, Bush and Rawlings

The mechanism proposed by Greene et al⁴⁷ to account for the forming process is founded on the assumption that under favourable circumstances certain solid state chemical reactions occur on the application of a high field across the insulator. It is directly analagous to the formation of colour centres in alkali halides by chemically unbalanced solid state electrolysis. The theory is developed for a hypothetical insulator MX consisting of M^+ and X^- ions, and is applicable to many different systems.

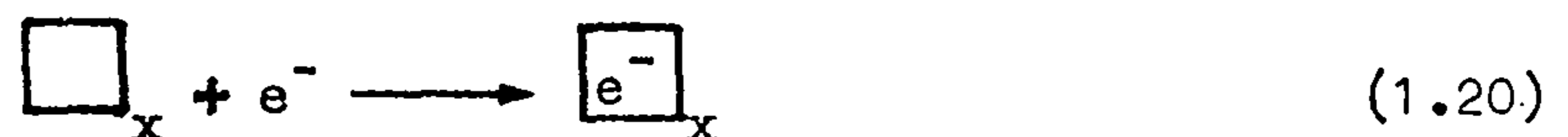
Typically the field across a thin film insulator is of the order 10^6 V cm⁻¹ and it is assumed that provided there are enough defects in the insulator solid state electrolysis will be possible. Normal low field electrolysis causes the following reactions to occur. At the anode the X⁻ anions liberate an electron with the evolution of O₂ (when the insulator is SiO). For halide devices the corresponding gas is given off. Thus



leaving behind an anion vacancy. At the cathode M⁺ cations are neutralised by the electron supply and neutral M atoms remain.



Under the high field conditions present injection of electrons into anion vacancies occurs at the cathode.



The diffusion of such vacancies towards the anode under the influence of the high electric field eventually leads to the establishment of chains of defect centres (probably of the F-centre type) which extend across the insulator from cathode to anode. It should be emphasised that throughout the lifetime of the device F-centres continually diffuse towards the anode, where they are discharged leaving behind a vacancy. Injection of electrons into vacancies at the cathode replenishes the F-centres lost at the anode. Thus the forming process is a continuous process which if inhibited, even after the establishment of defect

chains, will result in de-forming of the device. Subsequent conductivity of the formed device is dominated by tunnelling of electrons, through the chains of diffusing F-centres, towards the anode.

In an oxygen environment a further reaction can occur at the cathode.



This reaction is so probable that when oxygen is present the supply of electrons at the cathode is reduced to such an extent that reactions (1.19) and (1.20) are limited. Moreover with high oxygen concentrations reaction (1.20) is completely inhibited and continuous forming cannot occur. Thus the importance of an oxygen atmosphere on the forming process becomes apparent.

When the anode material (M_a) is chemically reactive the following reaction takes place



These positive metal ions together with negatively charged oxygen molecules from reaction (1.21) will both be absorbed into the insulator under the action of the field. We therefore have a situation where material is entering the insulator by reactions (1.21) and (1.22) and leaving by (1.18) and (1.19). If the rate of material entering exceeds the rate of material leaving the insulator, the insulator thickens, the field across it is reduced and forming via reaction (1.20) is diminished. Consequently, for optimum forming conditions an inert anode material should be employed and the ambient oxygen pressure should be kept to a

minimum.

The properties of the device after forming are explained in terms similar to those used by Simmons and Verderber², but minor modifications to the theory are necessary. Electron tunnelling takes place between allowed states in the insulator energy gap; but in this case the states are defects of the F-centre type and not injected Au ions. When the applied bias reaches a certain level electrons tunnelling from the cathode may reach the conduction band of the insulator and then be able to enter the un-formed regions of the insulator. Trapping in the un-formed regions produces a long lived space-charge. Negative resistance and memory are thought to be a consequence of this. The current falls at voltages greater than that at which trapping starts, but when the traps are filled the current starts to rise once more. Trapped charge which remains after the device has been switched off modifies the characteristic up to V_T . It can then be released by excitation out of the traps; the particular mechanism by which this is achieved is unclear but excitation by some form of energy transfer from electrons in the tunnelling path is suggested.

High noise levels in the negative resistance region are explained by a dynamic equilibrium process between the conducting paths, some switching on and some switching off in a similar way to the rupturing and re-forming of filaments in Dearnaley's model⁴³. The stepwise growth of current during switching⁴⁷ is also consistent with this idea.

Electron emission is caused by electrons in the conduction band being accelerated by the field to an energy sufficient to overcome the barrier at the anode. Further details are not discussed.

1.5.4 Barriac, Pinard and Davoine

It is first assumed that in an un-formed device there exist imperfect regions where the insulator is thinner than normal. On the application of a voltage the field in these regions approaches a critical value at which electrical arcing across the region takes place accompanied by a considerable release of heat⁴⁴. This causes local melting of the insulator resulting in the establishment of holes or cavities in the insulator. Vaporised metal atoms are adsorbed on the surface of the cavities and under the influence of the field a current of positive ions is established in the direction of the cathode. In the region of the cathode the ions create a positive space-charge which perturbs the field in such a way that the voltage is not now dropped over the whole thickness of the insulator d_0 but over an "effective thickness" $\delta \ll d_0$. δ varies with the amount of space-charge, saturating to a value Δ when a certain level is reached; δ is therefore dependent on V_b at low voltages. The effective field in the cathode region is thus V_b/δ and at some voltage after which δ has saturated to Δ the field V_b/Δ reaches a level at which tunnelling of electrons from the cathode begins. The tunnelling electrons are of relatively low energy and the majority are not able to surmount the "ionic barrier" to make an additive contribution to the total current. Instead they create electrically neutral pairs with the positive ionic charge carriers and form "pseudo-atoms". The bonding between the positive and negative carriers is of a chemical nature and is unstable in the absence of a sufficient maintaining field. The effect of this process is to diminish the ionic current by an amount equal to the tunnelling current in the cathode region. The resulting drop in I_c is the beginning of the negative resistance region. When I_c falls to very low values the space-charge is neutralised to such an extent that δ

begins to vary once more with V_b , causing an accelerated fall of I_c with V_b .

The foregoing processes are applicable in four different voltage ranges and the I_c - V_b characteristic can be divided up into four ranges corresponding to combinations of different conduction mechanisms and values of δ ^{44,49}.

In the low voltage range the conduction is purely ionic and δ is voltage dependent. The ionic current is given by a variation of equation (1.1)

$$I_{\text{ionic}} = 2 \lambda_s v n \exp\left(-\frac{U_s}{kT}\right) \exp\left(\frac{q\lambda_s F}{kT}\right) \quad (1.23)$$

where λ_s is the surface diffusion length of the ions, v the ionic vibration frequency, n and q the number and charge of ionic carriers and U_s a surface activation energy. k is Boltzmann's constant, T the absolute temperature and F the electric field. In the presence of the space-charge the effective field $F = V_b/\delta$ and so equation (1.23) becomes

$$I_{\text{ionic}} = 2 \lambda_s v n \exp\left(-\frac{U_s}{kT}\right) \exp\left(\frac{q\lambda_s V_b}{kT \delta}\right) \quad (1.24)$$

If we substitute

$$A = 2 \lambda_s v n \exp\left(-\frac{U_s}{kT}\right) \quad (1.25)$$

and

$$a' = \left(\frac{q\lambda_s}{kT}\right) \frac{1}{\delta} \quad (1.26)$$

the current in the first region is given by

$$I_1 = A \exp(a' V_b) \quad (1.27)$$

In the second range the space-charge reaches such a level that δ saturates to Δ and a' attains a constant value a , thus

$$a = \left(\frac{q\lambda_s}{kT} \right) \frac{1}{\Delta} \quad (1.28)$$

and the current is

$$I_2 = A \exp (aV_b) \quad (1.29)$$

The Fowler-Nordheim equation for the high field region is of the form

$$I_{\text{tunnel}} = \underline{B} V_b^2 \exp \left(- \frac{\beta'}{V_b} \right) \quad (1.30)$$

and is a variation of equation (1.2). The shape of the potential barrier makes only a limited contribution to the magnitude of the tunnel current and so the values of \underline{B} and β' for a rectangular barrier are given.

$$\underline{B} = S \frac{e^3}{8\pi h \phi} \frac{1}{\delta^2} \quad (1.31)$$

and

$$\beta' = \frac{8\pi \phi^{3/2} (2m)^{1/2} \delta}{3eh} \quad (1.32)$$

where S is the metal surface work-function, ϕ the metal-insulator barrier height, e and m the electronic charge and mass and h is Planck's constant. When $\delta = \Delta$ the above two equations saturate to constant values B and b thus

$$B = S \frac{e^3}{8\pi h \phi} \frac{1}{\Delta^2} \quad (1.33)$$

and
$$b = \frac{8\pi\phi^{3/2} (2m)^{1/2} \Delta}{3eh} \quad (1.34)$$

In the third voltage range the saturated value of δ still persists and the tunnel current in the high field region will be characterised by equation (1.30), replacing \underline{B} and β' by the constant values B and b from equations (1.33) and (1.34). The ionic current is given by equation (1.29) as in the second voltage range, the total current being the difference between the ionic and tunnelling currents. Hence

$$I_3 = A \exp(aV_b) - B V_b^2 \exp\left(-\frac{b}{V_b}\right) \quad (1.35)$$

In the fourth and final voltage range δ again varies because of the effective reduction of the positive ionic space-charge and the total current is the difference between the unsaturated ionic and tunnelling currents from equations (1.27) and (1.30). Thus

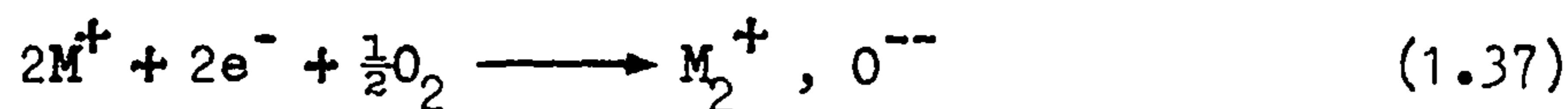
$$I_4 = A \exp(a'V_b) - \underline{B} V_b^2 \exp\left(-\frac{\beta'}{V_b}\right) \quad (1.36)$$

The magnitude of the current in any region is given by the relevant equation (1.27), (1.29), (1.35) or (1.36). The values of the constants can be obtained by graphical means. a and b are not found to vary with the type of structure and are usually in the range 0.6-1.5 and 17-25 respectively. A and B are dependent on many features, especially the nature of the oxide and counter electrode. They are also dependent on the previous history of the device and vary greatly between samples, making an estimate of the activation energy U_s impossible. Nevertheless they remain constant for the duration of one characteristic and are worthwhile parameters in describing the conduction process.

It is interesting to note that this theory predicts the value of the voltage for maximum current, V_m . Since the peak current occurs in region 3, V_m can be found from the zero of dI_3/dV_b . This is dependent on all the constants a , A , b and B and since a and A are temperature dependent the theory predicts a temperature dependent value of V_m .

In order for emission to take place the electrons must not form neutral pairs as previously described and must have sufficient energy after passing the "ionic barrier" to overcome the top electrode work-function. It is the low number of electrons satisfying the former condition which limits the emission efficiency of these devices.

Lastly, the influence of oxygen on the performance of the device becomes apparent in the light of the following reaction which occurs at high oxygen pressures.



The ions now form a stable metallic oxide in preference to neutral pairs and are thus permanently neutralised. A space-charge region is therefore not maintained in the cathode region.

1.5.5 Dearnaley, Morgan and Stoneham

This model is based essentially on the novel assumption that during forming a large number of conducting filaments are created which extend from one electrode to the other⁴³. Revesz⁹⁹ and Dearnaley⁴² have suggested that under favourable circumstances conducting chains of Si and O can be formed in films of SiO_x . Revesz considers that the channel formation is due to a correlated distribution of Si-O-Si bond angles which favours π orbital overlap along the channel¹⁰⁰. Dearnaley suggests that under the influence of an electric field

oxide films which are deficient in oxygen can undergo a process whereby conducting channels are propagated. There is a statistical chance that somewhere on the Au-SiO interface there will be ordered chains of Si and O atoms; these terminate on the Au electrode which provides good conditions for nucleation. In similar structures with free electron π orbitals electronic conduction along such a chain occurs and in the present case a similar mechanism is thought possible. A high electric field exists at the free end of the chain which exerts an anisotropic dielectric stress at its end point in the insulator. Nucleation can occur along the direction of the high field in such a way that the filament eventually propagates through the insulator to the other electrode. Formation of filaments by this process is however limited to SiO_x and other comparable structures. Since forming occurs in such a wide range of materials the forming process must be of a more general nature than that described above. The growth of chains of metal atoms alternating with anion vacancies is a possibility and gas release observed during forming supports this view.

Conduction subsequently occurs through the conducting chains. For simplicity it is assumed that conduction through each filament is ohmic and it is not necessary to introduce an energy band model. Each filament is assumed to have at least one weak spot along its length and its effective resistance is taken to be determined by this. As the voltage is increased the lattice temperature rises and phonon scattering increases, particularly at the weak spots. At a certain voltage thermal vibration at a weak spot attains such a level that rupture of the filament occurs and conduction ceases. The combined effect of many filaments rupturing at slightly different voltages is a gradual fall of current with voltage in the negative resistance region. Electrons released from the broken filaments are scattered into the surrounding

insulator where they are trapped. Polarisation of the insulator takes place, but as the traps relax by thermally assisted Poole-Frenkel emission the degree of polarisation falls, until after the dielectric relaxation time polarisation is absent altogether. Under these conditions re-joining of the filaments by ionic migration is considered to be possible. Thus after rupture a filament may re-establish itself after the dielectric relaxation time, which is dependent on the temperature of the insulator. At low temperatures filaments do not re-join because the dielectric relaxation time is extremely long. Thus after a device has been cycled above the negative resistance region at low temperature the device remains in its high impedance state as has been observed experimentally²⁵. The reason why switching from the low to the high impedance state is relatively rapid (approximately 10^{-9} s) while switching from the high to the low impedance state is much slower (approximately 10^{-7} s) now becomes apparent. Rupturing of filaments and scattering of hot electrons is a fast process while re-joining involves ionic migration, a much slower process. The long dead-time between switching cycles³¹ is a result of dielectric relaxation in the un-formed insulator.

Some further properties are also successfully explained by this model. In the negative resistance region filaments are continually breaking and re-joining leading to large current fluctuations. The noise level is therefore much higher than at lower and higher voltages where the filaments are either all unbroken or all ruptured.

Hot electrons produced by the high fields at the filamentary weak spots are responsible for electron emission into vacuum. Hot electrons produced at weak spots near the anode will not be heavily scattered and will be emitted with energies corresponding to the full bias across the device. Emitted electron energies measured by a number of workers have

shown the existence of electrons with energies of this magnitude^{33,38,74}. The sudden appearance of electron emission at voltages corresponding to that at which filaments start breaking is another consequence of the filamentary model.

The model can be summarised by a number of equations, which lead to a distribution of filament resistances. Joule heating of the filaments causes their temperatures to rise, and we can associate a local lattice temperature T with each filament. It is assumed that for a specific filament rupture will occur if T exceeds T_{\max} . It has previously been assumed that the behaviour of a filament is characterised by a weak spot somewhere along its length. It is this point of resistance ρ where the bulk of the voltage across the length of the filament is dropped and is also the point where the filament temperature T is highest. Changes in the value of T are determined by two factors, Joule heating and heat loss to the insulator. Heat loss is taken to be proportional to $T - T_0$ where T_0 is the temperature of the insulator. The filamentary local temperature is then given by

$$\frac{dT}{dt} = a'' \frac{V_b^2(t)}{\rho} - \frac{1}{\tau_c} (T - T_0) \quad (1.38)$$

where a'' and $1/\tau_c$ are proportionality constants characterising the heating and cooling processes. At a specific constant voltage V_b we assume that a thermal equilibrium has been reached so that $dT/dt = 0$. The steady state solution of equation (1.38),

$$\rho = \frac{\tau_c a'' V_b^2}{T - T_0} \quad (1.39)$$

gives us a direct relationship between a filament's temperature and its resistance. Because all filaments where $T > T_{\max}$ are assumed to rupture,

the resistance ρ_{\min} at which $T = T_{\max}$, is a critical resistance which determines whether a filament is broken or unbroken at a particular voltage. At voltage V_b filaments with $\rho < \rho_{\min}$ are therefore broken and those with $\rho > \rho_{\min}$ are still unbroken. Only these unbroken filaments contribute to conduction. ρ_{\min} is given by equation (1.39) when $T = T_{\max}$. Thus

$$\rho_{\min} = \frac{\tau_c a^n V_b^2}{T_{\max} - T_0} \quad (1.40)$$

The total current carried by the unbroken filaments is then given by

$$I = \int_{\rho_{\min}}^{\infty} d\rho \frac{V_b}{\rho} P(\rho) \quad (1.41)$$

where $P(\rho)$ is the probability distribution of the filament resistances.

Clearly

$$\int_0^{\infty} d\rho P(\rho) = 1 \quad (1.42)$$

The detailed shape of the $I_c - V_b$ characteristic is obviously determined by the distribution $P(\rho)$. Below V_T the device may be cycled without noticeable filament rupture. It is evident therefore that not many filaments exist with $\rho < \rho_T$ where

$$\rho_T = \frac{\tau_c a^n V_T^2}{T_{\max} - T_0} \quad (1.43)$$

Similarly there are few filaments with $\rho > \rho_u$ where

$$\rho_u = \frac{\tau_c a^n V_u^2}{T_{\max} - T_0} \quad (1.44)$$

and V_u is the voltage where the circulating current is a minimum. At voltages in excess of V_u filamentary conduction is not the predominant conduction mechanism and we can take it that all filaments are broken.

The distribution of filaments $P(\rho)$ may be deduced from the $I_c - V_b$ characteristic by using

$$\frac{P(\rho)}{\rho} \propto \frac{d(I_c/V_b)}{d(V_b^2)} \quad (1.45)$$

which yields a roughly triangular filament distribution. Negative values of $P(\rho)$ appear for low ρ but this is due to tunnelling at low voltages and is neglected in the subsequent analysis. Normalisation of the distribution can be performed if N , the number of filaments per unit area, can be estimated. $\tau_c a''$ is calculated by using the simplifying approximation that each filament is of constant radius d' and length L and is imbedded in a cylindrical heat sink of radius D . Thus ρ can be determined from equation (1.39), and N (estimated to be $5 \cdot 10^6$ filaments per cm^2), derived from the initial resistance of a device. Current-voltage behaviour deduced from a simplified triangular filament distribution neglecting tunnelling effects gives an excellent agreement with measured characteristics.

1.5.6 Ralph and Woodcock

The model developed by Ralph and Woodcock⁵ is an attempt to reconcile a phenomenological filamentary model of the type proposed by Dearnaley to the currently accepted theories of impurity band tailing in amorphous insulators. Thus although conduction takes place through filamentary regions, a band structure is ascribed to each filament. It is the modifications to the energy band picture under bias conditions which

determines the conduction behaviour and other related properties.

In common with the models of Simmons² and Hickmott³² conduction takes place via an impurity or defect band somewhere within the insulator energy gap. By considering the properties of impurity bands in disordered materials a band model of a filament can be proposed. Amorphous and impure semiconductors and insulators show a conduction and valence band which differs from the normal crystalline model. Because of the lack of long range order the band edges smear out into a range of low mobility localised states. There is a sharp change in mobility between the non-localised high mobility states and the localised states; the boundary where the mobility changes is termed the mobility edge, and the energy difference between the mobility edges of conduction and valence bands is referred to as the mobility gap. Instead of a reasonably well-defined energy gap we now have a mobility gap where the energy bands tail off into a range of localised states. Furthermore, the edges of the impurity band will also smear out into a range of localised states¹⁰¹, giving a mobility bandwidth which is less than the density of states bandwidth. The distribution of states into localised and non-localised regions appears to be determined by the ratio V_0/J' ^{101,102}, where $V_0^2 = \langle V^2 \rangle$; V is the random excess potential at each impurity site and J' is the bandwidth which would occur in a perfect crystal due to the overlap of the individual state wave-functions. A critical value of V_0/J' exists, above which all the levels in the band are localised. Anderson has given a value of 5.0 while Ziman¹⁰³ has estimated this to be 2.8. Below this critical value the impurity band is divided into a range of propagating states with localised density of states tails.

The energy band model for a filament is then proposed in which an impurity band of the type previously described is present. Band

tailing in the conduction and valence bands is also present although this is not important in the conduction process. Due to local fluctuations in V_0 and density of centres throughout the structure, there will be regions where the mobility bandwidth is low; a corresponding increase in the density of states bandwidth also occurs. These regions are referred to as constrictions and the proposed band model of a filament in the region of a constriction under zero bias is shown in figure 5a.

Under low bias the current flow in a filament is by way of iso-energetic tunnelling through the centre region of the impurity band. The shape of the $I_c - V_b$ characteristic in this range is of the form $I_c \propto \sinh K V_b$ which has been shown to be explicable by this type of mechanism². As the voltage is increased there comes a point where electrons are hot enough to leave the centre of the impurity band and enter the localised states. This is shown as (a) in figure 5b. The filament may still conduct via the trapping states by recombination (b), thermal degradation (c) and field emission (d), but finally trapping causes the filament to switch off leading to a falling current in the negative resistance region.

Two methods are described by which conduction through a filament can be inhibited. Firstly, trapping in the localised levels at a constriction will cause a change in the local value of V_0 . In order to ascertain whether V_0 will increase or decrease we first consider the factors contributing to the local value of V_0 . In the case of traps which are neutral when full and positive when empty, the compensating negative charges will reside in other unspecified sites. Pairs of positive and negative charges existing side by side would give a low energy configuration and it is therefore assumed that the charges are distributed in this fashion. The interaction between the positive

and negative charges determines the value of V_0 . Trapping of electrons neutralises some of the positive centres leaving isolated negative charges in the vicinity of neutralised centres. The magnitude of the local field near the centre will thus be higher, increasing the value of V_0 and consequently V_0/J' . If the value of V_0/J' exceeds the critical value all the states in the mobility band will become localised at the constriction and conduction will effectively cease.

The second method whereby the filaments are caused to switch off involves the trapping of a negative space-charge in the un-formed matrix surrounding the filaments. This induces positive charges in the conducting region of the filament which, if it is near a constriction, can lower the Fermi level into the localised tail at the bottom of the impurity band. Thus conduction along the filament is inhibited.

The memory phenomena are a consequence of the retention of trapped charge after the applied voltage is reduced. As long as the trapped charge persists some filaments remain non-conducting and current levels will be lower than in the absence of the trapped charge. Erasure of the memory state occurs when trapped charge is released by field emission into the conduction (or valence) band. Clearly the field is highest at the constrictions inside the filaments and once this reaches a sufficient level electrons trapped in the localised states within the filaments will be rapidly released. The voltage V_T at which memory erasure is initiated, is determined by the traps inside the filaments. Trapped charge outside the filaments (which can also inhibit conduction as described earlier) must also be released before all the filaments can be returned to the conducting state. This will not normally occur by simple field emission of the trapped charges, because of the relatively low field intensity in the un-formed matrix.

Therefore it is proposed that the charge outside the filaments must relax into the traps inside the filaments where it is then released by field emission in the normal way. The time dependent dead-time between switching cycles is thus a consequence of the time constant associated with the relaxation process. Hence the values of the threshold voltage and dead-time are both determined by trapping phenomena; in the former case by traps inside the filaments and in the latter by traps in the un-formed insulator.

Electron emission is caused by hot electrons which reach the conduction band by field emission from the traps within the filaments. The onset of emission will therefore occur at the same voltage as that at which memory erasure occurs. The emission intensity will rise quickly in the negative resistance region, where progressively more current is carried by electrons entering traps with subsequent release by field emission. As explained by the model of Dearnaley the noise levels in this region are high because of the different switching thresholds of many different filaments.

In common with the model of Hickmott electroluminescence is taken to be caused by radiative recombination between hot electrons and holes. The upper limit of photon energies measured by Ralph and Woodcock corresponded to the applied voltage, as expected.

1.5.7 Discussion

In the previous sections the history of the forming effect has been traced from the time of the original observations by Kreynina et al¹⁸. The earlier theories proposed to account for this effect were generally band models, and the conduction models of Hickmott³² and Simmons and Verderber^{2,17} assumed that the conduction medium was uniform, even though electron emission was observed to arise at discrete

spots. Nevertheless these models were able to give good quantitative as well as qualitative agreement with various device parameters, and Simmons was able to predict V_F in SiO with some degree of accuracy. Hickmott's model was also able to accommodate the effect of the high field region, which had been difficult to fit in to the other models.

With the advent of the observation of the forming effect in a wide range of materials in addition to Al_2O_3 and SiO, Greene et al⁴⁷ proposed that the forming effect was by means of a type of solid-state electrolysis. The model had the added advantage of being able to explain the reason for the emission of gas during forming, and also the effect of a gaseous environment. The observation that conduction takes place through chains of defect centres was a recognition of the fact that conduction was not of a uniform nature.

A further approach by Barriac et al^{44,49} was also successful in explaining the effect of an oxygen environment. This model accommodated the concept of a high field region, but assumed that conduction was uniform throughout the film. It also wrongly predicted the value of V_m , and was not a great improvement on earlier theories.

More recently the filamentary theory of Dearnaley et al⁴³ has had considerable success in explaining device properties. The model is applicable to many materials and does not assume a specific band structure. It is applicable not only to insulators and semiconductors, but also to organic monomolecular layers¹⁶. Modifications of the theory⁷³ can explain not only the high values of V_m in sulphides (which cannot be explained on a band model), but also the increase in V_m with time. Further experimental evidence for the filamentary model is given by the emission of electrons from point sources^{38,58}, the existence of SiO_4 tetrahedrons parallel to the electric field in SiO⁶⁰, and the

existence of an Si_2O_3 pseudophase in resistively prepared SiO_2 ⁶⁹. Dearnaley et al⁹ have fully reviewed the various conduction mechanisms and shown that the filamentary model is capable of explaining most of the observed phenomena. In particular the filamentary theory takes account of the localised nature of the conduction phenomena, and the rupturing and re-joining of filaments in such regions accounts for the difference in switching times between high to low and low to high impedance states. Moreover the very long device memory is more compatible with structural changes in the insulator than with a relatively short lived space-charge storage mechanism. The wider applicability of the filamentary theory, together with its success in explaining device properties, provides a good basis for formulating a more comprehensive theory. Such factors as the precise mechanism of forming, the role of the high field region and the actual mechanism of conduction within the filaments, remain unsolved. However, a more realistic conduction mechanism through the filaments has already been proposed by Ralph and Woodcock⁵, which goes a long way in reconciling the filamentary model to the accepted theories of conduction in non-crystalline materials.

1.6 Aim of the Experimental Work

$\text{Au-SiO}_x\text{-Au}$ devices were used throughout for the detailed experimental work, since these materials are relatively easy to evaporate, and the results could be compared with those of other researchers using the same insulator.

In addition to their interesting physical properties formed devices are worthy of investigation because of their possible industrial applications. Although their use as a memory element is unlikely to be competitive with conventional devices, the work of Hogarth and Bidadi⁹⁵

has shown that increased values of transfer ratio ($\alpha = I_e/I_c$) can be obtained under certain circumstances, and potential development as a cold-cathode electron emitter has not been ruled out. Considerable improvement is probably possible, and a general aim of current research is to seek ways in which this can be accomplished.

In the present case it was felt that sufficient research had not been performed on general device properties, such as higher voltage effects, time dependence and device temperature, all of which may have some bearing on the value of α . Consequently these aspects were investigated (see 3.1), together with estimates of attenuation lengths in SiO_x (see 3.3) and the mechanism of electron emission (see 3.4). Studies of the high field region (see 3.2) were performed, since this is an important device property which must be further investigated before the device conduction mechanisms can be fully understood. Forming was also observed in $\text{SiO}_x/\text{B}_2\text{O}_3$, CaBr_2 and Si_3N_4 (see 3.5) and this extended the range of materials in which device parameters had been measured.

CHAPTER 2

APPARATUS AND EXPERIMENTAL TECHNIQUES

2.1 Preparation of Devices

2.1.1 The Evaporation System

Thin films used in this investigation were produced by vacuum evaporation in a Balzers BA 510 19" coating unit. A DUO 25 rotary pump backing a DIFF 1500 9" diffusion pump was capable of producing an ultimate chamber pressure of 10^{-6} torr and this could be improved to 10^{-7} torr when liquid nitrogen cooling was employed. A radiant heater was incorporated into the bell-jar assembly which was used for heating substrates and also for baking out the system to achieve lower ultimate pressures. The bell-jar assembly was water-cooled and could be raised by a hydraulic hoist to permit easy access to evaporating materials and substrates. The interior of the chamber was visible during evaporation through a reinforced Pyrex window. Chamber and backing pressures were continuously monitored with Balzers Pirani and Penning gauges. Facilities for ionic bombardment cleaning of substrates were available in the chamber.

The evaporating sources were positioned 30 cm below the substrate holder and were screened from each other to avoid contamination. Power for the evaporating sources was drawn from an internal 2 kV A supply with secondary transformer windings delivering 4-32 V. An external supply was also used, so that two substances could be evaporated simultaneously if necessary. The techniques of co-evaporation have been previously described by Hogarth and Wright¹⁰⁴. Quartz crystals, used for monitoring the thickness and rate of deposition of evaporants, were located directly above each evaporating source. The crystals were shielded to minimise temperature induced frequency drifts and were collimated so that each crystal detected deposited

material only from its own evaporation source.

A rotary substrate holder was employed which was capable of holding four 3" x 1" substrates at a time. Masks could be rotated below the substrates by an external rotary seal, and a maximum of four different layers could be deposited. An aluminium shield, located directly below the masks enabled the substrates to be isolated from the evaporant until initial evaporating conditions had stabilised. A shutter was let into the bell-jar through one of the ports provided. This enabled portions of the masks to be successively shut off during evaporation, allowing devices of different electrode or insulator thickness to be deposited on a single substrate. At the end of a deposition sequence the substrate holder itself could be rotated and in this way it was possible to perform further depositions on three more sets of four substrates without breaking vacuum. It was thus possible to perform depositions on sixteen substrates in one pump-down sequence. In practice this number was limited by the capacity of the evaporating boats and the need for separate substrates for thickness measurements. Deposition on more than four different substrates was only rarely performed during one evaporation sequence.

2.1.2 Deposition Procedures

Films were deposited on Corning 7059 glass substrates. The less expensive Chance microscope slides were used when depositing material for thickness measurements. Substrates were thoroughly cleaned by boiling in a solution of Teepol in water for 10 minutes. They were then rinsed in boiling distilled water and final traces of grease and Teepol were removed by immersing in warm isopropyl alcohol. The substrates were finally dusted with a Selvyt cloth and any remaining dust particles were blown off, after mounting in the substrate holder,

by using a stream of compressed nitrogen. Final cleaning by ionic bombardment during the pump-down sequence was also employed.

On each substrate a maximum of nine devices could be deposited. Firstly a bottom (base) electrode of width 0.250" (6.4 mm) and standard thickness 500 Å was deposited on the clean slide. This was followed by the insulating layer and then by a thick strip of insulator to cover the edge of the bottom electrode. This is a frequent area of preferential dielectric breakdown^{27,28} and the thick insulating strip helped to diminish the high field in this region. The final deposition of the top (counter) electrode of width 0.125" (3.2 mm) completed the structure. A diagram of the device arrangement used is shown in figure 6.

Insulating materials were evaporated from covered molybdenum, or occasionally tantalum, boats. The cover reduced the effects of unequal heating which often caused insulators to be ejected from open boats. Au was evaporated from open molybdenum boats while Al was evaporated by hanging pieces of Al wire on a tungsten spiral. The depositions were carried out at a pressure of $5 \cdot 10^{-6}$ - $1 \cdot 10^{-6}$ torr at a substrate temperature of 200°C. Films showed greater adhesion to the substrates when deposited at this temperature, and the electrical behaviour was more stable.

Standardised optimum evaporation rates were adhered to throughout. These were 5 Å s^{-1} (Au), 7 Å s^{-1} (Al), 6 Å s^{-1} (SiO_x), 0.8 Å s^{-1} ($\text{SiO}_x/\text{B}_2\text{O}_3$), 4.5 Å s^{-1} (CaBr_2) and 0.3 Å s^{-1} (Si_3N_4). The parameter R/P (evaporation rate/evaporating pressure) is often a good indication of device structure and properties. In this case R/P for SiO_x was $1.2 \cdot 10^6 \text{ Å s}^{-1} \text{ torr}^{-1}$. Using refractive index measurements of SiO_x films Timson and Hogarth¹⁰⁵ have shown that this value corresponds to a predominantly SiO structure.

The deposition sequence proceeded in the following order. Firstly the interior of the evaporator chamber assembly was cleaned to reduce the risk of contamination of the evaporated films. The cleaned substrates, together with the evaporating boats and materials were loaded into the chamber, and aluminium shields to prevent soiling of the chamber by evaporants were inserted. The stability of the quartz crystal monitor circuits was checked before starting the pump-down sequence, as failure at a later stage usually necessitated repeating the whole sequence. When the chamber pressure had reached 0.5 torr the roughing valve was closed and the high vacuum valve opened so that the chamber was then pumped by the diffusion pump. The chamber needle valve control was adjusted so as to give a chamber pressure of 0.1 torr and the substrates were cleaned by ionic bombardment for a few minutes. The needle valve was then closed and the pressure allowed to fall to less than 10^{-5} torr. At this stage the substrate heater was turned on and the chamber temperature allowed to rise until the substrates were at approximately 200°C . This temperature was maintained for approximately 2 hours during which time the pressure fell further. After this bake-out the liquid nitrogen trap was filled and the deposition commenced.

The aluminium shield was positioned between the masks and boat, while the current through the boat containing the metal for the base electrode was adjusted until a uniform evaporation rate was attained. This was monitored using the calibrated quartz crystal monitors. The deposition was allowed to continue until the required thickness was reached, when the shutter was again used to close off the masks and the evaporation was curtailed. This procedure was repeated for the various layers and the shutter was used as necessary to deposit devices with different layer thicknesses on the same substrate. After deposition

the heater was switched off and the whole system allowed to cool before admitting air to the system. The substrates were removed as quickly as possible and kept in an evacuated desiccator until required.

2.1.3 Thickness Measurements

Thicknesses of films were monitored during evaporation using a pair of Edwards quartz crystal film thickness monitors¹⁰⁶. The quartz crystals were positioned near the substrates and the evaporant was allowed to deposit on them through a hole in the case. The frequency of the crystal, driven by an oscillator unit, varies linearly with the thickness of material deposited. Thickness could be determined once the crystal had been accurately calibrated using Talystep thickness measurements described below. The deposition rate could also be measured by electronically differentiating the oscillating frequency with respect to time. The deposition rate is proportional to rate of change of frequency.

After deposition, insulator thickness could be checked optically by making use of an interferometric technique. Special samples were used which had an insulating layer step covered with a metal layer. These samples were fabricated at the same time as the electrical samples. A semi-transparent aluminium coated optical flat was placed in contact with the substrate. Illuminating this with parallel monochromatic light of wavelength Λ and observing through a low powered microscope revealed interference fringes at the oxide step. By careful positioning of the optical flat the fringes could be made to run at right angles to the oxide film step. By measuring the number of fringes displaced (Q) in the pattern at the oxide step, the thickness (d) of the film could be deduced from the following equation

$$d = Q \frac{\Lambda}{2} \quad (2.1)$$

The accuracy of this method is limited to some extent by the deviations from flatness of the substrate, and by the accuracy to which the fringe displacement can be estimated. For film thicknesses of greater than 300 Å, however, the accuracy of this method was within 5% of the more accurate Talystep measurements described below.

Accurate thickness measurements were performed using a mechanical instrument, the Rank Taylor Hobson Talystep 1. In this instrument thicknesses are measured by a diamond stylus which traverses the substrate. Vertical movement of the stylus arm varies the inductance of a sensitive coil, which is electronically amplified and fed to a pen recorder which traces a greatly enlarged section of the film step. Typical traces are shown in figure 7. Film thickness could be obtained directly from the trace.

2.2 Electrical Measurements

2.2.1 The Vacuum Test System

Because forming and subsequent formed characteristics normally only occur under vacuum conditions, all electrical measurements were performed in a subsidiary high vacuum system which also served to protect devices from air and water vapour. A photograph of the test system is shown in figure 8. The diffusion pump was a 4" water-cooled Edwards EO4 and this was backed by an Edwards ES 200 rotary pump. Isolation of the chamber from the diffusion pump during roughing out was performed by an Edwards QSB4 butterfly valve. Backing and chamber pressures were monitored with Sadla-Vac Pirani and Penning gauges, and an Edwards needle valve assembly allowed the chamber pressure to be varied in the range 10^{-6} -1 torr.

A 12" bell-jar was positioned above the 1" thick aluminium base-plate. A 0.5" top-plate was used in conjunction with this, except when

temperature variations and emission patterns were being observed. Rubber seals between the chamber and the plates completed the vacuum seal. Glass-to-metal seals in the base-plate allowed screened leads for electrical connections and thermocouples to be introduced into the chamber. Screened co-axial electrical connectors allowed connections to the external circuitry to be made. A 5 kV lead-through was also let into the base-plate to transmit the high voltages necessary to observe emission patterns. This was also used as the lead-through for electrical connection to the electrometer when making emission current measurements. Leads were kept as short as practicable, and were rigidly tied down and screened to reduce spurious induced signals at low current levels.

Substrates were mounted on a Perspex assembly positioned in the centre of the chamber, and a photograph of this can be seen in figure 9. The devices were connected by means of spring contacts and good contact was ensured by lightly coating with silver paste. This was not applied in close proximity to the device active area and could not enhance the conductivity by seepage into the insulator. A thermocouple could be attached to the substrate if temperature data was required. The aluminium anode for emission current measurements, was positioned 2 cm vertically above the substrate. This was screened by an earthed aluminium plate, which was found to increase the electron capture efficiency of the anode.

2.2.2 Forming

Devices were formed in the bell-jar at pressures of less than 10^{-5} torr. A Solartron AS1414.2 60 V, 1 A power supply which was capable of delivering voltage in steps of 0.1 V was utilised. The voltage was increased in 0.1 V steps with an approximately 20 s delay

between steps. This was because some samples did not form immediately at the forming voltage, but required a few seconds to adjust to the new bias. After forming, devices were normally run for 10 minutes before readings were taken to allow the current to stabilise.

2.2.3 Circuits

The basic requirement of the circuit to measure I_c and I_e was the DC Solartron voltage source, an accelerating voltage source (Keithley 240A 1.2 kV, 10 mA) and a suitable measuring instrument capable of detecting 10^{-13} A or less. A Keithley 602 battery-operated electrometer, which was capable of being floated up to 1.5 kV was employed. Direct connection of this to the accelerating voltage source detected a constant level of induced DC noise, which could not be eliminated even by extensive screening. A solution was found by biasing the voltage source circuit, which supplied the voltage V_b across the device, at -100 V below earth potential. The anode was thus at a potential of +100 V relative to the base electrode of the device and electrons collected by the anode circuit drained away to earth through the electrometer. A diagram of this circuit is shown in figure 10a. A three terminal device is shown in the figure to illustrate the connection of a digital volt-meter (Solartron IM 1619) which was used in the potential distribution measurements. The voltage between any pair of electrodes (cathode (c), grid (g) or plate (p)) could be measured by suitable switch positioning.

Observations of emission patterns on a phosphor screen were performed using a slightly simpler circuit. The electrometer was dispensed with and a phosphor-coated conducting anode at a potential of 3 kV (provided by an Isotope Developments 532/A EHT unit) was utilised. The circuit is shown in figure 10b. There was no need in this case to

bias the voltage source circuit at -100 V.

2.2.4 Current-Voltage-Time Characteristics

Much of the work entailed measuring the variation of I_c and I_e with V_b under different conditions. Due to the high noise level of I_e it was impossible to obtain accurate readings directly from the electrometer. A method of time-averaging was employed in which the electrometer was used to measure the charge flow over the averaging period (usually 30 s). The average current was obtained by dividing the charge by the period of averaging.

Since this study was partly concerned with the operation of devices at high voltages ($V_b > 20$ V) it was necessary to ensure that the accelerating voltage remained constant. This was achieved by increasing the output of the high voltage source each time V_b was increased. The accelerating voltage was kept constant at +100 V relative to the device counter electrode, the high voltage source always being set at $V_b + 100$ V.

The time dependence of I_c and I_e at constant V_b were recorded using a Servoscribe chart recorder connected to the current measuring instruments. Current variations from immediately after the forming process, were recorded.

2.2.5 Temperature Measurements

The temperature of the device active area was occasionally required. This was obtained by attaching a chromel-alumel thermocouple to the surface of the device with a non-conducting adhesive (Araldite).

Earlier measurements of the variation of I_c and I_e with temperature had shown large current fluctuations as a result of the varying temperatures⁵⁹. In view of this, it was decided to design a system whereby measurements could be made at a range of constant temperatures.

The apparatus consisted of a brass box soldered to stainless steel tubes which were soldered to a 0.5" thick stainless steel top-plate. Brass and stainless steel were chosen for the parts of the system which required, respectively, a high and low thermal conductivity. Liquid nitrogen was introduced into the box from outside the vacuum system allowing temperatures of 80 K to be obtained. Substrates were stuck to brass plates with Araldite and these were securely screwed onto the base of the box. A thermocouple attached to the substrate recorded the temperature. Intermediate higher temperatures could be obtained by two methods. Firstly an electric heater could be inserted between the substrate and the box and a thermal equilibrium obtained between the heating and cooling processes. The temperature could be varied by varying the voltage across the heater. The second method consisted of attaching the substrate to the box on top of a number of stainless steel spacer plates. By varying the number of plates and the rate at which the liquid nitrogen was replenished a range of different temperatures could be obtained. Higher temperatures were obtained by using the heater without the liquid nitrogen supply, or by blowing steam through the brass box assembly.

2.2.6 Attenuation Lengths

Equation (1.9) predicts a linear variation of $\log I_e/I_c$ with the counter electrode thickness. Preliminary results in section 3.3 suggested that this type of variation held even when the thickness of the insulator was varied instead of the thickness of the counter electrode. Measurements of the attenuation lengths in insulators therefore required a set of devices with a constant thickness counter electrode, but with varying thicknesses of insulating layer. These could easily be fabricated in the evaporator unit using the shutter

to screen successively different parts of the substrate during insulator deposition. The value of the SiO_x attenuation length (λ_{SiO}) could be obtained directly from plots of $\log I_e/I_c$ against SiO_x thickness (d_{SiO}).

Emitted electron energy distributions were obtained by holding V_b , temperature and other variables constant, and observing the variation of I_e/I_c when a retarding voltage (instead of an accelerating voltage) was applied to the aluminium anode. Graphical differentiation of I_e/I_c with respect to retarding voltage gave the energy distribution.

2.2.7 Spatial Distribution of Emitted Electrons

It has previously been observed that electron emission from devices is non-uniform, and small area samples have been used to examine diffraction effects in the counter electrode^{37,38,41,58}. Work has also been performed on larger area devices where the angular distribution of emitted electrons averaged over the entire emissive surface was determined^{55,66,96}. The results of such determinations are normally compared to the theoretical model of Hrach^{46(d)}, and the shape of the distribution can give a useful guide to scattering properties in the insulator. Since both counter electrode diffraction and scattering in the insulator are of importance in determining the conduction and emission properties, it was decided to investigate electron emission using both the above techniques.

2.2.7.1 Diffraction of Emitted Electrons

Diffraction of emitted electrons by the Au counter electrode was originally investigated by Simmons et al^{37,38} who observed arcs consistent with (111) diffraction at pinholes in the top electrode. Lancaster⁴¹ and Gould and Collins⁵⁸ have both observed diffraction

through the counter electrode and a second (200) diffraction ring was reported. In order to avoid breakdown effects at the voltages necessary to observe (200) diffraction, a pulsed bias technique was used. This involved applying 20 V DC across the device together with a superimposed pulsed bias V_p , so that $V_b = V_p + 20$ V. It could be argued that the pulsed bias technique was responsible for the appearance of the second ring and that both rings were caused by (111) diffraction, the inner ring corresponding to $V_b = 20$ V and the outer ring to $V_b = V_p + 20$ V. Although this argument did not appear to explain the phenomena as satisfactorily as the assumption of (200) diffraction, it was decided to attempt to duplicate these results using a DC bias only and if possible to try and detect (220) diffraction. In section 3.4.1 it will be shown that this requires a voltage of 56.6 V so some alternative solution was required to alleviate the problem of high voltage breakdown. This was accomplished by evaporating multi-layer structures of two or three insulating layers sandwiched between three or four Au electrodes. The procedure was then to form successively each of the SiO_x layers and apply the final high voltage between base and counter electrode. In many cases the voltage drop was entirely in one region of the structure and breakdown occurred at 20-30 V voltage levels. However, with care in the evaporating procedure the layers could be "matched" to each other and uniform voltage drops across the different insulating layers were obtained. It was then possible to apply voltages in excess of 60 V without destruction of the structure.

The circuit shown in figure 10b was used. Emission patterns were viewed on a phosphor screen prepared in the following manner. Pyrex glass was made conducting by coating the heated screen with the vapour formed over molten stannous chloride. A few drops of concentrated

phosphoric acid were dissolved in 1 ml of methanol and this solution applied to the conducting surface. Powdered phosphor (Type H 918, Levy West Laboratories Ltd.) was sprayed onto the surface with an atomiser and excess phosphor tapped off. The screen was then baked in vacuum at 400°C for 1 hour which increased the adhesion of the phosphor to the screen. Contact to the screen was made with fine copper wire attached with silver paste.

Devices usually showed many arcs on the phosphor screen and in order to reduce the number many devices were masked with thin mica sheet to cut the emitting area down to 1 mm^2 . In this way the most favourable emitting areas for observation of diffraction phenomena, could be isolated.

2.2.7.2 Angular Distribution of Emitted Electrons

The angular distribution of emitted electrons was determined using a hemispherical anode collector, divided into ten bands. These were constructed from aluminium sheets of width $0.250''$ (6.4 mm) and were insulated from each other by $0.131''$ (0.8 mm) sheets of polythene. The hemisphere, of diameter $5.312''$ (13.49 cm), was gauged out of a block made up of alternate aluminium and polythene layers. A diagram and photograph are shown in figure 11. Each of the bands could be connected via the electrometer to earth (using the circuit in figure 10a) so that the emission current deflected into the solid angle subtended by the band could be measured. All the other bands were earthed so that the accelerating field was constant in all directions. The emission current deflected into each of the ten bands could thus be obtained, and the emitted angular distribution derived. In order to increase the symmetry of the emitting system the samples used for the measurements were circular, of diameter $0.187''$ (4.8 mm); these were

always carefully positioned at the centre of the anode.

CHAPTER 3

RESULTS AND DISCUSSION

3.1 DC Device Stability and Operation

3.1.1 Variation of I_c and I_e with V_b

The variation of I_c and I_e with V_b in SiO_x has been investigated by a number of researchers. The majority of these measurements were concerned with the device behaviour in the negative resistance region, and voltages in excess of 15 V were rarely applied. At voltages greater than this value destructive breakdown effects normally became apparent and a gradual fall of I_c and I_e at $V_b > 16$ V has been interpreted by Collins and Gould⁷⁴ as single-hole dielectric breakdown of the type observed by Budenstein and Hayes⁷⁵. In the present investigation DC voltages as high as 60 V were applied, and results typical of more than fifty sets of substrates are shown in figure 12 for a device with SiO_x thickness 5200 Å. (Devices with insulator thickness greater than 3000 Å readily formed, in contrast to earlier observations by Verderber et al¹⁷). The voltage was applied in 0.1 V steps and the figure represents a single increasing voltage trace. Note that the normal practice of plotting I_e on a logarithmic scale has been followed, and I_c has also been plotted in this way so that the variations in I_c at lower current levels can be easily seen. The behaviour of both I_c and I_e up to the current minimum was in agreement with previous measurements^{2,39,74}. I_c increased to a maximum at a voltage $V_m = 2-4$ V followed by a rapid fall to a current minimum at $V_u = 9-12$ V. I_e was first detected at 2 V and rose rapidly until V_m was reached. I_e continued to rise in the negative resistance region, although the rate of increase was much reduced. When V_u was exceeded

there was a further gradual increase in I_c , and I_e increased rapidly. Eventually both I_c and I_e reach a second maximum at 16-25 V, and increasing the voltage above this value resulted in a lessening of I_c and I_e . The fall was not reversible and decreasing the voltage decreased the current (see figure 13d). Increasing the voltage still further resulted in a series of discontinuous current drops (1), (2) and (3) which were evidently of a destructive nature. These were clearly distinguishable from the continuous fall of I_c in the voltage range following the second current maximum, and invariably showed an associated discontinuous fall in I_e . Such discontinuous current drops are definitely associated with an increase in resistance of a high field region of the insulator and this is fully described in section 3.2.3.

Before discussing the interpretation of the current-voltage characteristic described above, the transient responses of I_c in the different voltage ranges of the I_c - V_b characteristic will be described. As well as providing some insight into the conduction processes responsible, this method also helped to distinguish between the continuous and discontinuous falls in current noted above.

In figure 13 the transient responses of I_c in different voltage ranges of the characteristic are shown. Note that these traces were not all obtained from the same sample and that the current levels and transient times varied widely between samples. In each case the voltage was increased by 1 V (instead of the normal 0.1 V) so that the transient behaviour and current changes were significant enough to be easily observed on a chart recorder trace. The current was then allowed to relax to a constant level (but not allowed to rise over long time periods as described in section 3.1.2)

and the voltage was then reduced to its original value.

In figure 13a the variation of I_c with time when the voltage was increased from 3 to 4 V is shown. This is in the rising part of the $I_c - V_b$ characteristic before the negative resistance region. On increasing the voltage the current rises sharply and then increases slowly over a period of 30 s to a new steady value. Decreasing the voltage once more to the original value, results in a sharp current drop followed by an almost constant current of value equal to the original current at 3 V. Clearly the rise and fall of current is merely a response of the device to the changed bias and cannot be linked to any particular conduction model described in section 1.5. The gradual rise in current after the voltage increase is, however, rather difficult to explain in terms of one of the electronic models. Electronic processes are notoriously fast and transients existing over a period of 30 s are untenable. Although the possibility of a slight increase in current due to the gradual establishment of a steady ionic current could be envisaged, a better explanation is perhaps afforded by one of the filamentary theories. Following Dearnaley et al⁴³ we assume that there exists a distribution of filaments, most of which are unbroken at this voltage. We assume that there are also present a small number of incomplete filaments, which because of their own particular geometry or localised non-stoichiometry of the insulator, have not penetrated the insulating layer or have not re-joined after fracture. On increasing the voltage the current flow through the existing filaments increases and at the ends of the incomplete filaments the uniaxial dielectric stress is increased. Under these conditions a number of the incomplete filaments could join resulting in a current increase as they do so. Clearly the rate of current

increase will be higher at first as the most favourable filaments join, while the least favourable filaments will take an increasingly longer time before joining. Indeed some filaments may remain broken for some hours before re-joining as described in section 3.1.2.

In the negative resistance part of the characteristic somewhat different transient behaviour is observed (figure 13b). Increasing the voltage from 5 to 6 V results in an immediate current drop, presumably due to the rupture of filaments at the higher voltage. After a period of 30 s the current has increased to a nearly constant value. As in the previous case this is probably due to filaments re-joining under the increased field. The level of current recovery in the present case is substantially greater than that in the increasing current region of the $I_c - V_b$ characteristic; this is undoubtedly a result of the far greater number of broken filaments in the negative resistance region. Filaments which re-join and are of the wrong geometry or impedance to remain joined will again rupture and a type of natural selection mechanism will operate, only allowing filaments with an impedance above a certain threshold level to remain joined. Decreasing the voltage again results in a small current drop, but lowers the threshold resistance of filaments which can remain stable. Re-joining of an increased number of broken filaments can then take place.

In the region following the negative resistance region a different type of behaviour is apparent. On increasing the voltage from 11 to 12 V the current rapidly increases but then quickly falls to a new constant level. Reducing the voltage after current stabilisation induces a sharp current decrease, the current then re-stabilises to the original level. In this range filament rupture and re-joining does not appear to be the main cause of the transient

effects. Dearnaley et al⁴³ have argued that there are very few filaments remaining unbroken in this voltage range, and so we assume that filamentary rupture and re-joining are not the main contributions to changes in the steady state current levels. The total current will be a combination of current carried by these high resistance filaments and also that carried by other processes unconnected with filamentary conduction. The contribution of the filamentary current to the total current will still be appreciable and changes in the resistance of filaments as a result of changing voltage levels will become significant. A qualitative explanation of the behaviour can then be proposed. On increasing the voltage the current rises due to the increased voltage; this corresponds to the sudden current increase in figure 13c. The increased current causes the local filament temperature to rise which increases the filament resistance (if we assume that the filaments have a metal-like positive temperature coefficient of resistance). The current then falls until a steady state current value is achieved. On lowering the voltage the reverse process occurs. The voltage decrease causes a drop in current which causes the local filament temperature to drop. The filament resistance falls and the current rises until a new steady state value obtains. Some slight filament rupture and re-joining on increasing and decreasing voltage in figure 13c is probably in evidence, but this is masked by the effect described above. The longer time necessary to stabilise at the 11 V than at the 12 V voltage level, suggests that a process with a longer time constant (filament re-joining) still occurs when the voltage is reduced.

When voltages in excess of the second maximum are applied destructive processes take place. Figure 13d shows the responses

when the voltage is increased from 19 to 20 V and then reduced again. The increased voltage results in a current drop indistinguishable from that observed in figure 13b which was ascribed to filament rupture. In the present case, however, the current does not rise after the current decrease, but drops slightly in the same way as in figure 13c. Decreasing the voltage again results in a further sharp decrease in current, followed by a rising current which stabilises at a lower value than that observed at the original lower voltage. The fact that the new current level is not as high as that previously recorded for the same voltage strongly suggests that a destructive breakdown event has occurred. Most probably this is a number of single-hole breakdowns of the type described by Budenstein and Hayes⁷⁵ and previously suggested by Collins and Gould⁷⁴ as the cause of the falling current in this region. The sharp decrease corresponds to this localised destruction of the device, while the further slight fall is due to increased resistance of the current filaments as suggested for figure 13c. The further drop in current when the voltage is reduced is merely a consequence of the decreased voltage, while the slight increase following this depends on the decreased filament resistance as described for figure 13c and probably does not involve any filament re-joining.

In figure 13e the transient behaviour observed on increasing the voltage from 25 to 26 V is shown. This corresponds to an event of type (1) shown in figure 12, and represents a fall in current of 76% compared with 15% for figure 13d. The difference between the two values is normally greater than this for the following reason. The traces shown in figure 13 were for 1 V increases, while the normal $I_c - V_b$ characteristics were taken using

0.1 V increases. The fall in I_c in the critical region when 0.1 V is applied would be similar to that when 1.0 V was applied, providing the increased voltage exceeded the critical value. A fall in current of order 76% was not uncommon. However, a voltage increase of 0.1 V in the region where the current is steadily decreasing, would only produce a drop in current of approximately one tenth that recorded if 1.0 V was applied. A fall in current in the $I_c - V_b$ characteristics of 1.5% was therefore more typical, and was easily distinguishable from the much greater drops at higher voltages. Apart from this difference the general shape of figure 13e is similar to figure 13d. The explanation of the various current levels is therefore likely to follow the argument given for figure 13d. The differences between the two types of destructive behaviour are indicative of two different types of dielectric breakdown mechanism.

Klein^{98,107} has distinguished between two types of dielectric breakdown. These are categorised as electric (single-hole) breakdowns which are the results of an electron avalanche inside the insulator and which produce a number of holes in the material, and thermal breakdowns which occur when the power dissipated in the sample exceeds the rate at which heat can be conducted away without significant temperature rises. The rate of electric breakdowns varies with the voltage applied, and as the voltage is increased a larger number of breakdown areas are created in the device. Devices with thin electrodes (less than 2000 Å) undergo a process where the electrode evaporates in the vicinity of the breakdown event, thus isolating the breakdown area from the remaining device area. In this case the breakdowns are known as "self healing" and their effect is to decrease the effective device

area and thus reduce the subsequent current carrying capacity. As the voltage is increased the number of single-hole breakdowns increases until at a certain voltage V_B the breakdown rate becomes so large that complete device destruction occurs within a fraction of a second as a result of multiple single-hole breakdowns. Many materials show thermal breakdown at a voltage $V_{dm} < V_B$; if this condition is fulfilled the single-hole breakdown rate does not become high enough for multiple single-hole breakdowns to destroy the device. Whether the device is destroyed by thermal or multiple single-hole breakdowns depends only on the magnitudes of V_{dm} and V_B . Whichever of the two types of device destruction first occurs is described by Klein as maximum-voltage breakdown, and the voltage at which this occurs is taken to be an intrinsic device property. In either case single-hole electric breakdown occurs at voltage levels below those for maximum-voltage breakdowns.

Budenstein and Hayes¹⁰⁸ argue that maximum-voltage breakdown is always initiated as a series of single-hole breakdowns, and that the maximum-voltage breakdown behaviour does not represent the ultimate dielectric strength of the material. The results of Budenstein et al¹⁰⁹ show two different breakdown voltage parameters, V_{max} which is the voltage at which single-hole breakdown takes place and V_{min} which is the voltage at which cessation of breakdown occurs. V_{max} appears to vary with insulator thickness such that $F_{max} \propto d^{-\frac{1}{2}}$ ($F_{max} = V_{max}/d$ where d is the dielectric thickness) and this supports a single-hole breakdown theory of Forlani and Minnaja¹¹⁰. Nevertheless the results of Smith and Budenstein¹¹¹ have indicated that certain device areas undergo destruction at lower voltages than other areas. In NaF samples the value of the leakage current was considerably reduced after the appearance of several hundred

breakdowns. CaF_2 samples showed an increase in V_{max} with the number of separate breakdowns, and it was suggested that V_{max} rises with the number of breakdowns due to the elimination of weak spots. Similarly varying values of breakdown voltage with the number of DC breakdown tests have also been observed by Klein⁹⁸.

In the present results in formed SiO_x material it is likely that a similar process occurs. We have seen that in the falling current range following the second current maximum (figure 13d) increasing the voltage causes an irreversible reduction of the film current carrying capacity. However considerable device destruction does not occur in this region and these effects cannot therefore be ascribed to maximum-voltage breakdown, of either the thermal or multiple single-hole variety. Collins et al⁷⁸ have observed self-healing breakdowns in formed $\text{Al-SiO}_x\text{-Ag}$ cathodes, which cause evaporation of part of the metal contact. In the $\text{Au-SiO}_x\text{-Au}$ cathodes therefore it is probable that the same process occurs, with many single-hole breakdowns taking place each time the voltage is increased. Micrographs of top electrode damage which can be seen in figure 17b indicate that this is indeed the process responsible.

At higher voltages the discontinuous drops in current start to occur. We shall refer to these as burnouts to distinguish between them and normal breakdown. It was observed for devices on the same substrate that the value of the voltage for the first burnout (which will be referred to as V_{β} to differentiate between it and the normally quoted breakdown voltage V_B) occurred at approximately the same voltage. This was also true for devices on different substrates and with different insulator thicknesses (see 3.2.1). Thus the value of V_{β} or (1) in figure 12 appears to

be a particular device property and is not of a random nature. The later burnouts (2) and (3) did not show this consistency however and appeared at random voltages after the first. It is clear from the earlier discussion that these are not the result of progressive single-hole breakdowns. It is more likely that V_{β} corresponds in some way to maximum-voltage breakdown, although whether this is of a thermal nature or multiple single-hole breakdown is not clear. Large scale destruction of the insulator occurs although complete failure rarely takes place at the voltage V_{β} . This is probably because breakdown does not occur over the whole insulator thickness (as discussed in sections 3.2.1 and 3.2.3) leaving part of the insulator intact. This may well be due to conduction of heat away from the breakdown area by the remaining insulator, if we assume that the burnout is of a thermal nature. As a result of the first burnout the potential distribution within the insulator as well as the structural features will be drastically changed. The value at which further burnouts occur will depend primarily on the previous burnout history and this will occur at unpredictable voltages after V_{β} .

Clearly the variation of V_{β} with insulator thickness and temperature, as well as the variation in potential distribution after a burnout are of importance. These aspects are described in sections 3.2.1, 3.2.2 and 3.2.3 respectively.

3.1.2 Time Dependence of I_c and I_e

The variations of I_c and I_e with time (t) were taken immediately after forming. There appeared to be a difference in the time dependence of I_c depending on whether the voltage level corresponded to the current maximum at V_m , or the current minimum at V_u . In

figure 14, the variations of I_c with t during a period of over 50 hours ($1.8 \cdot 10^5$ s) are shown for Au-SiO_x-Au films of thickness 1000\AA . Figure 14a shows the variation of the maximum current when $V_m = 3.4$ V; figure 14b shows the variation of the minimum current with $V_u = 10$ V. Unfortunately both these sets of results could not be obtained on the same device, because running the device for long periods generally increases the conductivity and subsequent traces would not therefore give comparable results; however both the traces shown were obtained from nominally identical devices on the same substrate, and are representative of more than thirty such traces.

Both of the curves show an increase in current with time. This levelled off to a maximum and then decreased in the case of $V_b = V_m$, but continued to increase until the test was terminated when $V_b = V_u$. The different degree of current increase after an arbitrary time period (say 10^4 s) is vastly different for the two traces. For V_m the current level is approximately 3 times the original value, while for V_u the current increases by a factor of 13.

An increasing value of I_c with t strongly indicates that a continuous forming process is in operation. Lomax and Simmons⁴⁰ observed similar continuous forming phenomena and suggested that final device failure may be due to dielectric breakdown initiated by the increased current levels. Clearly any of the models involving atomic re-arrangement or ion injection will be susceptible to variations in I_c with t . The model of Hickmott does not appear to be applicable as conduction is limited by the number of structural faults and foreign atoms introduced into the insulator during preparation. The model of Simmons et al appears to be somewhat more applicable to this type of behaviour, since the injection of

extra metal ions and thus an increase in the ion density in the insulator is possible. However Verderber et al¹⁷ have postulated that the degree of forming depends on the solubility of the metal in the insulator; Simmons and Verderber² have proposed that the density of injected ions is a function of temperature and voltage (and not of time). On this basis then, time dependent behaviour is unlikely. More concrete evidence against this type of model is afforded by the work of Dearnaley et al⁴³. They have shown, by means of Rutherford back-scattering, that formed SiO_x from devices with one Au electrode does not contain nearly a sufficient number of Au ions to support Simmons' theory.

The models of Greene et al and Pivot et al are both dependent on ionic motion. Although in Greene's model there is not significant contribution to I_c from an ionic current (the current is carried by tunnelling between defect sites of the F-centre type produced as a result of negative ion discharge at the anode) the density of such sites will be dependent on the ionic conduction process. It is well known that if ionic transport is the main conduction mechanism the resistivity of the film under a DC voltage will increase with time⁶ and thus a reduction in the current is predicted. Joffe¹¹² has suggested that a space-charge occurs at the electrodes due to undischarged carriers. The voltage is then dropped over the space-charge and a uniform field across the insulator (assumed in equation (1.1)) does not remain. The current falls as a result of the ionic space-charge. A second explanation suggests that a dielectric relaxation process is responsible. The initial current is then the sum of the value given by equation (1.1) and a further transient relaxation term. As the time increases the transient term decreases and we are left with the steady state ionic current. The discrepancy

between the current-time measurements in formed material and the established current variations in ionic conductors makes it unlikely that ionic conduction is the principle mechanism involved.

Previous observations of variations in current levels have been explained in terms of the filamentary theory by Sutherland et al^{73,88}. They observed variations in the value of V_m after running ZnS and CdS devices for a few minutes at V_u . They suggested that this could be due to a change in the filamentary distribution caused by the application of the steady voltage. This causes the destruction of the most highly conducting filaments, while additional positive centres are created in the remaining filaments; this reduces the average effective spacing between the centres.

In the present case similar variations in the value of V_m are not apparent and thus a permanent change in the distribution of filament resistances is not implied. In figure 14a there is a steady increase in current up to $5 \cdot 10^4$ s. This may be ascribed to re-joining of broken filaments and the field induced growth of new filaments. The broken filaments will be those with original resistances between ρ_T , given by equation (1.43), thus

$$\rho_T = \frac{\tau_c a'' V_T^2}{T_{max} - T_o}$$

and ρ_m where

$$\rho_m = \frac{\tau_c a'' V_m^2}{T_{max} - T_o} \quad (3.1)$$

ρ_m is the solution for ρ_{min} in equation (1.40) when $V_b = V_m$. Clearly any filaments re-joining with values of $\rho < \rho_m$ will again rupture as a result of the high temperature generated at the weak spots. Thus

only filaments which re-join with $\rho > \rho_m$ will be capable of carrying current. After a period of time, however, the broken filaments will again re-join and will continue to do so until most of them become re-established with a suitable resistance $\rho > \rho_m$. Due to the close value of ρ_m and ρ_T the proportion of broken filaments at $t = 0$ and voltage V_m will be fairly small. The main contribution to the increase in current is probably due to the establishment of new filaments. These will propagate at a low rate from relatively unfavourable nucleation sites (all the favourable sites will have associated filaments established during the original forming process). The decrease in current after $5 \cdot 10^4$ s is clearly of a permanent nature and persisted for approximately 40 hours, after which the test was terminated. Dielectric breakdown is unlikely, especially at the low voltage level, V_m . The following point may be of importance in explaining this time dependent failure mechanism. We refer to the model of Dearnaley et al in section 1.5.5. For any voltage $V_b > V_T$ there will, at $t = 0$, be some broken filaments because of thermal rupture. The minimum resistance of an unbroken filament at voltage V_b is given by equation (1.40)

$$\rho_{\min} = \frac{\tau_c a'' V_b^2}{T_{\max} - T_o}$$

The maximum current flow through a filament at V_b must then be V_b/ρ_{\min} or

$$I_{\max} = \frac{T_{\max} - T_o}{\tau_c a''} \frac{1}{V_b} \quad (3.2)$$

We then postulate that the probability of permanent destruction of a single filament (where this means that the filament cannot subsequently

re-join under any circumstances) increases with the current density through the filament. The actual mechanism is not clear although gradual evaporation of the electrode at high current density regions is probable. This is reasonable in view of the fact that permanent destruction most probably takes place at the electrode, otherwise re-joining is always possible. Since $V_u > V_m$, and using equation (3.2)

$$I_{\max}(V_m) > I_{\max}(V_u) \quad (3.3)$$

The rate of permanent filament destruction will depend on the probability of destruction of a single filament as well as the number of filaments. Since both these variables are initially higher at V_m , the rate of filament destruction will be higher. When the rate of permanent filament destruction exceeds the rate of re-joining and establishment of new filaments, the circulating current will fall as is observed in figure 14a.

Initially at $V_b = V_u$ most of the filaments are ruptured. However, we have assumed that re-joining of filaments will occur after long time periods and that eventually all the filaments will re-join with new resistances greater than ρ_u , which is given by equation (1.44)

$$\rho_u = \frac{\tau_c a'' V_u^2}{T_{\max} - T_o}$$

This partially explains the much greater increase in I_c with t at V_u in figure 14b. At V_m most of the filaments are joined, only those with resistances between ρ_T and ρ_m are capable of re-joining. At V_u nearly all the filaments are ruptured and so the capacity for

filament re-joining is greatly increased. Furthermore, establishment of extra filaments at V_u is more probable than at V_m due to the increased field in the insulator. The rapid increase in I_c with t will thus mask any small current decreases due to permanent filament destruction as discussed earlier. Over longer time periods, when all the filaments have re-joined and the current increase from the establishment of new filaments is outweighed by the decrease due to permanent filament destruction, it may be possible to detect a decrease in current. This was not apparent in the present study where the maximum time for which devices were tested was approximately 50 hours.

We have assumed that over long time periods ruptured filaments can re-join under the action of the field even though their original resistance may have been less than ρ_{min} . The re-joined filaments will be of resistance $\rho > \rho_{min}$ where ρ_{min} is given by equation (1.40). It follows therefore that the distribution of filament resistances will vary with time, and shift towards increasing resistance with increasing time. Sutherland⁷³ has shown that this leads to an increasing value of V_m , but this was not evident in the present work. Therefore at low voltages the low resistance filaments must re-establish themselves. This will be easier for filaments which have re-joined at higher voltages than for filaments which remain broken. Clearly, there must also be a mechanism whereby high resistance filaments do not gradually thicken up at the high field weak spots, thus causing a shift to lower filament resistances. In actual fact the weak spot dimensions of the filament cannot increase to such a value that the thickness of the remaining filament is exceeded. Thus the filament resistance is unlikely to be much less than its original resistance immediately after forming.

A comparison between the results of Sutherland et al^{73,88} and the present results provides some interesting contrasts. In ZnS and CdS the observed variation in the value of V_m was ascribed to the permanent rupture of low resistance filaments after having run the device for several minutes at V_u . A similar explanation was proposed above for the decrease in I_c with time in figure 14a. In this case permanent filament destruction was considered more probable at V_m than at V_u because of the greater number of conducting filaments and a higher maximum current density per filament at the lower voltage. Nevertheless, even at the more favourable voltage level for permanent filament destruction, this did not become detectable until after several hours, while a similar effect was observed by Sutherland after a few minutes at unfavourable voltage levels in sulphides. The permanent destruction of low resistance filaments therefore appears to take place far more quickly in sulphides than in SiO_x . This is probably determined by the actual conduction mechanism through the filaments. - If a filamentary band structure model of a type similar to that proposed by Ralph and Woodcock⁵ is assumed then the current flow through a filament will depend, at least in part, on the conductivity of the semiconductor or insulator. Filaments in a semiconductor will therefore carry a much higher current density than those in an insulator, thus indicating why the permanent destruction of filaments occurs at a higher rate than in SiO_x .

In SiO_x the rate of re-joining and establishment of extra filaments appears to be higher than in sulphides. If the re-joining rate was as high in sulphides as in SiO_x we would expect the re-establishment of low resistance filaments at lower voltages, as suggested earlier for SiO_x . There would not then be the shift to

higher resistances, which appears to be characteristic of sulphides. Similarly a high rate of filament establishment and re-joining, sufficient to mask the fall in current due to the permanent destruction of filaments, would increase the time necessary to shift the filamentary distribution to higher resistances. The higher rate of filament establishment and re-joining in SiO_x is most probably dependent on the ease of forming of the particular insulator or semiconductor. Sutherland⁸⁹ has suggested that the establishment of conducting filaments will occur most readily in materials which show a high degree of ionic bonding. An estimate of this can be obtained from equation (1.12) and the percentage ionic character of the various substances considered is CdS (15%), ZnS (19%) and SiO_x (55%). We would therefore expect a higher degree of filament establishment and re-joining in SiO_x from this theory. Indeed Sutherland has suggested that forming in sulphides is probably only possible at all (in view of the low ionic character) because of the diffusion of electrode material into the insulator as a result of the power dissipated in the two-stage forming process characteristic of sulphides.

It thus appears that the differences between the results for sulphides and SiO_x depend on the rate of permanent filament destruction and also on the rates of filament establishment and re-joining after the original forming process. In sulphides, which show a high rate of filament destruction and low rate of establishment and re-joining of filaments, a shift to higher filament resistances occurs within a few minutes; in SiO_x where the filaments are more stable and can propagate and re-join relatively easily this does not occur. Instead an increase in I_c with t occurs until the permanent destruction rate becomes significant after a period of several hours.

Variations in the value of I_e with t were not reproducible between samples although some factors were common to all samples. Figure 15a shows the variation of I_e at the voltage for maximum current, $V_m = 3.4$ V. The sharp drop in I_e over the first 10^3 s was evident in most of the samples tested, although the variations in I_e after that time differed widely between samples. Clearly there is no direct correlation between the behaviour of I_c and I_e , I_c increasing and I_e falling in the initial 10^3 s. Since it is extremely likely that regions of the device where the local temperature or electric field is high will be areas of high electron emission (caused by thermionic or field emission) and since these regions are those most likely to suffer early destruction (by filament melting or localised dielectric breakdown) it is probable that the initial high emission current is a consequence of the high emission efficiency of such regions. These are quickly destroyed during the initial stages of running the device. A corresponding drop in I_c is not evident since such regions are not necessarily regions of high current density. Further evidence of the initial destruction of regions of high emission efficiency was obtained when the variation of I_e with t was repeated. Such traces did not show the fall in I_c in the first 10^3 s, suggesting that the regions had already been destroyed during the earlier measurements. At values of t in excess of 10^3 s the emission is thus from the more stable device areas. The fluctuations in I_e could not be accounted for in terms of corresponding fluctuations in I_c , and are most probably due to field variations in the insulator. Such spontaneous variations in the field distribution have been observed, and are described in section 3.2.3.

At V_u the initial drop in I_e was not observed. A typical example is shown in figure 15b, where $V_u = 12$ V. At higher voltages it is

probable that nearly all the regions of high emission efficiency are already destroyed due to the high field. Similar random variations were obtained as at V_m , although at V_u the amount of variation was greater. The shape of the curve in figure 15b is by no means characteristic of all the devices tested at the higher voltage. Many curves fell below the initial level of I_e and then rose after a period of time. Also the value of I_e was often increasing when the test was terminated, instead of decreasing as in figure 15b. All that can be said about these measurements is that over a period of over 10^5 s there was a slow random variation in I_e of a similar nature to that observed at V_m . The greater variation in I_e at V_u is most probably a consequence of more local field variations, resulting from the higher applied voltage.

3.1.3 Device Temperature During Operation

In order to test the possibility of elevated temperatures within the sample which may lead to thermal breakdown at high voltages, a thermocouple was attached to some devices and the device temperature (T_c) monitored. Typical results are shown in figure 16 where I_c is also plotted for comparison. The temperature was allowed to stabilise after each increase in voltage, so that steady state conditions were achieved.

As expected the temperature increased as I_c increased; this is merely a consequence of Joule heat dissipation within the device and is not considered an important factor in breakdown, since this region of the curve is normally traversed without destruction. More significant is the increase in temperature in the voltage range 17-22 V, while the current level continued to fall. The slope of the T_c - V_b curve increases rapidly in this range, indicating the

onset of a rapid temperature rise within the device. A steady state value of T_c and I_c was obtained at 22 V, but when the voltage was increased to 22.2 V burnout occurred, and T_c and I_c subsequently fell to new levels. Due to the very short time of breakdown processes (about $80 \mu s^{97}$) no catastrophic increase in T_c or I_c could be observed. However the increase in device temperature, which nearly always accompanied device burnout, is a strong indication of the existence of abnormal thermal processes within the insulator. Such processes may well lead to thermal breakdown behaviour.

Note this type of behaviour is different from that observed in Al-SiO_x/B₂O₃-Al devices (see 3.5.1). For these devices I_e falls at high voltages, and this can be ascribed to a spreading out of the high field region. Under these circumstances such abnormal behaviour may not occur, and thus there is no increase in temperature at higher voltages.

3.1.4 Microscopic Investigation of Device Damage

Observation of the top electrode after subjecting samples to various different voltage levels, gives an interesting insight into the destructive processes occurring in such samples. New samples which are not formed show a uniform surface region with few visible faults. After forming the general pattern is similar, and breakdown holes and peeling of the top electrode are not in evidence.

After forming some samples were cycled at voltages up to V_m , and were subsequently run at that voltage for a few minutes. In no case was the voltage allowed to exceed 8 V. Observation of such samples under the microscope revealed some areas of the device which had escaped damage, while other regions showed many areas of localised wrinkling. A photomicrograph of such areas is shown in figure 17a.

The wrinkled areas were typically 100 μm in diameter; the top electrode was not penetrated and the localised regions did not link up to form larger areas. The existence of such regions is probably due to non-uniform heating of certain areas of the device, due to the high current passed at V_m which could lead to non-uniform expansion of the top electrode. The evolution of oxygen may also contribute to the appearance of such areas⁷⁵.

(When higher voltages are applied to the device different types of destructive behaviour are observed. When a maximum of 10 V was applied no new features other than those in figure 17a appeared, but when the maximum voltage was raised to 15 V many single-hole breakdown spots were observed. These are shown in figure 17b. Typically the diameter of such breakdown holes was 10-50 μm although the large hole at the bottom left-hand corner was nearer 100 μm in diameter. Similar single-hole breakdowns of diameter 10-100 μm were observed in SiO films by Budenstein and Hayes⁷⁵. The outer region of the breakdown hole corresponds to vaporisation of the top electrode. The darker region in the centre of the hole is a destructive area penetrating right through to the other side of the device. Smaller single-hole breakdowns often nucleate on the edges of existing holes (in accordance with Budenstein and Hayes¹⁰⁸) and an example of this is visible on the right-hand side of the picture. As the maximum voltage level is increased the density of such breakdowns increases and large areas of the top electrode are destroyed. The falling current in figure 13d is undoubtedly a consequence of such localised destruction.

In figure 17c a micrograph of electrode damage is shown for a device which had been repeatedly cycled up to 20 V and left at that voltage level for a period of 48 hours. Such a picture is typical

of devices which have been used for long periods (such as those used for the time dependence measurements in section 3.1.2), but which have not exceeded the burnout voltage. Large device areas are seen to be destroyed probably as a result of a link up of many single-hole breakdowns of the type in figure 17b. The long striations on the right-hand side of the picture indicate a method of propagation of such areas. New single-hole breakdown areas nucleate at the peripheries of existing holes (as in figure 17b) causing a growth of the breakdown chain. The striations are of width approximately $50 \mu\text{m}$ which is of the order of breakdown holes. Crossing of such breakdown areas can electrically isolate many areas of the electrodes (even though they may not be destroyed) making an even greater contribution to the fall in current.

Conversely figure 17d shows a device which has been run for only a few minutes, but where the burnout voltage has just been exceeded. Note in this case there is no tendency for the breakdown holes to link up, and the difference between this and the previous photograph appears to be the different lengths of time for which the voltages were applied. Large scale linking up of breakdown areas in these devices is therefore a time dependent process at voltages less than V_{β} . The other interesting feature of figure 17d is the wrinkling of the top electrode around the breakdown areas on the left-hand side of the picture. Such behaviour was not observed in devices which had not exceeded V_{β} , but was frequently observed when V_{β} had been exceeded. The appearance of such wrinkling, which is visually distinguishable from the type observed after V_m in figure 17a, must therefore be connected with the burnout process. Increased temperatures at V_{β} (see 3.1.3) and also significantly at V_m , are most probably contributory factors to this type of behaviour. Current densities around the

breakdown areas are likely to be higher than the average, due to localised melting of the electrode and the destruction of part of the insulator, and thus the temperature in these areas is probably higher than that in the bulk of the device. The burnout process, which is accompanied by an increase in temperature, is thus indicated by wrinkling of the top electrode around previously destroyed single-hole breakdown areas, where the current density and thus the temperature is probably higher than in the bulk.

In figure 17e the top electrode surface is shown, of a device where a voltage of 35 V had been maintained for several minutes. The general features visible in figure 17d are still apparent as scattered areas of destroyed material. However the wrinkling around the breakdown spots has mostly disappeared. Why this is so is not clear, as the temperature and current density above V_{β} are lower than at lower voltages. Even at this high voltage breakdown areas have not linked up to the extent of those in figure 17c, however some overlapping of breakdown areas is visible on the left-hand side of the picture, where a small area of wrinkled top electrode is still visible. The main features appearing in this figure are the straight "tunnels" between breakdown areas (top right-hand area of picture) and also the meandering paths (bottom left-hand area close to overlapping breakdown areas). Also visible are many small dots in the breakdown areas. An enlarged view of part of the device in figure 17e is shown in figure 17f.

This shows a tunnel (bottom centre) between two breakdown areas. The diameter is approximately 12 μm , which is considerably less than the typical size of breakdown areas. Figure 17e shows that the diameter of most tunnels is approximately the same. Detailed observation reveals that the tunnels are in fact raised regions of the

top electrode, which often form a path between breakdown areas. The top of the tunnel is out of focus in figure 17f, indicating that it is raised above the plane of the top electrode. Comparison of the tunnels with the wrinkling in figure 17a, shows them to be of essentially the same diameter, and their origin is probably thermal in nature. Significantly they are always joined at one end to a breakdown area where the current density is probably high. There is no evidence of actual breakdown behaviour beneath the tunnel regions, although the wrinkling of the top electrode might be as a result of a heat dissipating process in the insulating layer or the bottom metal electrode. The evolution of oxygen as suggested for figure 17a may also contribute to the appearance of the tunnel regions.

An enlarged view of a meandering path in the top electrode is visible on the top right-hand corner of figure 17f and is of diameter 3 μm . This appears to be evaporation of the top electrode. In common with the tunnels these paths are always connected to a breakdown area and are probably the result of electrode melting initiated at the breakdown.

Finally the appearance of small dots in the breakdown regions is typical of many devices. These are shown as small spherical objects in figure 17f. The diameter of these dots is a maximum of 1.5 μm . These globules are very similar to balls of crystalline silicon which are often found at breakdown areas⁷⁵. Typically the diameter of such crystalline regions is 0.1-2.0 μm . They are usually situated at the end of a dark track, indicating movement of the globule across the burned-out insulator region.

To summarise, photomicrographs of breakdown areas show many features common to breakdown processes in Al-SiO-Al capacitors. These include single-hole breakdowns, nucleation of new breakdowns

on the edges of existing ones, and the appearance of globules (probably of crystalline silicon) in the breakdown regions. In addition wrinkling of the top electrode occurs when the device temperature rises at V_m and V_β , and in the latter case this occurs mainly at the edges of existing breakdown holes.

3.2 The High Field Region

3.2.1 Dependence of V_β on Insulator Thickness

In section 3.1.1 various mechanisms of dielectric breakdown were discussed in order to explain the behaviour in the second falling current region and the existence of burnouts exhibited in figure 12. It was concluded that these two effects originated from different types of dielectric breakdown, and the micrographs in figure 17 support this view. In the decreasing current range an increase in voltage produces additional single-hole breakdown areas, whereas when the device voltage is made to exceed V_β similar additional single-hole breakdown spots are not apparent. In order to investigate the behaviour of V_β further, a series of sets of devices was fabricated with insulator thicknesses varying from 100 to over 6000 Å. Each substrate supported nine devices and thus each value of V_β for a set of devices was the average of nine such determinations. In figure 18 the variation of V_β with insulator thickness d is shown. The points are the average values of V_β on a particular substrate and the extent of the error bars indicate the spread of values on that substrate.

It is apparent that within experimental error the value of V_β remains constant over the entire insulator thickness range. Furthermore the average field when the first burnout occurs varies between $2.5 \times 10^7 \text{ V cm}^{-1}$ and $3 \times 10^5 \text{ V cm}^{-1}$. In un-formed materials

the breakdown field normally decreases with insulating thickness and frequently a relation of the type $F_B \propto d^{-\frac{1}{2}}$ is obeyed^{75,109,111}.

F_B is the average field across the dielectric layer. More generally a relation of the type $F_B \propto d^{-\gamma}$ obtains¹¹⁰ and the value of γ

typically ranges from 0.3-0.65. Clearly a correlation between this type of relation and the above results will only occur if $\gamma = 1$.

The justification for assuming such a fortuitous variation of F_B with d is slim in view of the following. Firstly the thickness

range over which such theories are normally applied is between

$1-10^4 \mu\text{m}$ (10^4-10^8 \AA) which is greatly in excess of the thickness range to which the present results pertain ($10^2-6 \cdot 10^3 \text{ \AA}$). Secondly

the temperature variation of V_B is more in accordance with thermal

breakdown characteristics than with electric breakdowns predicted

by the Forlani-Minnaja theory¹¹⁰ (see 3.2.2). Thirdly the assumption

that the field is uniform within the insulator in formed materials

is undoubtedly unjustified. The experimental results of Hickmott³²

and Gundlach and Kadlec⁹¹ both suggest that most of the voltage is

dropped over a high field region. Similar results were obtained

in the present study and are described more fully in section 3.2.3.

Furthermore, both the theories of Hickmott and Barriac et al⁴⁹ predict

the existence of a high field region within the insulator. In the

latter case this saturates to a constant thickness at a voltage

less than V_m . An explanation of the experimental results based on

the assumption of a high field region within the insulator thus

appears to be more applicable to formed materials than a theory

which does not take into account the existence of the high field

region. Assuming that the high field region is the region where

breakdown is initiated, the constancy of V_B with d can be explained

in one of two ways. Either the thickness of the high field region

(δ) remains constant with V_b and the burnout occurs when the voltage distribution is such that an intrinsic burnout field (F_β) is applied across the high field region; or F_β varies with δ in some way analagous to that predicted by the Forlani-Minnaja theory and δ varies with V_b in such a way that the variation of F_β with δ is largely cancelled out. While distinguishing between these two alternatives is extremely difficult without much more experimental work on the subject, the following maximum experimental values of δ have been obtained. Hickmott³² obtained a value of 120 Å in formed SiO, while Gundlach and Kadlec⁹¹ observed the entire high field region in a nine monolayers thick layer of cadmium arachidate (234 Å). In the present study the thinnest SiO_x layer in which the high field region was observed was 310 Å (see 3.2.3). Thus the maximum value of δ does not appear to exceed 310 Å in SiO_x. Furthermore if we assume that δ is approximately 100 Å the field across the region at a burnout voltage of 25 V is $2.5 \cdot 10^7$ V cm⁻¹. This is considerably higher than the typical breakdown voltage of 10^6 V cm⁻¹ in un-formed materials^{109,111}, although it does represent an estimate of the dielectric strength of the high field region in formed SiO_x. A lower value of δ at lower voltages would probably lead to increased fields in the insulator, thus initiating breakdown at lower voltages. Similarly the probability of tunnelling through the layer, with a subsequent rise in current, would be increased at low values of δ . Thus in the absence of any evidence to the contrary, the simpler explanation that δ remains constant with V_b near the burnout voltage will be assumed. The maximum limit of δ is fairly well defined, but there are no experimental measurements of the minimum limit.

On the above assumption a tentative explanation of the breakdown process can be proposed. On forming a high field region is set up at some region in the insulator. This is of thickness δ and probably remains roughly constant with voltage and temperature. Both self-healing and maximum-voltage breakdown processes are initiated in the high field region. Self-healing breakdowns will penetrate completely through the remaining insulator in the lower field regions. Destruction of layers many times the thickness of the breakdown layer have previously been reported¹⁰⁹. A maximum-voltage breakdown will occur when the field across the high field region reaches a particular value, F_{β} ; the burnout voltage V_{β} will then be given by $V_{\beta} = F_{\beta} \delta$. Destruction of that region is most likely due to thermal runaway or multiple single-hole breakdowns (see 3.2.3). Complete device destruction does not occur since the low field region may well escape relatively undamaged.

3.2.2 Dependence of V_{β} on Temperature

Since it appears probable that the burnout voltage signifies the onset of a breakdown process originating in a high field region of the insulator, a study of the temperature dependence of V_{β} should give an indication whether such an assumption is correct. Figure 19 shows the dependence of V_{β} on T over a range of 80-360 K. Such a variation of average breakdown field F_{β} , with T is characteristic of thermal dielectric breakdown. It is not possible to plot the actual field in the high field region in figure 19, since the thickness δ is unknown; if a thickness of 100 \AA is considered the field when 70 V is applied is $7 \times 10^7 \text{ V cm}^{-1}$. Although this is high, a dielectric strength of $4 \times 10^7 \text{ V cm}^{-1}$ has been observed in SiO_2 films¹¹³. In the present study, where the structure of

the oxide is undetermined, a field of this magnitude may not be unreasonable.

Electric breakdowns, which have been identified from the linear dependence of F_B on $d^{-\frac{1}{2}}$ do not show the type of temperature dependence shown in figure 19. SiO capacitors in the thickness range 1200-9600 Å normally show a temperature independent value of F_B from 80-310 K^{75,109}. There is no correlation between conduction before breakdown and during breakdown, pre-breakdown conduction being strongly temperature dependent. It is unlikely therefore that this type of breakdown mechanism is responsible for device burnouts in formed SiO_x devices.

A comparison of the temperature dependence of figure 19 with published work for thermal breakdowns is a more promising exercise. Klein and Gafni¹¹⁴ observed a roughly linear variation of F_B with T in SiO films. Departures from linearity were taken to be due to the variation of the thermal conductance of the film with T. Sze¹¹⁵ observed a linear variation of $F_B^{\frac{1}{2}}$ with T in Si₃N₄ films. Both these sets of results were attributed to thermal dielectric breakdown, and the thermal breakdown field was calculated in the following way. The structure is assumed to reach an equilibrium temperature under steady state conditions. This is given by equating the Joule heat with heat losses. Following Klein and Gafni¹¹⁴

$$\sigma \frac{A}{h} V_b^2 = \Gamma (T_c - T) \quad (3.4)$$

where A is the effective capacitor area, h the effective device insulator thickness, Γ the thermal conductance of the device and T_c and T the respective device and ambient temperatures. An empirically determined variation of conductivity σ with field and temperature can then be substituted into equation (3.4). Equation (3.4) can then

be solved by plotting the Joule heat for different values of the field, and also the heat lost against T_c . The points of intersection of the heat loss line with the Joule heat curves give the equilibrium temperature for different values of the electric field. The field for which the Joule heat curve is a tangent to the heat loss line is the maximum field which can be applied without destruction. At a certain temperature (which corresponds to the field F_B) the derivatives with respect to T_c of both sides of equation (3.4) will be equal. From the equation thus obtained and from equation (3.4) the temperature variation of F_B can be obtained. The different types of variation obtained by Klein and Gafni and Sze occur because of the different functions for σ which were used. In the present case no generally accepted equation for the variation of σ has been proposed and a similar calculation for F_B cannot be performed. However a plot of $V_\beta^{\frac{1}{2}}$ against T gives a series of points through which a straight line can be drawn (see figure 20). Clearly this is not sufficient justification for assuming that a conduction relation of the type proposed for Si_3N_4 by Sze applies. It does however indicate that a systematic variation exists between V_β and T , in spite of possible variations of δ with V_b and T , F_β with δ and Γ with T . An increased value of burnout voltage at low temperatures (which is characteristic of thermal breakdown due to better heat conduction) is clearly apparent.

The fact that breakdown does not occur at V_m where the energy dissipation is generally higher than at the burnout voltage is an interesting feature of these devices. At V_m there is a mechanism whereby the power dissipation is reduced; melting of high resistance regions of the filaments leads to a decrease in the current flow. At the higher voltage most of the current is not carried by filaments

and such a limiting mechanism does not take place. Instead the power dissipation continues to rise leading to breakdown.

To summarise, the temperature dependence of V_{β} is not in accordance with that observed for single-hole dielectric breakdowns. The continuous fall of V_{β} with T is characteristic of thermal dielectric breakdown, and the results are not at variance with a thermal breakdown process originating in the high field region of the insulator. A direct comparison of results such as these with thermal breakdown theory cannot be attempted until the thickness of the high field region is better established and a suitable expression for σ is proposed.

3.2.3 Potential Distribution Measurements

In view of the earlier suggestion that there exists within the insulator a high field region, it was decided to attempt to observe any non-linearity in the internal field. The structure used was Au-SiO_x-Al-SiO_x-Au. Al was used for the centre (grid) electrode as this is a metal which normally shows poor forming properties and would therefore be less likely to induce forming between the negative (cathode) or positive (plate) electrodes. The grid was used only for potential measurements and voltages were not applied directly to the grid. Devices were always formed directly between cathode and plate. The voltage between cathode and grid will be referred to as V_{cg} and that between grid and plate as V_{gp} . V_{cp} is the voltage across the whole device and corresponds to V_b in diodes.

Figure 21 shows the variation of V_{cg} and V_{gp} with V_{cp} for an un-formed device of total thickness 1700 Å. The cathode-grid region was of thickness 1360 Å and the grid-plate region 340 Å. At low

voltages the curves are nearly linear and the potential divides in the ratio 1:3.3 (at $V_{cp} = 3$ V). This compares with 1:4 for the ratios of the thicknesses and is typical of results obtained on more than fifty samples. Thus at low voltages the voltage divides over the two layers in approximately the same ratio as their thicknesses. A similar correlation has been observed by Hickmott³² and Gundlach and Kadlec⁹¹.

As the voltage was increased the $V_{gp} - V_{cp}$ curve became increasingly sublinear, while an increasing proportion of the voltage was dropped over the cathode-grid region. Thus there is a steady increase in the relative resistance of the cathode-grid region as V_{cp} increases, and there are occasional more noticeable changes in the potential distribution. This is apparent in figure 21 at 3.9 V (arrowed). After the appearance of such instabilities the device formed at $V_F = 4.7$ V and a dramatic change in the potential distribution occurred. Nearly the whole of the voltage was dropped over the cathode-grid region leaving a voltage drop of initially only 3 mV over the grid-plate region.

Over a wide range of triode structures with insulating layers of thickness varying between 150 and 5000 Å, the following general properties of the forming process emerged. At low voltages the potential distribution was essentially uniform and divided over the insulating layers in proportion to their thicknesses. As the voltage was increased the potential distribution became increasingly non-linear, until after forming nearly the entire voltage was dropped over one region. The location of the region of high voltage drop did not necessarily occur in the cathode-plate region. In the majority of samples tested by Hickmott this was the case, although it was recognised that the high field region could exist in the

grid-plate region and that field emission from the cathode was not therefore the process responsible for the negative resistance characteristics. The present results are more in agreement with the results of Gundlach and Kadlec where there was no preferred location for the high field region. Indeed, in the present case the high field region was nearly always in the thicker of the two insulating regions irrespective of whether this was the cathode-grid or grid-plate region. (To check this on each substrate half of the devices were connected so that the thin region was the cathode-grid region; the other half were connected so that the thin region was the grid-plate region). In no case where the thick region was more than twice the thickness of the thin region did the high field region appear in the thin region. As the thicknesses of the two regions became more equal the number of cases where the high field region occurred in the thin region increased. For example, for a set of fourteen devices with insulating layers of 620 and 930 Å (ratio of thicknesses = 1.50) the proportion of devices showing the high field region in the thin layer was 28.6%. A set of devices with thicknesses 200 and 250 Å (ratio of thicknesses = 1.25) the proportion was 42.8%. The location of the high field region within the insulator appears to be of a random statistical nature, determined only by the thicknesses of the two layers. A further explanation suggested by Gundlach and Kadlec that the position of the high field region is determined by the symmetry (or otherwise) of the triode structure is also possible. In the present case and in the case of the results of Gundlach and Kadlec both the cathode and plate were of the same material. Conversely Hickmott used Al for the cathode and Au for the plate electrode. The preponderance of the high

field region in the cathode region may have therefore been due to the assymetrical nature of the devices tested.

The performance of a typical device after the establishment of the high field region in the cathode-grid region is shown in figure 22. The cathode-grid region was of thickness 1360 \AA while the grid-plate region was 340 \AA . I_c (figure 22a) is very similar to the curve shown in figure 12 for a diode structure, exhibiting VCNR behaviour and a burnout at 22 V. The value of V_m is somewhat higher than that associated with diodes, and such minor deviations from normal diode behaviour were sometimes observed in triodes. However, the normal features of diode behaviour were retained. Figure 22b shows the voltage drop over the cathode-grid region. This is nearly the whole of the applied voltage and is much in excess of the 80% of the voltage drop expected from the relative insulating layer thicknesses. The existence of a high resistance region in the cathode-grid region is indicated by this behaviour. Figure 22c shows the behaviour of V_{gp} with V_{cp} . The variations of V_{gp} with V_{cp} follow I_c almost exactly, and the resistance in the grid-plate region remained constant at all points in the I_c - V_{cp} curve. This is compatible with ohmic filamentary conduction in the thin low resistance region, providing the conduction process is dominated by processes in the high field region.

So far the present results have confirmed the results of Hickmott and Gundlach and Kadlec and show that the field is non-linear in the insulator, with most of the voltage being dropped in a high field region and ohmic conduction in the remaining low field region. The existence of such a region was suggested in the discussion in sections 3.2.1 and 3.2.2. However, it was also postulated that destructive processes originate in the high field

region, and in order to confirm this V_{cp} was increased until the burnout voltage was exceeded. In the majority of cases the potential changed as shown in figure 22. (In exceptional circumstances a different shift in potential occurred, but only in devices which had shown anomalies in their $I_c - V_{cp}$ curves. These will be discussed later). The burnout was characterised by a fall in voltage in the low field region as a result of increased resistance in the high field region. Resistances in the grid-plate region were 2.34Ω before burnout and 2.2Ω after burnout. Such a variation is well within experimental error and thus it appears that the conductivity in the low field region is essentially unchanged by the burnout process. Conversely in the cathode-grid region the average resistance changed from $1.65 \cdot 10^4$ to $5.5 \cdot 10^4 \Omega$. Such a large permanent increase in the resistance in the high field region is a strong indication that destructive breakdown processes are initiated in that region. Burnout can then be defined as a permanent increase in resistance in the high field region.

Exceptionally burnout behaviour coincided with a drastic switch in the voltage drop from one side of the device to the other. This occurred only when the device also showed anomalous current peaks or shifts of the high field region at lower voltages. When this type of behaviour occurs the voltage drop slowly shifts to the previous low field region of the insulator. Typically after burnout the voltage drop in the previous high field region changed from 26.95 V to 2 mV while the voltage drop in the previous low field region increased from 42 mV to 27 V . Such a redistribution of voltage indicates the establishment of a very low resistance path in the previous high field region. The long time necessary for the redistribution to take place (up to 3 minutes) is suggestive

of a metallic diffusion process as a result of the high field region. This apparently occurs in a small number of devices (less than 5%) in preference to breakdown behaviour.

Such behaviour is readily distinguishable from normal burnouts by the associated anomalous behaviour in the $I_c - V_{cp}$ characteristics. The low incidence of such behaviour in diodes suggests that shorting of the high field region occurs primarily in triodes, where a low resistance contact between the grid and one of the metal contacts across the high field region, can occur.

The stability of the high field region at voltages less than V_β was also investigated. Occasionally spontaneous changes in the position of the high field region from one region to the other were observed. This did not produce an associated drop in I_c (as with the anomalous burnout behaviour) and would not be distinguishable in diodes. Such behaviour was also observed by Gundlach and Kadlec. The high field region could sometimes be moved into the previous low field region by reverse-biasing the structure. This did not always take place and such behaviour agrees with the results of Hickmott. However it was possible by this method to obtain an estimate of the maximum thickness of the high field region. Clearly when the high field region occurs in the thickest portion of the insulator (as normally happens), it is only possible to estimate the maximum thickness of the high field region as equal to the thickness of the insulator to which the high field region is confined; the average field over the two layers for the sample in figure 22 just before burnout was $1.62 \cdot 10^6 \text{ V cm}^{-1}$ in the thicker region and $8.25 \cdot 10^2 \text{ V cm}^{-1}$ in the thinner region. The actual field in the high field region which is confined in the thicker portion of the insulator is likely to be somewhat higher than the average value.

A more extreme example of the voltage drop being confined to a narrow region was observed in devices with insulator regions of thickness 5140 and 310 Å. Originally the voltage drop occurred in the 5140 Å region, which was adjacent to the cathode. After running the device at reverse bias for a number of hours the high field region had moved to the thinner region and the average field in the two regions at 20 V was $9 \times 10^2 \text{ V cm}^{-1}$ (thicker region) and $6.45 \times 10^6 \text{ V cm}^{-1}$ (thinner region). In this case the high field region was confined to a region of the insulator less than 6% of the total thickness.

The general conclusions obtained from the potential distribution measurements are

(i) Before forming the voltage drop is roughly proportional to the insulating layer thicknesses.

(ii) After forming nearly the whole voltage drop occurs in one region of the insulator (usually the thickest).

(iii) The average field in the high field region of the insulator is typically 3-4 orders of magnitude greater than in the low field region.

(iv) The higher field region may be shifted to the thinner region by reverse-biasing. This serves as a method of estimating the maximum thicknesses of the high field region, since it is then confined to a small proportion of the insulator thickness. There is evidence that the high field region can be contained in a region 310 Å thick, although the thickness of the high field region may be less than this.

(v) Burnouts occur when the resistance in the high field region discontinuously increases. The low field region of the insulator remains undamaged. The field in such a region is comparable to dielectric breakdown fields, and the variation

of V_{β} with insulator thickness and temperature (in sections 3.2.1 and 3.2.2) is further evidence of breakdown behaviour. Device temperature measured before burnout (section 3.1.3) indicates thermal breakdown behaviour.

3.2.4 Low Temperature Characteristics

Low temperature characteristics in Al_2O_3 have been observed by a number of authors^{19,25,36}. Similar effects have also been observed in SiO_2 . The results described below are in good qualitative agreement with the earlier results of Hickmott²⁵.

On decreasing the temperature the value of I_c fell. The negative resistance region persisted until the temperature fell below a certain critical value. This varied somewhat between samples but was usually in the range 180-230 K. At temperatures below the critical value the first characteristic was very similar to that at room temperature and an example is shown in figure 23a for a device of thickness 1800 Å at 210 K. Decreasing the voltage resulted in a high impedance reverse characteristic. Further tracing of the I_c-V_b characteristic for both forward and reverse directions resulted in a stable reproducible high impedance characteristic. In figure 23b this high impedance, low temperature characteristic is shown for the same device. This shows a very rapid increase in current of over 3 orders of magnitude in the voltage range up to 20 V. The low impedance negative resistance could not be obtained again at low temperatures, and could only be recovered by increasing the temperature above the critical value. In accordance with the results of Simmons and Verderber² devices showed irreversible thermal-voltage memory effects. The magnitude of I_c in the second and subsequent I_c-V_b traces was determined by

the maximum voltage to which the previous low temperature characteristic had been cycled. Thus the curve in figure 23b is the result of the first low temperature characteristic, where the voltage had not exceeded 20 V.

Simmons explains this behaviour in terms of a dead-time effect. Normally the memory state is erased when stored charge, which is injected under the original voltage bias and which subsequently tunnels towards the centre of the insulator at zero voltage, is swept away to the anode at V_T (see 1.5.2). The length of time the electrons take to tunnel to the centre of the insulator is given by the dead-time. The dead-time is inversely proportional to the phonon-assisted tunnelling probability, and at low temperatures this will be very low, effectively increasing the dead-time to very large values. Thus there is insufficient time for the stored charge to diffuse to the centre of the insulator, and the memory state cannot be erased, unless the dead-time is decreased by raising the temperature. Another explanation, also involving the release of trapped charge has been described by Dearnaley et al⁴³ (see 1.5.5). In this case the dead-time corresponds to the relaxation time of the polarised insulator. Only after the insulator is unpolarised are the filaments considered to be capable of re-joining and thus restoring the low impedance characteristic. Relaxation of the polarised insulator is assumed to be due to a thermally activated Poole-Frenkel effect, and a long dead-time is expected at low temperatures. Hence both the explanations of the disappearance of the low impedance characteristic and the negative resistance involve a temperature dependent dead-time, which corresponds to a movement of trapped charge in the insulator. However, as yet no detailed investigation of the high impedance $I_c - V_b$ characteristic has been attempted.

In the present case it was considered that an investigation into the conduction phenomena at low temperatures could be useful not only in explaining the low temperature device behaviour, but may also have some bearing on device properties where for some reason or other the normal conduction mechanism has been suppressed. Examples of this are at higher voltages where filaments are expected to be broken, or after very long time periods (of duration greater than that investigated in section 3.1.2) where permanent filament destruction may well have occurred. The behaviour of devices before forming may also fall into this category.

Devices were tested at voltages of up to 60-70 V. As this normally entailed going through at least one burnout event in the course of tracing the characteristic, the curves were taken on devices when the burnout had already occurred. This did not appear to alter the shape of the characteristics, although the value of I_c was always reduced after a burnout event.

Current-voltage curves were examined in the light of the various conduction mechanisms described in section 1.2, and a correlation was also attempted between $\log I_c$ and $\log V_b$ in order to determine whether a power law dependence of the type described by Jonscher¹¹⁶ and by Timson and Hogarth⁸⁷ applied. The only correlation that could be obtained was a linear variation between $\log I_c$ and $V_b^{\frac{1}{2}}$. This is normally an indication of Schottky or Poole-Frenkel mechanisms which are described by equations (1.4) and (1.5). Typical results are shown in figure 24, for two devices. Device A was of thickness 1800 Å at a temperature of 210 K and gave a value of $\beta = 1.39 \cdot 10^{-5} \text{ eV m}^{\frac{1}{2}} \text{ V}^{-\frac{1}{2}}$ in equation (1.5), for Poole-Frenkel conduction. Device B was of thickness 1400 Å at a temperature of 127 K and gave a value of $\beta = 0.88 \cdot 10^{-5} \text{ eV m}^{\frac{1}{2}} \text{ V}^{-\frac{1}{2}}$. Such values are considerably lower than

a value of $1.99 \cdot 10^{-5} \text{ eV} \cdot \text{m}^{\frac{1}{2}} \text{V}^{-\frac{1}{2}}$ which can be deduced from the published data of Simmons and Verderber² for an un-formed device of thickness 400 \AA at 300 K. No positive correlation can therefore be drawn between conduction processes in un-formed devices, and in formed devices at low temperatures.

The possibility of a Schottky effect in SiO has been discounted by the work of Jonscher and Ansari¹¹⁷. In general, the experimental values of β are midway between the theoretical values for β_S and β_{PF} and thus the numerical value of β is not really a good indication of the conduction mechanism responsible. A distinction can only be drawn if it is otherwise known whether the process is electrode or bulk limited. Current-voltage characteristics were taken by Jonscher and Ansari on a series of Al-SiO-Al, Cu, Ti or Mg devices. Irrespective of the electrode material these gave a value of $\beta = 2.2 \cdot 10^{-5} \text{ eV} \cdot \text{m}^{\frac{1}{2}} \text{V}^{-\frac{1}{2}}$. Thus the conduction process was not electrode dependent and was bulk limited. Similar experiments by Hartman et al¹¹⁸ and Hirose and Wada¹¹⁹ showed a similar independence of the current-voltage characteristic on the electrode material. Stuart¹²⁰ similarly concluded that conduction was bulk limited. Because of the substantial evidence in favour of a bulk limited conduction process in SiO, the results will be described in terms of the Poole-Frenkel mechanism, and the Schottky effect will not be considered further.

The theoretical value of β_{PF} is given by

$$\beta_{PF} = \left(\frac{e^3}{\pi \epsilon_0 \epsilon} \right)^{\frac{1}{2}} \quad (3.5)$$

To obtain β_{PF} in terms of the normal units of $\text{eV} \cdot \text{m}^{\frac{1}{2}} \text{V}^{-\frac{1}{2}}$ it is necessary to divide the value given by equation (3.5) by the electronic charge $e = 1.6 \cdot 10^{-19} \text{ C}$. ϵ is normally taken to be the high frequency

dielectric constant, although Hill¹²¹ has suggested that a function of both the low and high frequency values is more appropriate. The typical theoretical value of β_{PF} is $3.8 \cdot 10^{-5} \text{ eV m}^{\frac{1}{2}} \text{ V}^{-\frac{1}{2}}$ as given by Jonscher and Ansari for a value of $\epsilon = 4$ in SiO. Typical experimental values of β in SiO_x are $2.1 \cdot 10^{-5}$ ¹²², $1.95\text{-}2.1 \cdot 10^{-5}$ ¹²³, $2.2 \cdot 10^{-5}$ ¹¹⁷ and $1.38\text{-}2.6 \cdot 10^{-5} \text{ eV m}^{\frac{1}{2}} \text{ V}^{-\frac{1}{2}}$ ¹²⁴.

A number of explanations for these and other similar low β values have been proposed. Johanson¹²² described his results in terms of a Schottky emission mechanism from regions of Si imbedded in SiO₂. Simmons¹⁰ has described an anomalous Poole-Frenkel effect, applicable for a system with shallow neutral traps and deep donors. The expected β value is then more in agreement with experimental values. Hill¹²⁵ has suggested that the low experimental β values arise as the result of thermal emission or tunnelling over the potential barrier between adjacent ionised donor sites. This leads to an effective value of β ranging from $\frac{1}{2}\beta_{PF}$ to β_{PF} . Adachi et al¹²⁶ considered the effect of carrier jumps from occupied Poole-Frenkel sites to empty ones in both the forward and reverse field directions. Their calculated results are in better agreement with experiment than the original Poole-Frenkel theory. Hall¹²⁷ considered the extent of the wave-function of an electron bound at a Poole-Frenkel site. A large number of localised Wannier-type states were considered and tunnelling effects were ignored. Two solutions for the current flow equation were derived, one dominating at high temperatures and the other at low temperatures. These equations were successful in explaining the results of Servini and Jonscher¹¹⁶ on SiO and also those of Adkins et al¹²⁸ on amorphous carbon.

It is clear from the above that the experimental values of β are not in good agreement with the theoretical values of β_{PF} ; also

there are a variety of different models which have been proposed to explain the experimental values. Nevertheless the very low values of β calculated in the present work are even lower than those quoted above, and require some additional explanation.

One of the main differences between formed devices and un-formed SiO_x films is the existence of the high field region which has been discussed in section 3.2.3. Such a field could well be an indication of a space-charge region within the insulator, which would have a profound effect on any Poole-Frenkel type mechanism. Barbe¹²⁹ has shown that the current level can be dominated by either space-charge limited conduction or the Poole-Frenkel effect, depending on the number of injected carriers. Moreover O'Dwyer¹³⁰ has considered the effect of emission processes in a dielectric where a space-charge build-up has occurred, and shown that a field emission mechanism can give a $\log I_c \propto V_b^{\frac{1}{2}}$ characteristic. Thus in the presence of a space-charge region this type of characteristic is not necessarily an indication of Poole-Frenkel or Schottky emission.

In the present case it was thought possible that the appearance of Poole-Frenkel type behaviour was due to the suppression of the normal conduction mechanism as a result of a redistribution of the high field region at low temperatures. The existence of the high field region is obviously a necessary accompaniment to VCNR behaviour, and the absence of VCNR was considered a possible indication of the disappearance of the high field region. In order to test this idea, measurements using triode structures of the type described in section 3.2.3 were repeated at low temperatures. These potential distribution measurements showed in fact that the high field region remained throughout the first and all subsequent characteristics. There was no sweeping away of the high field region during the first characteristic

with uniform fields thereafter. In fact the conduction process did not appear to be ohmic in the lower field region as the voltage drop across this region was not proportional to I_c . The existence of the high field region appears, therefore, to be a necessary but not a sufficient condition for the observation of VCNR.

Two salient experimental facts have emerged from the above. Firstly the $\log I_c \propto V_b^{\frac{1}{2}}$ behaviour, which is indicative of a field-lowering mechanism of the Poole-Frenkel or Schottky type, and secondly, the existence of the high impedance region at low temperatures, which must be a significant factor in determining the conduction process. The experimental values of β are not in agreement with the Poole-Frenkel effect and any explanation of this discrepancy must take into account the existence of the high field region. Two different explanations were considered, one involving the Poole-Frenkel effect over a limited thickness of the insulator; the other that a different (but similar) type of field-lowering mechanism occurred. The first explanation was rejected for the following reasons. In section 3.2.3 typical average fields in the insulator regions were given as $8.25 \cdot 10^2$ and $1.62 \cdot 10^6$ V cm⁻¹. Clearly the Poole-Frenkel effect cannot occur in the low field region as this is well below the normally accepted minimum fields for Poole-Frenkel behaviour. Also calculations of β assuming the voltage drop over the high field region produce β values of $0.53 \cdot 10^{-5}$ and $0.41 \cdot 10^{-5}$ eV m^{1/2} V^{-1/2} for curves A and B in figure 24. This is even more incompatible with Poole-Frenkel behaviour than assuming uniform conduction. Timson¹³¹ has suggested that in rapidly evaporated B₂O₃ films a different type of field lowering mechanism can occur. Timson found values of $\beta = 0.61-8.9 \cdot 10^{-5}$ eV m^{1/2} V^{-1/2} in B₂O₃ with wide variations between individual samples. He suggested that the field-lowering effect occurred at a positive

ionic space-charge potential barrier which was set up within the insulator. In the present case it is known that a definite non-linearity of the field occurs, and this is most probably the effect of a space-charge region. Such an explanation is more in accordance with experimental fact than assumptions of unnecessary temperature parameters or excessively high values of the dielectric constant.

3.3 Attenuation Lengths in SiO_x

Electron emission from formed devices has led to the proposal of using thin film sandwich structures as cold-cathode emitters^{25,39}. For this purpose suitable emission stability, uniformity and intensity are required. Factors which affect the magnitude of I_e are thus of special importance; in particular scattering in the top metal electrode and in the insulating layer. Attenuation lengths measured in the top metal layer are usually measured in devices of this type using the definition of attenuation length given by Hickmott³³ in equation (1.9)

$$\frac{I_e}{I_c} = K \exp\left(-\frac{d}{\lambda}\right)$$

where d is the thickness of the top metal layer, K is a pre-exponential factor and λ is the attenuation length. A series of devices, identical except for varying values of d is then prepared. Values of I_e/I_c are then measured on each device for various voltages, and the attenuation length for a particular voltage can be obtained by plotting the value of $\log I_e/I_c$ at that voltage against d . Each value of $\log I_e/I_c$ and d is obtained from a device with a different top electrode thickness. The slope of such a plot is $-1/\lambda$ from which the attenuation length can be derived. Typical values of attenuation lengths measured by

this method using formed devices are 200 Å between 3 and 8 V for Au³³, 60-88 Å between 2.8 and 3.4 V for Au⁵⁷, 700-3000 Å between 3 and 20 V for Au⁷⁴ and 150-450 Å between 9 and 20 V for Ag⁷⁸.

These results are generally at variance with the accepted theoretical predictions of Quinn⁷⁶ and Motizuki and Sparks⁷⁷.

Figure 25 shows Quinn's theoretical variation of mean free path l in Ag, with electron energy E computed from the equation

$$l(\text{Å}) = \frac{14.5}{(m^*)^{\frac{1}{2}}} \frac{E_0^{5/2} \beta^{3/2}}{\left[\tan^{-1}(\beta^{-\frac{1}{2}}) + \beta^{\frac{1}{2}}/(1+\beta) \right]} \frac{1 + E/E_0}{E^2} \quad (3.6)$$

as given by Crowell et al¹³². E_0 is the Fermi energy in eV, m^* is the electron effective mass in units of the free electron mass and is assumed to be unity for the purposes of this calculation, and

$$\beta = \left(\frac{4}{9\pi} \right)^{1/3} \frac{r_s}{\pi} \quad (3.7)$$

where r_s is the radius, measured in terms of the Bohr radius, of a sphere equal in volume to the volume per electron. The value of E_0 was taken to be 5.5 eV¹³³ and an r_s value of 3.036 (calculated directly from electron concentration) was used. The variation of mean free path for electrons in Au was also calculated but the identical value of E_0 and near identical value of r_s of 3.011 produced a curve virtually indistinguishable from the Ag curve. These theoretical predictions show an E^{-1} dependence of mean free path for large E and an E^{-2} dependence for small E . It is the small E values which concern us here. In direct contrast with these variations are the attenuation lengths measured by the method described by Hickmott. Although strictly speaking mean free paths should not be compared with attenuation lengths¹³⁴, numerical values

are generally within an order of magnitude agreement and for the present approximate argument we may consider them to be equivalent. Measured attenuation lengths invariably increase with bias and are typically 2 orders of magnitude greater than the theoretical predictions. The most recent measurements are those for Au of Collins and Gould⁷⁴ and for Ag of Collins et al⁷⁸ which are given above. In both cases the attenuation length increases roughly linearly with bias, from 700 Å at a bias of 3 V to 3000 Å at 20 V in the case of Au, and from 150 Å at a bias of 9 V to 450 Å at 20 V in Ag. Collins et al suggest these discrepancies are probably due to structural features of the sandwich, in particular preferential electron emission through locally thin areas and localised emission from breakdown craters and the surrounding metal. While these effects can be of importance, another factor influencing the results is the heavy scattering in the oxide layer. This reduces the energy of electrons entering the top electrode so that their energies then range from zero up to the full applied bias across the device. Collins and Gould have measured the variation of transfer ratio ($\alpha = I_e/I_c$) with retarding potential for different applied voltages (see figure 4 of reference 74). By graphically differentiating these curves the actual energy distribution could be obtained^{59,135}. The distributions showed a peak at an energy much less than that corresponding to the full applied bias across the device. For applied voltages of 7.5 and 17.5 V respectively the distribution peaked at energies of 1.5 and 3.0 eV, and therefore scattering in the oxide was of such an extent that the greatest contribution to the measured attenuation lengths came from the low energy electrons. Since, from figure 25, these low energy electrons have very long mean free paths, the measured value of λ for the distribution will be greatly in excess of predicted

mean free paths of mono-energetic electrons of energy corresponding to the full applied voltage.

Furthermore the amount of scattering in the insulator is obviously determined to a large extent by the insulator thickness. Measured values of λ in Au rise with the thickness of insulator used^{59,135}. The proportion of low energy electrons clearly increases with the thickness of insulator because of the heavier scattering in thicker insulators. Thus the thicker the insulating layer the greater the proportion of low energy electrons entering the metal and the longer the measured attenuation length.

As we have seen above interactions in the insulator are extremely important when considering device emission properties not only because of scattering in the insulator, but also because prior scattering in the insulator can influence measurements of attenuation lengths in the counter electrode. Measurements of attenuation lengths in the oxide are thus of great interest.

We may define an attenuation length λ_{SiO} in terms of the device transfer ratio $\alpha = I_e/I_c$ ¹³⁶. Thus

$$\frac{I_e}{I_c} = \underline{K}(V_b, \psi_{\text{Au}}, L) \exp\left(-\frac{d_{\text{Au}}}{\lambda_{\text{Au}}}\right) \exp\left(-\frac{d_{\text{SiO}}}{\lambda_{\text{SiO}}}\right) \quad (3.8)$$

where d_{Au} and d_{SiO} are the top electrode and oxide film thicknesses, λ_{Au} is the electron attenuation length in the Au layer, and \underline{K} is a function of V_b , ψ_{Au} (the Au work-function) and L , where L is a function containing interfacial scattering factors and any non-exponential scattering dependence. The factor L will also depend on d_{SiO} in a non-exponential manner, as the heavy scattering in the oxide will affect the shape of the energy distribution of the electrons entering the Au layer. This (unknown) variation of L with d_{SiO} is the

major limitation in the accuracy to which λ_{SiO} may be determined. The justification for assuming such an exponential dependence of I_e/I_c on d_{SiO} is entirely empirical and an example of such variations is shown in figure 26 for devices with constant d_{Au} (1400 Å), but with d_{SiO} ranging from 500-4000 Å. These yielded plots of $\log I_e/I_c$ against d_{SiO} through which a reasonable straight line could be drawn. However there does appear to be some slight curvature, particularly at the thicker values of d_{SiO} , and this presumably depends on the variation of L with d_{SiO} discussed above. Curvature to the extent of that observed by Eckertova and Bocek⁹⁵ on Al-Al₂O₃-Au structures was not observed, even though the internal field distribution was non-linear as discussed earlier in section 3.2.3.

λ_{SiO} as a function of V_b was determined from a series of plots of the type in figure 26. In figure 27 the measured values of λ_{SiO} at 77 and 300 K are plotted for the bias range of 4-20 V. The room temperature results were previously determined by the author at the University of Lancaster⁵⁹. The scatter in the results is considerable, primarily due to the current instabilities associated with this type of device and also the variation of L with d_{SiO} discussed earlier. The dotted lines indicate the maximum scatter of experimental points. Errors are typically ± 100 Å for $V_b < 7$ V and ± 250 Å for $V_b > 7$ V. The attenuation lengths are seen to lie in the range 400-1000 Å. Although there do not appear to be any comparable measurements of electron attenuation in amorphous SiO_x a number of workers have studied attenuation in Al₂O₃. These results have usually yielded values in the range 5-24 Å^{24,137,138}. However Hickmott³³, by studying the variation of I_e/I_c with V_b for different oxide thicknesses, obtained an attenuation length of greater than 200 Å for Al-Al₂O₃(120-930 Å)-Au(255 Å) devices. Systematic

measurements of the variation of $\lambda_{\text{Al}_2\text{O}_3}$ with V_b were not however attempted. Furthermore, Malter-effect cathodes with dielectric layers several thousand angstroms thick yield appreciable emission currents for a variety of oxide, fluoride and chloride layers¹³⁹⁻¹⁴¹.

The simple explanation given above for long attenuation lengths in metals cannot be extended to the case of insulators. The theoretical predictions of mean free paths in metals are not applicable to insulators, and there is no theoretical justification for arguing that low energy electrons exhibit long mean free paths in the oxide layer. The suggestion of Collins et al⁷⁸ that the discrepancy between attenuation length measurements on formed devices and those measured by other means is a consequence of structural features of the sandwich, is still valid. Indeed, the polyfilamentary conduction model, which is also applicable to Malter cathodes, may provide an explanation for the long attenuation lengths. Emission of electrons from filamentary weak spots near the anode would give an increased value of I_e/I_c , and this would be especially noticeable for thicker insulators where normal scattering processes in the insulator significantly attenuate the value of I_e/I_c . (The divergence of the experimental points from the average straight lines to increasing values of I_e/I_c for $d_{\text{SiO}_2} > 3000 \text{ \AA}$ in figure 26 is probably an indication of this). Emission from weak spots near the anode is not significantly attenuated in the short distance between the weak spot and the emitting electrode, and is probably the main contributory factor in giving the long measured attenuation lengths. The long attenuation lengths appear, therefore, to be associated with the particular conduction and emission processes in formed materials.

The temperature independence between the results for 77 and 300 K is also an interesting point. Undoubtedly some variation is masked by the spread of results, but no really significant difference is apparent. In order to investigate this further, retarding potential measurements were made of the emitted electrons, and the dependence of I_e/I_c on retarding potential V_r , for a device at 77 and 300 K is shown in figure 28. The voltage bias was $V_b = 5$ V. Following normal practice I_e/I_c was plotted to minimise any time dependent drifts in I_e caused by I_c . Such plots normally showed a gradually decreasing value of I_e/I_c with V_r and there was some evidence of emission even when V_r approached V_b . (This is not apparent on the graph due to the linear I_e/I_c scale). Complete saturation of I_e/I_c did not occur at $V_r = 0$ and higher emission currents could usually be drawn when a higher accelerating voltage was used. Such effects could be eliminated by biasing the aluminium plate, normally used to screen the anode, at a suitable positive voltage. This procedure was not employed, however, due to the non-uniform fields set up in the vicinity of the sample.

Differentiation of retarding potential curves gives a direct measure of the energy distribution of the emitted electrons. An example of energy distributions for electrons of energy E ranging from 0-5 eV is shown in figure 29. The general shape of the distributions are in agreement with retarding potential measurements of energy distributions of emitted electrons in tunnel cathodes^{24,142} and in formed materials⁹⁶. The shape, height and width of the energy peak depends on the various scattering mechanisms involved; in general, scattering shifts the energy peak to an energy much lower than that corresponding to the full applied voltage. It is evident from figure 29 that both the curves peak at approximately the same

energy and that the shapes of the distributions are similar for electrons of low energy. Measured attenuation lengths are thus expected to be similar for the two temperatures. Although the structure of the oxide film is not well defined, it seems likely in the vacuum deposited amorphous mixture of Si and SiO_x, electron-defect and electron-impurity scattering will predominate over electron-phonon scattering. The temperature independence of the present results supports this view. A further explanation of the temperature independence of the emitted electron energy distribution is also possible. The electron energy distribution is characteristic of the temperature of the emitting regions of the device. These may be similar even though the bulk temperatures are widely different.

3.4 Spatial Distribution of Emitted Electrons

3.4.1 Electron Diffraction Through the Top Electrode

Simmons and Verderber³⁷ have shown that the radii of emission arcs produced as the result of first order electron diffraction in the top Au electrode of formed sandwich structures are given by an equation of the type⁵⁸

$$r = \frac{24.54 s}{d_{hkl} V_a^{\frac{1}{2}}} \left(1 - \frac{37.6}{d_{hkl}^2 (V_b + \eta)} \right)^{\frac{1}{2}} \quad (3.9)$$

where r is the radius in cm, s is the cathode-screen separation, d_{hkl} is the lattice spacing in Å, V_a is the accelerating potential and η is the Fermi energy of the Au electrode. Furthermore, the condition for emission of electrons through the top surface of the Au was given by Gould and Collins^{58,59} as

$$(V_b + \eta) - (\eta + \psi_{Au})^{\frac{1}{2}} (V_b + \eta)^{\frac{1}{2}} - \frac{75.2n^2}{d_{hkl}^2} > 0 \quad (3.10)$$

where ψ_{Au} is the Au work-function and n is the order of diffraction. By substituting suitable values of η (5.5 eV), ψ_{Au} (5.3 eV) and d_{hkl} the minimum voltage for the appearance of electron diffraction from a particular set of diffraction planes can be calculated. The values of this threshold voltage for electron diffraction are given in the following table.

Diffraction plane	d_{hkl}	Threshold voltage for electron diffraction
(111)	2.355 Å	26.7 V
(200)	2.039 Å	33.0 V
(220)	1.442 Å	56.6 V
(311)	1.230 Å	73.4 V
(222)	1.177 Å	79.0 V

It can thus be seen that voltage levels in the region of 60 V are required to observe more than two diffraction rings, and as described in section 2.2.7.1 multilayer structures were required.

Diffraction patterns observed on devices at voltages not exceeding 20 V showed many random arcs of the type described by Simmons et al³⁷ and Gould and Collins⁵⁸. At these low voltages diffraction cannot be through the top electrode as the condition in equation (3.10) is not fulfilled. Simmons et al^{37,38} have suggested that in this case emission occurs through the edges of pinholes in the top electrode. Patterns obtained on multilayer structures of Au and SiO_x are shown in figure 30 for voltages ranging from 20-70 V. It can be seen that one diffraction ring is visible at $V_b = 20$ V, two rings at 30 and 40 V, three rings at 50, 60 and 70 V and also a possible fourth ring at 70 V. The radii of these patterns were measured and plotted in the form of r^2 against $1/(V_b + \eta)$ in figure 31. (The error bars represent the maximum and minimum of the measured values of r). From equation (3.9)

these should lie on a straight line. Equation (3.9) is also plotted as a straight line in figure 31 for (111), (200), (220) and (311) diffraction, using the values of d_{hkl} from the above table. All the photographs were taken at a screen-sample distance $s = 5$ cm, and accelerating voltage $V_a = 3$ kV.

The first point to note from figure 31 is that all the experimental points lie on one of the theoretical lines denoting diffraction from a particular set of planes. Thus the inner ring corresponds to (111) diffraction, and the other rings to (200) and (220) diffraction. The short arc appearing in the 70 V photograph appears to be a result of (311) diffraction at the higher voltage, although such a designation cannot be conclusive on the basis of measurements on such a short arc.

Secondly, the above table also predicts the minimum voltage at which diffraction phenomena from a particular set of planes will occur through the surface of the counter electrode. The extent of the voltage range where such behaviour should be observed is shown by the breaks in the straight lines in figure 31; to the left of the break diffraction should be observed, while to the right the voltage is insufficient to give the electron enough energy for emission. In all cases the first appearance of a diffraction ring occurred at a voltage just below that given in the table. This appears to be an effect of surface irregularities⁵⁸ which can distort the electric field close to the emitting surface. The intensity of the diffraction rings, which should be in the ratio of approximately 10:5:3 could not be directly observed. However there was a general tendency for the outer diffraction rings to be of lower intensity than the inner rings.

In the 60 and 70 V photographs in figure 30 an arc appeared which was roughly parabolic in shape. This type of arc frequently appeared when attempting to observe diffraction phenomena, and is probably due

to diffraction from another area of the device in a direction not perpendicular to the electrode plane.

To summarise, these results have shown that diffraction of electrons through the polycrystalline Au counter electrode can occur in formed devices. Diffraction from the (111), (200) and (220) planes was positively identified, and possible diffraction from the (311) planes was also observed, thus confirming and extending earlier work by Simmons et al^{37,38}, Lancaster⁴¹ and Gould and Collins⁵⁸. Diffraction appears to arise from numerous localised areas, and is not therefore in disagreement with the filamentary theory.

3.4.2 Angular Distribution of Emitted Electrons

Figure 32 shows the variation of the angular distribution of emitted electrons from thin film structures. The function $\Delta(\theta)$ is plotted as a function of θ , where the angle θ is measured from the normal to the plane of the film. $\Delta(\theta)$ represents the emission current deflected into a particular band of the hemispherical collector shown in figure 11, normalised to unit space angle and divided by the total emission current. Plotting the data in this fashion permits direct comparison between the present results and those of Thevenard et al⁵⁵ and Hrach and May⁶⁶. Moreover an isotropic energy distribution is characterised by a circular plot when the co-ordinates are plotted in this way.

Figure 32a was obtained from a single thickness device of thickness 400 Å. The dependence of the angular distribution on increasing the voltage level can clearly be seen. At $V_b = 7$ V the distribution shows a pronounced forward maximum, while at $V_b = 14$ V this has broadened considerably and the distribution is more isotropic. Figure 32b, which was obtained on a 700 Å triode device to allow higher voltages

to be applied, shows a continuation of this trend. The curve for $V_b = 25$ V still shows a slight forward maximum, while for $V_b = 40$ V the distribution is virtually isotropic.

Hrach^{46(d)} has theoretically analysed the dependence of $\Delta(\theta)$ on θ for various different device parameters. The main conclusion was that an isotropic angular distribution requires short mean free paths for elastic interactions with phonons, and large mean free paths for collisions with traps. It follows, therefore, that an isotropic emitted electron angular distribution is an indication of predominantly elastic scattering within the insulator, while a distribution with a pronounced forward maximum signifies an appreciable interaction with traps. Thevenard et al and Hrach and May have both observed results very similar to those shown in figure 32a, and have concluded that the diminishing importance of the central maximum at higher voltages is a result of a greater proportion of elastic scattering in the higher energy electrons. It has previously been argued in section 3.3 that the low energy (5 eV) emitted electrons of figure 29 do not undergo a significant proportion of phonon collisions. Moreover an energy analysis of emitted electrons performed by Hrach⁹⁶ has established that electrons emitted at small values of θ have much lower energies than those emitted at large θ . This is consistent with low energy electrons (from traps) comprising the central maximum and higher energy elastically scattered electrons comprising the isotropic background. The diminishing importance of the central maximum at higher voltages is thus accounted for.

In the present case similar results to these were obtained, and at higher voltages the trend towards a disappearing central maximum continued. The present results therefore confirm the earlier measurements. However there is a further point with regard to the

diminishing central maximum that is worth considering. As can be seen from figure 32a the disappearance of the central maximum occurs mainly in the range 7-14 V. Furthermore figure 32b shows that it has nearly disappeared when a voltage of 25 V is applied. The main contribution to the disappearance of the central maximum occurs, therefore, in the voltage range where the filamentary theory predicts that filament rupture is at its greatest level. The process continues during further filament rupture up to 25 V. A correlation between these two effects may be more than co-incidental. At low voltages the filamentary theory predicts that most of the current is carried by filaments while at high voltages other conduction mechanisms may play an increasing role. Electrons emitted from the ends of conducting filaments would be those of low energy (since the filaments are ruptured at higher energies) and would most probably be emitted in the forward direction. The isotropic distribution at higher voltages would therefore correspond to conduction other than by filamentary means.

As well as the effects of traps and elastic scattering, the effects of changing from a filamentary to a non-filamentary conduction process ought therefore to be considered when discussing the angular distribution of emitted electrons. It would be interesting to observe whether a correlation between the disappearance of the forward maximum and that of the filamentary conduction process is also observed in other materials where V_m may be higher than in the case of SiO_x .

3.5 The Forming Effect in Other Materials

Exploratory measurements were performed on the systems Al- $\text{SiO}_x/\text{B}_2\text{O}_3$ -Al, Au- CaBr_2 -Au and Au- Si_3N_4 -Au. The results were restricted to the forming process, current-voltage measurements, sample temperature ($\text{SiO}_x/\text{B}_2\text{O}_3$) and dead-time effects (CaBr_2 and Si_3N_4).

The measurements were intended merely as a first look at these systems, to see if the forming process occurred and if properties peculiar to the particular systems were observed.

3.5.1 $\text{SiO}_x/\text{B}_2\text{O}_3$

The results described in this section were obtained jointly with E. H. Z. Taheri, who also prepared the samples.

Recent research work in this department has shown that co-evaporated films of mixtures of $\text{SiO}_x/\text{B}_2\text{O}_3$ (prepared by using a technique described by Hogarth and Wright¹⁰⁴) show interesting dielectric properties. Timson and Hogarth⁸⁷ have shown that Al- $\text{SiO}_x/\text{B}_2\text{O}_3$ -Al sandwiches of thickness $1-2 \cdot 10^4 \text{ \AA}$ give a DC current-voltage relationship of the form $I_c \propto V_b^n$ (see equation (1.11)) where n was of the order of 4-6. The AC conductance σ_{AC} at frequency f was of the form $\sigma_{AC} \propto f^n$ where n varied between 0.9 and 1.0. Hogarth and Taheri⁸⁶ have extended these measurements to thinner films having $\text{SiO}_x(70\%)/\text{B}_2\text{O}_3(30\%)$ layers of thickness 3000-6000 \AA . These films showed different behaviour to the thicker films, typically higher currents were passed for a given voltage even though the resistivity was high ($10^{15}-10^{16} \text{ \Omega cm}$) and currents tended to decrease above a certain voltage level. The observation of the current maximum has certain similarities with VCNR behaviour, and the possibility of electron emission into vacuum, and also other properties of formed devices was considered worthy of investigation. A mixture of $\text{SiO}_x(70\%)/\text{B}_2\text{O}_3(30\%)$ was used in this work since these films show a high sensitivity to water vapour for concentrations of B_2O_3 greater than 50%. Al electrodes were used in spite of early work which had suggested that forming with Al electrodes would not occur. The more recent work of Pivot et al⁶⁰ and Doucas and Walsh⁸⁰ has shown that Al electrodes are not necessarily a barrier to

forming. Hickmott⁸⁴ has formed bisulphate anodised Al-Al₂O₃-Al devices but was unable to form pure samples. He attributed the increased ability to form to the impurities present and this explanation may also hold for the samples of Doucas and Walsh which had an additional CdS layer and of Hogarth and Taheri which contained a large proportion (30%) of B₂O₃ in addition to the SiO_x.

In the present study current measurements showed that a forming process did indeed occur⁹⁴. Typical current increases were from 10⁻⁵ to 10⁻³ A and were not as significant as current increases of 8 orders of magnitude sometimes observed in SiO films¹⁷. The forming voltage was somewhat variable between samples but was usually in the range 12-20 V. When forming was complete the bias voltage was reduced to zero and then reapplied to give the formed characteristic. In some cases the device would spontaneously un-form and then re-form and general device stability was not as good as with Al or Au-SiO-Au devices. However the devices did show remarkable dielectric properties and some samples could withstand voltages up to 400 V.

Figure 33 shows a typical I_c-V_b curve. A peak current is exhibited at V_m = 30 V followed by a negative resistance region. Above the maximum the general level of current falls although there are sudden increases in current at voltages greater than V_m. The value of I_c was quite low and certainly not so high as for simple oxide devices. This result is consistent with the improved dielectric properties of these glasses previously reported¹⁰⁴.

Figure 34 shows the I_e-V_b curve. I_e appears at low voltages and rises very sharply at about 10 V to a maximum which occurs at the same voltage (V_m) as the maximum value of I_c. I_e then sharply decreases until at some voltage (approximately 100 V) I_e falls very steeply and sometimes disappears altogether. Subsequent retracings of the

characteristic show the same general form and current levels of the same order, thus indicating that dielectric breakdown has not begun to destroy the samples.

Figure 35 shows the variation of transmission ratio ($\alpha = I_e/I_c$) with V_b . The maximum value of α is 10^{-3} on films of thickness 3000 \AA with electrodes of thickness 500 \AA . This is comparable to the maximum estimate for SiO films⁷⁴ of thickness 800 \AA and assuming a top electrode having zero thickness and thus no attenuation effect. We may expect to obtain even higher values of α on thinner films with a thinner top electrode.

As in section 3.1.3 the sample temperature (T_c) was monitored during operation. The variation of T_c with V_b and I_c is shown in figure 36. In general the T_c - V_b curve follows the I_c - V_b curve and the maximum temperature occurs when the current flow is highest. In contrast to figure 16 for Au-SiO_x-Au devices the temperature at higher voltages relaxes to the ambient temperature and no significant heat dissipation is detectable. In this case the temperature measurements are not a direct indication of thermal dielectric breakdown. The very high dielectric strength of the mixture allows high voltages to be applied across the insulator without breakdown occurring. Although currents are low the high applied voltage means that considerable power is being dissipated in the device. For example, values of $V_b = 300 \text{ V}$ and $I_c = 0.33 \text{ mA}$ correspond to a power dissipation of 0.1 W . Although this is of the same order as power dissipated in simple oxide devices, the low values of I_c may be expected to lead to more stable operation.

The temperature measurements, which show that the temperature is a maximum before the onset of negative resistance, are in agreement with the theory of Dearnaley et al⁴³. Furthermore the values of V_F and V_m are very high in the present case, the V_m value even exceeds

that quoted by Sutherland⁷³ for ZnS devices. Sutherland has pointed out that for any of the band models the value of V_m is determined by a factor inherent in the band structure, while the value of V_F is given by equation (1.16), for the model of Verderber et al¹⁷. Clearly both of these measured values of V_F and V_m for $\text{SiO}_x/\text{B}_2\text{O}_3$ are more in agreement with the filamentary theory than with the various band models.

Beyond the current maximum the temperature falls and there is no evidence of thermally induced breakdown. The failure of emission at voltages in excess of 100 V must therefore be a consequence of some other process unconnected with dielectric breakdown. The clue to the explanation of this effect probably lies in the existence of a high field region which has been discussed (for SiO_x) in section 3.2.3. The suggestion is that at very high voltages the potential distribution across the sample becomes more uniform and therefore the sample will not subsequently behave with the properties of formed devices, and I_c will fall. Alternatively, electrons are not accelerated through a region of such high field intensity, and therefore normal scattering processes decrease their energy below the emission threshold. It should be pointed out that simple SiO_x sandwiches⁷⁴ (see 3.1.1) do not show this effect and breakdown occurs while emission is taking place. This is probably due to the large values of I_c in SiO_x .

3.5.2 CaBr_2

All the experimental results described in this section were obtained on Au-CaBr_2 (1000 Å)-Au devices.

Current-voltage characteristics obtained before forming differed widely from those of SiO_x devices. In particular the current typically exceeded 100 mA and the I_c-V_b characteristic was nearly linear. Examples of the I_c-V_b characteristic are shown in figure 37 for two different

samples; these give way to formed characteristics at 4.9 and 6.3 V. Such behaviour is not uncommon in thin film devices and is usually taken as an indication of a short circuit between the two electrodes; in the present case high currents were always obtained initially and this appeared to be a characteristic of the sample materials used. Sutherland et al⁸⁸ have also observed currents of several amps in Al-CdS-Au or Ag devices which eventually gave way to a formed characteristic. In the present case a similar process occurred, and electron emission appeared. The high current before forming may be as a result of electrode diffusion, porosity of the insulating layer or the absorption of water vapour during evaporation or subsequent transferral to the test system. The latter appears to be a likely possibility as CaBr_2 is hygroscopic. Trapped water vapour would lead to a greatly increased current density and the high temperatures thus generated could lead to evaporation or melting of low resistance paths. Un-forming of the device when stored at atmospheric pressure also supports the supposition that absorbed water vapour is the cause of the low impedance ohmic characteristic. The value of the forming voltage is uncertain, as this may occur at voltages below that at which the original low impedance characteristic is destroyed; however the appearance of electron emission at this voltage indicates that the two processes occur simultaneously. The voltage at which this occurs is 4.5-7.5 V, which may be taken as an upper limit of the forming voltage.

Typical examples of the variation of I_c and I_e with V_b after forming are shown in figure 38. Note this is the first formed characteristic. There are many similarities between these characteristics and those for SiO_x in figure 12. However the value of V_m is normally approximately 10 V and there is no second maximum in I_c . Furthermore electron emission was not detected until voltages exceeding 5 V were applied, and

burnout behaviour was not observed. The most marked difference between CaBr_2 and SiO_x devices is, however, the non-reversibility of the $I_c - V_b$ curve in CaBr_2 . Provided the maximum voltage (V_1) applied during the first trace had exceeded V_m (where V_m is the voltage for maximum current during the first characteristic), the maximum current of the new characteristic appeared not at V_m , but at V_1 . Moreover, provided the voltage for maximum current for the second characteristic was not exceeded, the second characteristic was reproducible up to the current maximum. These properties are illustrated in figure 39. Figure 39a shows the variation of I_c with V_b when the voltage was increased to 10 V, decreased to zero and then increased to 20 V. (1) denotes the first increasing voltage trace, (2) the reverse trace and (3) the second increasing voltage trace. Within the error expected for this type of device (1), (2) and (3) follow the same path and the characteristic below V_m is reproducible. Similarly, provided the voltage for current maximum in any subsequent characteristic is not exceeded, the characteristic up to the maximum is reversible and reproducible in later tracings. Different behaviour is observed if V_m is exceeded. In figure 39b the voltage was increased to 12 V (passing V_m at 9 V), decreased to zero and then increased to 20 V. ((1), (2) and (3) have the same meanings as in figure 39a). Here it can be seen that the decreasing voltage trace does not follow the increasing voltage trace, following a higher impedance characteristic as the voltage is reduced. The next forward voltage trace follows the decreasing trace until the voltage $V_1 = 12$ V is reached. I_c then steadily decreases with V_b . Effectively, therefore, within certain limits, the $I_c - V_b$ characteristic of a sample can be changed simply by applying a certain voltage, which is greater than V_m , to the device. All subsequent characteristics at voltages less than that used to induce the new characteristic will be

reproducible, and of a higher impedance than the original characteristic. If the voltage used to induce the new characteristic is exceeded, a further even higher impedance characteristic will be generated.

The explanation of such phenomena in CaBr_2 is not clear, but the results of Bernard et al⁷² on Al_2O_3 devices are an interesting comparison with the above. By heat treating formed devices at temperatures greater than 200°C they observed that a negative resistance region appeared for the first forward trace, but did not occur for the reverse trace, or for further increasing voltage traces. Furthermore the maximum voltage applied to a device determined the $I_c - V_b$ characteristics for all subsequent runs with lower voltages, and behaviour identical to that shown in figure 39b was also observed (see figure 4 of reference 72). They concluded that these effects corresponded to an increase in the dead-time from some milliseconds to a few hours as a result of the heat treatment. Restoration of VCNR after a waiting period of 10-20 hours indicated that this behaviour was in fact a dead-time effect. In the present case no heat treatment was used, but the high currents generated before forming and shown in figure 37, must have produced high temperatures. The experimental conditions of Bernard et al may well have been duplicated as a result of the high current.

The explanation proposed by Bernard et al assumes that the dead-time corresponds to the time necessary for electrons to pass from traps to "liberation states". An increase in the activation energy for this process is assumed to occur as a result of the heat treatment. While this particular model is speculative, there is good evidence that a dead-time effect is involved. In the present case the original characteristic could not be recovered, even after a waiting period of 24 hours; this does not preclude an increased dead-time effect however,

but merely sets a lower limit. The close correlation between the present results and those of Bernard et al is a strong indication that a similar explanation may hold. Whether the hypothesis of Bernard et al is correct, or whether some other explanation applies (possibly involving a gradual dielectric breakdown effect) must await further experimental work. This should be directed at determining whether in fact CaBr_2 experiences a greatly increased dead-time or whether the new characteristic is permanent; also low temperature characteristics, which are especially sensitive to dead-time effects, should be investigated.

3.5.3 Si_3N_4

Due to the high melting point of Si_3N_4 (approximately 1900°C) great difficulty was encountered during vacuum evaporation. The system was set up with the evaporating boat run at the maximum permitted current, and even under these circumstances the evaporation rate was only 0.3 \AA s^{-1} . However, it was possible to fabricate some samples, although evaporation was normally terminated after several minutes, to avoid excessive overheating. Consequently the samples used in this study had rather thin Si_3N_4 layers (typically 100 \AA).

In common with the CaBr_2 devices described in the previous section, very high currents of up to 1 A were initially passed. Such measurements show that a thin layer of Si_3N_4 sandwiched between Au electrodes does not necessarily act as an insulator. This behaviour is shown in figure 40 for two different devices. The current rose linearly with voltage at low voltages, eventually decreasing in slope and giving way to a formed characteristic at 6-9 V; in the examples shown this occurred at 7 and 8 V. The origin of this type of behaviour is probably connected with the thinness of the insulator, which would clearly increase the

possibility of electrode diffusion or shorting through local flaws. It is unlikely that the effect of water vapour has any significant contribution to the high current levels drawn. Devices could be stored for long periods at atmospheric pressure without significant changes to the device properties, and un-forming did not occur.

After the elimination of the very low impedance characteristic, normal formed behaviour could be observed. Typical $I_c - V_b$ and $I_e - V_b$ characteristics are shown in figure 41. These are comparable to figures 12 and 38 for SiO_x and $CaBr_2$ respectively. The value of V_m for Si_3N_4 was in the range 12-25 V, and this differed widely between samples. Burnout behaviour was not always observed, but in figure 41 one can be seen at 51 V. In general the current-voltage characteristics were not radically different from those of other materials, with the exception of the rather high value of V_m .

In figure 42 an $I_c - V_b$ characteristic is shown, where the voltage was reduced three times during the course of the characteristic. It is evident that this behaviour is very similar to that observed in section 3.5.2 for $CaBr_2$, and is also identical with that described by Bernard et al⁷² for Al_2O_3 devices which had undergone prolonged exposure to high temperatures. A similar explanation to that offered for this effect in $CaBr_2$ is likely to apply also to Si_3N_4 . It is possible that the high temperature to which the device is raised during the very low impedance pre-forming characteristic can cause a drastic increase in the dead-time. Further work on Si_3N_4 is necessary to establish this fact. The extension of measurements to thicker layers of Si_3N_4 , prepared by sputtering or electron bombardment, would be interesting, since the initial high current level may only be as a result of the thin Si_3N_4 layers used.

CHAPTER 4

CONCLUSIONS AND SUMMARY

4.1 DC Device Stability and Operation

The dependence of I_c and I_e on V_b was investigated at voltages up to 60 V in Au-SiO_x-Au systems. At voltages less than 20 V, the normal effects of negative resistance and the onset of electron emission were observed. At voltages greater than 20 V sudden discontinuous drops in I_c and I_e were often observed. These drops were irreversible and were of a destructive nature.

The transient effects of increasing and decreasing the voltage at certain points in the I_c - V_b characteristic were investigated. The behaviour of the transient currents could be explained in each of the different voltage ranges by rupturing and re-joining of filaments and the establishment of new filaments, and changes in the filament resistance due to localised heating at high voltages; irreversible breakdown effects were identified in the higher voltage range. It was possible to distinguish between single-hole breakdowns and maximum-voltage breakdowns by the different degree of current drop associated with the breakdown behaviour. It was established that the first maximum-voltage breakdowns occurred at a voltage V_β in the voltage range 20-30 V, irrespective of device thickness. V_β , which was designated the burnout voltage, appeared to be a characteristic property of formed devices.

Time dependence measurements of I_c and I_e produced some interesting results. I_c increased at both the voltage for current maximum V_m , and the voltage for current minimum V_u . I_c reached a maximum after several hours at V_m , while at V_u , I_c continued to increase. I_e showed a steadily decreasing characteristic at V_m , but the behaviour was unpredictable at V_u . It was shown that the increasing value of I_c was compatible with re-joining of broken filaments and the establishment of

new filaments. The degree of current increase was higher at V_u due to the greater capacity for filament re-joining (most of the filaments are ruptured at V_u), and also because the establishment of new filaments would occur at a faster rate at the higher voltage. It was established that the maximum current a filament could carry was higher at V_m than at V_u . It was postulated that permanent filament destruction was the cause of the decreasing value of I_c observed at V_m , and that such a decrease in I_c would be dependent on both the number of filaments and the individual filament current. Both these variables are initially higher at V_m and consequently a maximum value of I_c is observed before any indication of such behaviour at V_u . Differences in the time dependence of SiO_x devices and published data for CdS and ZnS, could be adequately explained in terms of higher currents along the filamentary paths in semiconductors, and the greater ease of forming (estimated by the partial ionic character) in SiO_x .

As expected it was found that device temperature peaked at the maximum of the I_c - V_b curve due to Joule heating effects. More surprisingly a rise in temperature was also observed at voltages slightly less than V_β , even though I_c was decreasing in this range. It was concluded that such abnormal thermal processes in the insulator were indicative of thermal dielectric breakdown at the burnout voltage.

Microscopic investigation of device damage showed wrinkling of the top electrode at V_m and also at voltages just above V_β . This was further evidence of a thermal breakdown process at the burnout voltage. Single-hole breakdowns were observed in the voltage range just below 20 V and after long periods these linked up to form larger burned-out areas. At higher voltages, linking of breakdown areas by wrinkling and evaporation of the top electrode was observed. Small spherical dots were observed in the breakdown regions, and these were of similar size

(1.5 μm) to balls of crystalline silicon which are often found in breakdown areas of SiO capacitors.

4.2 The High Field Region

Results showed that in the thickness range 100-6000 \AA V_{β} remained constant irrespective of insulator thickness. Thus the average field across the insulator at burnout varied with the insulator thickness. It was suggested that on forming, a high field region of constant thickness δ is set up within the insulator, and that burnout corresponds to dielectric breakdown occurring across this region. The temperature dependence of V_{β} was not in accordance with that previously observed for electric breakdowns; however a continuous fall of V_{β} with T was further evidence of thermal dielectric breakdown. A linear dependence of $V_{\beta}^{\frac{1}{2}}$ on T was observed, and if it is assumed that δ remains constant, this implies a breakdown field-temperature variation of the same type as that previously observed in Si_3N_4 .

Potential distribution measurements confirmed that a high field region, over which most of the voltage is dropped, is set up at the onset of forming. This region did not appear primarily at the cathode but could be located nearly anywhere between the cathode and anode. The thickness of the region was estimated to be not greater than 310 \AA . It was shown that at the burnout voltage the resistance in the high field region increased substantially, while in the low field region the resistance remained constant. This is good evidence that the burnout does correspond to substantial destruction of the high field region, as has been tacitly assumed in explaining the dependence of V_{β} on insulator thickness and temperature.

At low temperatures negative resistance behaviour was not observed for the second and subsequent characteristics, although the high field

region remained. A linear correlation between $\log I_c$ and $V_b^{\frac{1}{2}}$ was observed, but values of β (from the Poole-Frenkel equation) were typically $0.88 \cdot 10^{-5}$ and $1.39 \cdot 10^{-5} \text{ eV m}^{\frac{1}{2}} \text{ V}^{-\frac{1}{2}}$. Such values are too low to support conduction by a simple Poole-Frenkel mechanism. Nevertheless a field lowering effect is indicated and it was suggested that this arises as a consequence of the high field region.

4.3 Attenuation Lengths in SiO_x

The discrepancy between the theoretical values of mean free path and experimental values of attenuation length of metals measured in formed devices was considered. It was demonstrated, with particular reference to Ag and Au, that a cause of this discrepancy could be the heavy scattering in the insulator before the electrons reach the top metallic layer. This produces an emitted electron energy distribution which peaks at energies less than that corresponding to the full applied voltage, and thus the measured attenuation length is an average over the whole emitted energy distribution. As is seen experimentally this would lead to longer measured attenuation lengths than those theoretically predicted.

Linear plots of $\log I_e/I_c$ against d_{SiO} were obtained by using sets of devices with different insulator thicknesses. The linearity of these plots showed that I_e/I_c follows an exponential relationship with insulator thickness, and thus the attenuation length in SiO_x could be derived. This was estimated to be in the range 400-1000 Å for voltages between 4 and 20 V, irrespective of whether the ambient temperature was 77 or 300 K. The long attenuation lengths were consistent with the filamentary theory, and the independence of these values with temperature was explained by considering the emitted electron energy distribution at the two temperatures. Both distributions were very similar, thus

explaining the independence of the temperature results. The similarity between the distributions was considered to be a consequence of the relative unimportance of electron-phonon scattering in amorphous SiO_x films, where electron-defect and electron-impurity scattering predominate.

4.4 Spatial Distribution of Emitted Electrons

By accelerating the emitted electrons onto a phosphor screen, electron diffraction through the top Au electrode of multilayer Au- SiO_x -Au sandwiches could be observed. Diffraction by the (111), (200) and (220) planes was identified, and possible diffraction from the (311) planes was also observed. The radii of the diffraction rings, as well as the minimum voltage level necessary for observing diffraction behaviour from a particular set of diffracting planes, were in excellent agreement with theory.

The angular distribution of emitted electrons showed a gradual decrease in the importance of the forward maximum, until at high voltages the distribution was nearly isotropic. Such results have previously been explained in terms of a gradual change in the origin of the emitted electrons with increasing voltage; at low voltages the emitted electrons are produced primarily by excitation from traps, while at higher voltages they are the result of elastic electron-phonon interactions. While such an explanation is not in disagreement with the present results it was considered that such a change may also be as a result of the cessation of filamentary conduction at higher voltages.

4.5 The Forming Effect in Other Materials

Exploratory measurements of forming and current-voltage characteristics were performed on systems of SiO_x (70%)/ B_2O_3 (30%) sandwiched between

Al electrodes, and on CaBr_2 and Si_3N_4 sandwiched between Au electrodes.

$\text{SiO}_x/\text{B}_2\text{O}_3$ films formed at between 12 and 20 V and the current maximum occurred at approximately 30 V. Values of the transmission ratio were higher than those in simple oxide devices. The samples also showed remarkable dielectric properties, some samples even withstanding voltages of 400 V. It was suggested that the failure of I_e at voltages in excess of 100 V was caused by a spreading-out of the high field region at the high voltage level.

Surprisingly, CaBr_2 and Si_3N_4 samples showed very similar properties. Before forming I_c was very high and increased linearly with V_b at low voltages, suggesting shorting between the electrodes. The origin of this effect was thought to be different for the two substances; for CaBr_2 which is hygroscopic it was suggested that trapped water vapour might have been responsible, while for Si_3N_4 , the thin insulating layer (100 Å) may have led to short-circuiting. In both cases the first forward characteristic was similar to that for SiO_x cathodes, V_m being approximately 10 V in CaBr_2 and 12-25 V in Si_3N_4 . The characteristic was not reversible in either substance, and subsequent characteristics were of higher impedance. Such effects were thought to be due to an increase in the dead-time between cycles, caused by the high temperatures generated during the initial high current characteristics.

REFERENCES

1. N. F. Mott, *Phil. Mag.* 19 (1969) 835.
2. J. G. Simmons and R. R. Verderber, *Proc. Roy. Soc. A* 301 (1967) 77.
3. N. F. Mott and W. D. Twose, *Adv. Phys.* 10 (1961) 107.
4. N. F. Mott, *Adv. Phys.* 16 (1967) 49.
5. J. E. Ralph and J. M. Woodcock, *J. Non-Crystalline Solids* 7 (1972) 236.
6. D. R. Lamb, *Electrical Conduction Mechanisms in Thin Insulating Films* (London: Methuen Monograph, 1967).
7. J. G. Simmons, *J. Phys. D: Appl. Phys.* 4 (1971) 613.
8. C. A. Mead, *Phys. Rev.* 128 (1962) 2088.
9. G. Dearnaley, A. M. Stoneham and D. V. Morgan, *Rep. Prog. Phys.* 33 (1970) 1129.
10. J. G. Simmons, *Phys. Rev.* 155 (1967) 657.
11. H. K. Henisch, *Scientific American* 221, 5 (1969) 30.
12. S. R. Ovshinsky, *Phys. Rev. Letters* 21 (1968) 1450.
13. C. F. Drake, I. F. Scanlan and A. Engel, *Phys. Stat. Solidi* 32 (1969) 193.
14. K. L. Chopra, *J. Appl. Phys.* 36 (1965) 184.
15. W. R. Hiatt and T. W. Hickmott, *Appl. Phys. Letters* 6 (1965) 106.
16. K. H. Gundlach and J. Kadlec, *Phys. Stat. Solidi (a)* 10 (1972) 371.
17. R. R. Verderber, J. G. Simmons and B. Eales, *Phil. Mag.* 16 (1967) 1049.
18. G. S. Kreynina, L. N. Selivanov and T. I. Shumskaia, *Radio Engng. Elec. Phys.* 5 (1960) 219.
19. G. S. Kreynina, *Radio Engng. Elec. Phys.* 7 (1962) 166.
20. G. S. Kreynina, *Radio Engng. Elec. Phys.* 7 (1962) 1949.
21. C. A. Mead, *Proc. Inst. Radio Engrs.* 48 (1960) 359.
22. C. A. Mead, *J. Appl. Phys.* 32 (1961) 646.
23. C. A. Mead, *Phys. Rev. Letters* 8 (1962) 56 and Erratum, *Phys. Rev. Letters* 2 (1962) 46.

24. H. Kanter and W. A. Feibelman, J. Appl. Phys. 33 (1962) 3580.
25. T. W. Hickmott, J. Appl. Phys. 33 (1962) 2669.
26. H. Kanter, J. Appl. Phys. 34 (1963) 3629.
27. S. R. Pollack, J. Appl. Phys. 34 (1963) 877.
28. S. R. Pollack, W. O. Freitag and C. E. Morris, Electrochem. Technol. 1 (1963) 96.
29. T. W. Hickmott, J. Appl. Phys. 34 (1963) 1569.
30. T. W. Hickmott, J. Appl. Phys. 35 (1964) 2118.
31. J. G. Simmons and R. R. Verderber, Radio Electr. Eng. 34 (1967) 81.
32. T. W. Hickmott, J. Appl. Phys. 35 (1964) 2679.
33. T. W. Hickmott, J. Appl. Phys. 36 (1965) 1885.
34. A. Cachard, J. Roger, R. Uzan, G. Mesnard and G. Dejardin, C. R. Acad. Sci. 261 (1965) 5333.
35. G. A. Filaretov, V. I. Stafeyev, G. A. Cherkashin, M. S. Lur'ie, Yu. Z. Bubnov and Zh. S. Asnina, Radio Engng. Elec. Phys. 11 (1966) 246.
36. C. Barriac, F. Giraud-Heraud, P. Pinard and F. Davoine, C. R. Acad. Sci. 262 (1966) 900.
37. J. G. Simmons, R. R. Verderber, J. Lytollis and R. Lomax, Phys. Rev. Letters 17 (1966) 675.
38. J. G. Simmons and R. R. Verderber, Appl. Phys. Letters 10 (1967) 197.
39. R. R. Verderber and J. G. Simmons, Radio Electr. Eng. 33 (1967) 347.
40. R. W. Lomax and J. G. Simmons, Radio Electr. Eng. 35 (1968) 265.
41. M. C. Lancaster, S.T.L. Technical Memorandum No. 604 (1967).
42. G. Dearnaley, Phys. Letters A 25 (1967) 760.
43. G. Dearnaley, D. V. Morgan and A. M. Stoneham, J. Non-Crystalline Solids 4 (1970) 593.
44. C. Barriac, P. Pinard and F. Davoine, C. R. Acad. Sci. 266 (1968) 423.
45. R. Pinto and B. M. Shaha, Japan. J. Appl. Phys. 7 (1968) 1542.

46. R. Hrach, Czech. J. Phys. B 18 (1968) 402 (a), 880 (b), 1117 (c), 1244 (d), 1356 (e), 1591 (f).
47. P. D. Greene, E. L. Bush and I. R. Rawlings, Proc. Symp. on Deposited Thin Film Dielectric Materials, Ed. F. Vratny (New York: The Electrochemical Society, 1968).
48. G. Dearnaley, Thin Solid Films 3 (1969) 161.
49. C. Barriac, P. Pinard and F. Davoine, Phys. Stat. Solidi 34 (1969) 621.
50. P. Hartmann, G. Niquet and P. Vernier, J. Vac. Sci. Technol. 6 (1969) 719.
51. J. Bernard, G. Delacote and Y. Mentalecheta, Phys. Stat. Solidi 31 (1969) 315.
52. A. A. Galkin and O. M. Ignat'ev, J.E.T.P. Letters 9 (1969) 407.
53. K. C. Park and S. Basavaiah, J. Non-Crystalline Solids 2 (1970) 284.
54. S. R. Jawalekar, Indian J. Pure Appl. Phys. 8 (1970) 36.
55. P. Thevenard, J. A. Roger and C. H. S. Dupuy, C. R. Acad. Sci. 270 (1970) 421.
56. R. Hrach, Czech. J. Phys. B 20 (1970) 1292.
57. G. Niquet, P. Vernier and P. Hartmann, C. R. Acad. Sci. 270 (1970) 1234.
58. R. D. Gould and R. A. Collins, Appl. Phys. Letters 16 (1970) 393.
59. R. D. Gould, M.Sc. Thesis, University of Lancaster (1969).
60. J. Pivot, M. Boudeulle, A. Cachard and C. H. S. Dupuy, Phys. Stat. Solidi (a) 2 (1970) 319.
61. J. Bernard, M. Decker and Y. Mentalecheta, C. R. Acad. Sci. 270 (1970) 1419.
62. P. Tronc, Thin Solid Films 5 (1970) R29.
63. R. R. Sutherland, K. O. Legg and R. A. Collins, Thin Solid Films 6 (1970) R39.
64. I. Emmer, Phys. Stat. Solidi (a) 3 (1970) K191.
65. F. L. Worthing, J. Electrochem. Soc. 115 (1968) 88.

66. R. Hrach and J. May, Phys. Stat. Solidi (a) 4 (1971) 637.
67. L. Frank, Phys. Stat. Solidi (a) 4 (1971) K135.
68. L. Frank, Phys. Stat. Solidi (a) 5 (1971) 269.
69. A. Cachard, J. A. Roger, J. Pivot and C. H. S. Dupuy, Phys. Stat. Solidi (a) 5 (1971) 637.
70. A. Cachard, J. Pivot and C. H. S. Dupuy, C. R. Acad. Sci. 270 (1970) 1058.
71. A. Cachard, J. A. Roger, J. Pivot and C. H. S. Dupuy, C. R. Acad. Sci. 272 (1971) 859.
72. J. Bernard, R. Haug, Y. Mentalecheta and Y. Tregouet, Phys. Stat. Solidi (a) 6 (1971) K127.
73. R. R. Sutherland, J. Phys. D: Appl. Phys. 4 (1971) 468.
74. R. A. Collins and R. D. Gould, Solid State Electronics 14 (1971) 805.
75. P. P. Budenstein and P. J. Hayes, J. Appl. Phys. 38 (1967) 2837.
76. J. J. Quinn, Phys. Rev. 126 (1962) 1453.
77. K. Motizuki and M. Sparks, J. Phys. Soc. Japan 19 (1964) 486.
78. R. A. Collins, I. A. Edge and K. O. Legg, Phys. Stat. Solidi (a) 9 (1972) 309.
79. R. A. Collins, G. Bowman and R. R. Sutherland, J. Phys. D: Appl. Phys. 4 (1971) L49.
80. G. Doucas and D. Walsh, Thin Solid Films 9 (1971) 25.
81. R. A. Collins, Thin Solid Films 11 (1972) 187.
82. G. Doucas and D. Walsh, Thin Solid Films 11 (1972) 447.
83. G. Dittmer, Thin Solid Films 9 (1972) 141.
84. T. W. Hickmott, Thin Solid Films 9 (1972) 431.
85. J. M. Woodcock and J. E. Ralph, J. Non-Crystalline Solids 11 (1972) 83.
86. C. A. Hogarth and E. H. Z. Taheri, Thin Solid Films 10 (1972) 455.
87. P. A. Timson and C. A. Hogarth, Thin Solid Films 10 (1972) 321.

88. R. R. Sutherland, J. P. A. Williamson and R. A. Collins, J. Phys. D: Appl. Phys. 5 (1972) 1686.
89. R. R. Sutherland, Ph.D. Thesis, University of Lancaster (1972).
90. L. Pauling, The Nature of the Chemical Bond, 3rd edition (New York: Cornell University Press, 1960) p98.
91. K. H. Gundlach and J. Kadlec, Thin Solid Films 13 (1972) 225.
92. A. Cachard, J. A. Roger, J. Pivot, C. Diaine and C. H. S. Dupuy, Thin Solid Films 13 (1972) 231.
93. L. Eckertova and J. Bocek, Thin Solid Films 13 (1972) 237.
94. E. H. Z. Taheri, C. A. Hogarth and R. D. Gould, Phys. Stat. Solidi (a) 12 (1972) 563.
95. C. A. Hogarth and H. Bidadi, Thin Solid Films 13 (1972) S27.
96. R. Hrach, Thin Solid Films 15 (1973) 65.
97. D. V. Morgan, M. J. Howes, R. D. Pollard and D. G. P. Waters, Thin Solid Films 15 (1973) 123.
98. N. Klein, J. Electrochem. Soc. 116 (1969) 983.
99. A. G. Revesz, Phys. Stat. Solidi 24 (1967) 115.
100. A. G. Revesz, J. Non-Crystalline Solids 4 (1970) 347.
101. N. F. Mott, Phil. Mag. 17 (1968) 1259.
102. P. W. Anderson, Phys. Rev. 109 (1958) 1492.
103. J. M. Ziman, J. Phys. C: Solid State Phys. 2 (1969) 1230.
104. C. A. Hogarth and L. A. Wright, Proc. Intern. Conf. on the Physics of Semiconductors, Moscow (1968) p1274.
105. P. A. Timson and C. A. Hogarth, Thin Solid Films 8 (1971) 237.
106. L. Holland (Ch.5, W. Steckelmacher), Thin Film Microelectronics (London: Chapman-Hall, 1965) p204.
107. N. Klein, Thin Solid Films 7 (1971) 149.
108. P. P. Budenstein and P. J. Hayes, J. Vac. Sci. Technol. 6 (1969) 602.

109. P. P. Budenstein, P. J. Hayes, J. L. Smith and W. B. Smith, J. Vac. Sci. Technol. 6 (1969) 289.
110. F. Forlani and N. Minnaja, J. Vac. Sci. Technol. 6 (1969) 518.
111. J. L. Smith and P. P. Budenstein, J. Appl. Phys. 40 (1969) 3491.
112. A. F. Joffe, The Physics of Crystals (New York: McGraw-Hill, 1928).
113. N. Klein, I.E.E.E. Trans. Electron Devices ED-13 (1966) 788.
114. N. Klein, I.E.E.E. Trans. Electron Devices ED-13 (1966) 281.
115. S. M. Sze, J. Appl. Phys. 38 (1967) 2951.
116. A. K. Jonscher, Thin Solid Films 1 (1967) 213.
117. A. K. Jonscher and A. A. Ansari, Phil. Mag. 23 (1971) 205.
118. T. E. Hartman, J. G. Blair and R. Bauer, J. Appl. Phys. 37 (1966) 2468.
119. H. Hirose and Y. Wada, Japan. J. Appl. Phys. 3 (1964) 179.
120. M. Stuart, Brit. J. Appl. Phys. 18 (1967) 1637.
121. R. M. Hill, Phil. Mag. 23 (1971) 59.
122. I. T. Johansen, J. Appl. Phys. 37 (1966) 499.
123. P. A. Timson and P. Wickens, Thin Solid Films 5 (1970) R55.
124. M. Deery, J. G. Perkins and K. G. Stephens, Thin Solid Films 8 (1971) R16.
125. R. M. Hill, Thin Solid Films 8 (1971) R21.
126. H. Adachi, Y. Shibata and S. Ono, J. Phys. D: Appl. Phys. 4 (1971) 988.
127. R. B. Hall, Thin Solid Films 8 (1971) 263.
128. C. J. Adkins, S. M. Freake and E. M. Hamilton, Phil. Mag. 22 (1970) 183.
129. D. F. Barbe, J. Phys. D: Appl. Phys. 4 (1971) 1812.
130. J. J. O'Dwyer, J. Appl. Phys. 37 (1966) 599.
131. P. A. Timson, Ph.D. Thesis, Brunel University (1971).
132. C. R. Crowell, W. G. Spitzer, L. E. Howarth and E. E. LaBate, Phys. Rev. 127 (1962) 2006.
133. C. Kittel, Introduction to Solid State Physics, 3rd edition (New York: Wiley, 1966) p208.

134. J. J. Quinn, Appl. Phys. Letters 2 (1963) 167.
135. R. D. Gould, Phys. Stat. Solidi (a) 9 (1972) K177.
136. R. D. Gould, C. A. Hogarth and R. A. Collins, J. Non-Crystalline Solids 12 (1973) 131.
137. R. E. Collins and L. W. Davies, Appl. Phys. Letters 2 (1963) 213.
138. E. D. Savoye and D. E. Anderson, J. Appl. Phys. 38 (1967) 3245.
139. L. A. Serebrov and V. I. Salin, Sov. Phys. - Solid State 7 (1965) 1261.
140. N. L. Yasnopol'skii and A. E. Shabel'nikova, Sov. Phys. - Solid State 10 (1968) 75.
141. E. L. Garwin and J. Llacer, J. Appl. Phys. 41 (1970) 1489.
142. R. M. Handy, J. Appl. Phys. 37 (1966) 4620.

FIGURES

1. Device properties
2. Band diagrams of un-formed and formed diodes (after Hickmott)
3. Band diagrams of un-formed device (after Simmons)
4. Band diagrams of formed device (after Simmons)
5. Model of Ralph and Woodcock
6. Device arrangement
7. Typical Talystep traces
8. The vacuum test system
9. Interior of test system chamber
10. Circuits
11. Hemispherical anode
12. Dependence of I_c and I_e on V_b
13. Transient responses of I_c at different voltages
14. Variation of I_c with time
15. Variation of I_e with time
16. Dependence of device temperature on I_c and V_b
17. Photomicrographs of device damage
18. Dependence of V_β on insulator thickness
19. Dependence of V_β on temperature
20. Dependence of $V_\beta^{\frac{1}{2}}$ on temperature
21. Potential distribution before forming
22. Dependence of I_c on V_{cp} and potential distribution after forming
23. Low temperature dependence of I_c on V_b
24. Low temperature dependence of $\log I_c$ on $V_b^{\frac{1}{2}}$
25. Dependence of mean free path in Ag on electron energy from the theory of Quinn
26. Dependence of $\log I_e/I_c$ on insulator thickness at different voltages
27. Dependence of attenuation length in SiO_x on V_b

28. Dependence of I_e/I_c on retarding potential
29. Emitted electron energy distributions at different temperatures
30. Electron emission patterns at different voltages
31. Linear dependence of square of emission pattern radius on $1/(V_b + \eta)$
32. Angular distributions of emitted electrons
33. Dependence of I_c on V_b in $\text{SiO}_x/\text{B}_2\text{O}_3$
34. Dependence of I_e on V_b in $\text{SiO}_x/\text{B}_3\text{O}_3$
35. Dependence of transmission ratio on V_b in $\text{SiO}_x/\text{B}_2\text{O}_3$
36. Dependence of device temperature on I_c and V_b in $\text{SiO}_x/\text{B}_2\text{O}_3$
37. Forming in CaBr_2
38. Dependence of I_c and I_e on V_b in CaBr_2
39. Dependence of I_c on V_b for increasing and decreasing voltages in CaBr_2
40. Forming in Si_3N_4
41. Dependence of I_c and I_e on V_b in Si_3N_4
42. Dependence of I_c on V_b for increasing and decreasing voltages in Si_3N_4

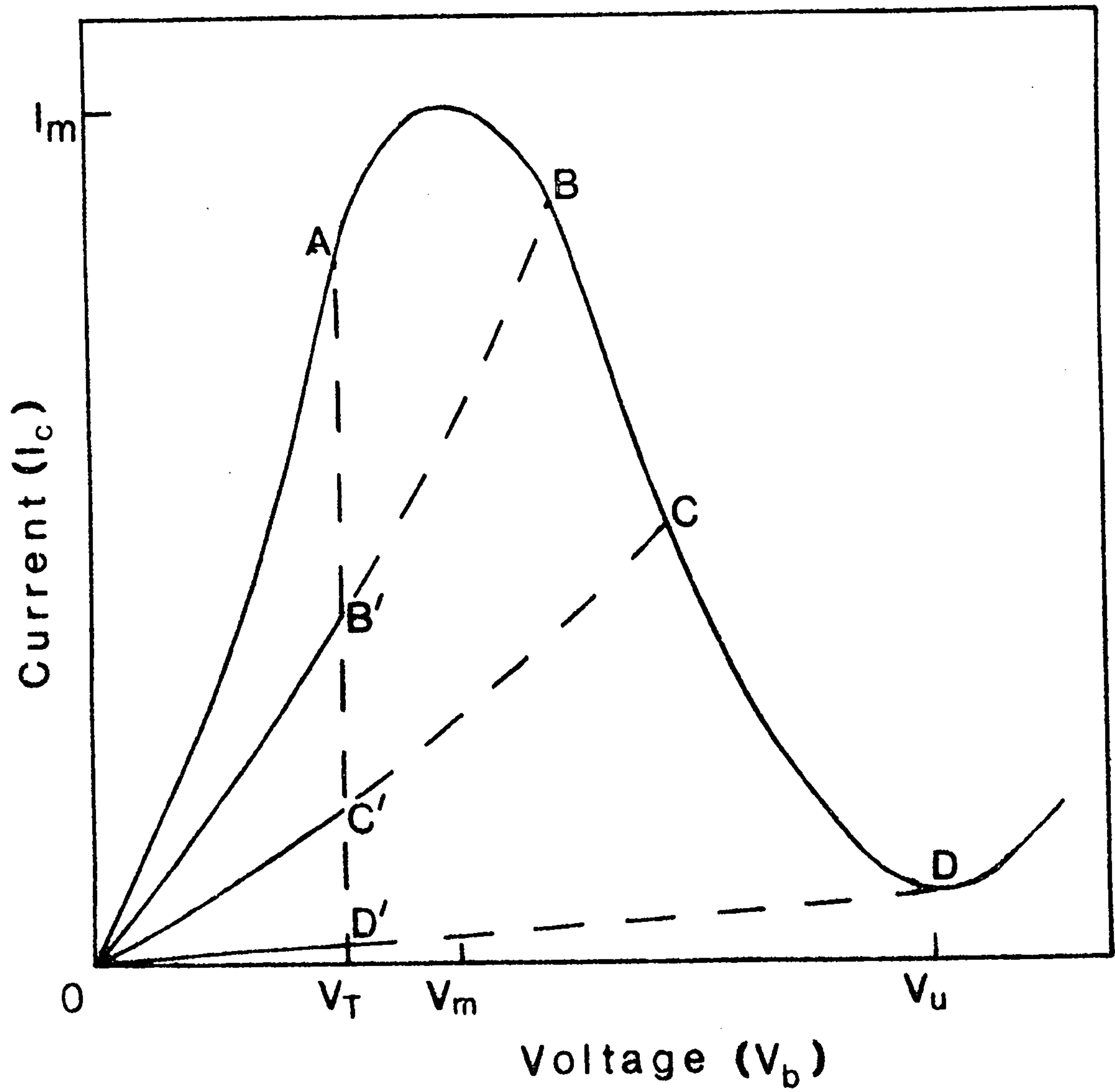
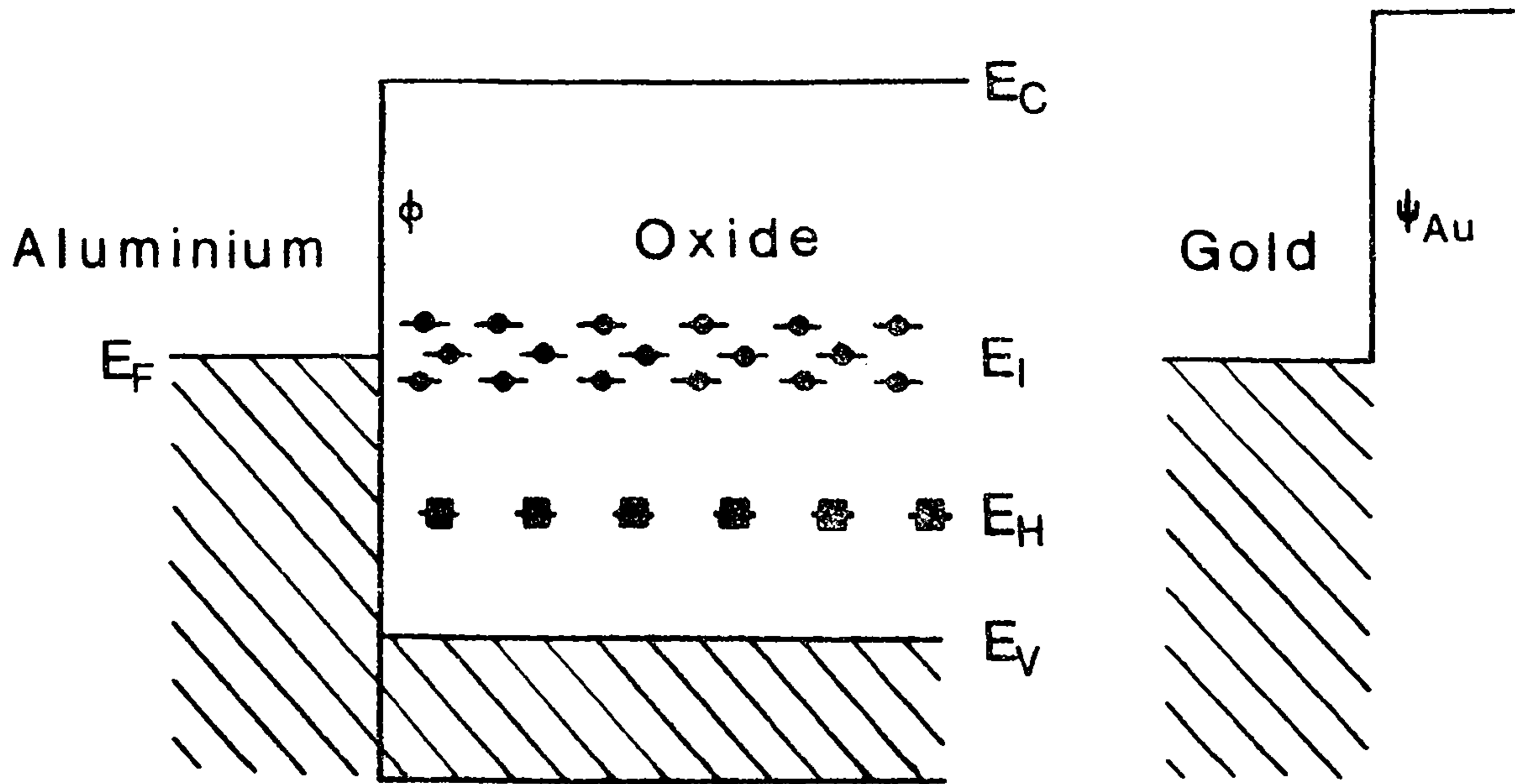
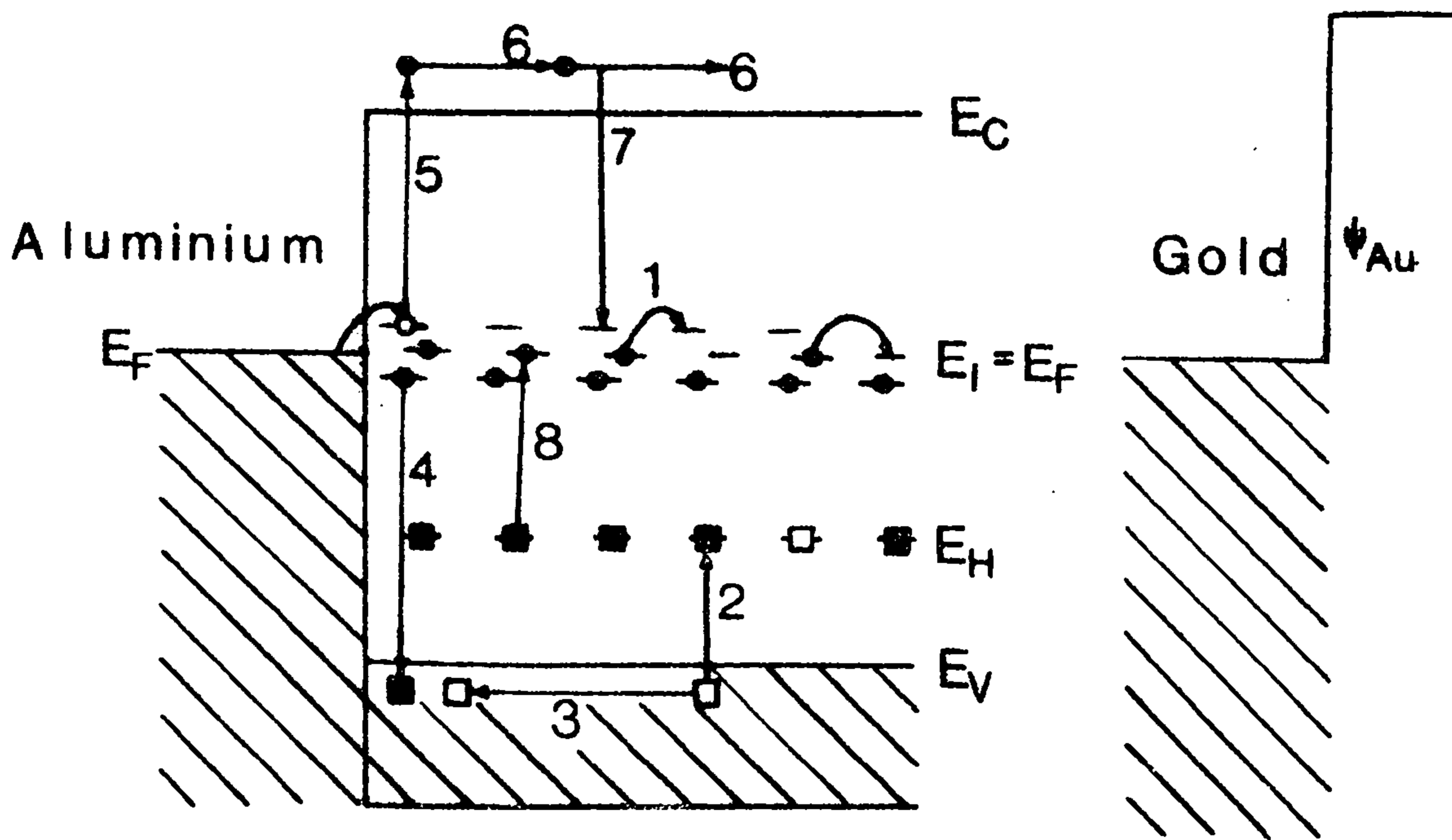


Figure 1. Device properties



a. Un-formed diode



b. Formed diode

Figure 2. Band diagrams of un-formed and formed diodes (after Hickmott)

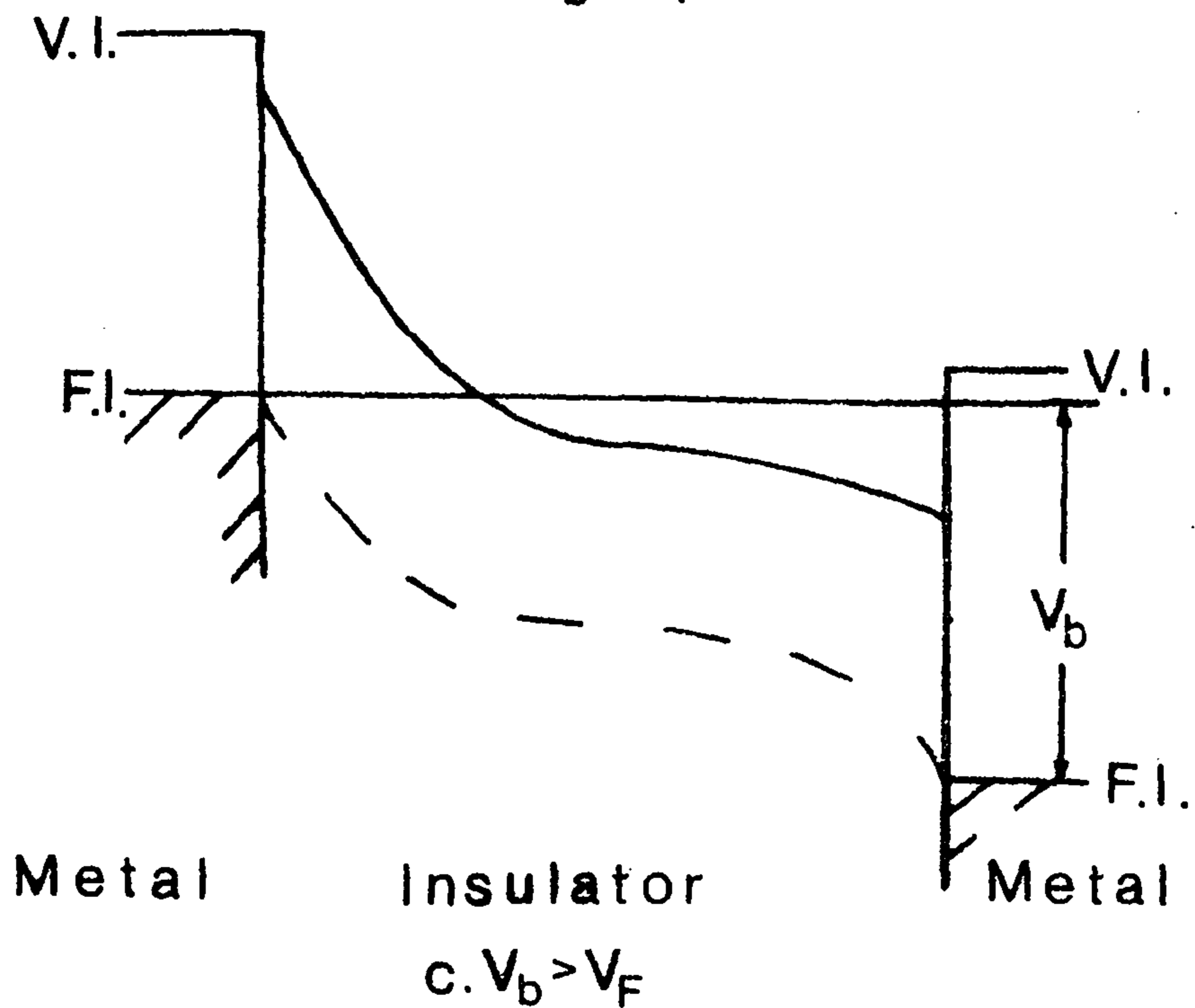
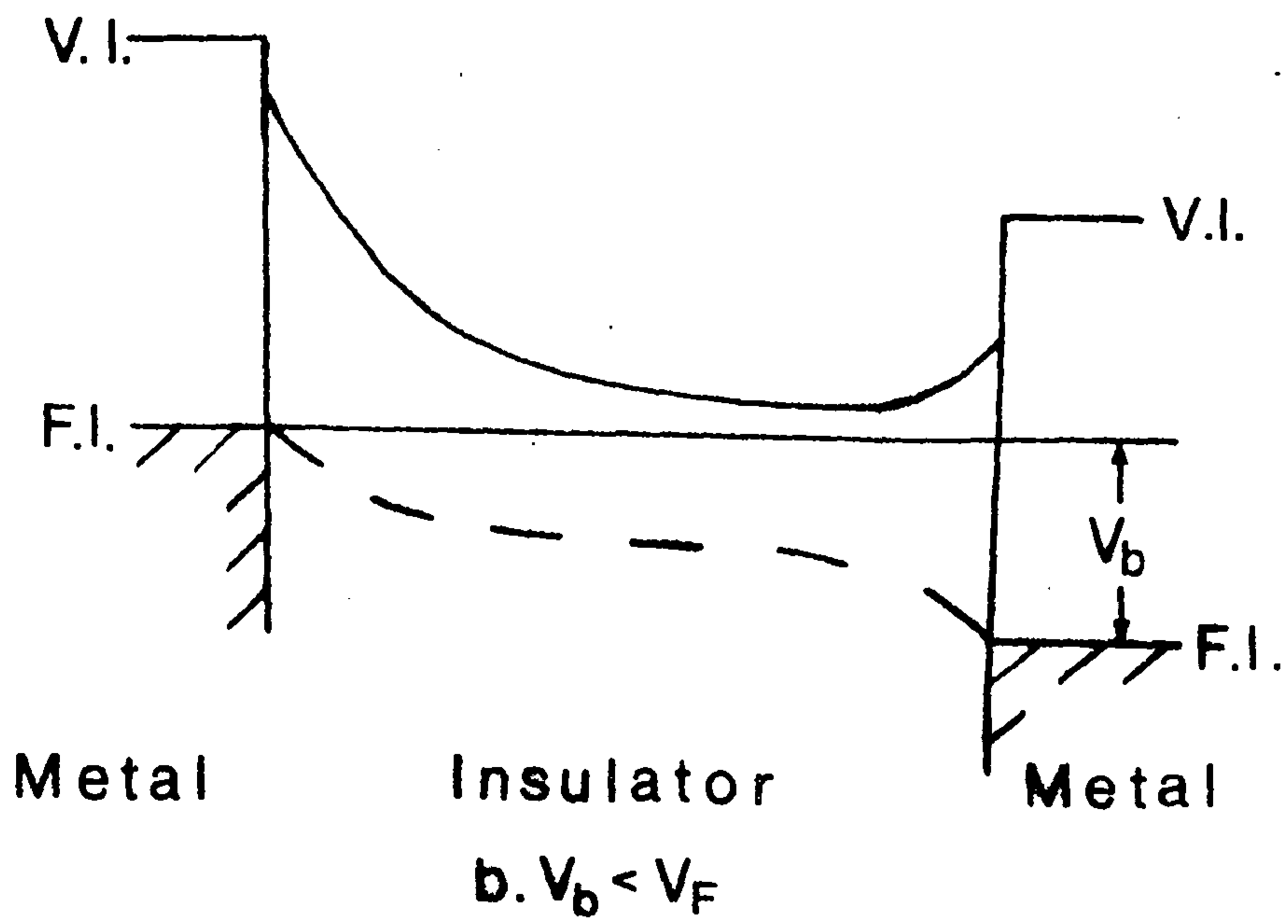
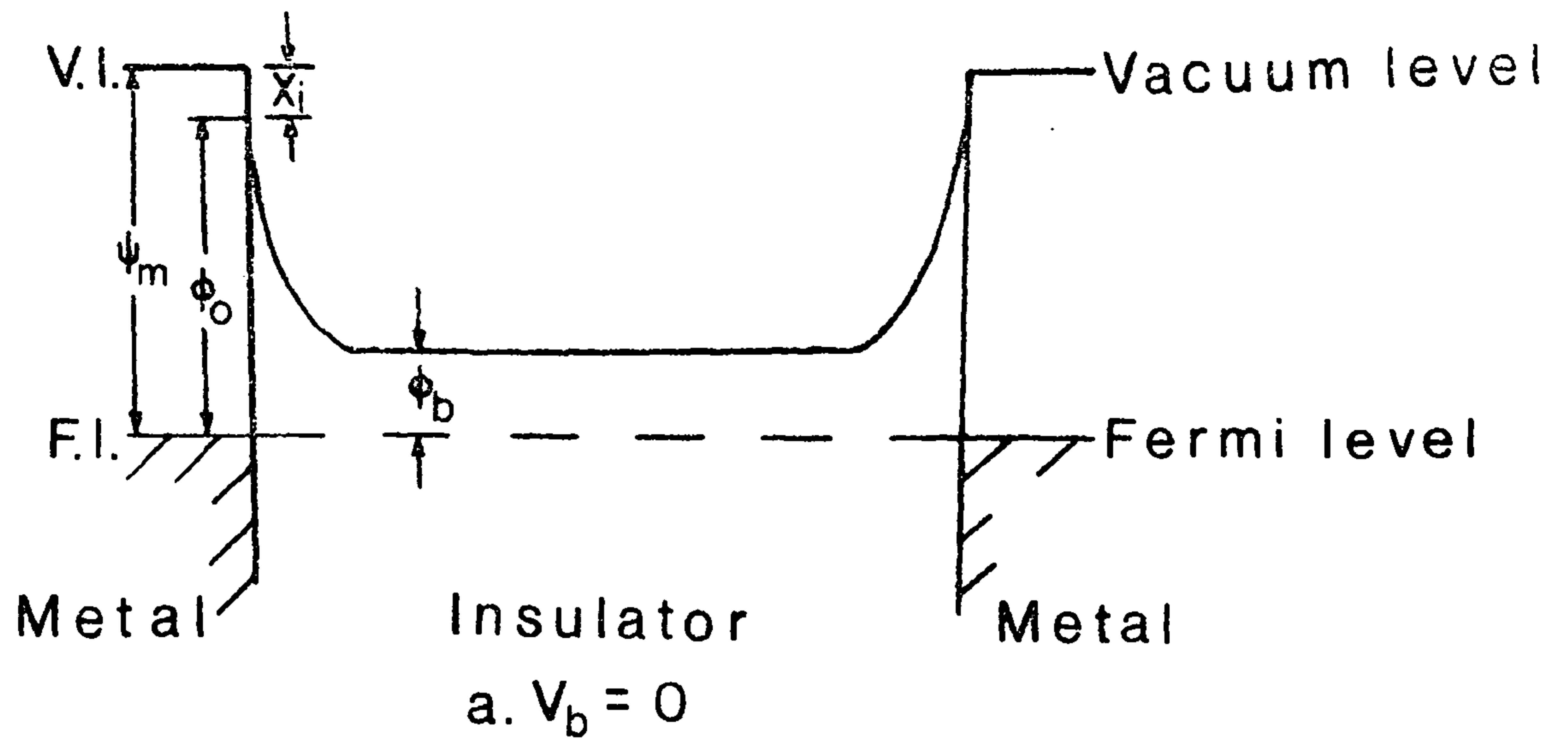


Figure 3. Band diagrams of un-formed device (after Simmons)

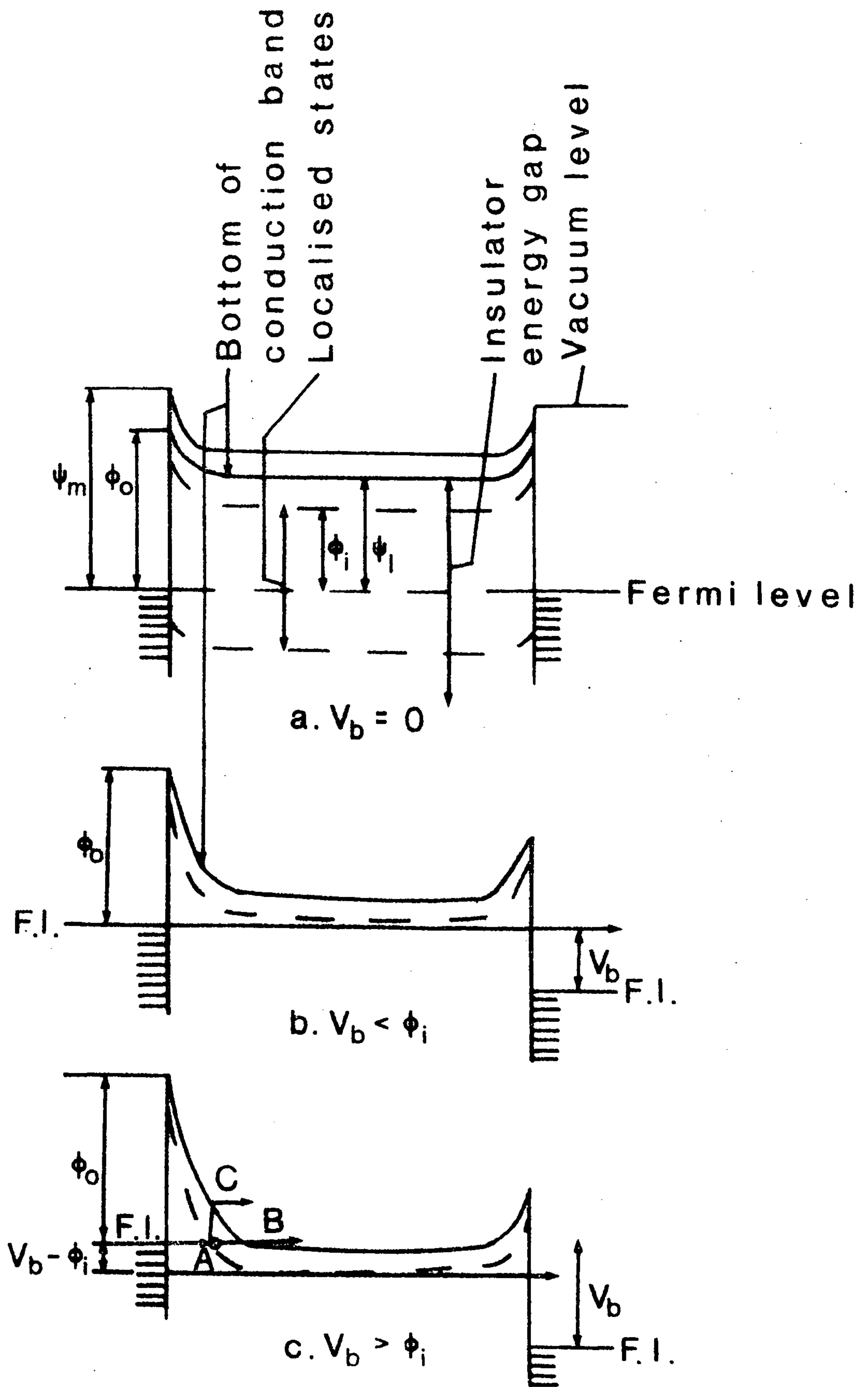
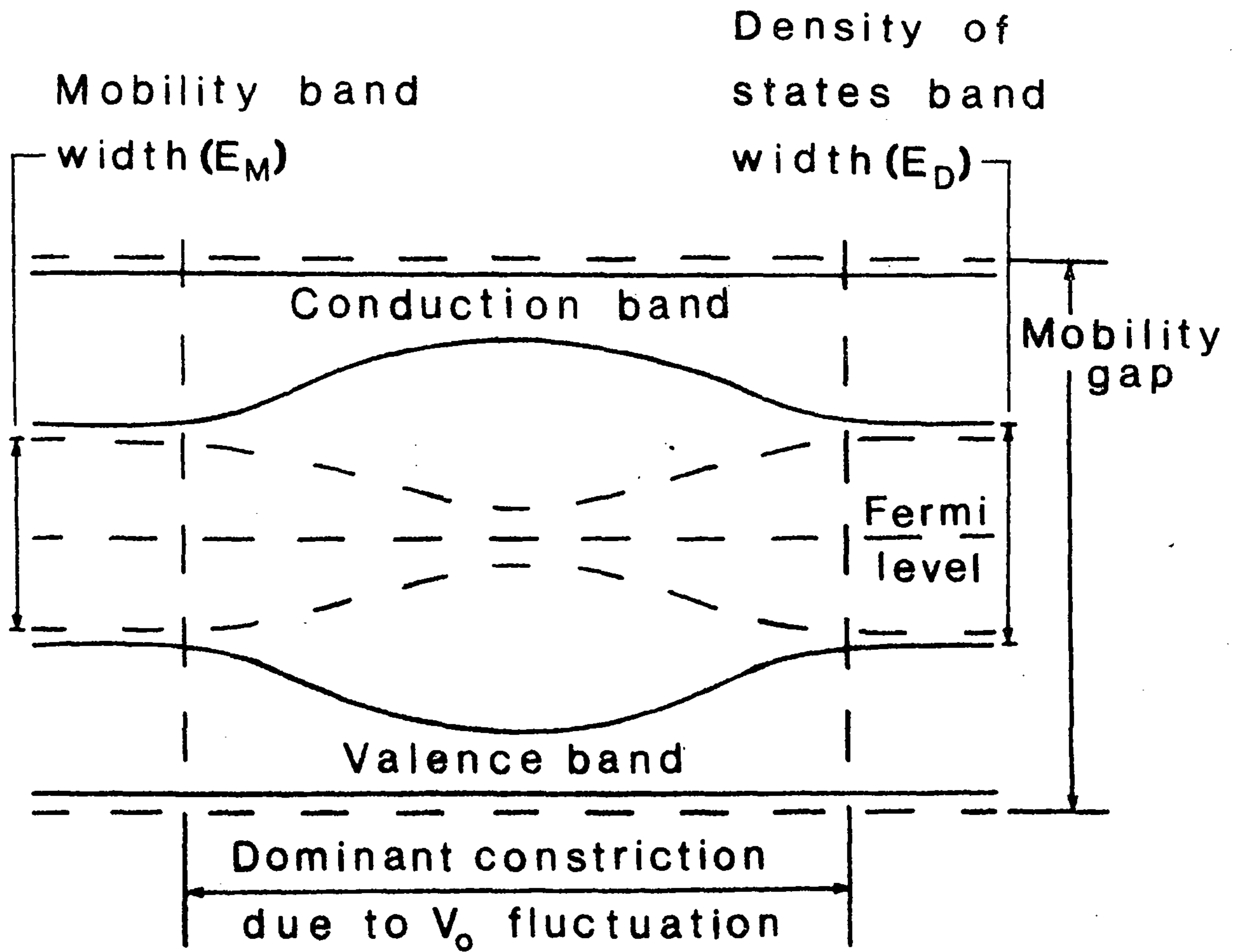
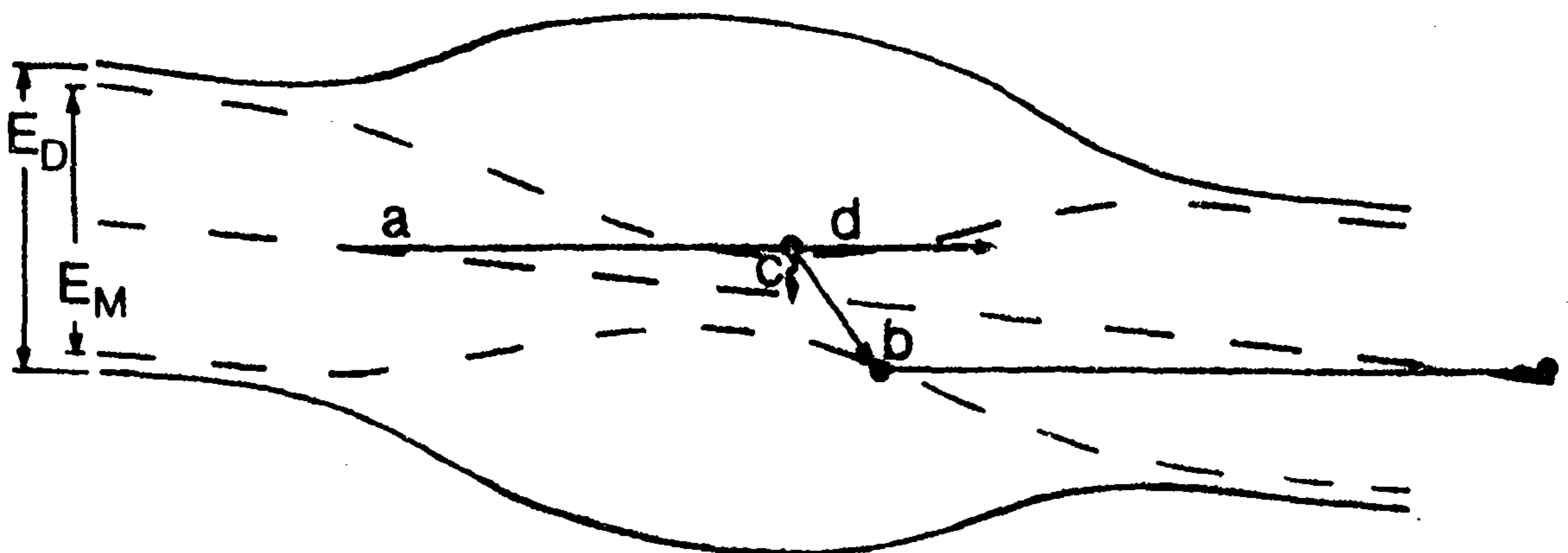


Figure 4. Band diagrams of formed device (after Simmons)



a. Band model of filamentary constriction at zero bias



b. Conduction processes at low bias

Figure 5. Model of Ralph and Woodcock

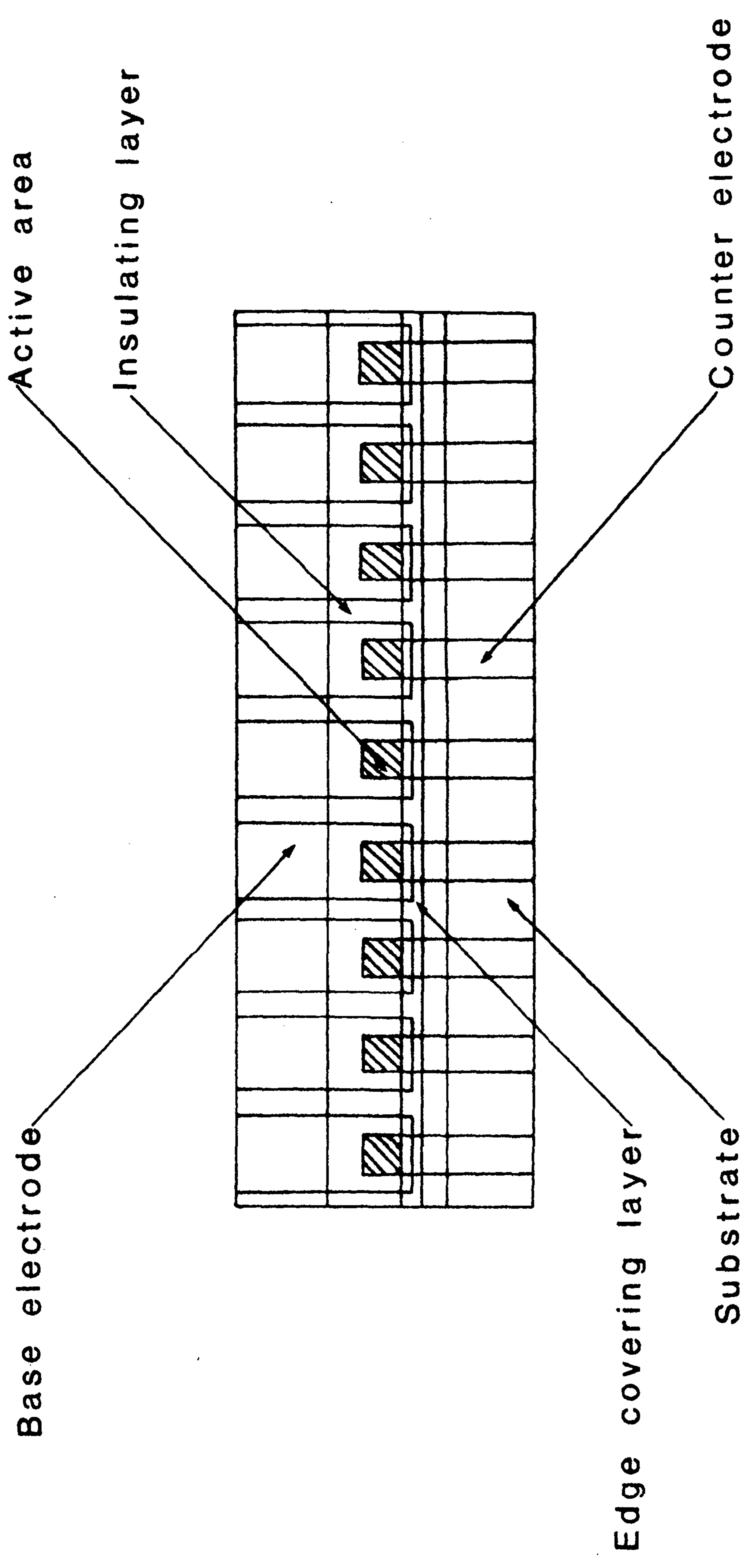
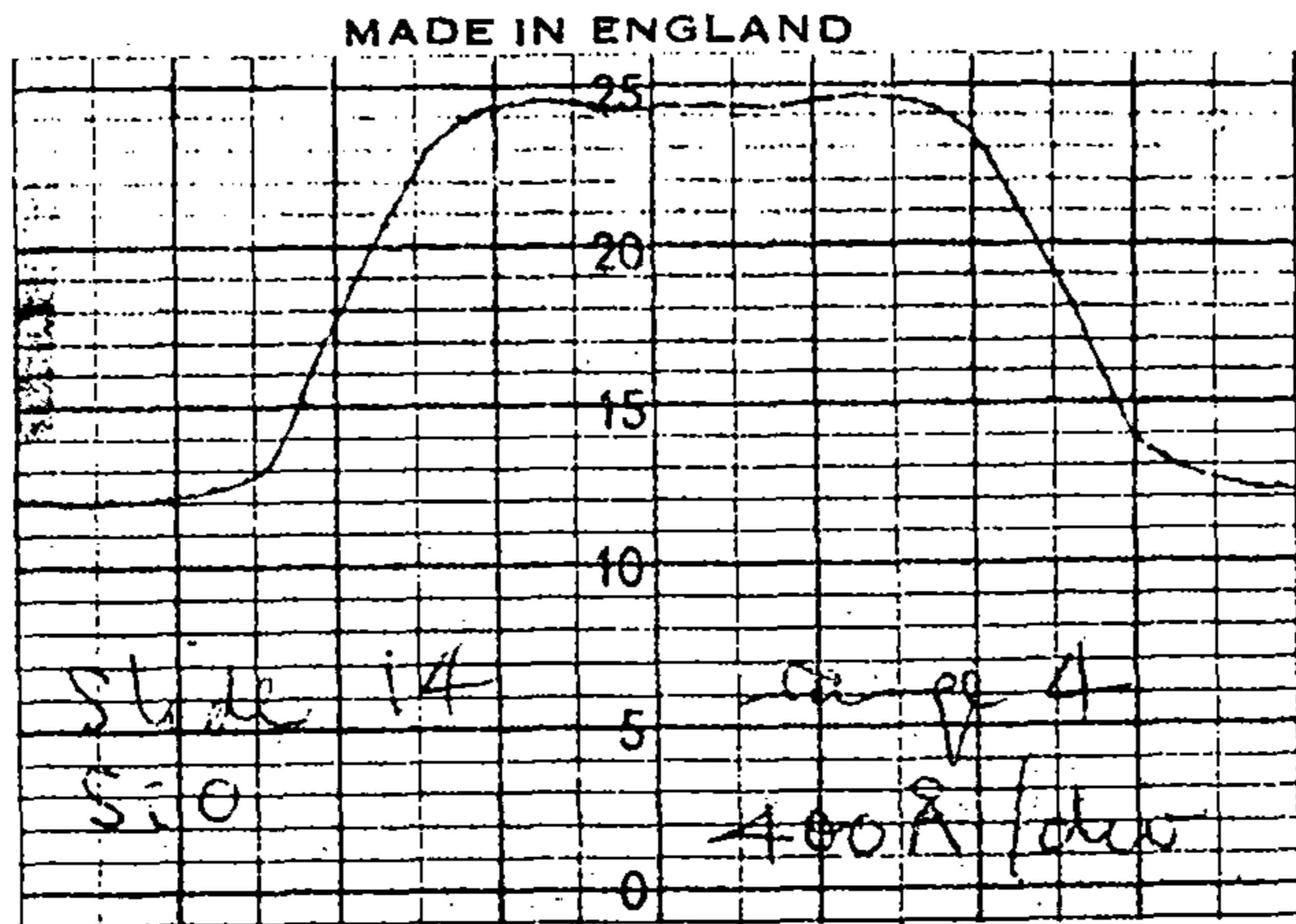
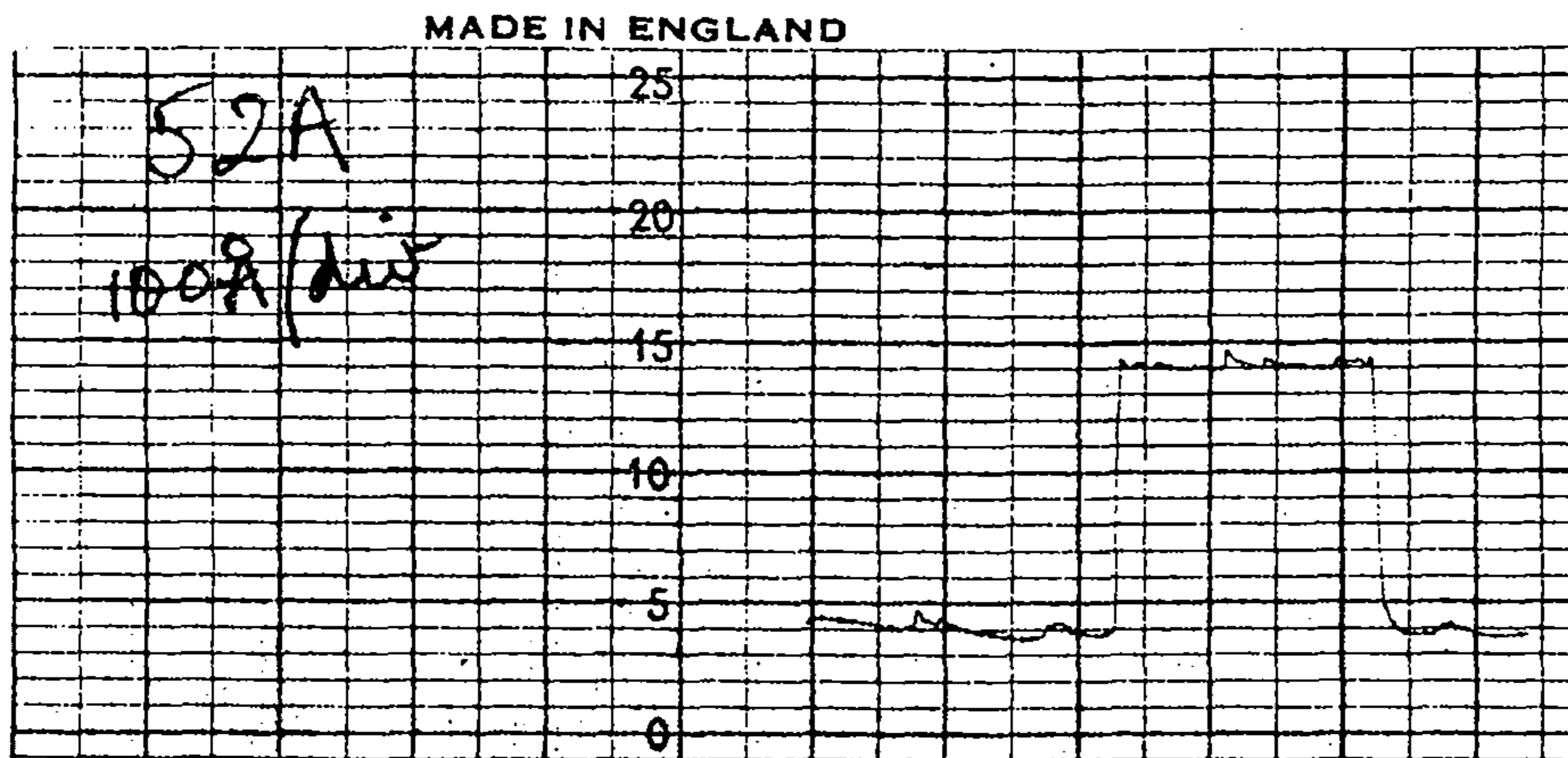


Figure 6. Device arrangement



5000 Å



1000 Å

Figure 7. Typical Talystep traces

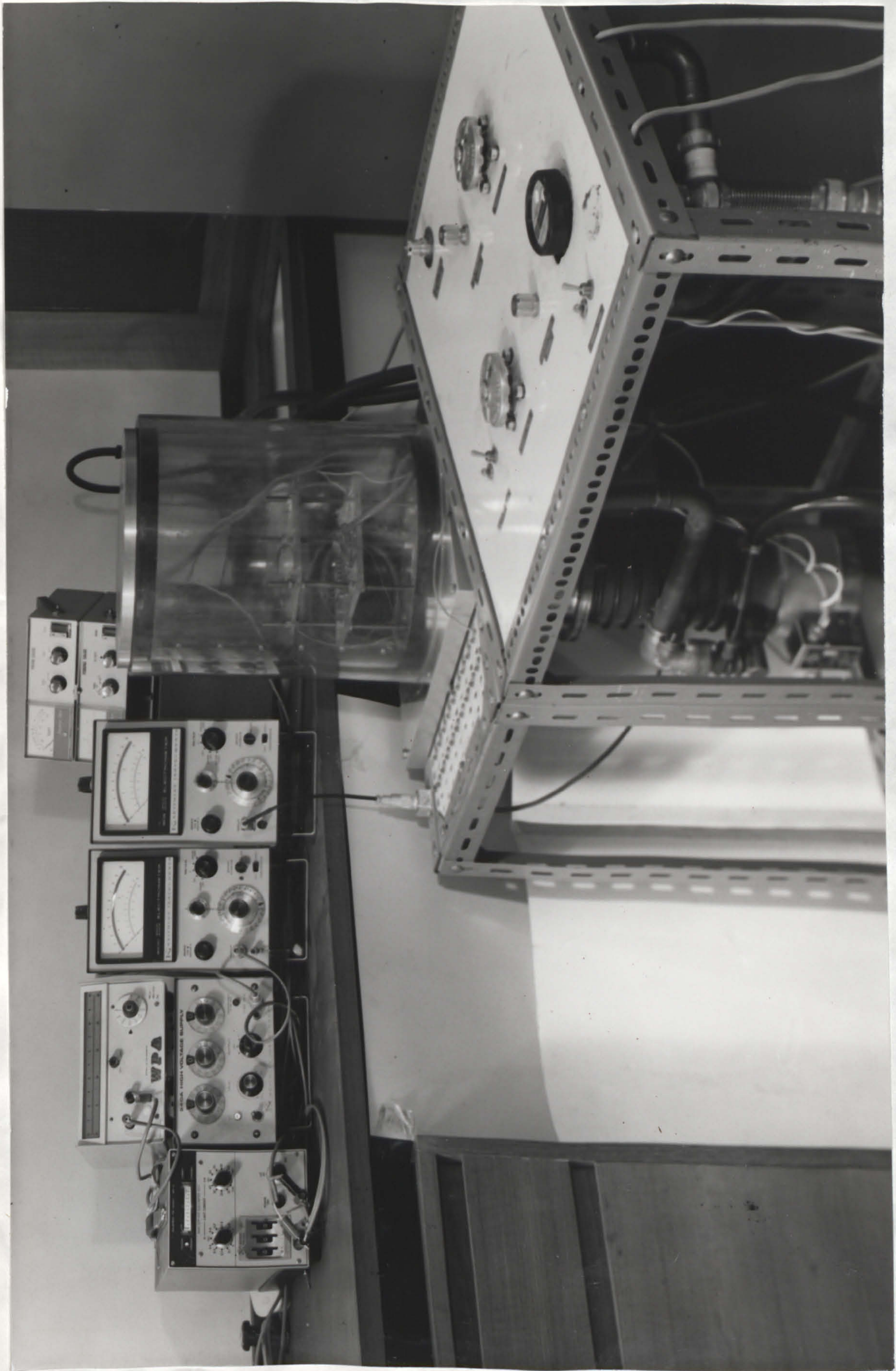


Figure 8. The vacuum test system

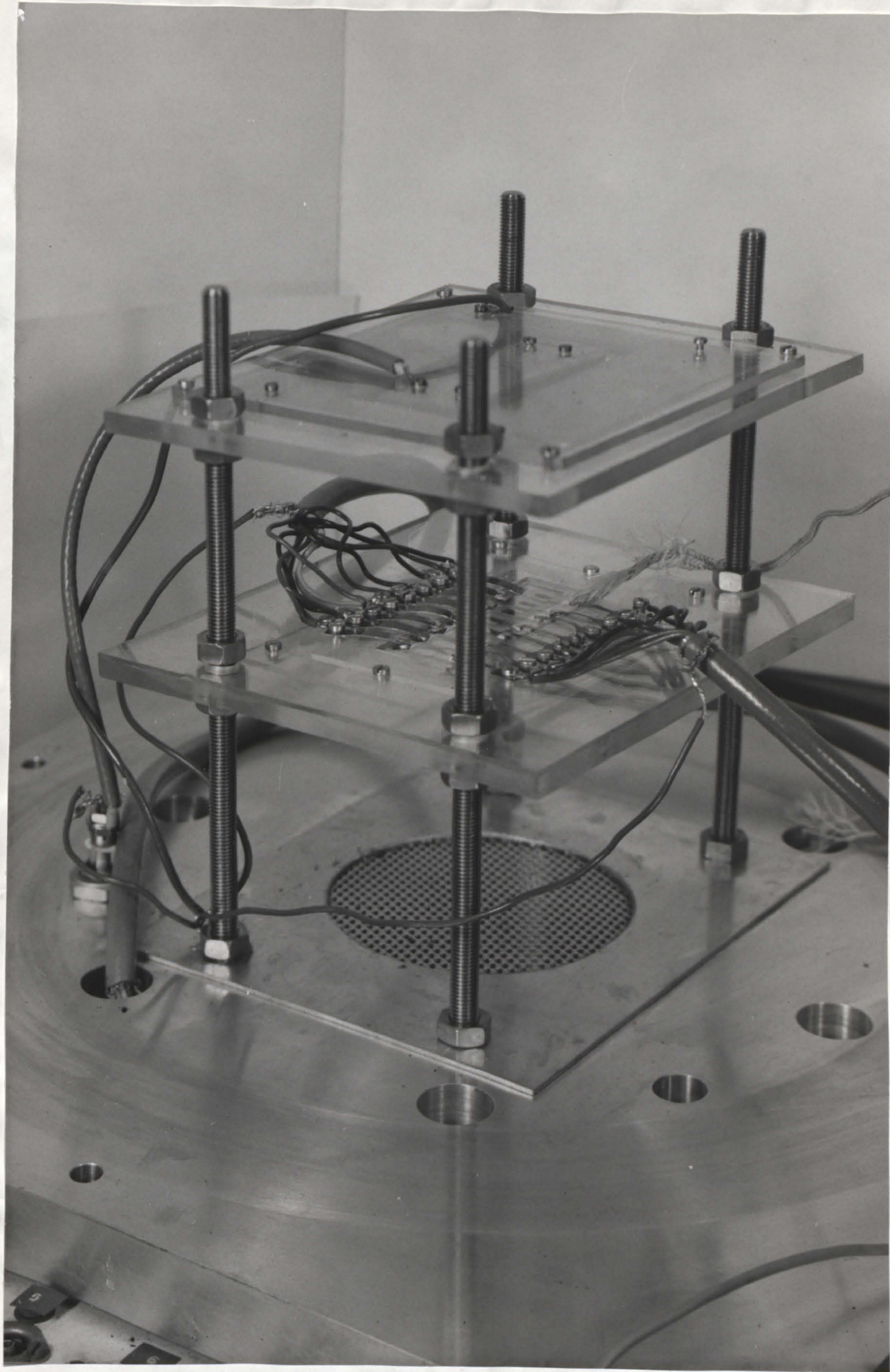
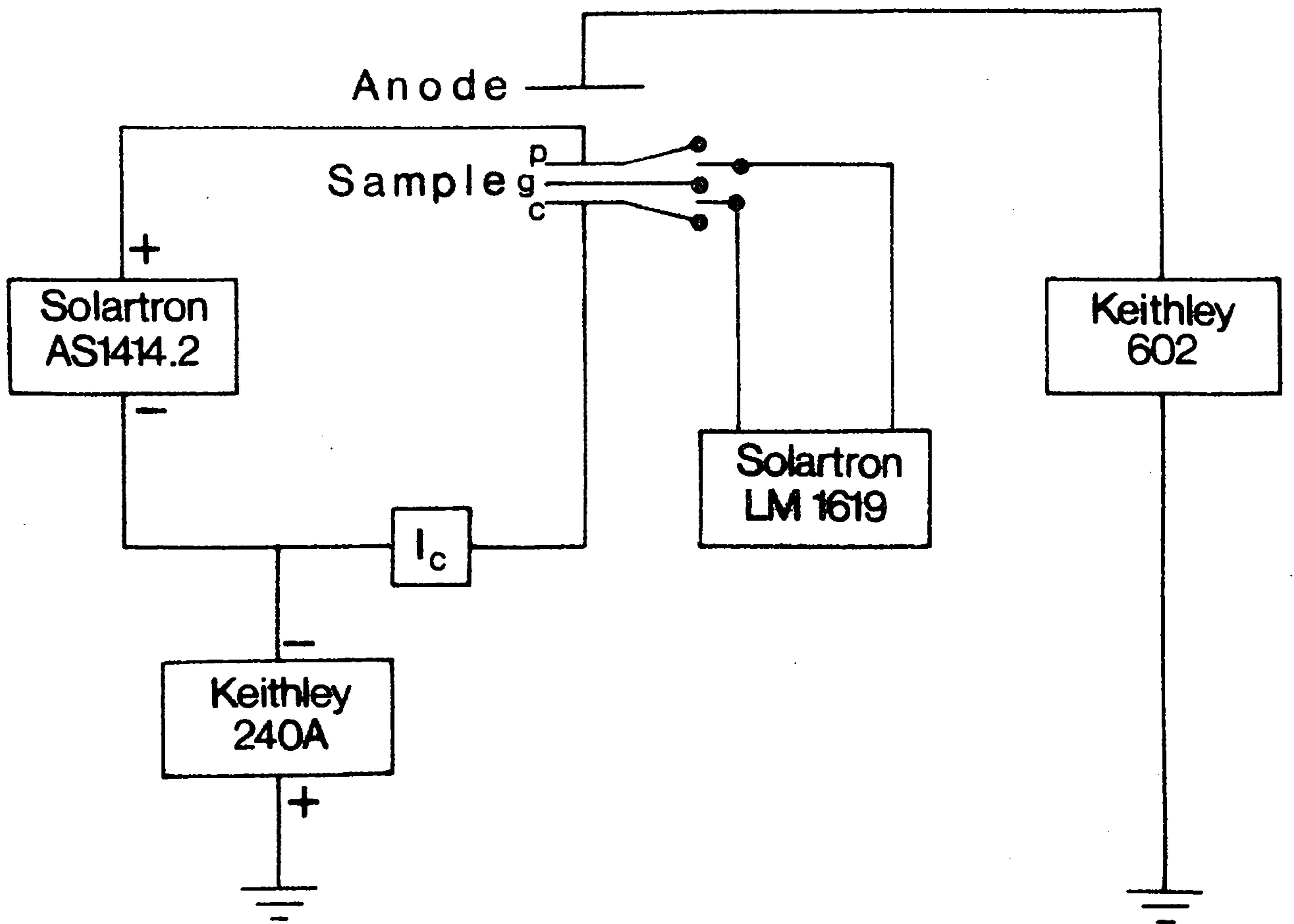
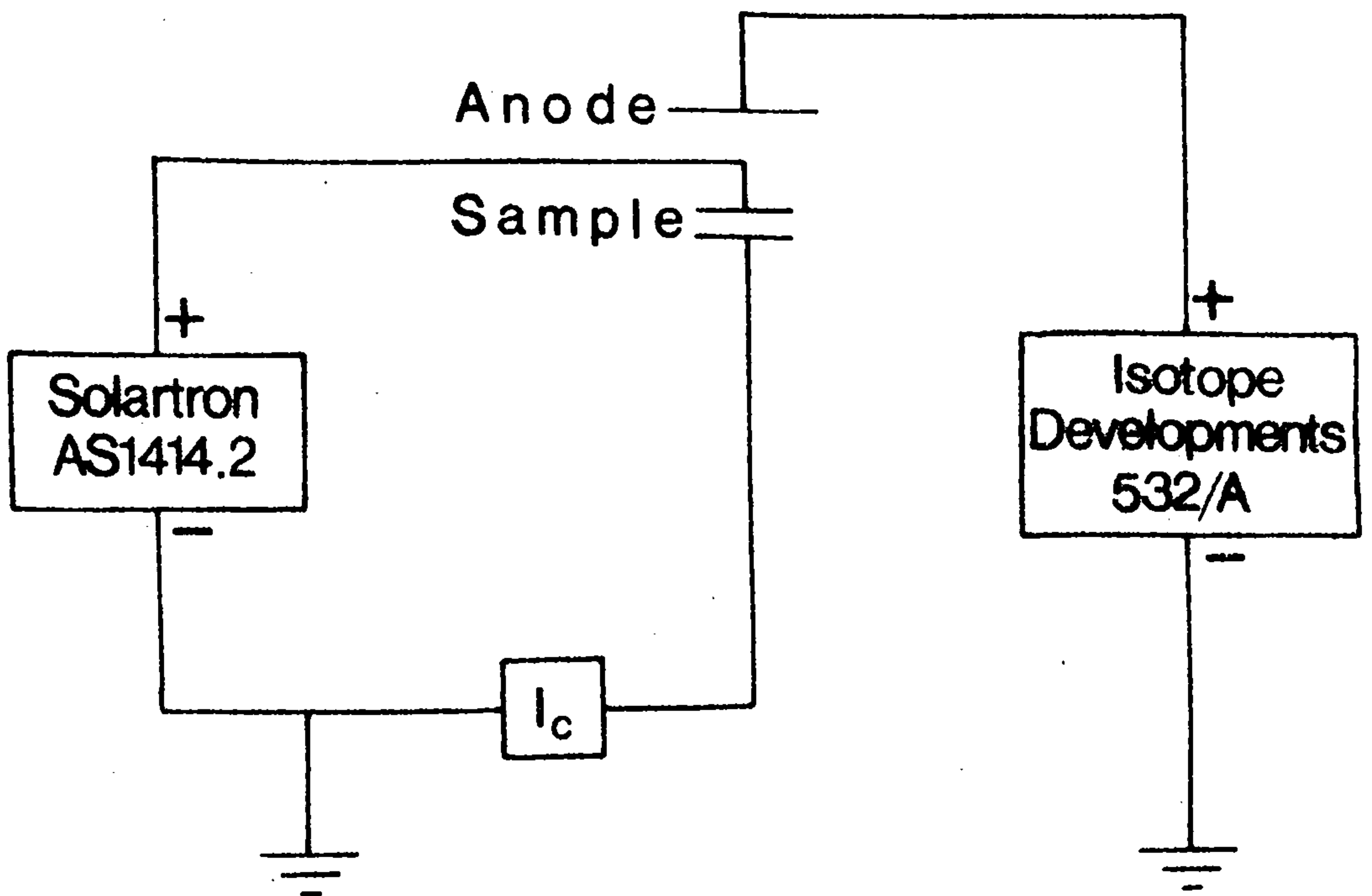


Figure 9. Interior of test system chamber

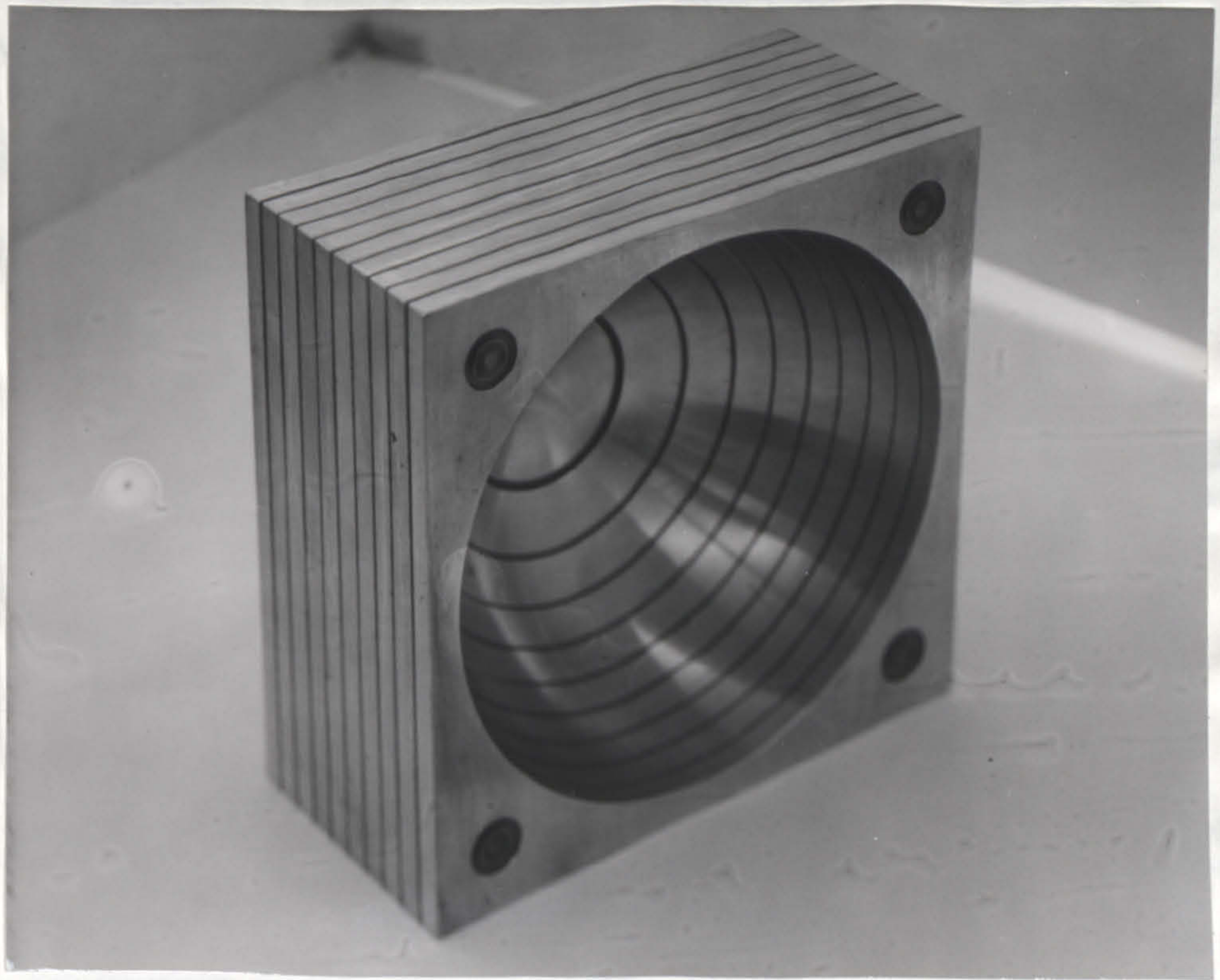


a. Circuit for electrical measurements

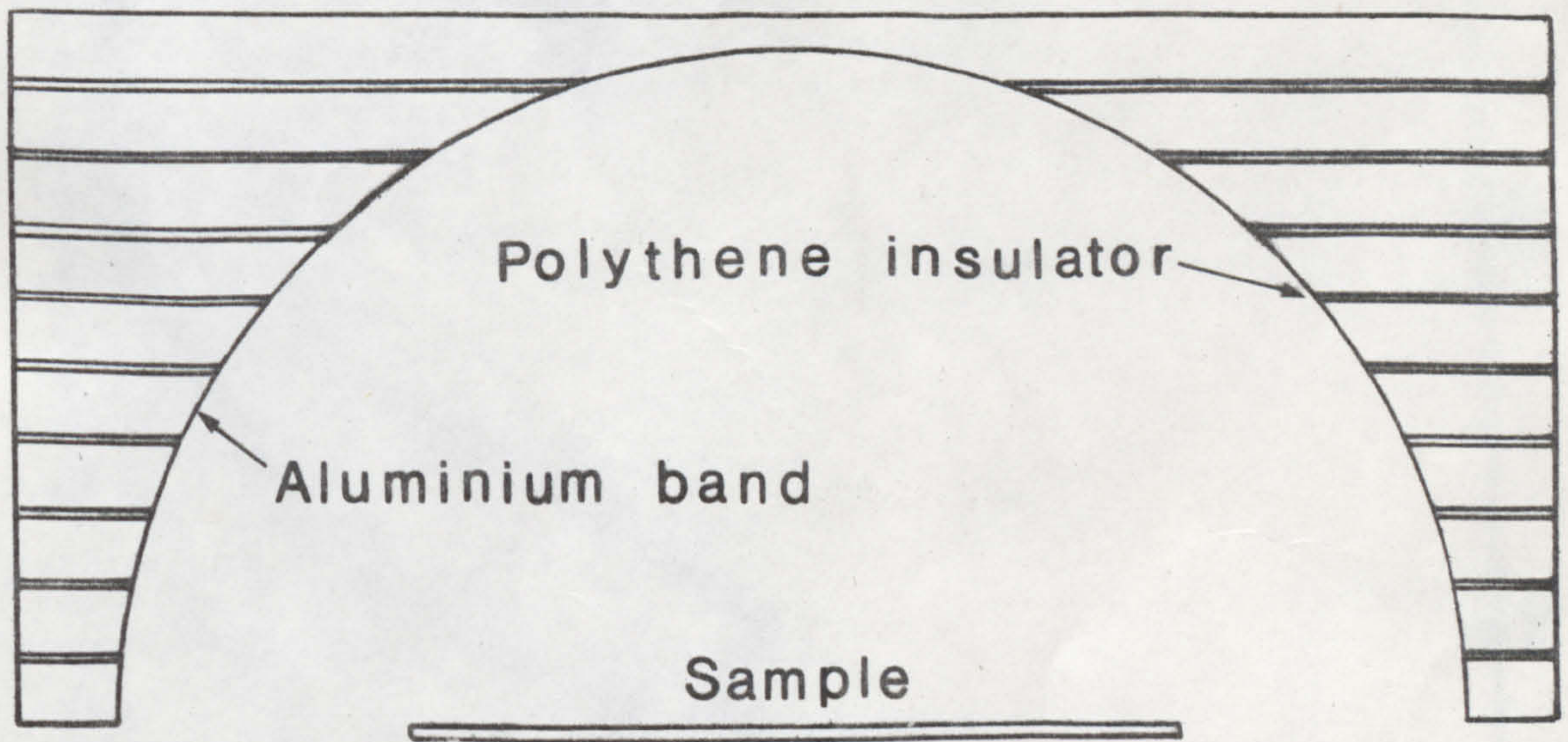


b. Circuit for observing emission patterns

Figure 10. Circuits



Photograph



Section through anode

Figure 11. Hemispherical anode

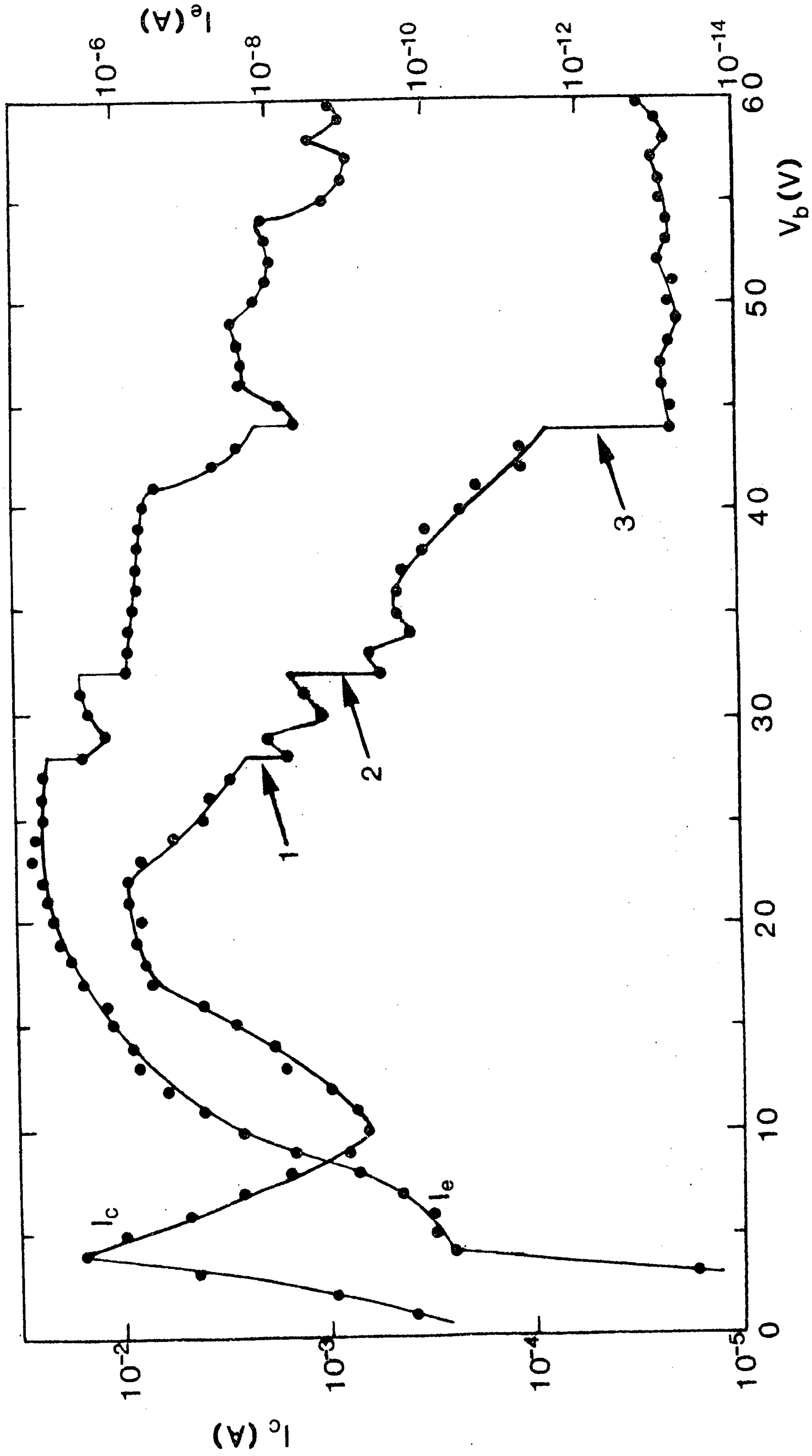


Figure 12. Dependence of I_c and I_e on V_b

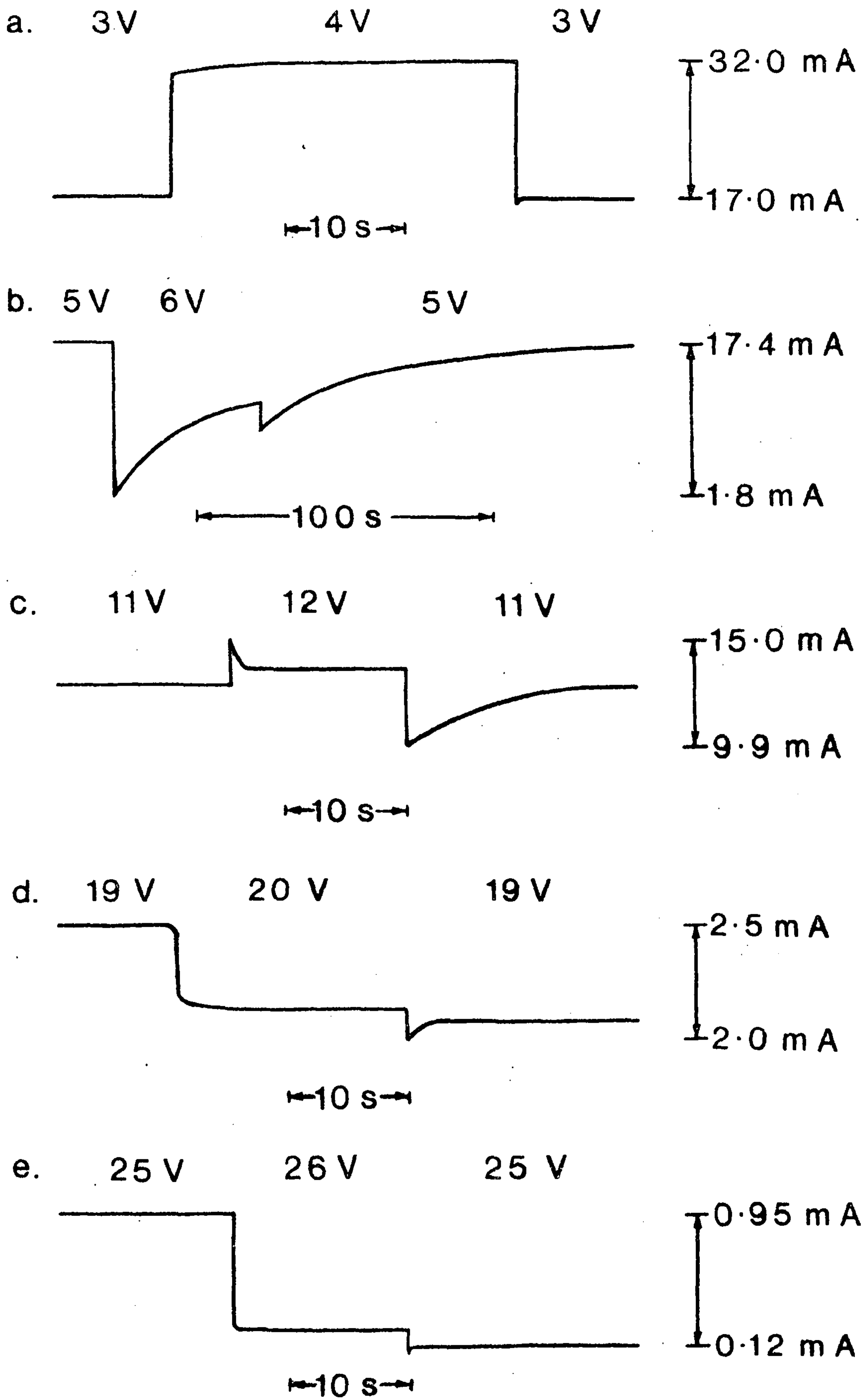
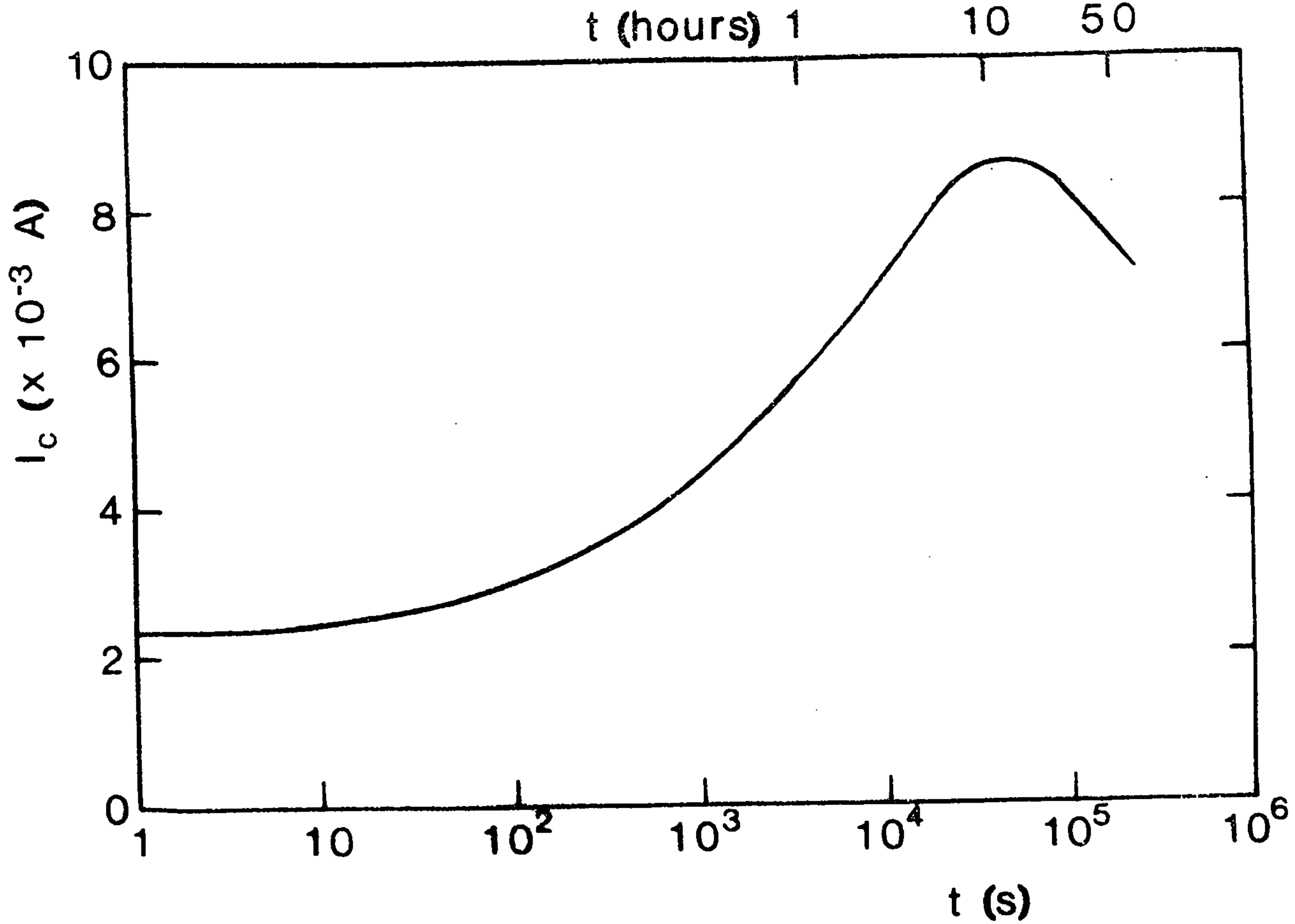
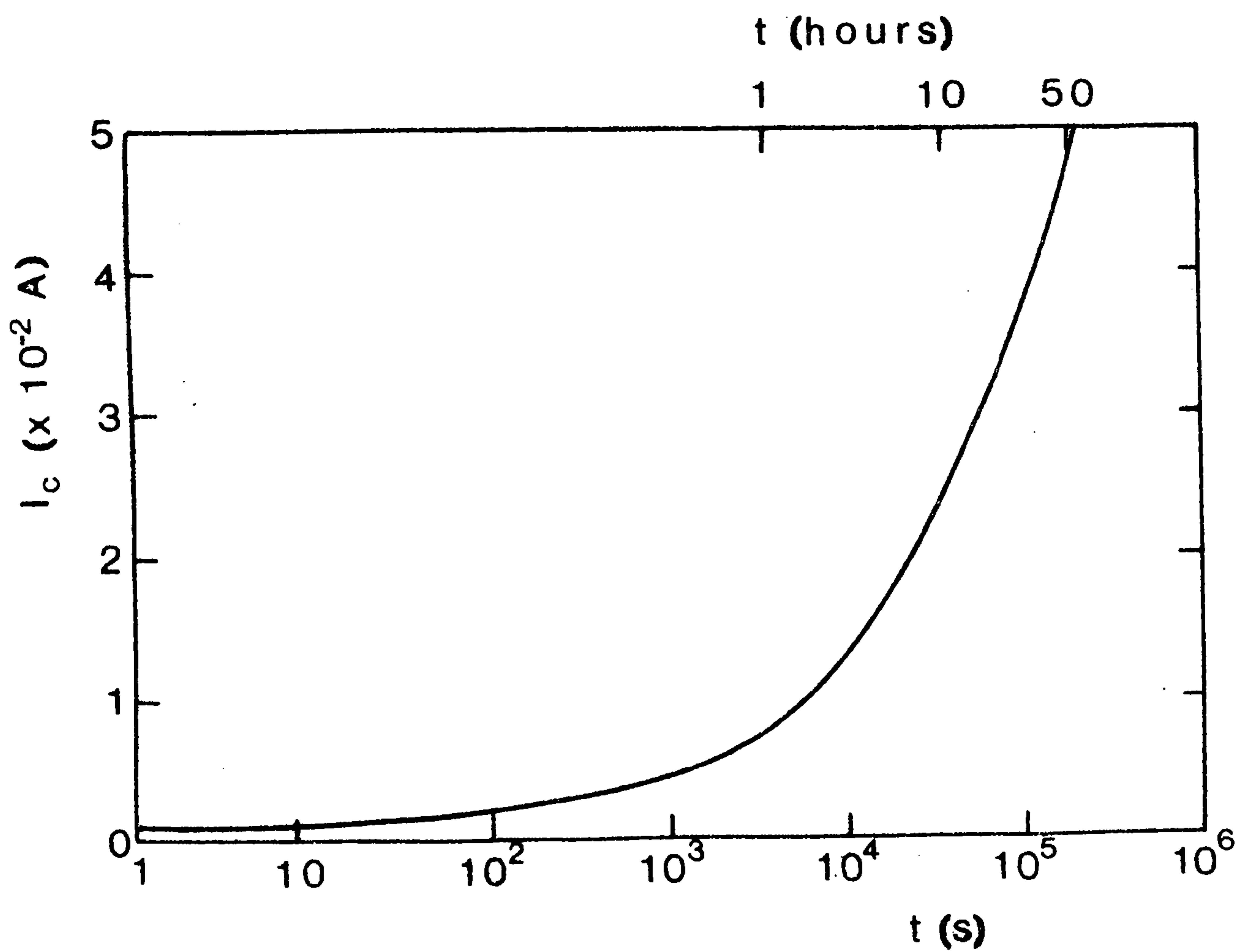


Figure 13. Transient responses of I_c at different voltages

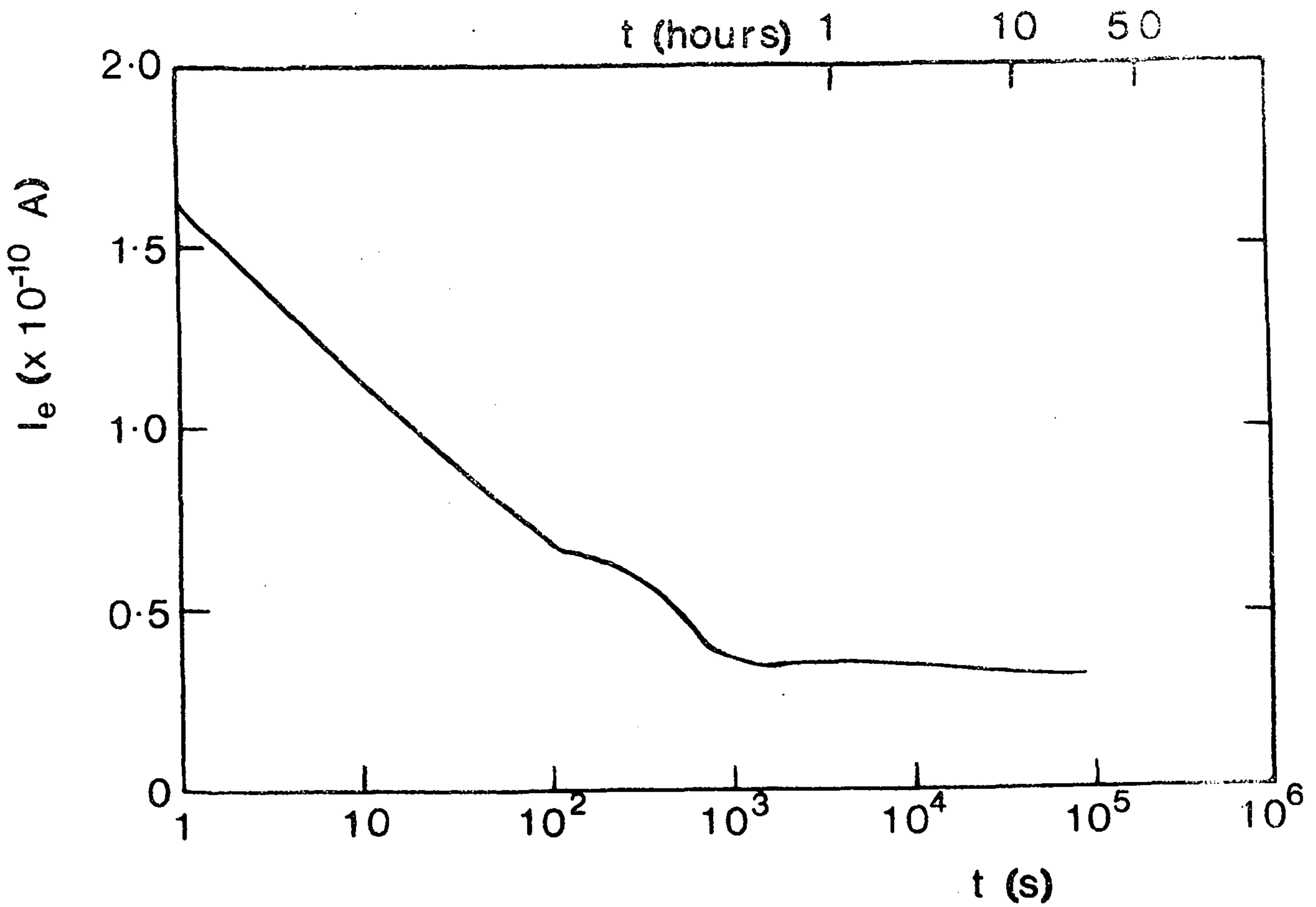


a. $V_m = 3.4$ V

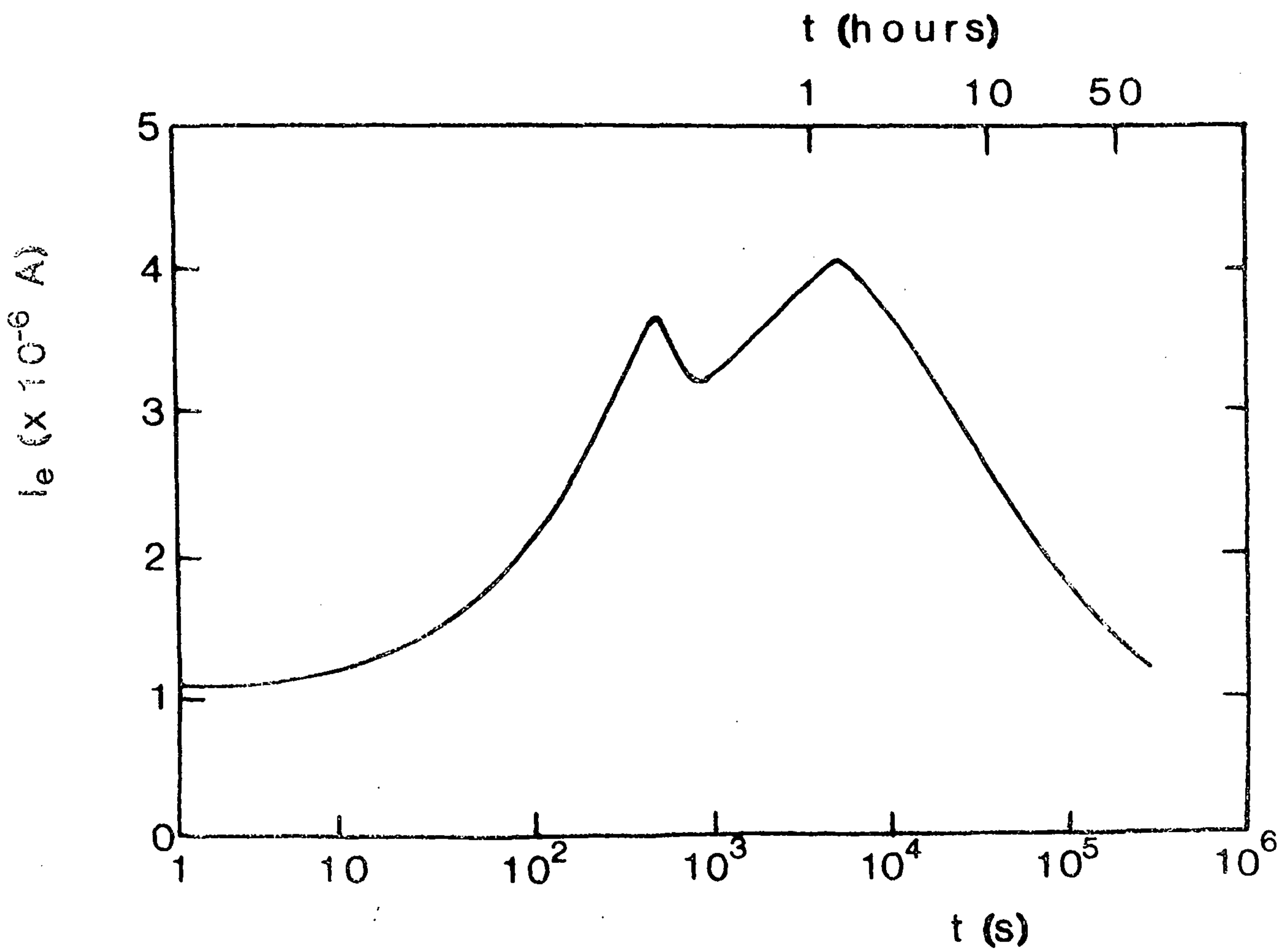


b. $V_u = 10$ V

Figure 14. Variation of I_c with time



a. $V_m = 3.4$ V



b. $V_u = 12$ V

Figure 15. Variation of I_e with time

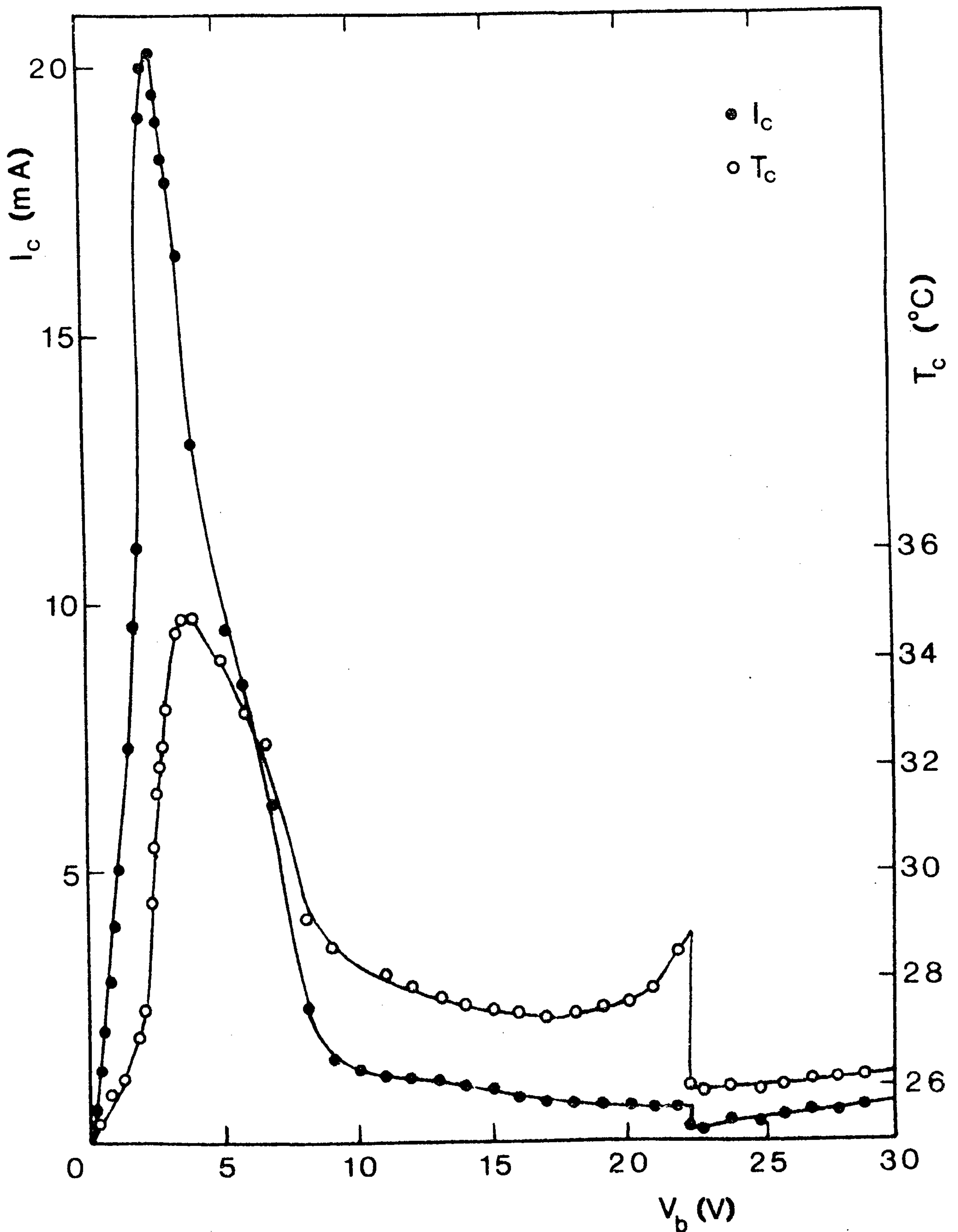
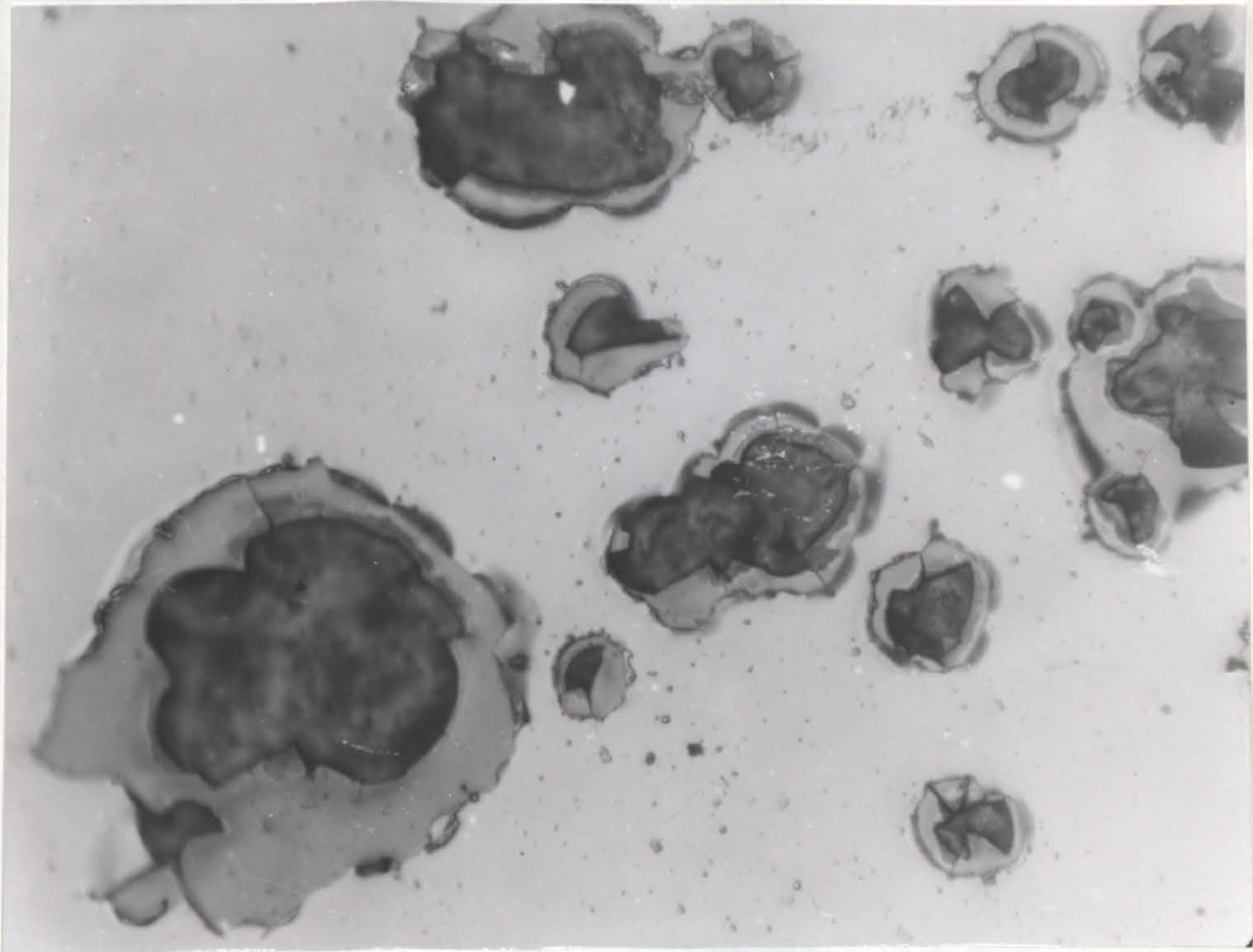


Figure 16. Dependence of device temperature on I_c and V_b



a.

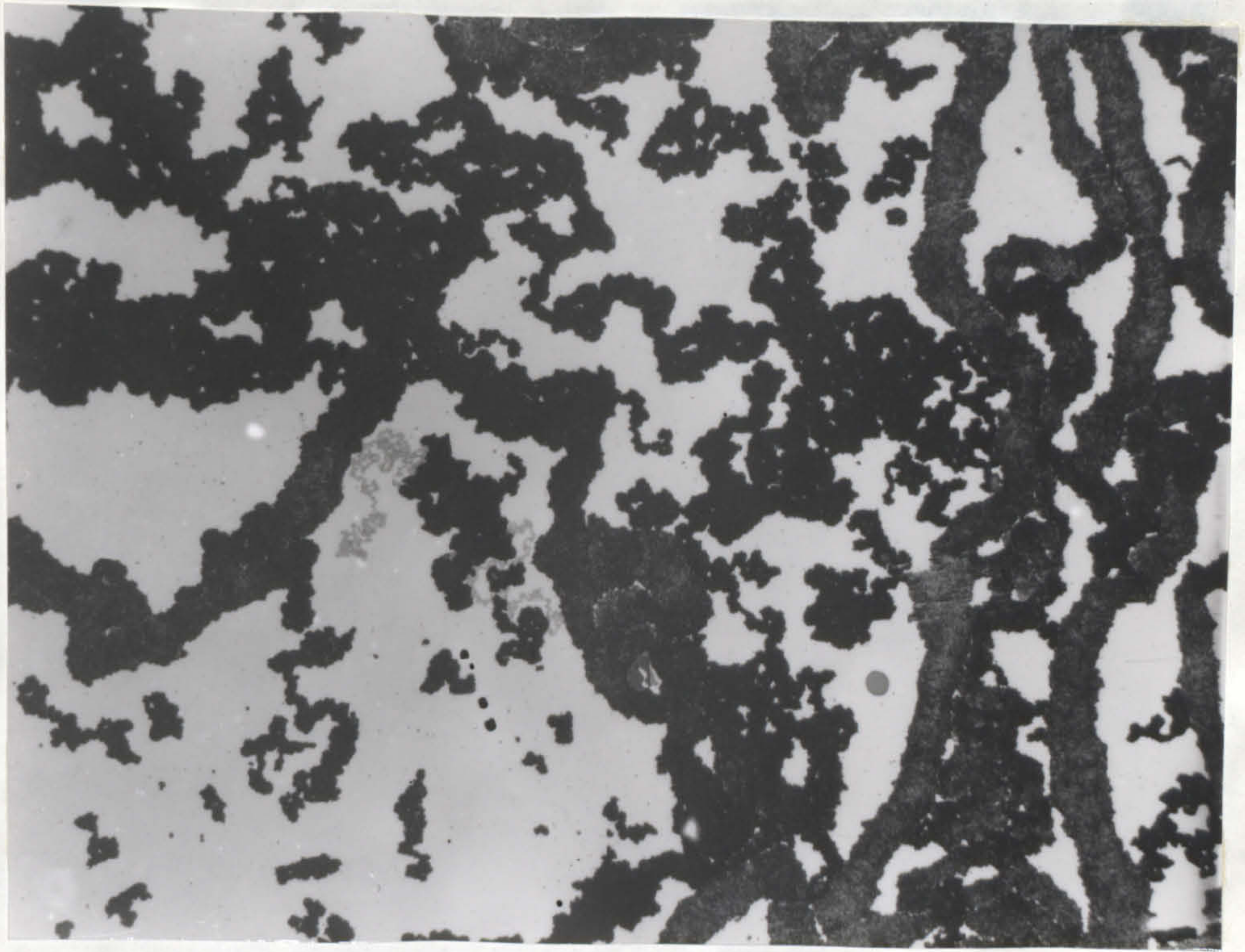
—|—| 100 μ m



b.

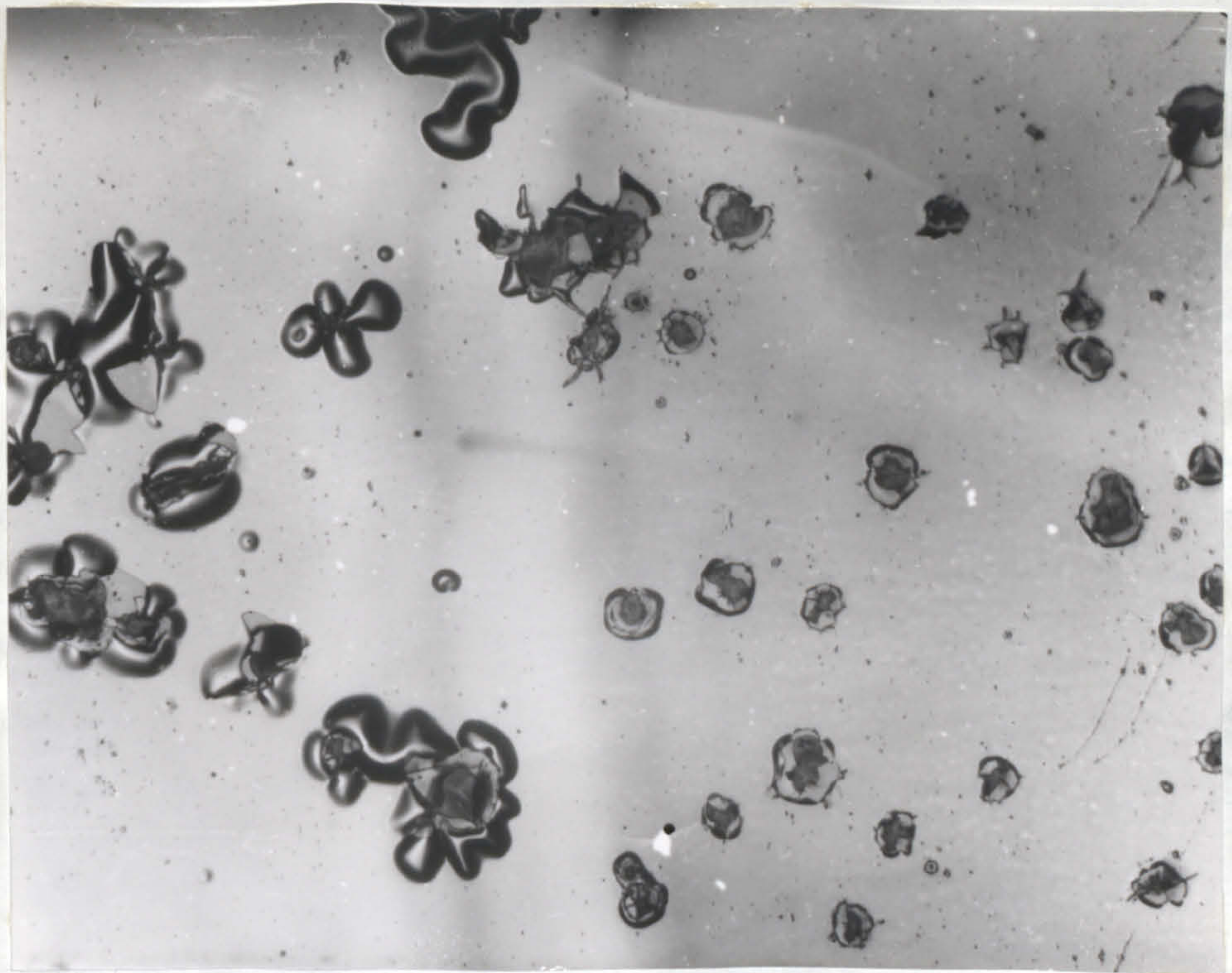
—|—| 10 μ m

Figure 17. Photomicrographs of device damage



c.

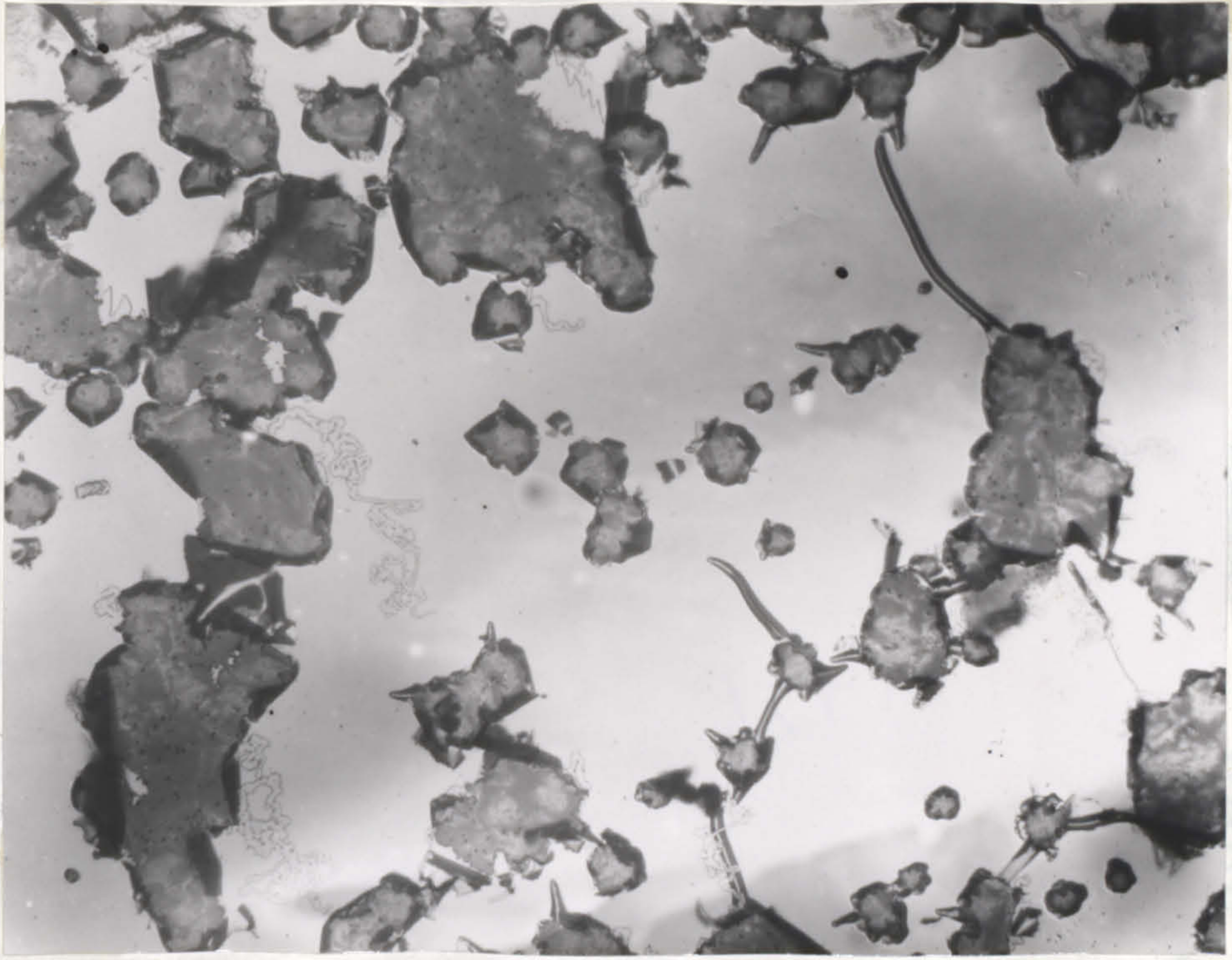
—|—| 100 μ m



d.

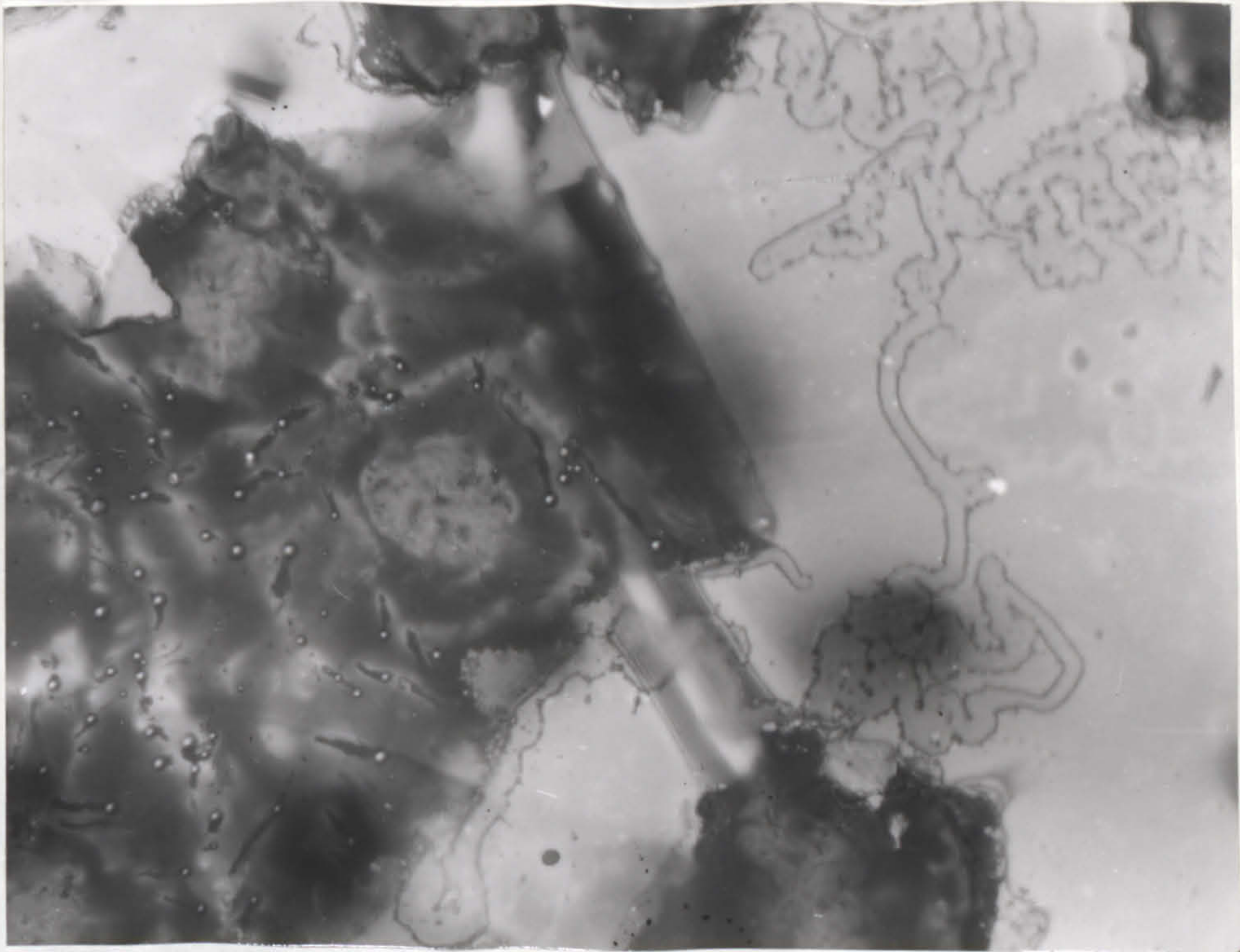
—|—| 100 μ m

Figure 17. Photomicrographs of device damage



e.

100 μm



f.

10 μm

Figure 17. Photomicrographs of device damage

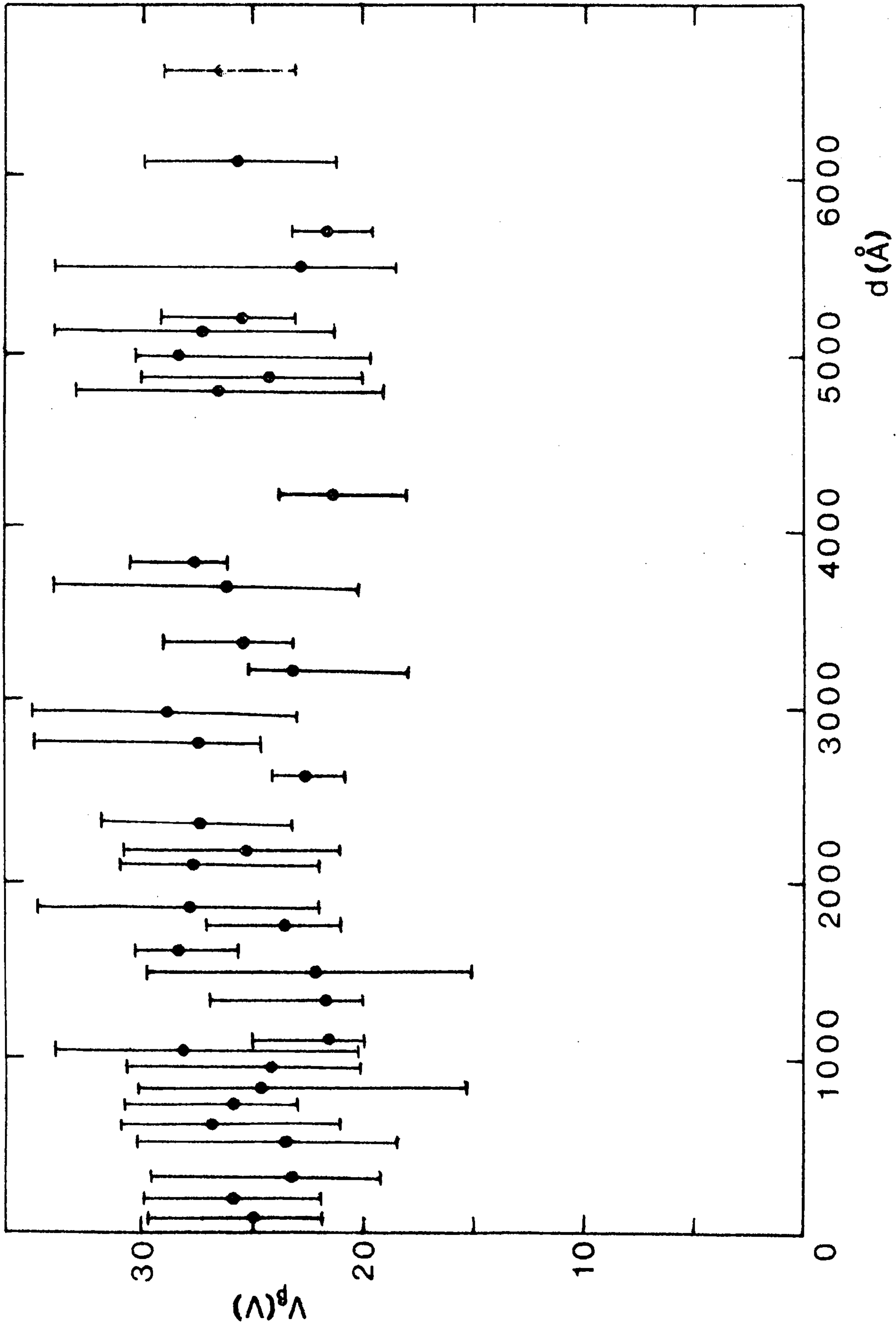


Figure 18. Dependence of V_β on insulator thickness

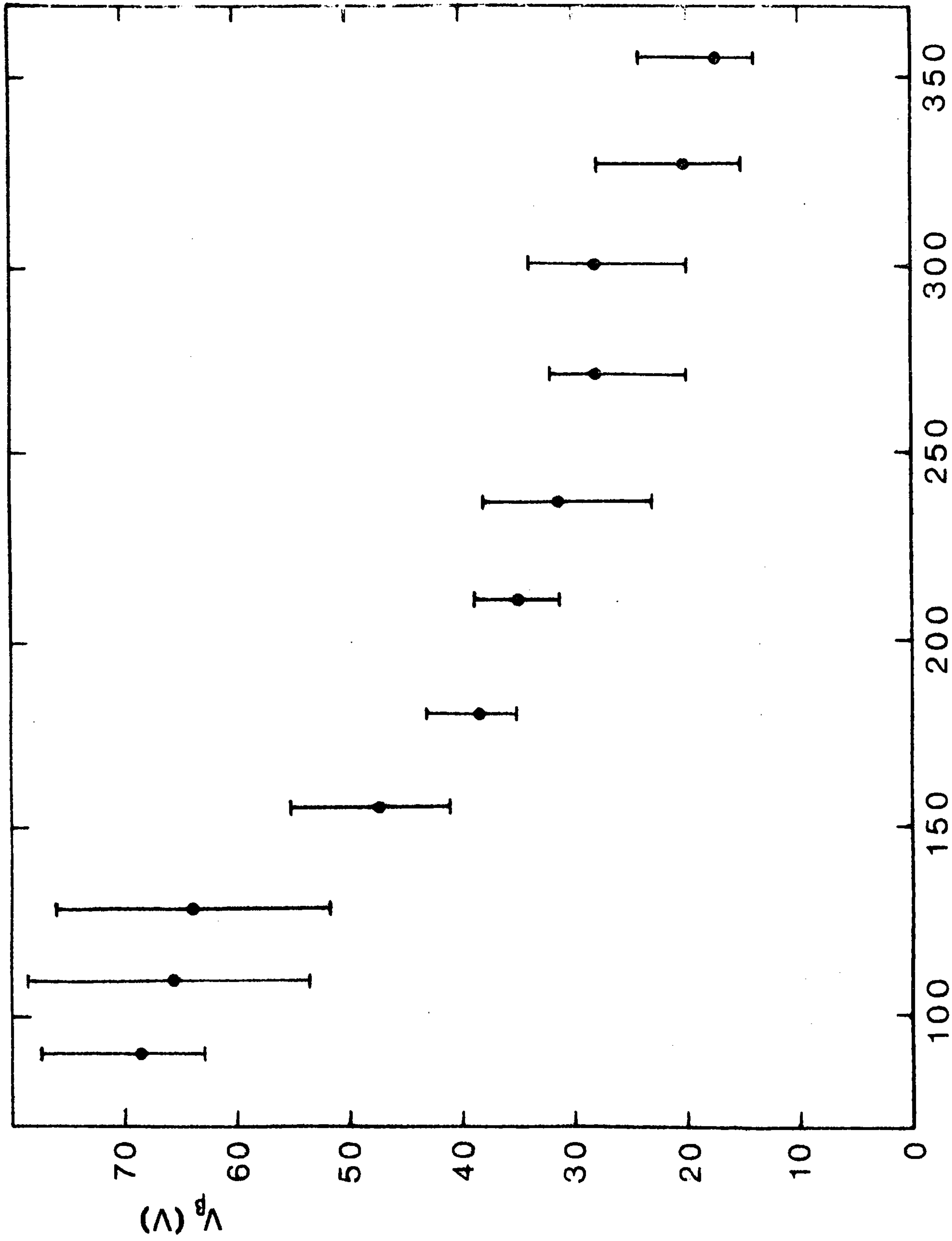


Figure 19. Dependence of V_{β} on temperature

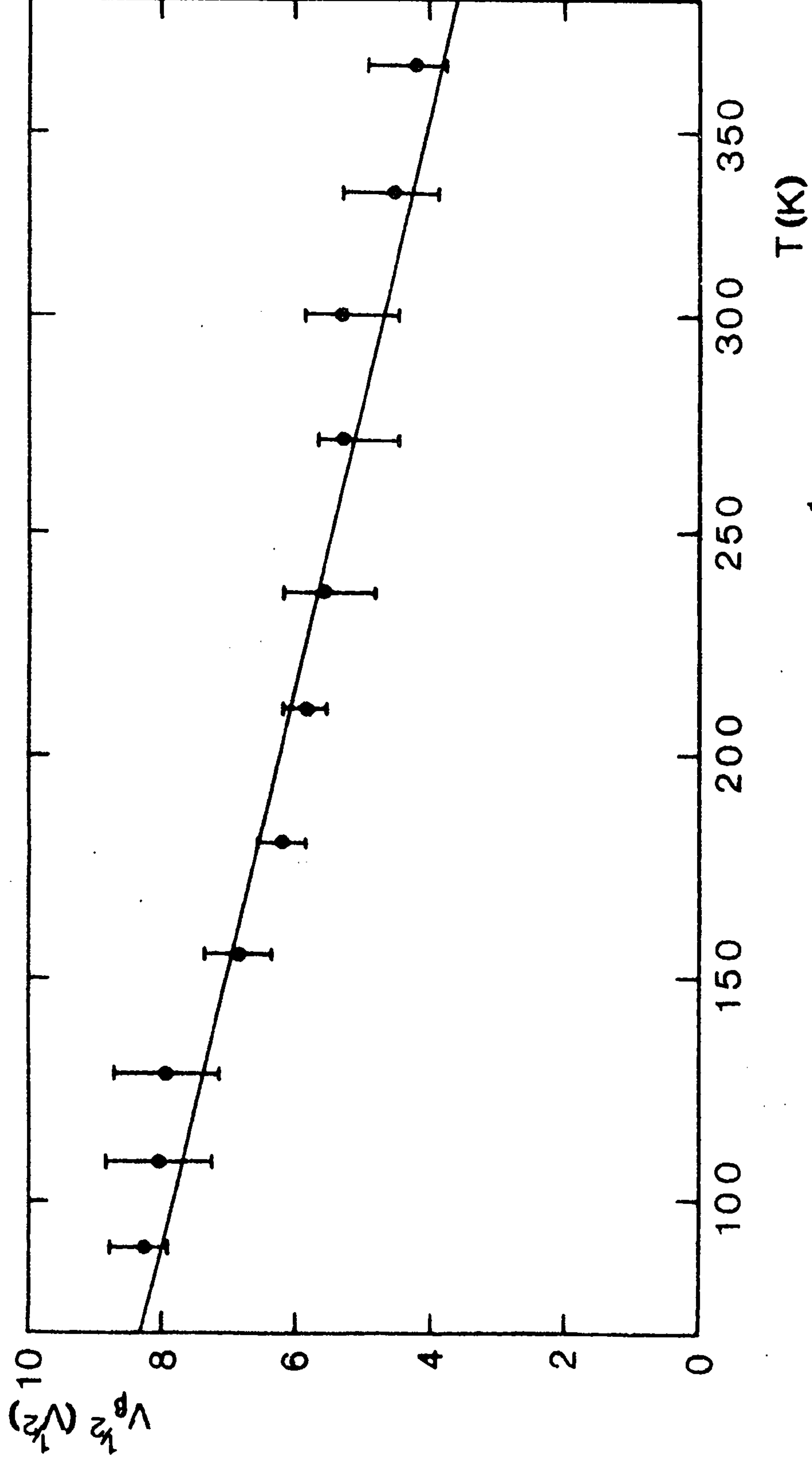


Figure 20. Dependence of $V_{\beta}^{1/2}$ on temperature

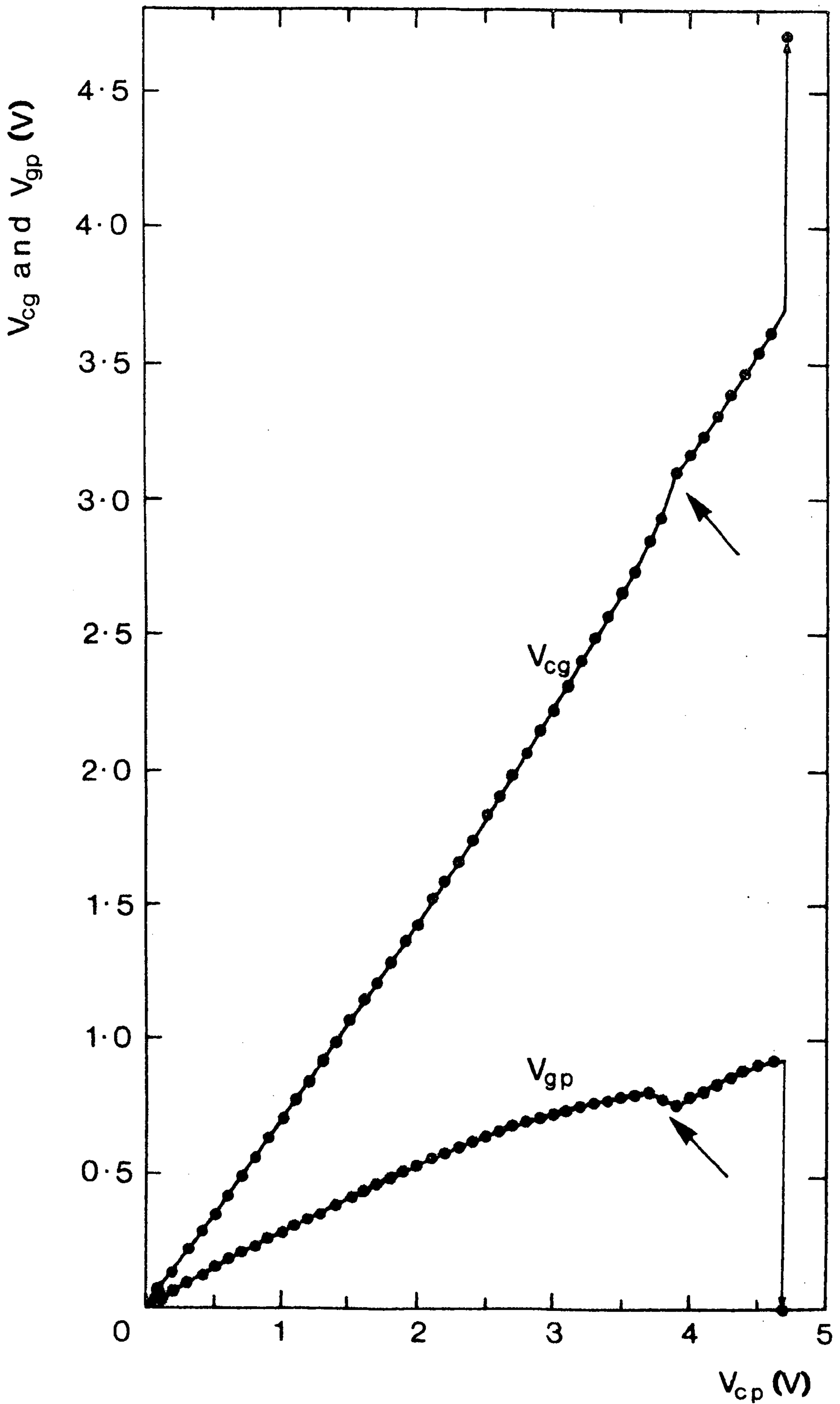


Figure 21. Potential distribution before forming

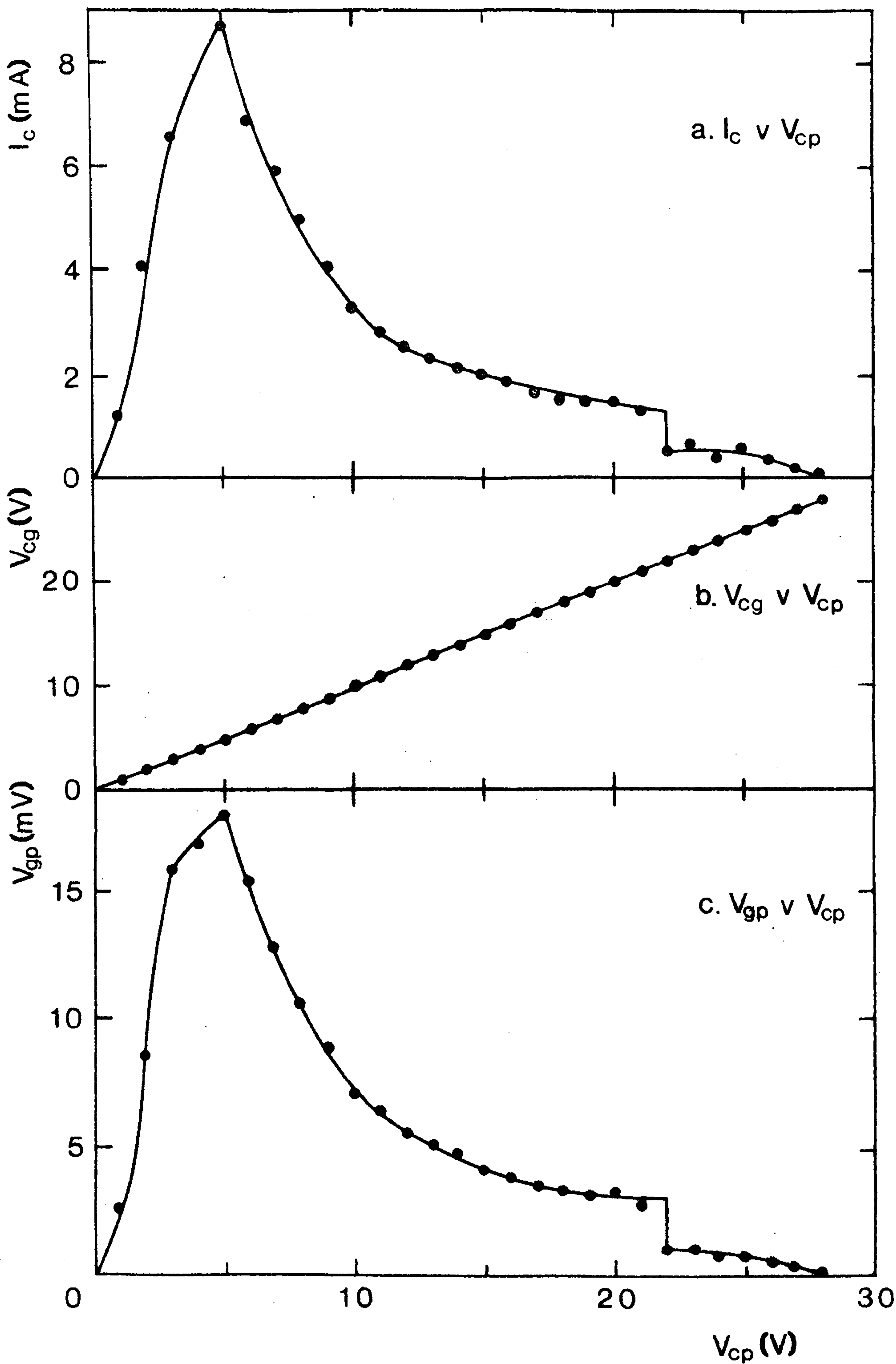
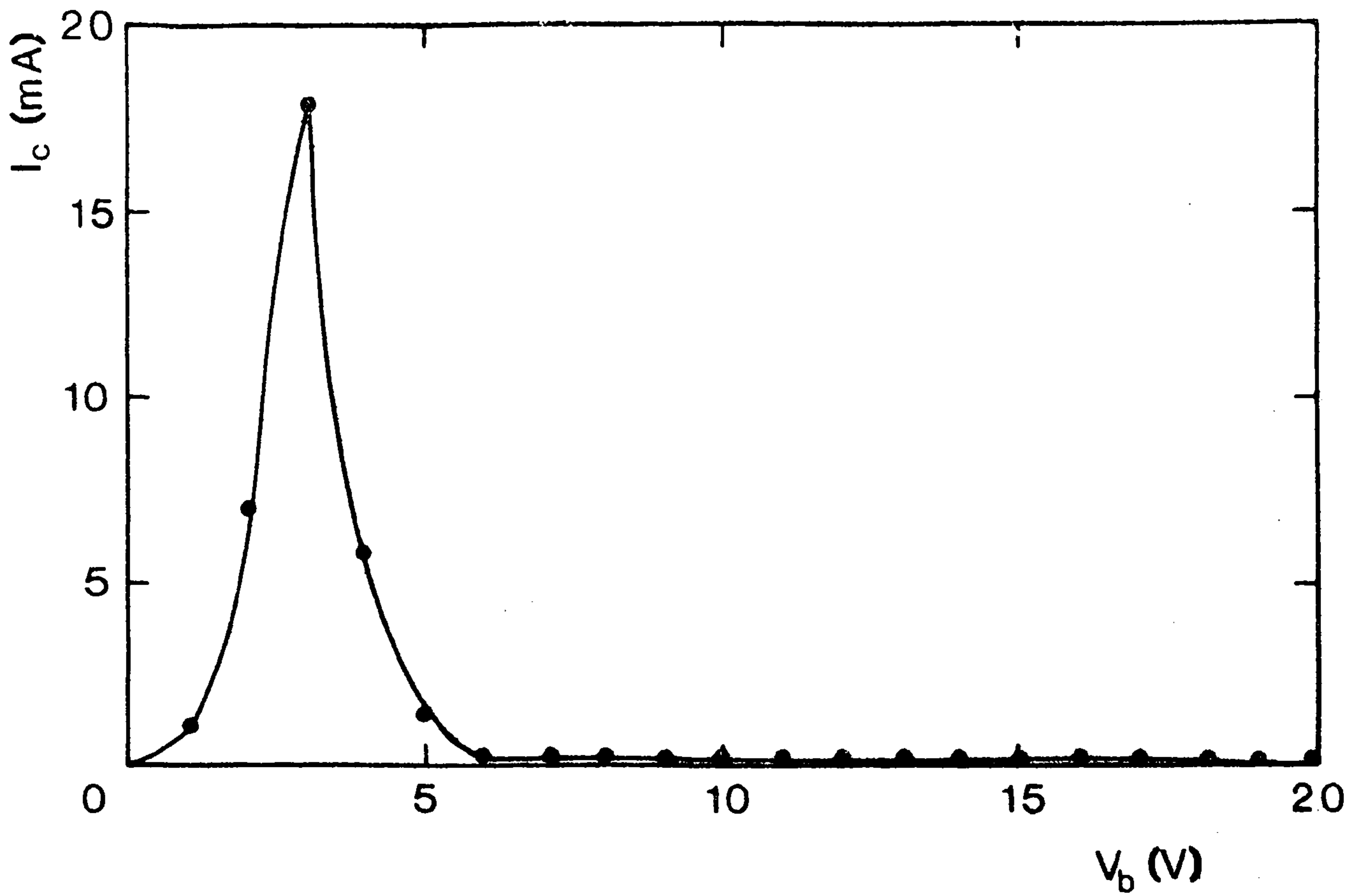
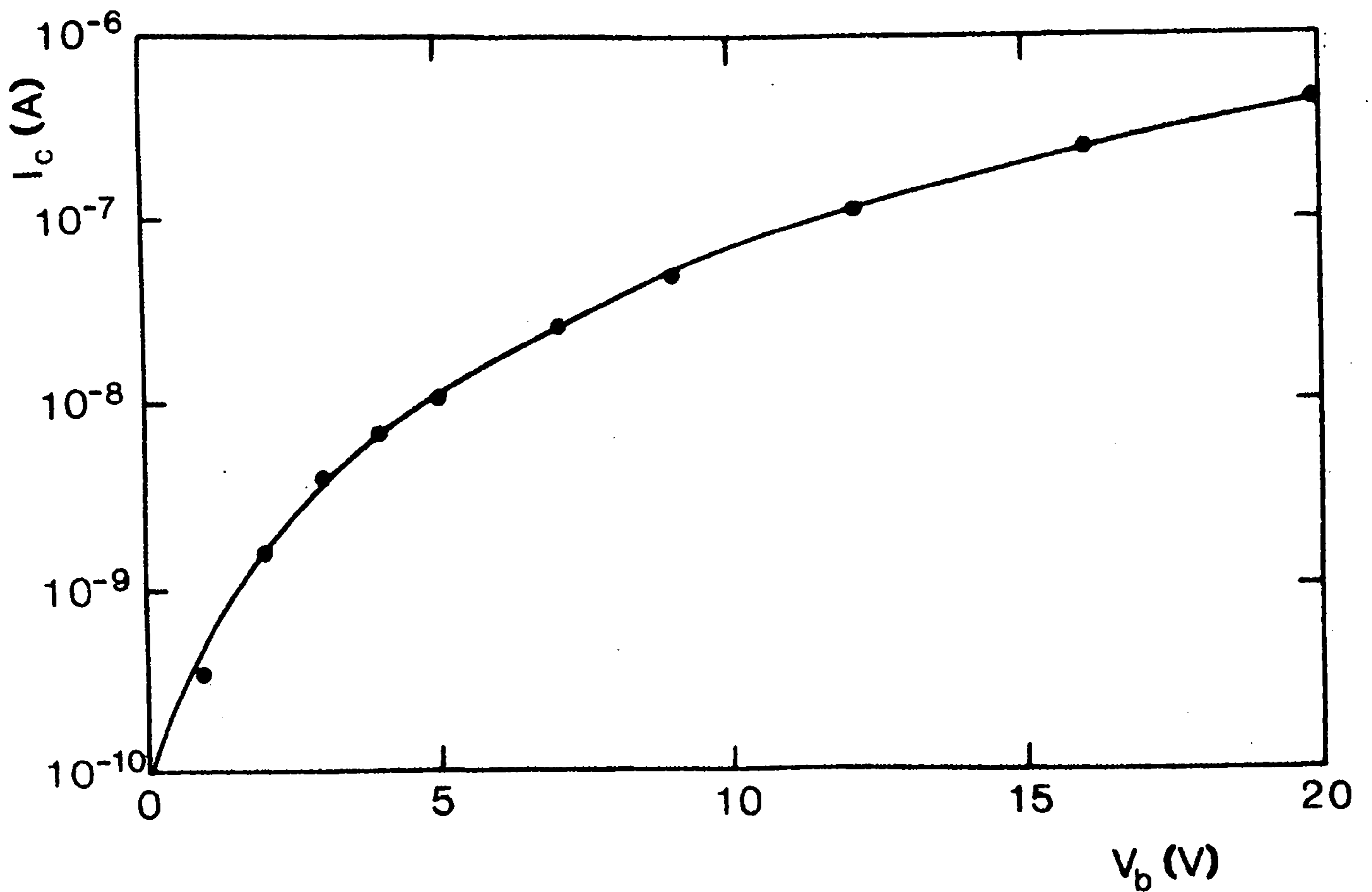


Figure 22. Dependence of I_c on V_{cp} and potential distribution after forming



a. First characteristic



b. Second characteristic

Figure 23. Low temperature dependence of I_c on V_b

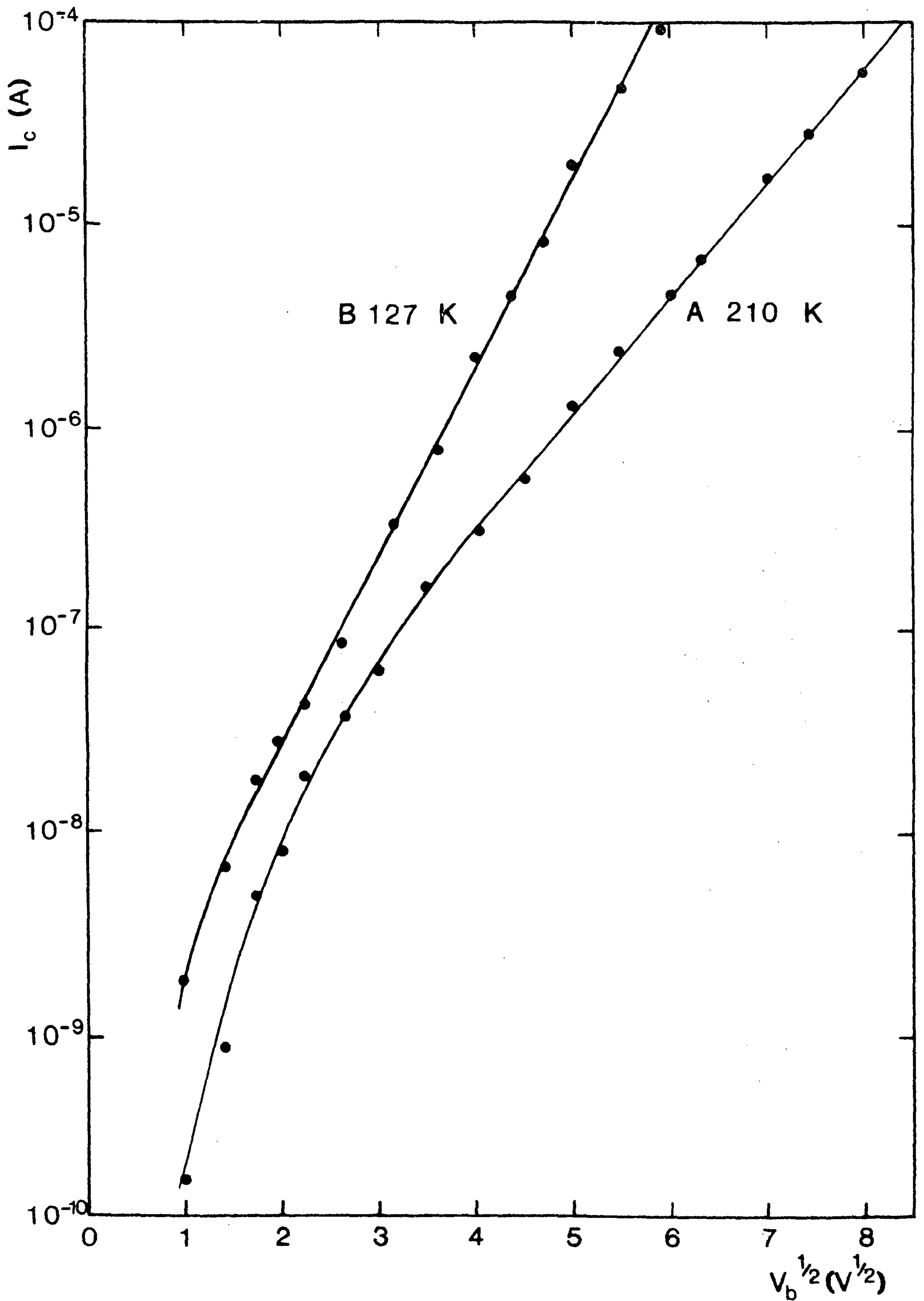


Figure 24. Low temperature dependence of $\log I_c$ on $V_b^{1/2}$

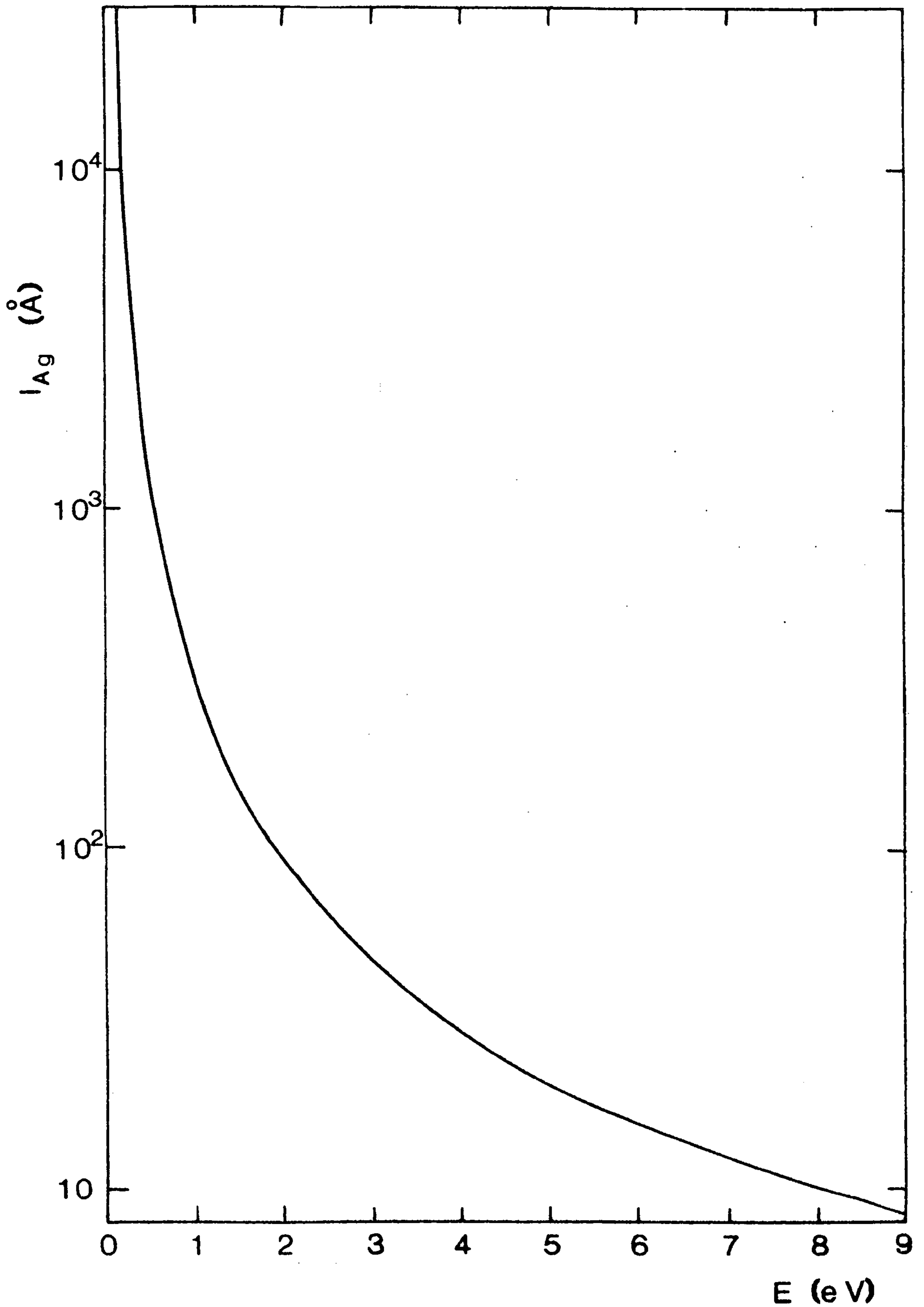


Figure 25. Dependence of mean free path in Ag on electron energy from the theory of Quinn

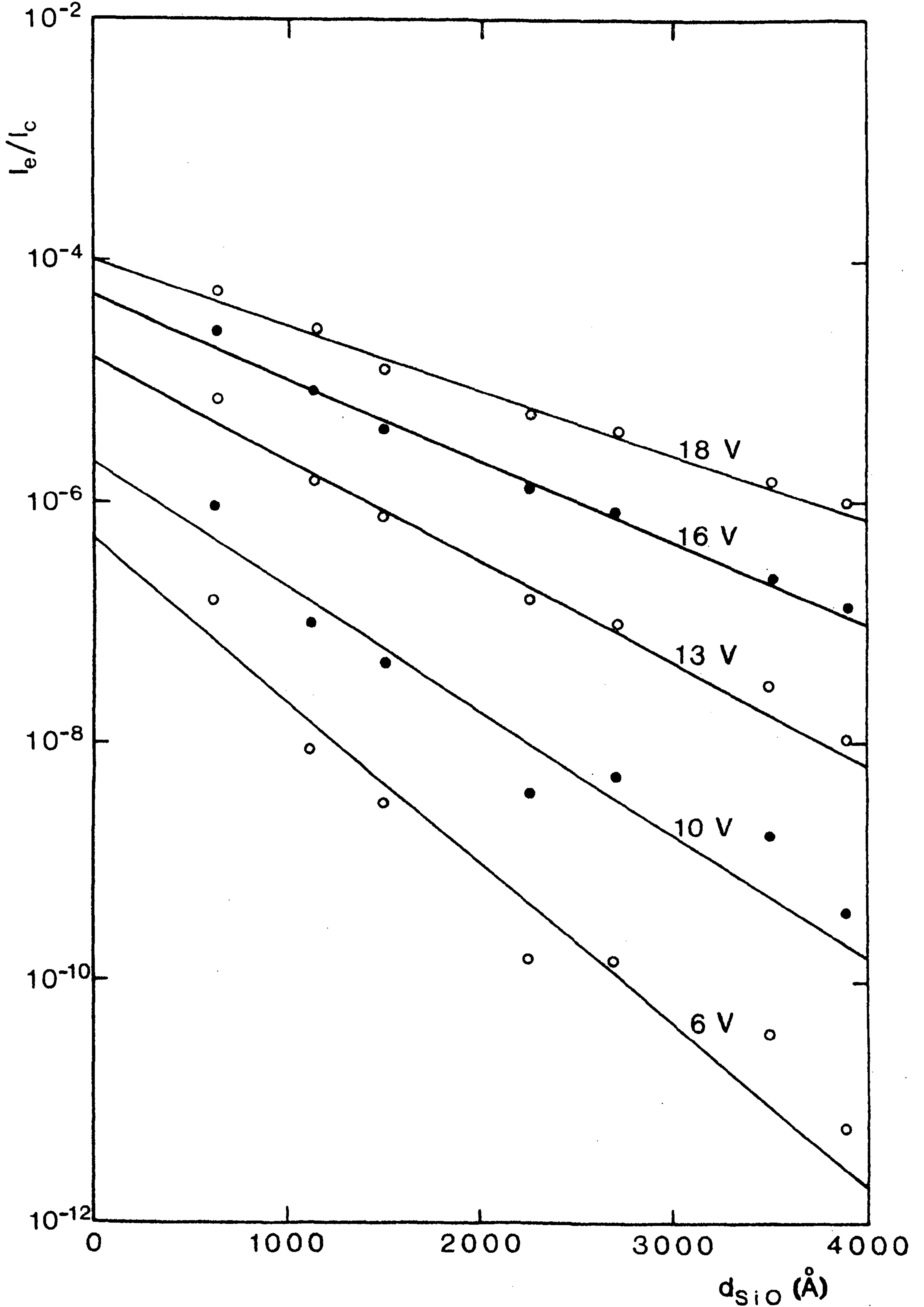


Figure 26. Dependence of $\log I_e/I_c$ on insulator thickness at different voltages

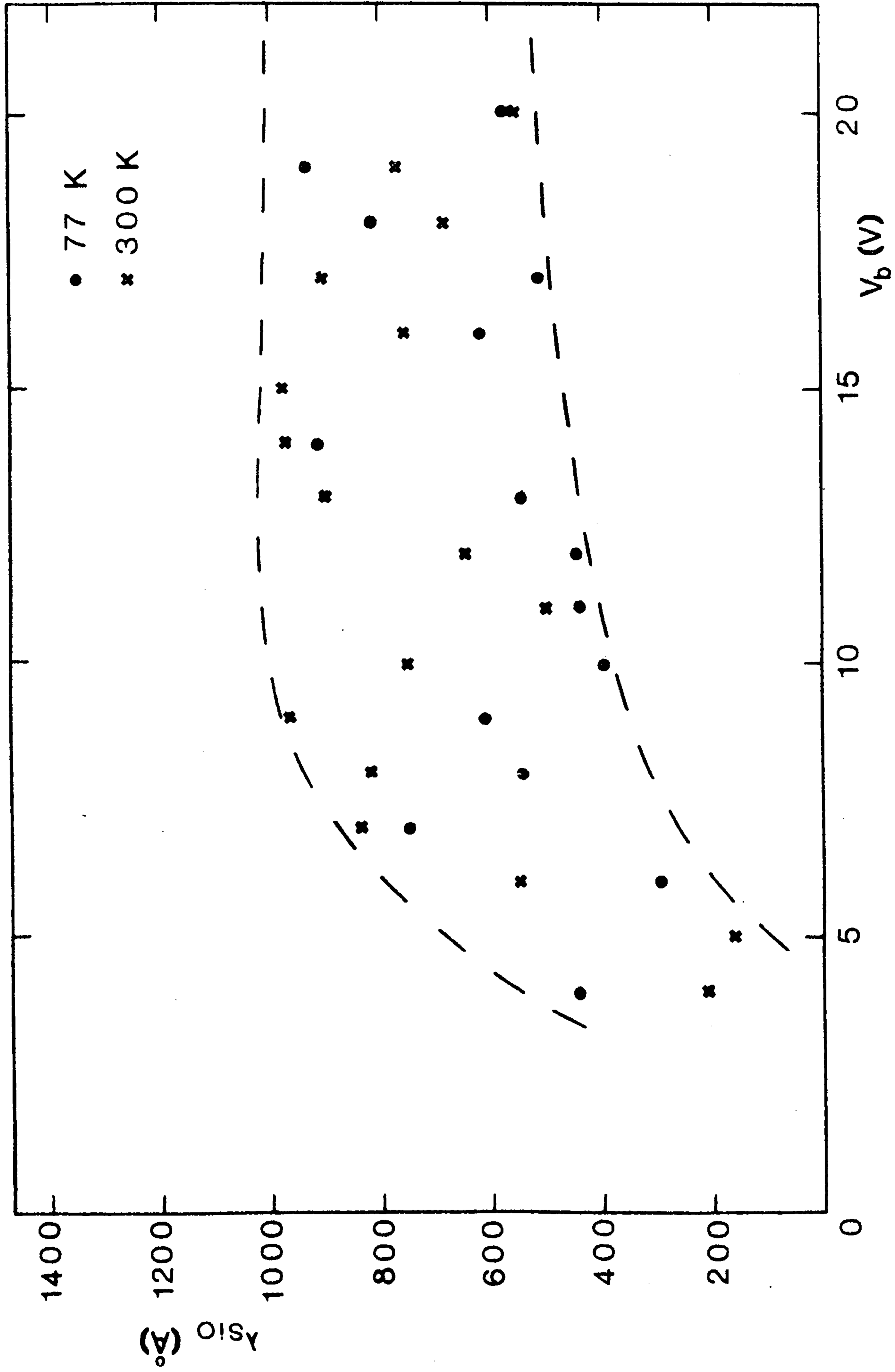


Figure 27. Dependence of attenuation length in SiO_x on V_b .

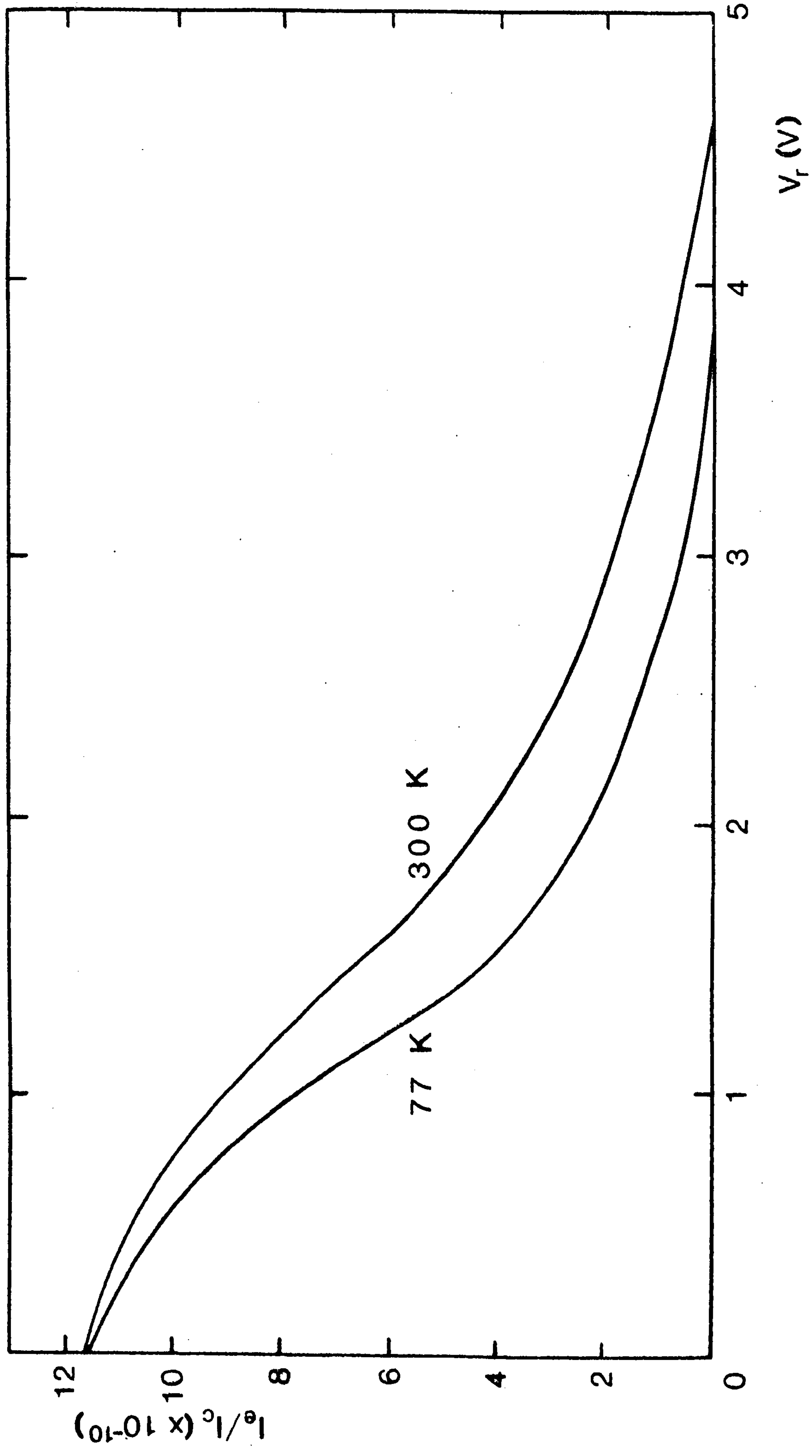


Figure 28. Dependence of I_e/I_c on retarding potential

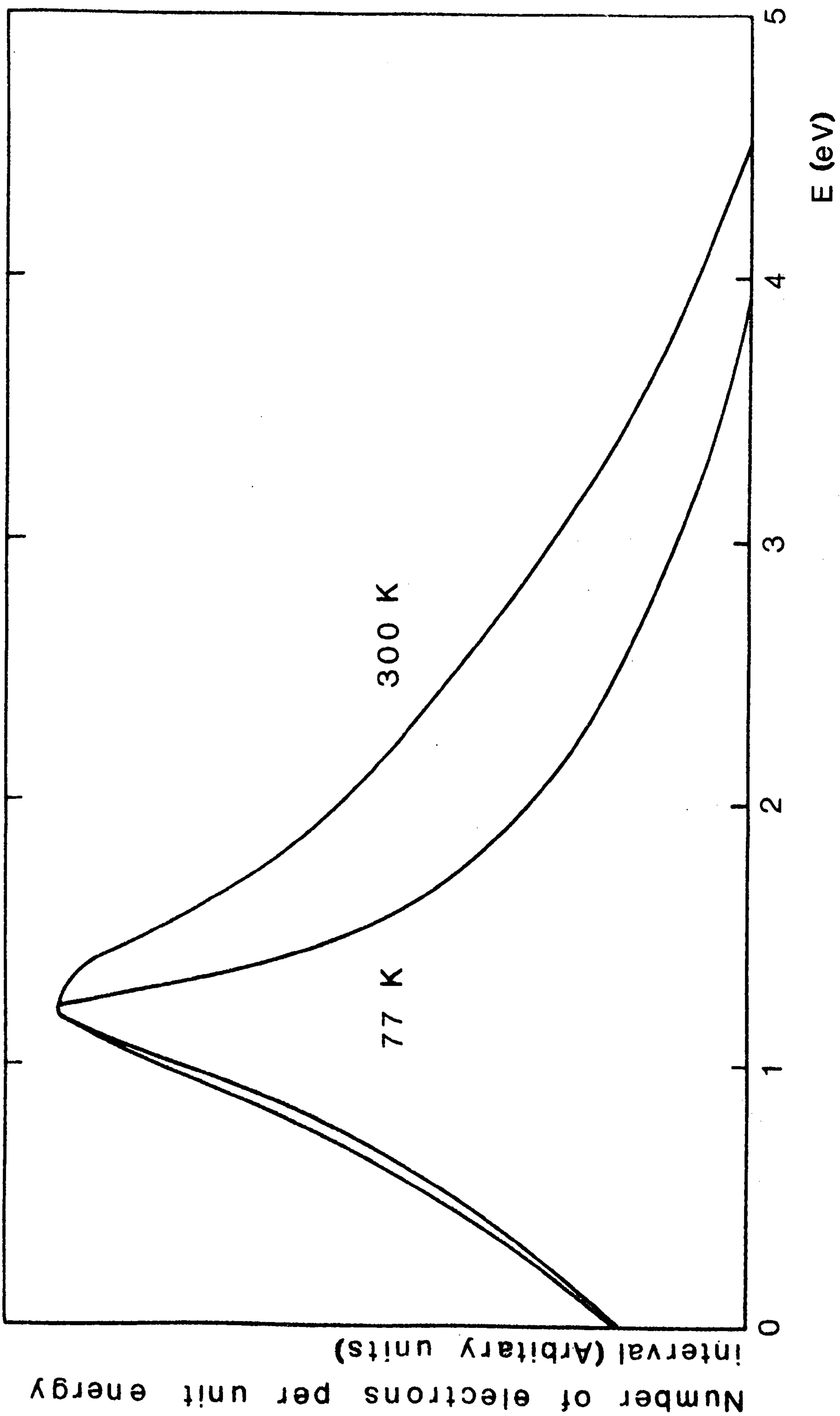
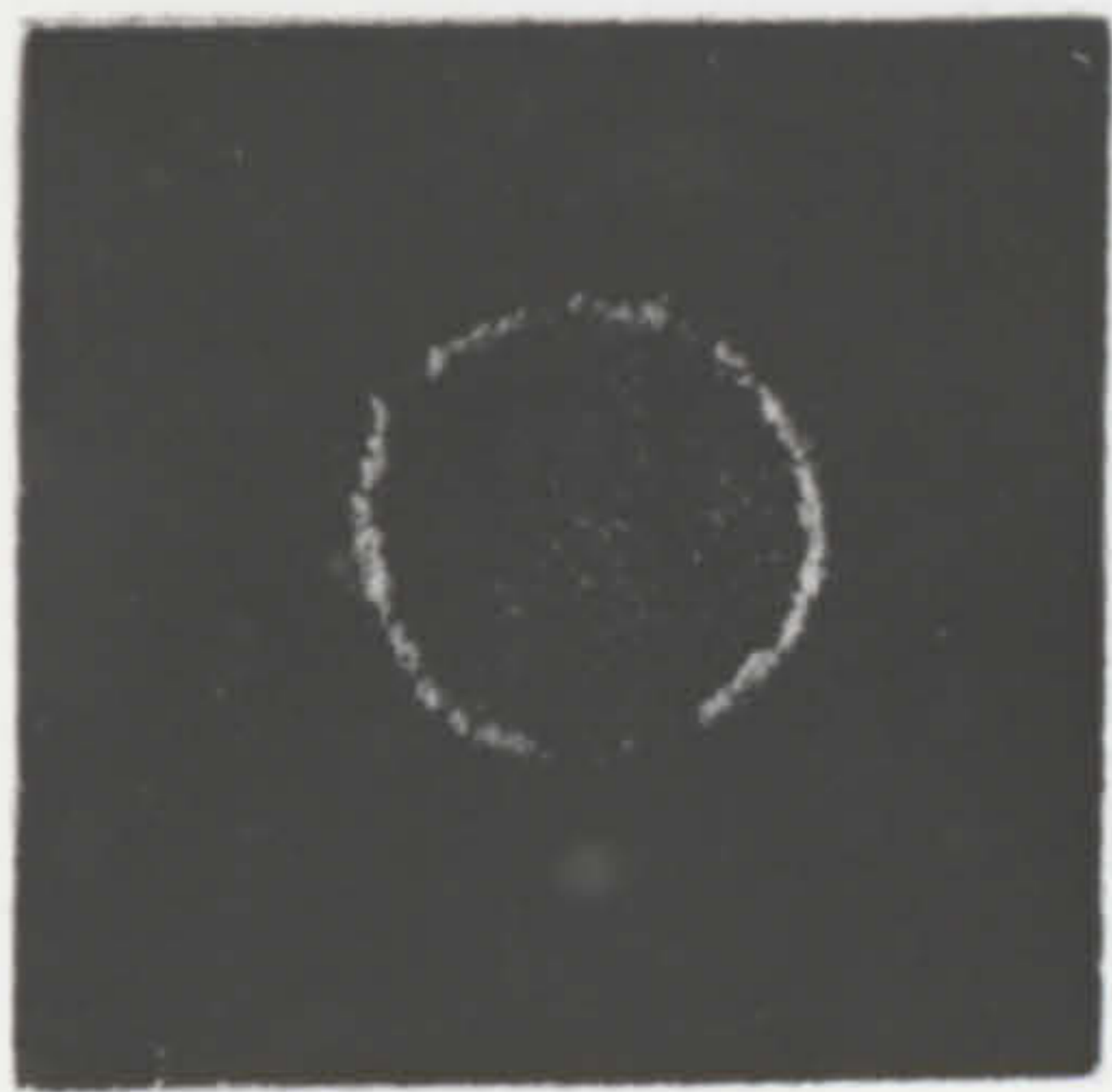
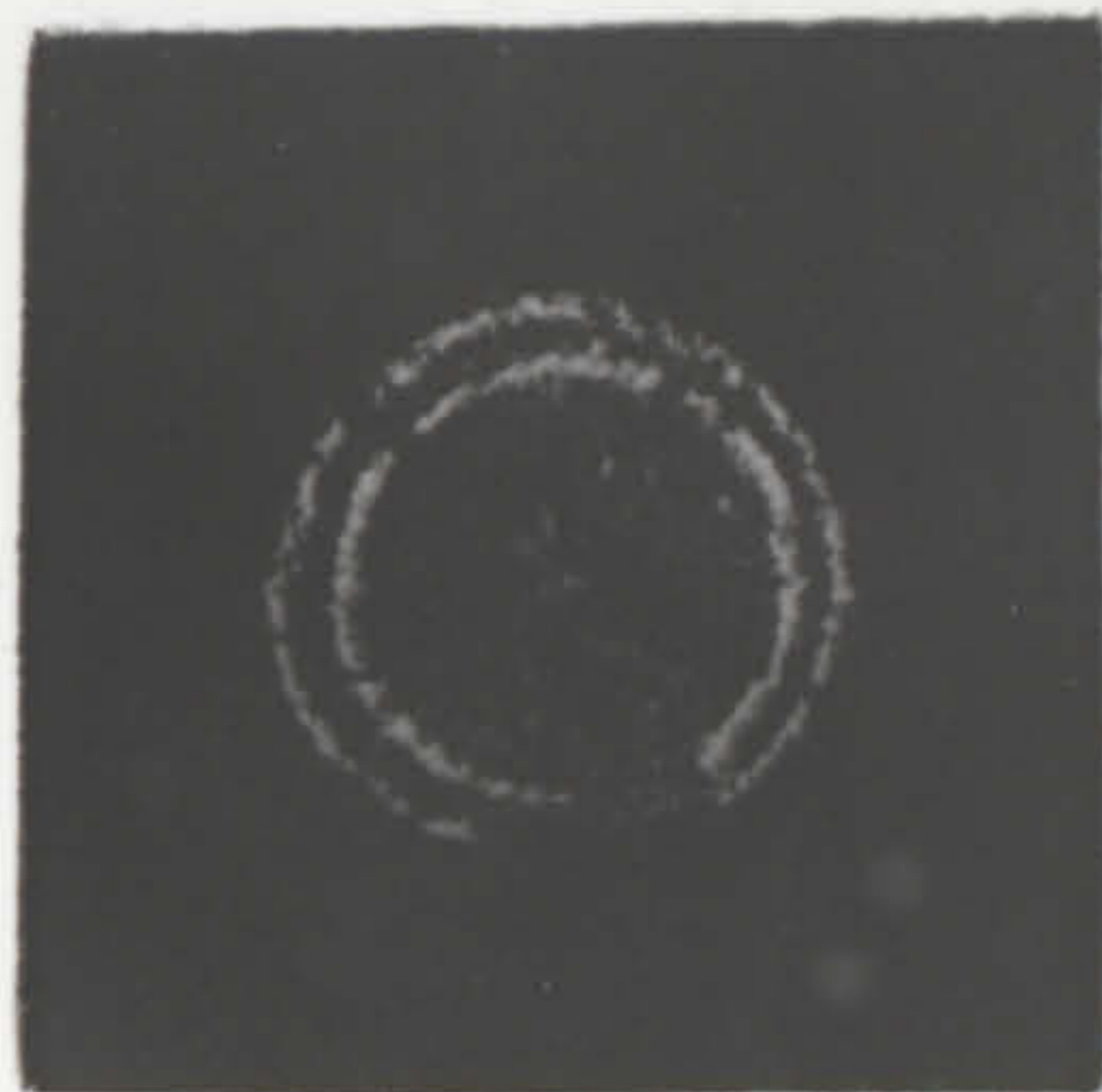


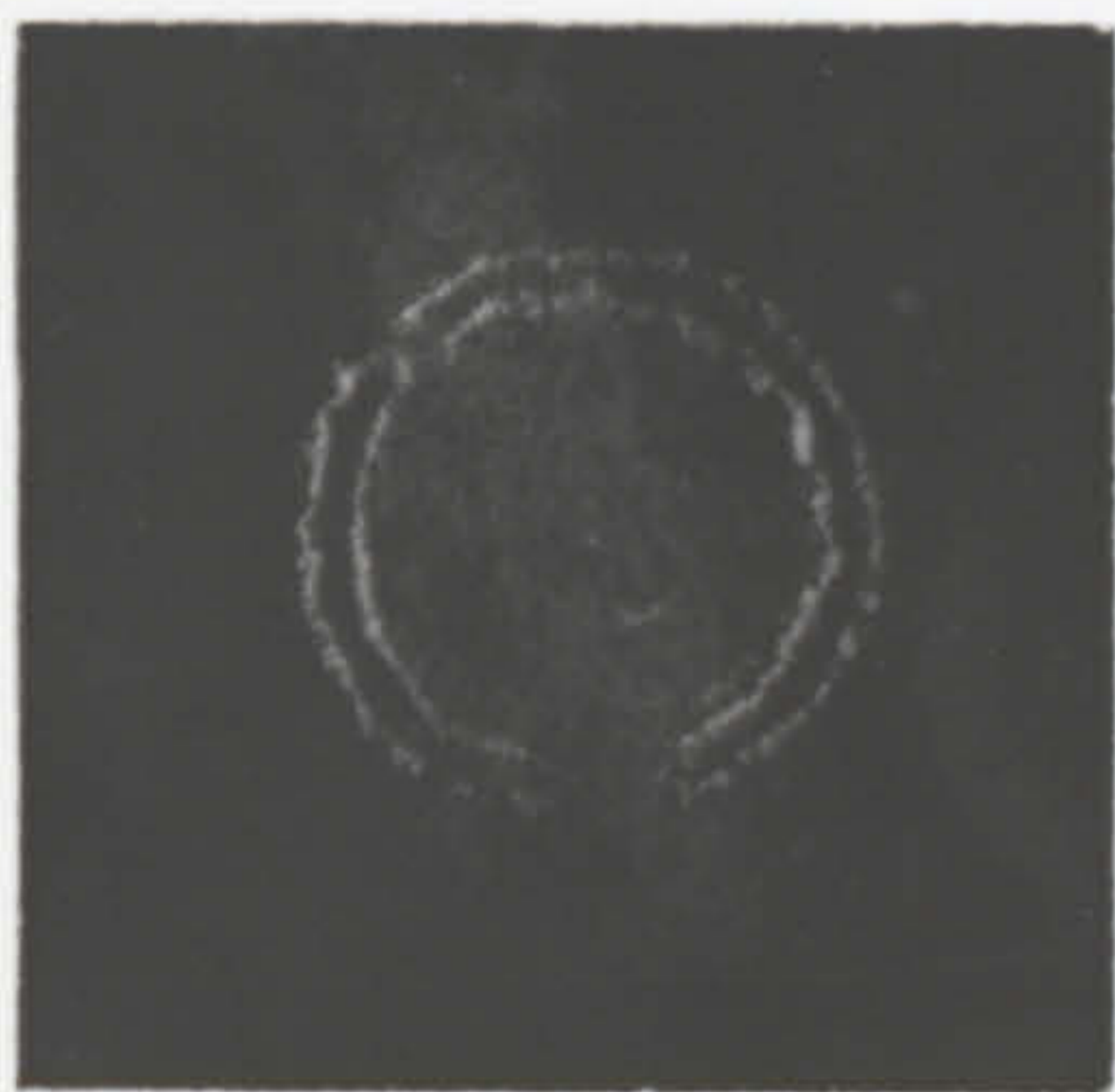
Figure 29. Emitted electron energy distributions at different temperatures



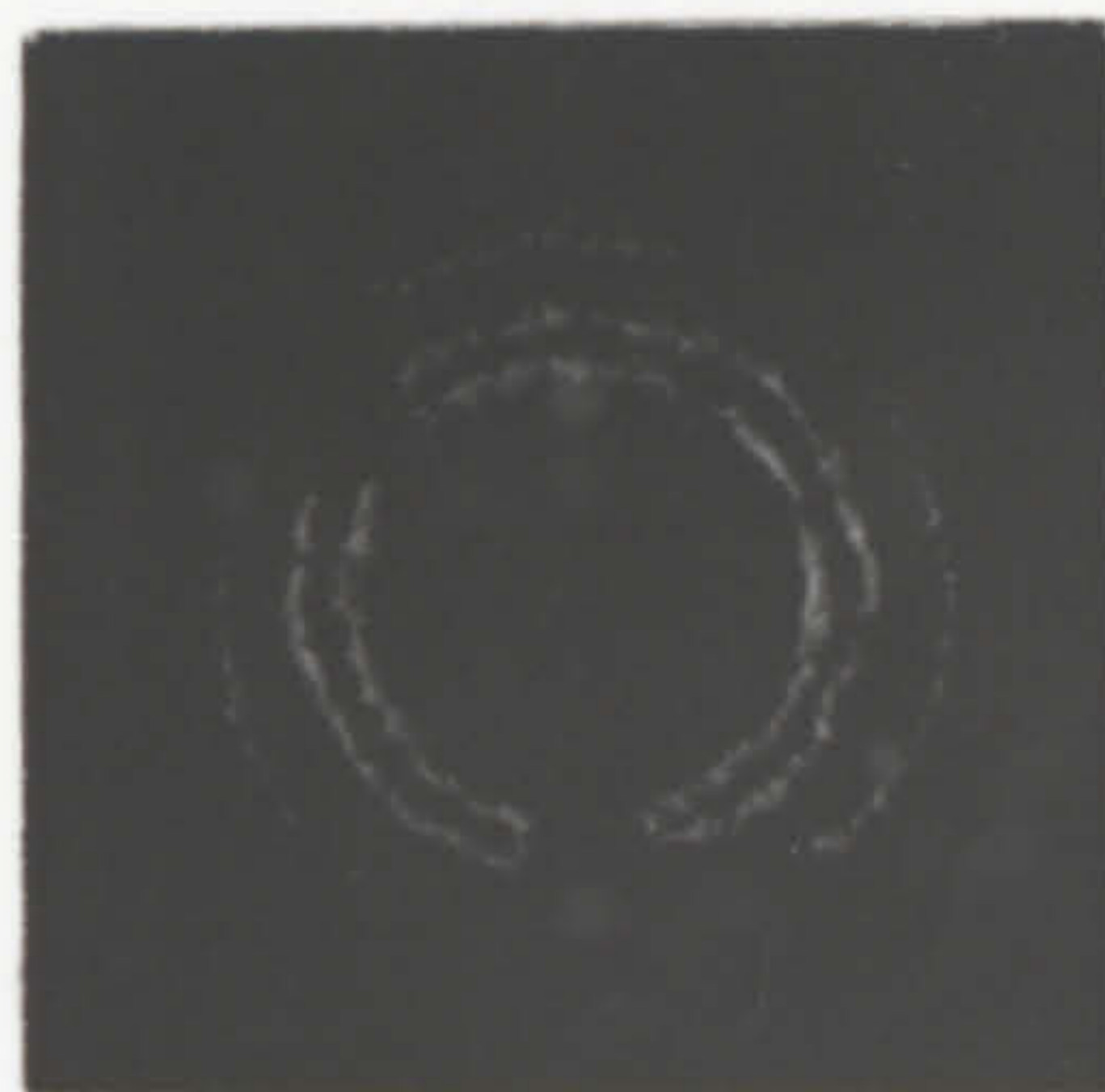
20 V



30 V



40 V



50 V



60 V



70 V

Figure 30. Electron emission patterns at different voltages

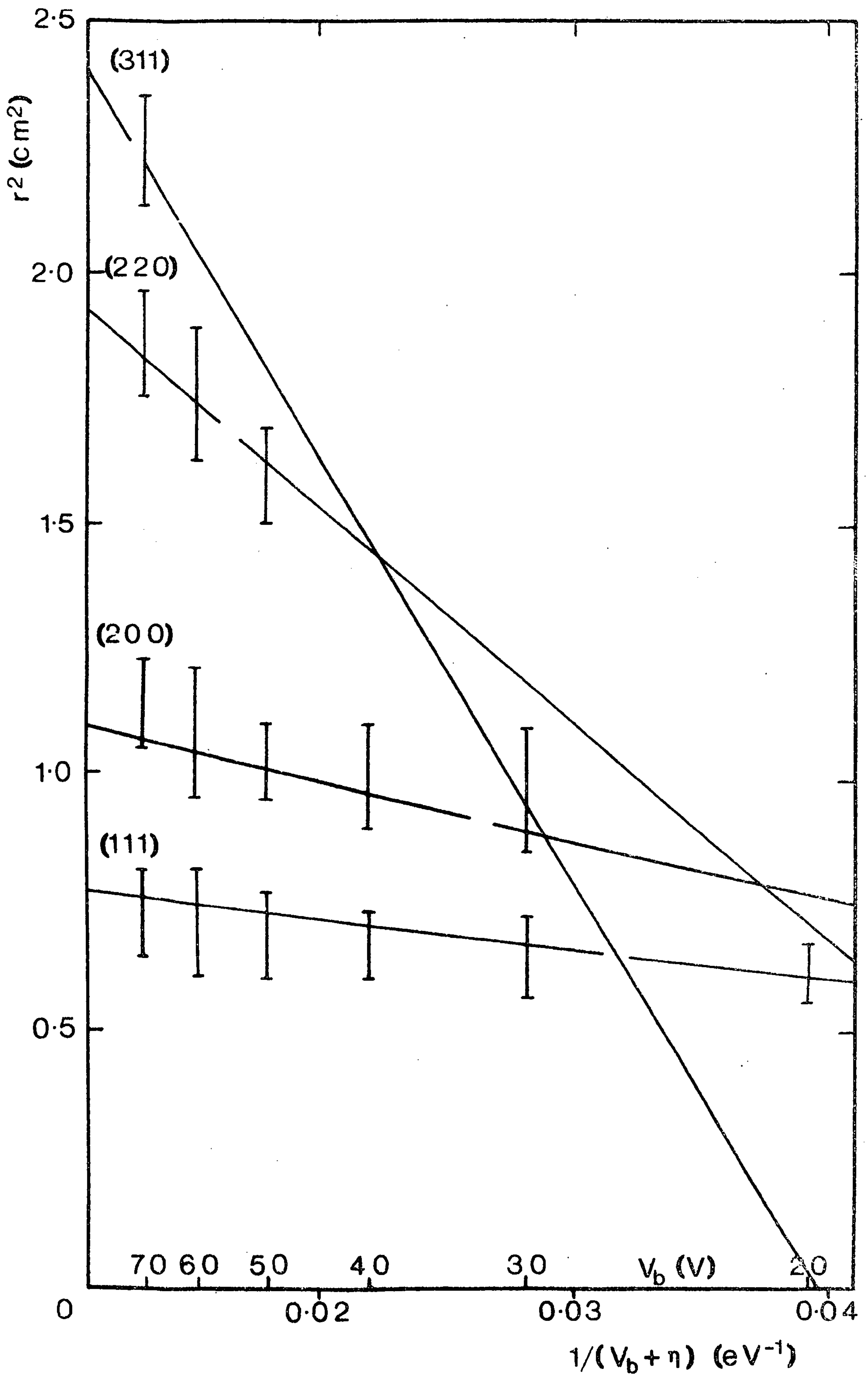


Figure 31. Linear dependence of square of emission pattern radius on $1/(V_b + \eta)$

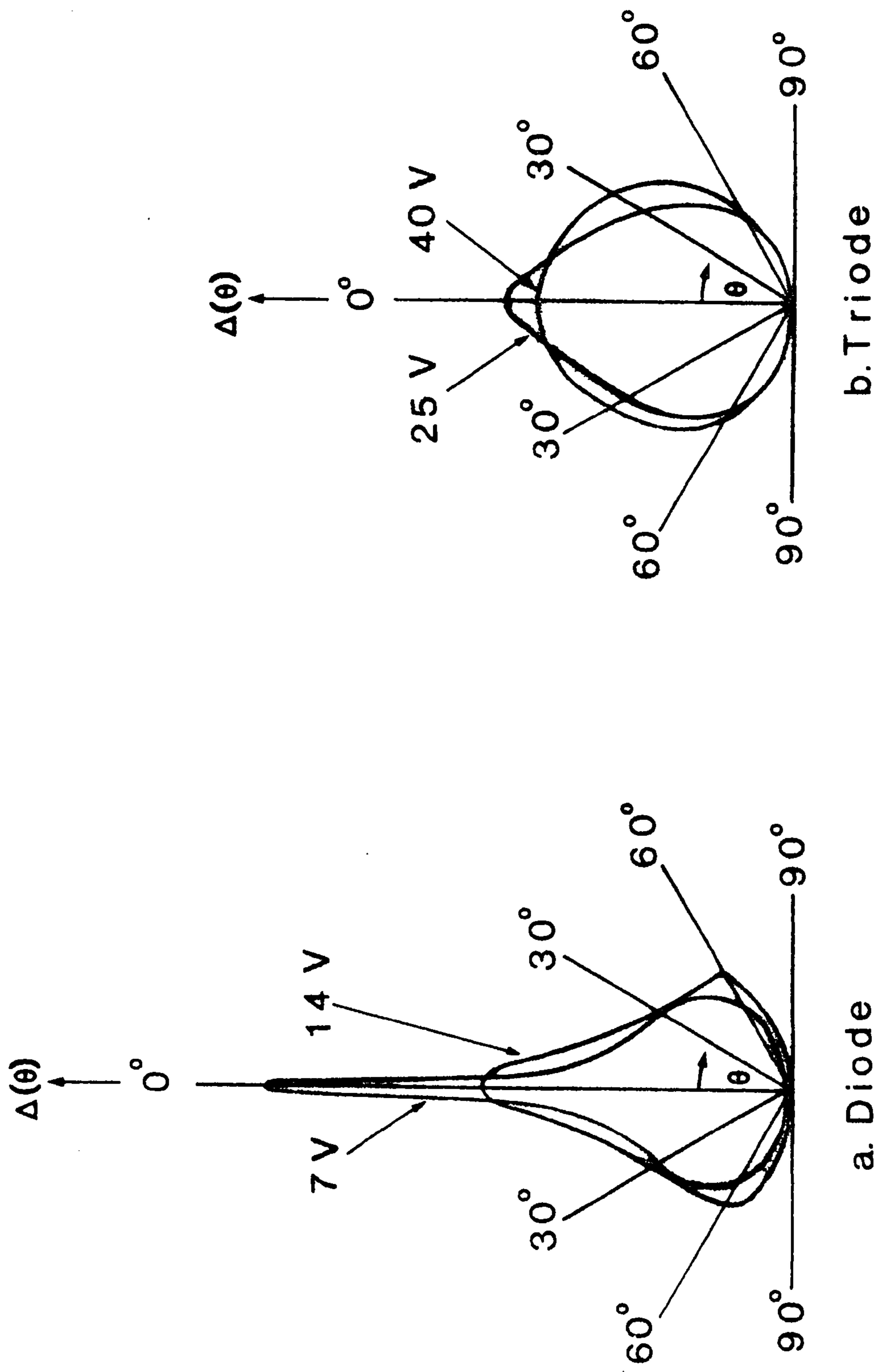


Figure 32. Angular distributions of emitted electrons

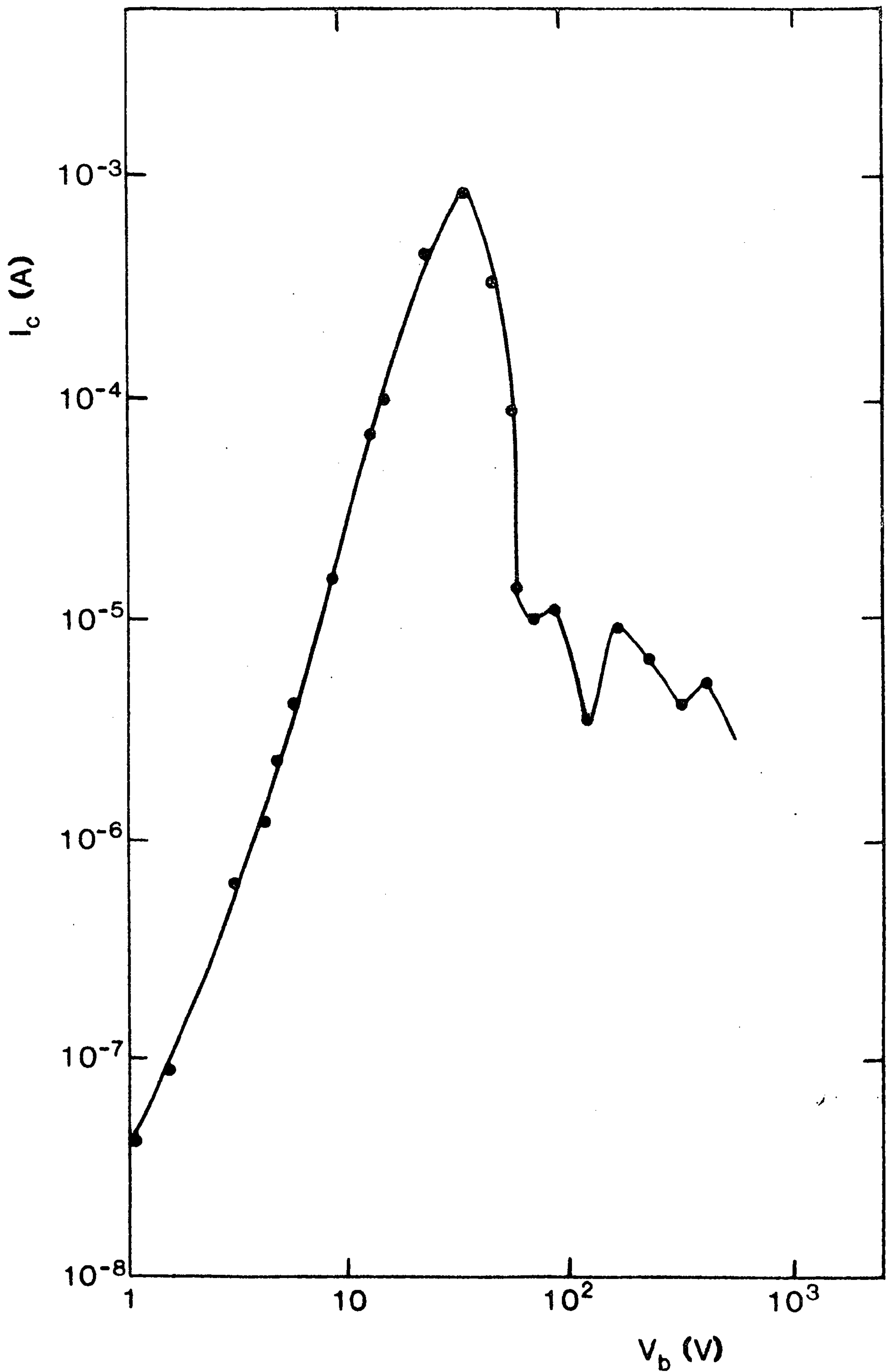


Figure 33. Dependence of I_c on V_b in $\text{SiO}_x/\text{B}_2\text{O}_3$

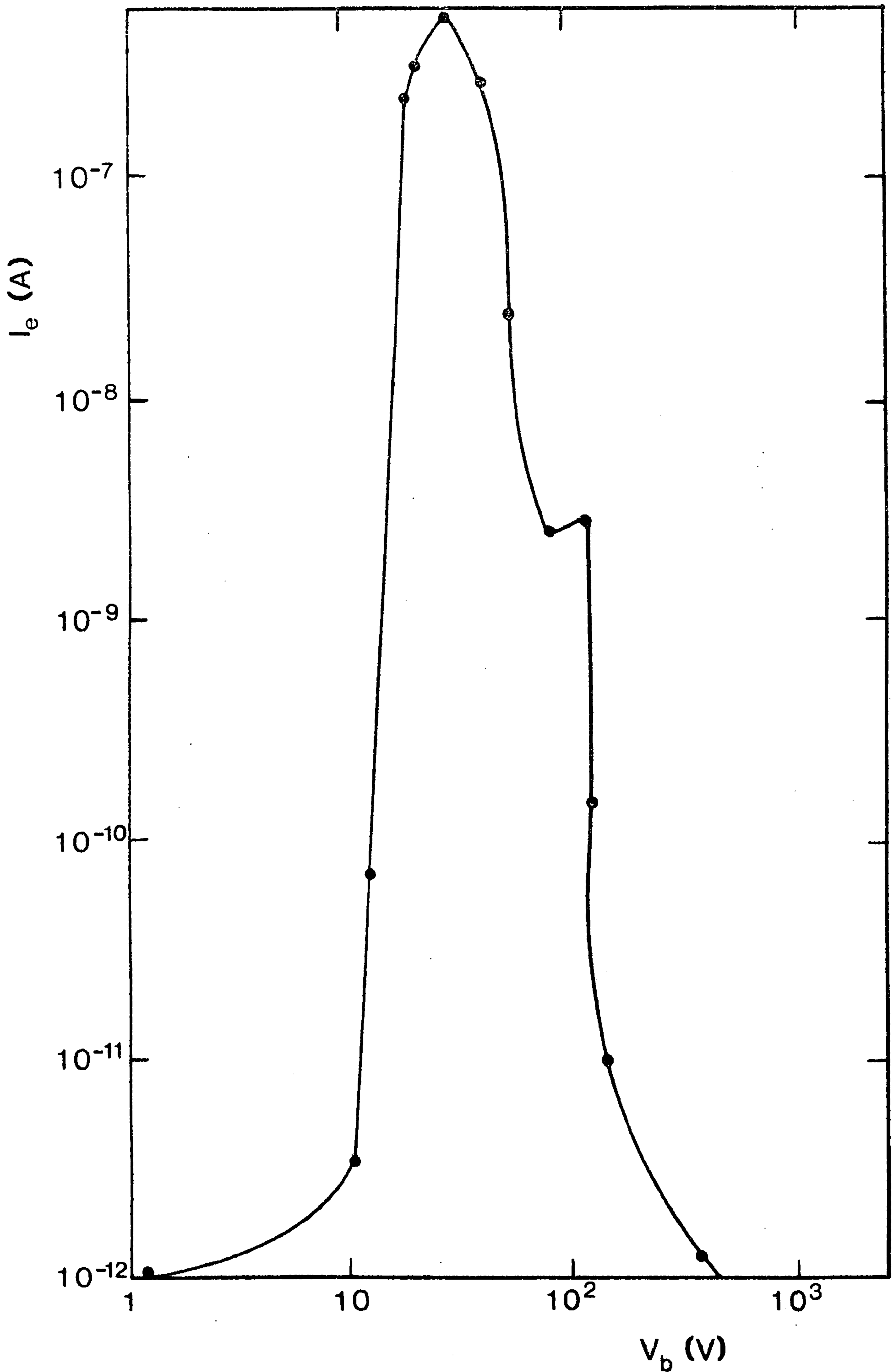


Figure 34. Dependence of I_e on V_b in $\text{SiO}_x/\text{B}_2\text{O}_3$

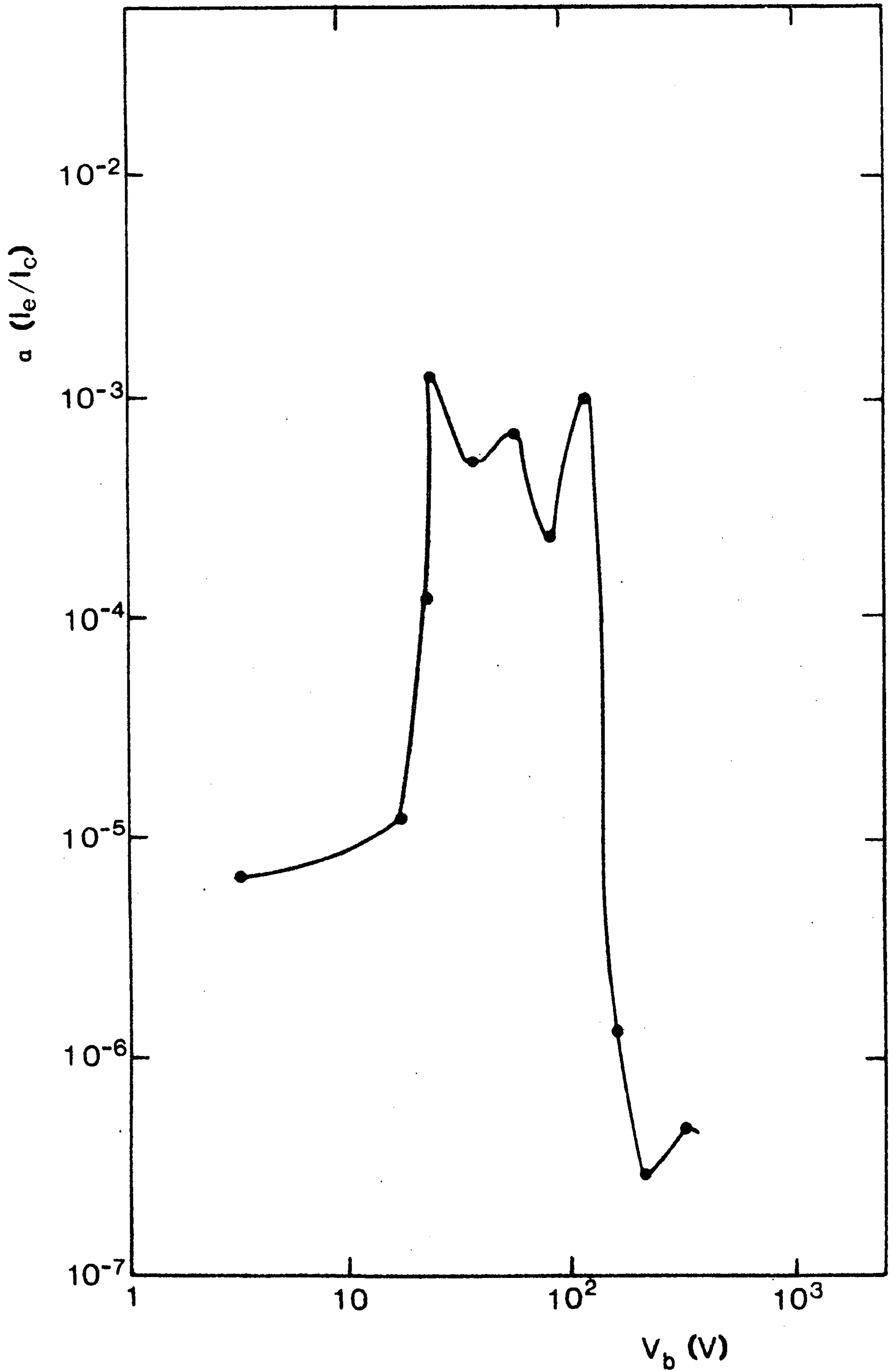


Figure 35. Dependence of transmission ratio on V_b in $\text{SiO}_x/\text{B}_2\text{O}_3$

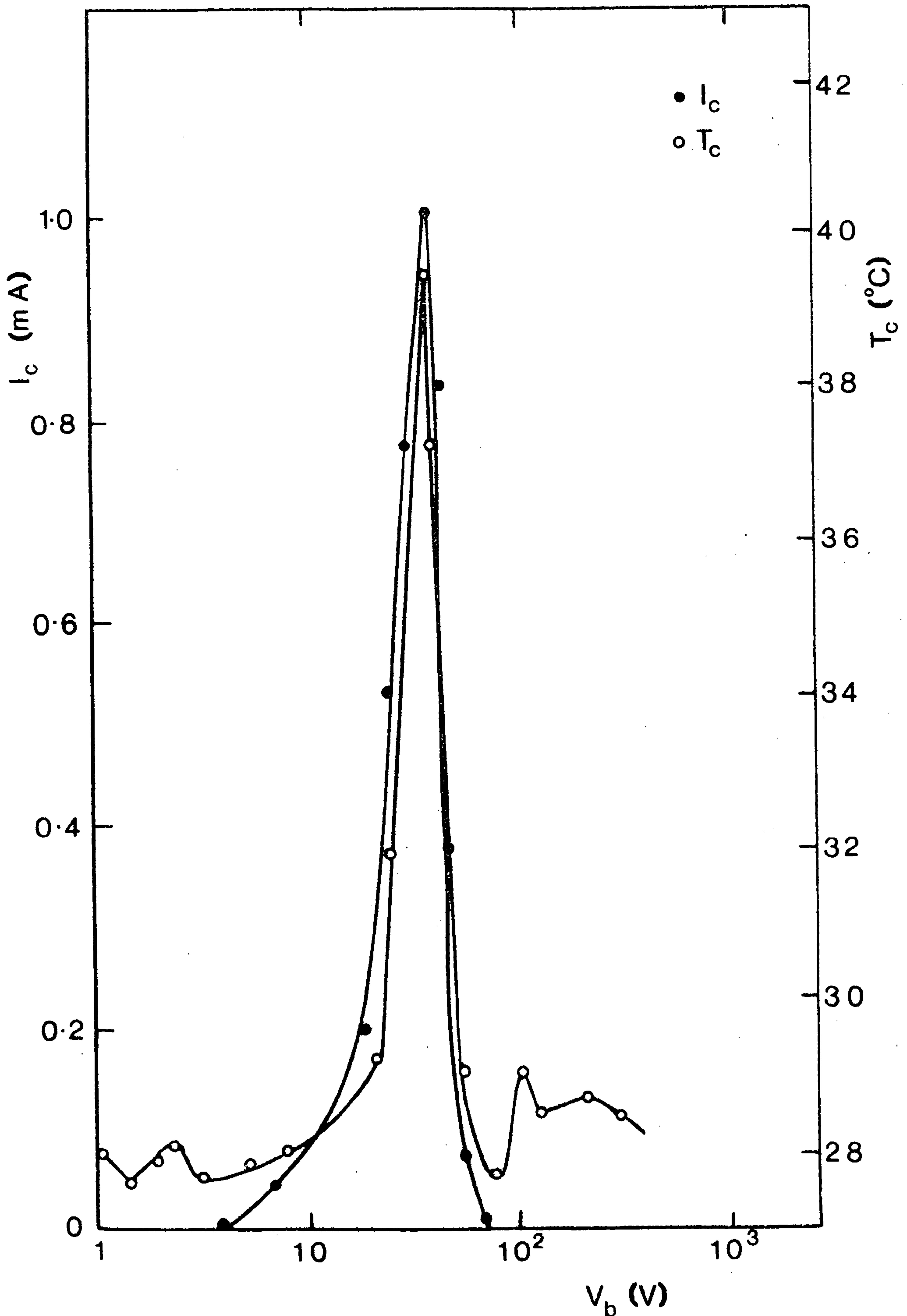


Figure 36. Dependence of device temperature on I_c and V_b in $\text{SiO}_x/\text{B}_2\text{O}_3$

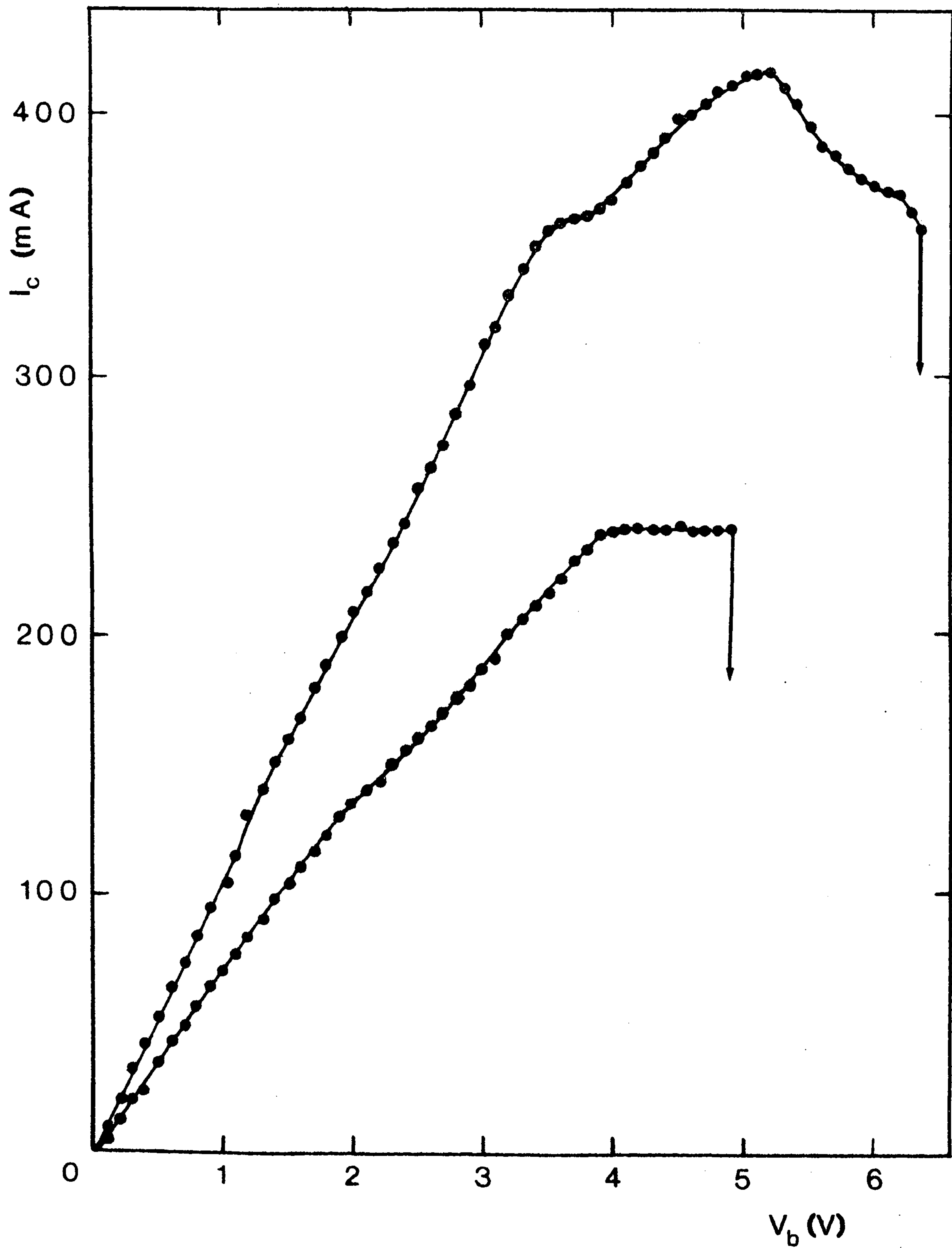


Figure 37. Forming in CaBr_2

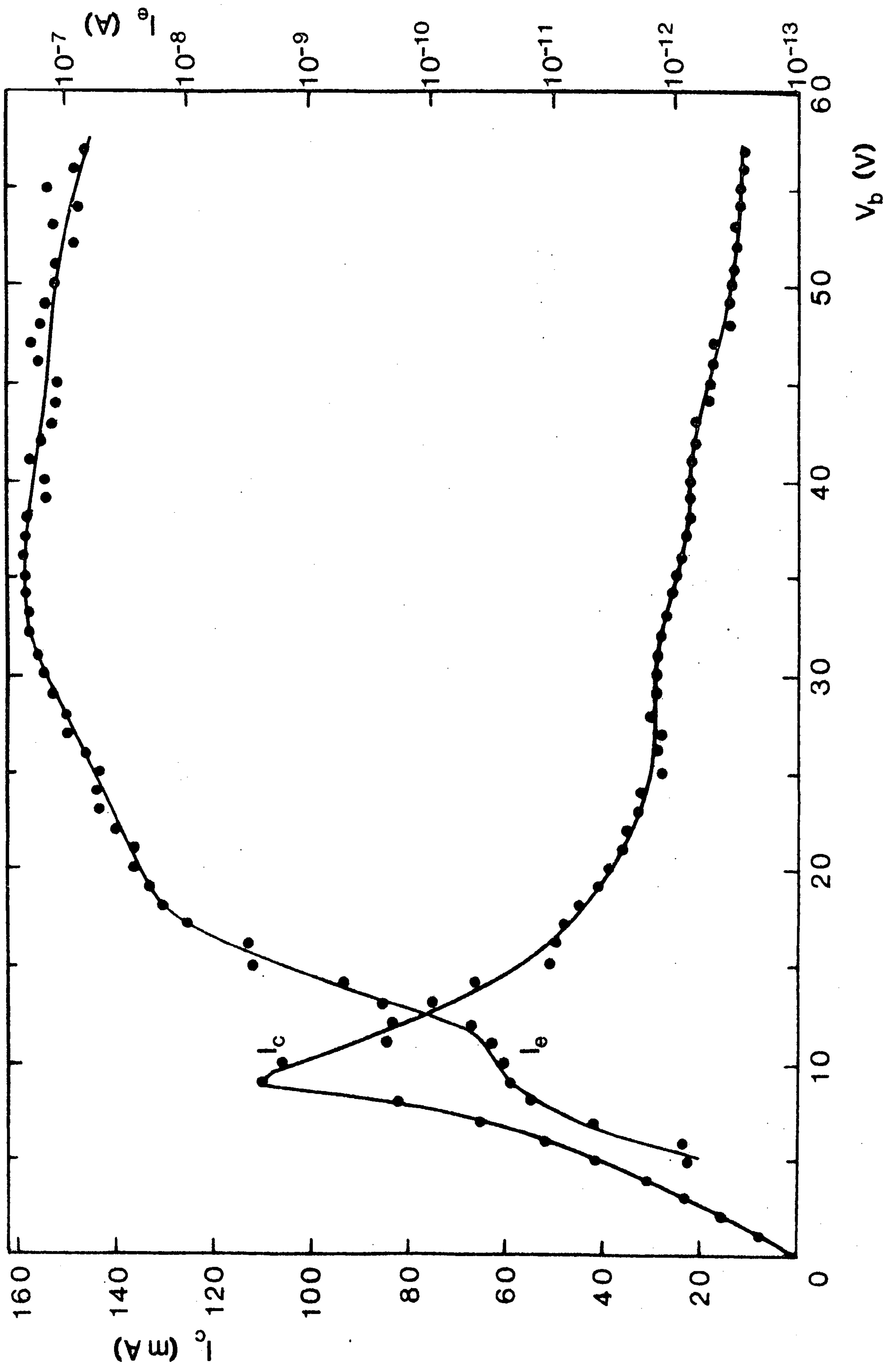


Figure 38. Dependence of I_c and I_e on V_b in $CaBr_2$

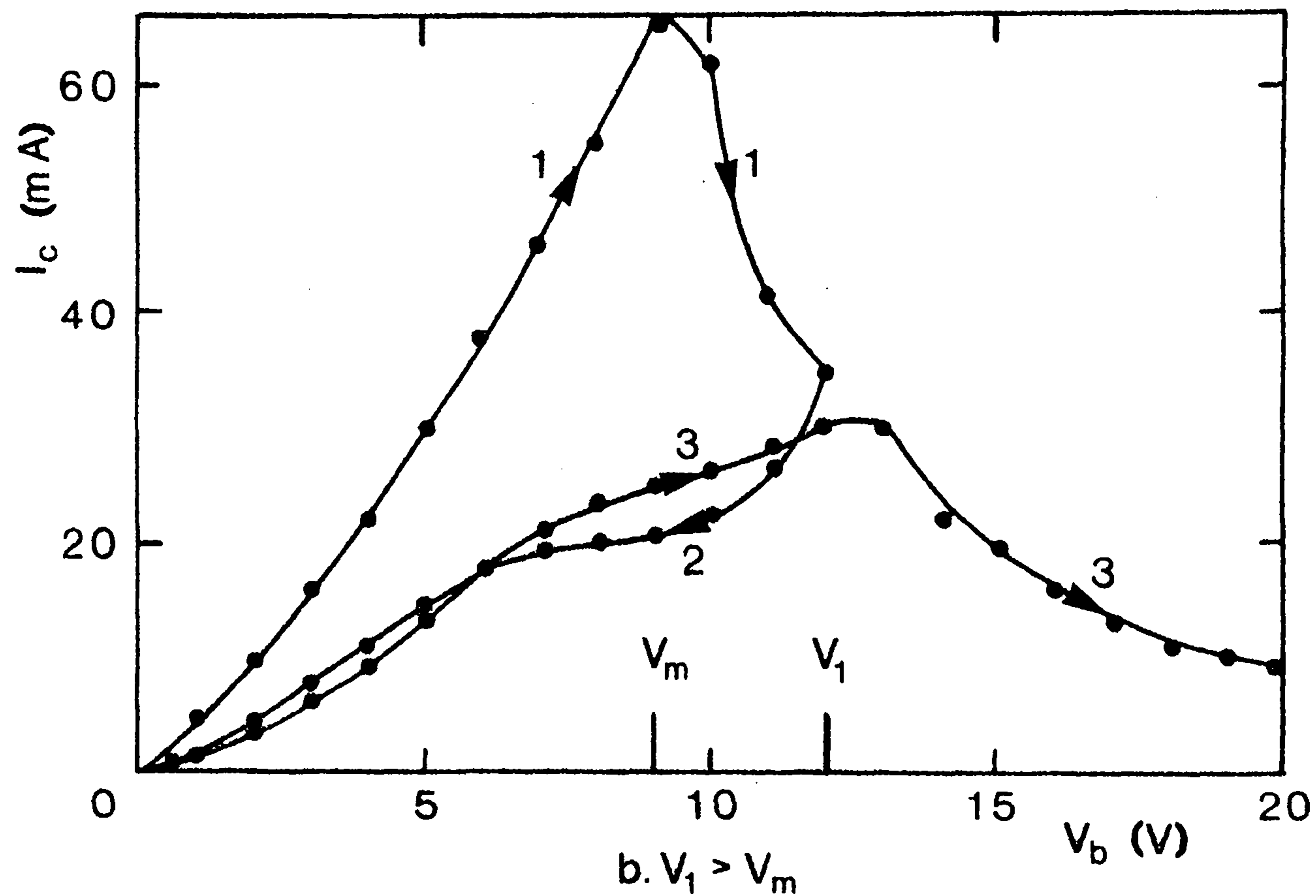
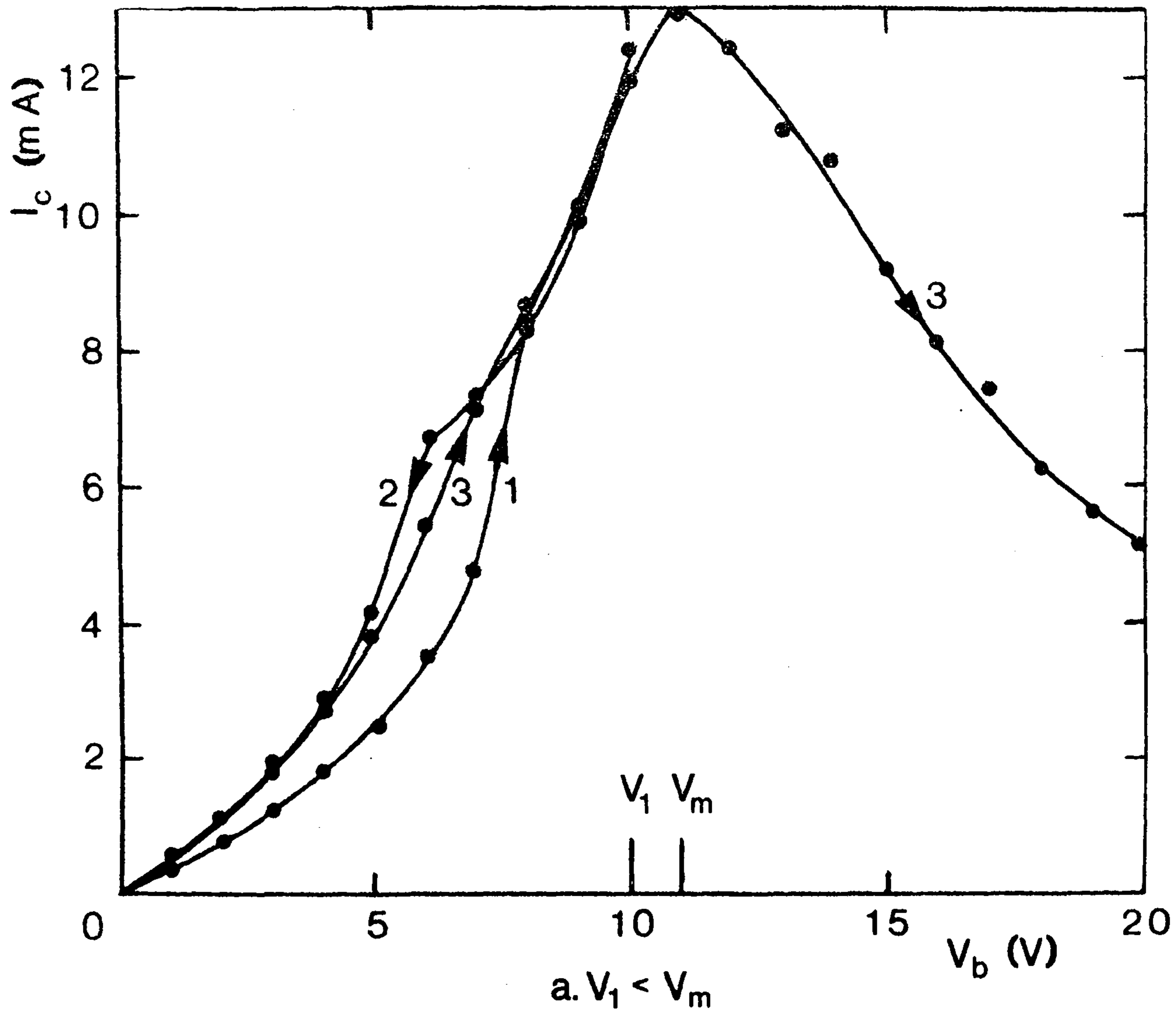


Figure 39. Dependence of I_c on V_b for increasing and decreasing voltages in CaBr_2

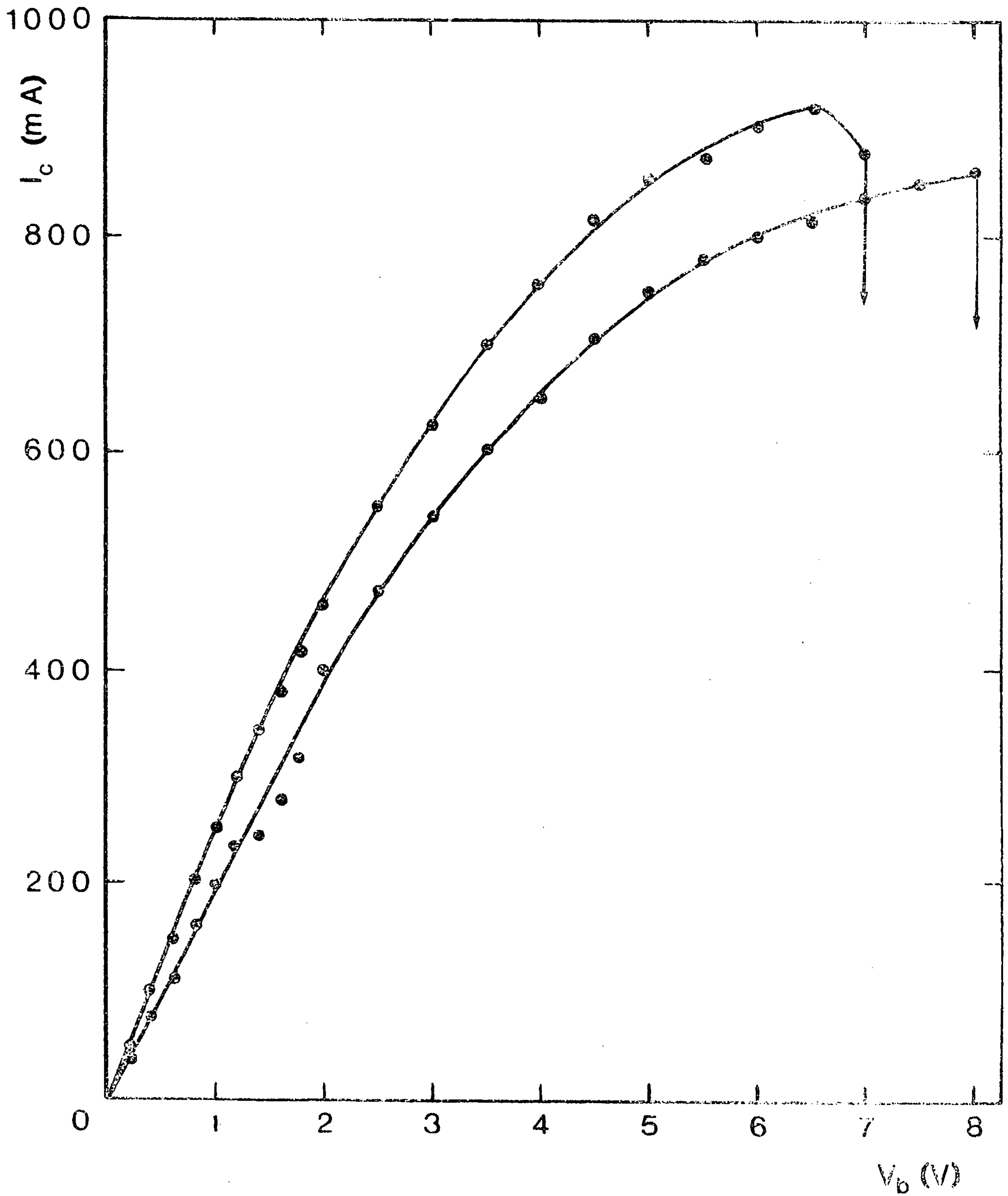


Figure 40. Forming in Si_3N_4

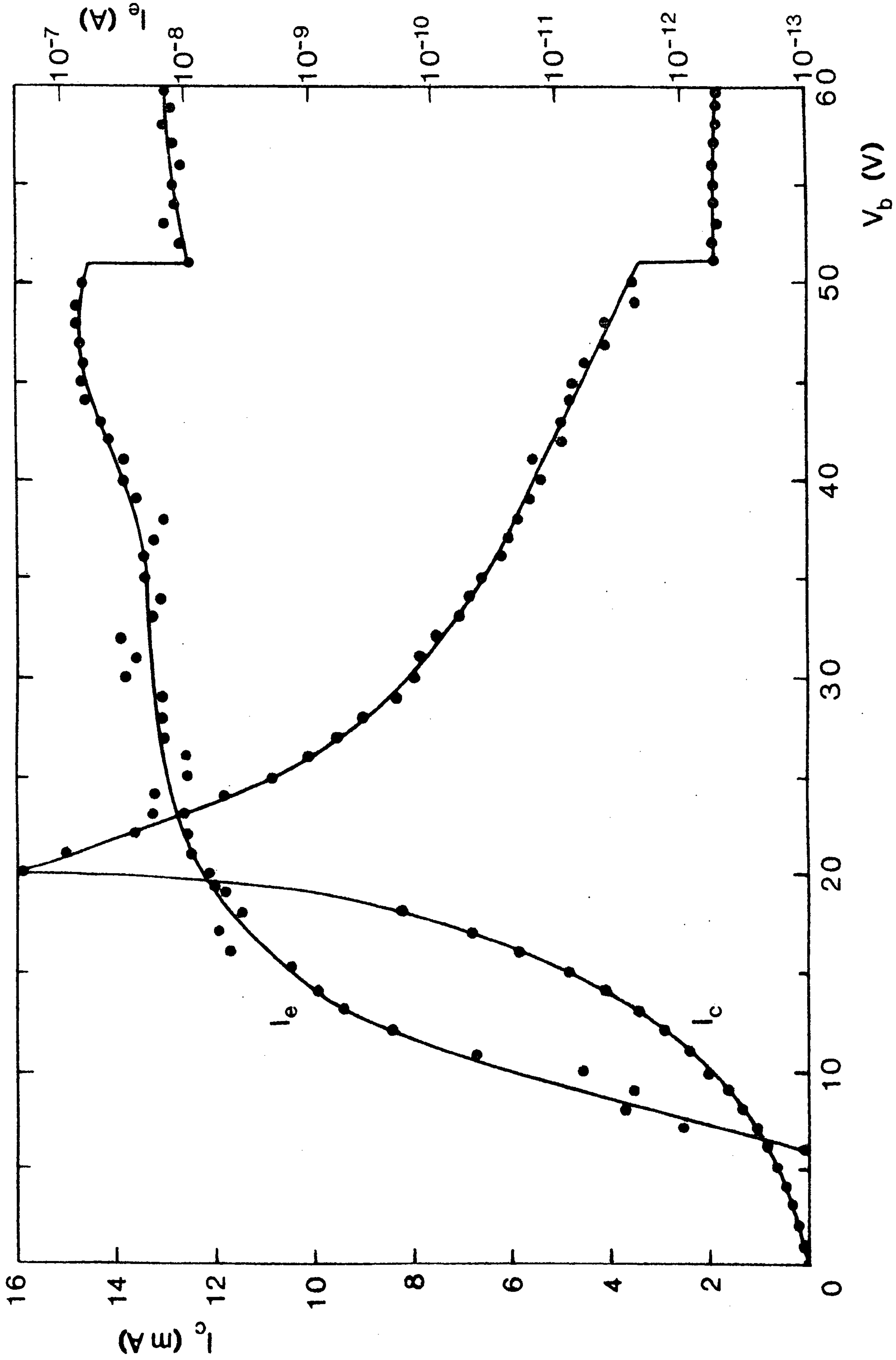


Figure 41. Dependence of I_c and I_e on V_b in Si_3N_4

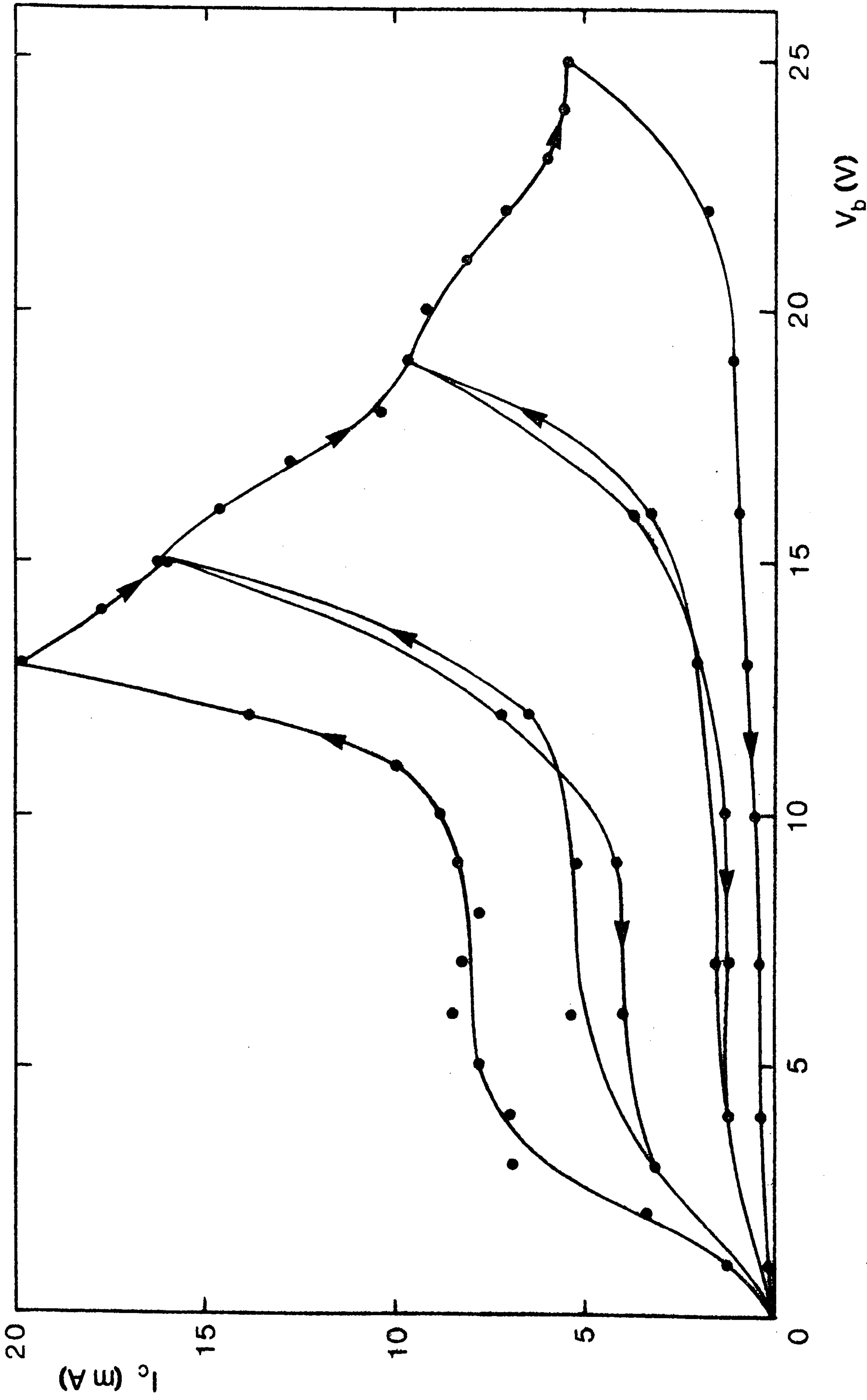


Figure 42. Dependence of I_c on V_b for increasing and decreasing voltages in Si_3N_4

'It did not last: the Devil howling "Ho!
Let Einstein be!" restored the status quo.'

Sir John Collings Squire

1884 - 1958